Numerical and series solutions for flows of non-linear fluids

By

Zaheer Abbas

DEPARTMENT OF MATHEMATICS
QUAID-I-AZAM UNIVERSITY
ISLAMABAD, PAKISTAN
2009

Numerical and series solutions for flows of non-linear fluids

By

Zaheer Abbas

Supervised by

Dr. Tasawar Hayat

DEPARTMENT OF MATHEMATICS
QUAID-I-AZAM UNIVERSITY
ISLAMABAD, PAKISTAN
2009

Numerical and series solutions for flows of non-linear fluids

By

Zaheer Abbas

A Thesis

Submitted in the Partial Fulfillment of the

Requirements for the Degree of

DOCTOR OF PHILOSPHY

IN

MATHEMATICS

Supervised By

Dr. Tasawar Hayat

DEPARTMENT OF MATHEMATICS
QUAID-I-AZAM UNIVERSITY
ISLAMABAD, PAKISTAN
2009

CERTIFICATE

Numerical and series solutions for flows of non-linear fluids

By

Zaheer Abbas

A THESIS SUBMITTED IN THE PARTIAL FULFILLMENT OF THE REQUIREMENTS FOR THE DEGREE OF THE DOCTOR OF PHILOSOPHY

We accept this dissertation as conforming to the required standard

1. _____
Prof. Dr. Muhammad Ayub
(Chairman)

2. _____ 18/12/09
Dr. Tasawar Hayat
(Supervisor)

3. _____
Prof. Dr. Muhammad Ozair Ahmed
(External Examiner)

4. _____ 18/12/09
Dr. Khalid Hanif
(External Examiner)

DEPARTMENT OF MATHEMATICS
QUAID-I-AZAM UNIVERSITY
ISLAMABAD, PAKISTAN
2009

Dedicated to

My beloved father
Haji Ashiq Hussain

&

supervisor
Dr. Tasawar Hayat

Acknowledgements

To begin with the name of Almighty Allah, the creator of the Universe, who bestowed his blessings on me to complete this thesis successfully. I offer my humblest, sincerest and million Darood to the Holy Prophet Hazrat Muhammad (PBUH) who exhorts his followers to seek knowledge from cradle to grave.

It is difficult to overstate my gratitude to my PhD supervisor, Dr. Tasawar Hayat due to his enthusiasm, inspiration, valuable instructions, intellectual suggestions and extraordinary efforts in explaining the basics of the subject clearly and simply. Without his efforts it is impossible for me to complete this research work.

I am grateful to the chairman, Department of Mathematics Prof. Dr. Muhammad Ayub for his successful efforts in maintaining the research atmosphere in the department and for being friendly with me all the way.

The financial assistance provided by the Higher Education Commission (HEC) under 5000 indigenous fellowship scheme (PIN # 063-111210-Ps3-048) and sponsoring my short visit to Germany under International Research Support Initiative Program (IRSIP) is greatly acknowledged.

I am highly indebted to Dr. Yongqi Wang and Prof. Martin Oberlack of Darmstadt University of Technology, Germany, for their guidance and help in learning numerical techniques.

I am heartily indebted to my close friends, Dr. Muhammad Sajid, Dr. Nasir Ali, Dr. Tariq Javed and Dr. Iftikhar Ahmed for providing a stimulating and fun environment in which to learn and grow. I never forget the hours of discussion on various issues of the subject particularly regarding the analytical solutions of highly nonlinear equations. We shared wonderful period of life at QAU all together.

I would like to share my sincerest thanks to my colleagues at International Islamic University and members of FMG at Quaid-i-Azam University, especially Dr. Masood Khan, Amir Nadeem, Niaz, Sabir, Umer, Qamar, Tariq Hussain, Nawaz, Qasim, Zahid, Sajjad, Amir Mann, Amjad and Ramzan. Sincerest thanks to my friends Ahmer, Hadayat Niazi and Zaigham, Shahzad, Atif Mushtaq and M.Sc. fellows.

Lastly and most importantly, I wish to thank my grandfather who always prays for my big achievements, my parents, they grow me up, supported and guided me throughout the course of my life. The moral support provided by my brothers Jamshid, Tahir, Nasir, Qaiser and Sikander, sisters, bhabhies, my uncle Shoukat Ali and all other family members is matchless.

And last but not least the support, sacrifice and sharing of difficult moments from my wife Javaria is unforgettable. No doubt she is a very special person. Nafaye my son suffered and missed me a lot during this time of study.

December 18, 2009 *ZAHEER ABBAS*

Contents

Preface

The flows of non-Newtonian fluids are important in chemical engineering, food processing, lubrication and tribology, polymer devolatisation, bubble columns etc. Analysis of the magnetohydrodynamic (MHD) effect on the flows of such fluids has shown an increasing amount of attention in recent times. Such interest stems because of the occurrence of these liquids in industrial processes. The shear dependent viscosity and the elasticity of non-Newtonian fluids can make the constitutive relationships between the stress and rate of strain quite complicated. Such effects add extra terms in the constitutive relationships. Consequently, the mathematical analysis for the flows of such fluids involves equations with more nonlinear terms. It is also noted, in general, that order of such equations hikes in comparison to the Navier-Stokes equations. Therefore, finding accurate solutions to equations of non-Newtonian fluids is not an easy task.

Most fluid phenomena that occur in daily life are concerned with chemical reactions. Such flows are mainly encountered in several engineering applications. The concept of molecular diffusion of species with chemical reaction is further important in diffusive operations. For better understanding of transport processes, the heat transfer is of great significance. This interest stems from numerous practical applications including chemical catalytic reactors, grain storage, high performance insulation of buildings, heat exchange between soil and atmosphere, electrochemical processes, beds of fossil fuels such as oil shale and coal and many others.

The boundary layer flows due to a stretching sheet are of great interest in many engineering applications. Some of the practical examples of such problems are glass fiber and paper production, continuous casting, hot rolling, cooling of electronic chips, the aerodynamic extrusion of plastic sheets, crystal growing, polymer melts and solutions, the cooling and drying of paper and textiles etc. There has been a renewed interest in developing analytical and numerical solutions for nonlinear problems of stretching / shrinking flows. Having in mind all the stated motivations above, the arrangement of present thesis is proposed as follows.

Chapter one aims to present some survey background of stretching flows and considerations of equations of second grade and Maxwell fluids. Concept of boundary layer flow, the homotopy analysis method and homotopy-Padé approximation also included.

Chapter two studies the MHD flow of an incompressible and thermodynamic second grade

fluid bounded by an oscillatory stretched sheet. Mathematical formulation for a time-dependent and nonlinear problem is developed. The resulting problem is solved both analytically and numerically. Analytic solution is derived in series form by homotopy analysis method (HAM) whereas finite difference method is employed for a numerical solution. A comparative study between the two solutions shows an excellent agreement. Skin friction coefficient is further computed. The amplitude of skin friction coefficient is found to increase when the viscoelastic parameter is enhanced. **The results of this chapter are published in "Int. J. Non-Linear Mechanics, 43, 783-793 (2008)".**

Chapter three is concerned with an investigation of the flow and heat transfer characteristics of the boundary layer flow of a viscoelastic fluid over a continuous moving surface with a parallel free stream. Elastico-viscous fluid model is chosen in the problem development. The problem statement is based upon laws of conservation of mass, linear momentum and energy. Series solution to the governing nonlinear problem is sought by homotopic approach. Homotopy-Pade technique is utilized in tabulating skin friction coefficient and local Nusselt number. Comparison of the present analysis of series solution is given to the corresponding numerical solution in a viscous fluid. It is concluded that the local Nusselt number increases when the value of Prandtl number increases. The behaviors of viscoelasticity on the skin friction coefficient and Prandtl number on the local Nusselt number are similar in a qualitative sense. **These observations have been accepted for publication in "Numerical Methods For Partial Differential Equations".**

Chapter four is devoted to the flow of a non-Newtonian fluid film over an unsteady stretched surface. The flow modeling is based upon the time-dependent equation for boundary layer flow in a second grade fluid. The stretching velocity is also taken time-dependent. Homotopy analysis method is used to solve non-linear ordinary differential system. Variations of the dimensionless velocity profiles for various pertinent parameters are sketched and discussed. The values of skin friction coefficient are also illustrated. It is noticed that velocity profiles are the increasing functions of unsteady parameter. Moreover, the magnitude of skin friction coefficient increases when second grade parameter is increased. **These results are published in "Mathematical and Computer Modelling, 48, 518-526 (2008)".**

Chapter five investigates the magnetohydrodynamic boundary layer flow of a second grade

fluid caused by a shrinking surface. The considered surface is porous. By making use of similarity transformations, the partial differential system is converted into an ordinary differential system. Exact and homotopy solutions are first developed and then compared. Tables and graphs are prepared for velocity profiles and skin friction with respect to several parameters of interest. The boundary layer thickness is found to decrease when second grade parameter increases. The influence of Hartman number, suction and second grade parameters on the boundary layer thickness is quantitatively similar. **Such conclusions are published in "ASME Journal of Applied Mechanics, 74, 1165-1171 (2007)".**

Chapter six describes the steady mixed convection in the stagnation point flow of a Maxwell fluid bounded by a stretching vertical sheet. Assisting and opposing flow situations are analyzed carefully. Similarity transformations are invoked in reducing resulting partial differential equations of flow and temperature to the ordinary differential equations. The analytic and numerical solutions of dimensionless velocity and temperature fields are computed. Convergence of the series solutions is explicitly discussed. Comparative analysis for the two solutions is carried out. Effects of embedded parameters are discussed. As expected for assisting flow, the wall heat transfer is a decreasing function of Deborah number. Furthermore, the effects of Deborah number on assisting and opposing flows are different. **These findings are accepted in "Nonlinear Analysis: Real World Applications".**

Chapter seven deals with the influence of mass transfer on MHD flow of an upper convected Maxwell fluid over a porous shrinking sheet. An attempt is made when a chemical reaction is present. Homotopy analysis method is used in obtaining series solutions of velocity and concentration fields. In addition, the skin friction coefficient, the surface mass transfer and the gradient of mass transfer are computed. Both cases of destructive/generative chemical reactions are analyzed. It is shown that an increase in suction parameter causes a reduction in the concentration field in both situations of destructive/generative chemical reactions. However, opposite trend of concentration field is noted for destructive and generative chemical reactions. **Such observations have been published in "Physics Letters A 372, 4698-4704 (2008)".**

Chapter eight aims to examine the boundary layer flow of a micropolar fluid toward a stretching surface with a stagnation-point on the wall, and tending to potential flow at infinity. The considered fluid model is useful to analyze the flow of colloidal solutions, liquid crystals,

suspension solutions, animal blood etc. The sheet is stretched in a non-linear manner and magnetohydrodynamic nature of fluid is chosen. The obtained series solutions of dimensionless velocity and skin frictions are compared with the existing solutions in the literature. A good agreement is achieved. The skin friction coefficient has monotonic behavior with respect to vortex viscosity of micropolar fluid. **The contents of this chapter are published in "Nonlinear Analysis: Real World Applications, 10, 1514-1526 (2009)".**

Chapter nine looks at the mixed convection flow of a micropolar fluid bounded by a nonlinear stretching surface. The problem formulation does not take into account the viscous dissipation effects. The dimensionless problems of velocity and temperature solved in the series forms. Convergence region of the obtained series solutions is determined. The used homotopy Pade approximation helps in obtaining the fast convergence of the series solutions. The microrotaion velocity is found to decrease when buoyancy parameter increases. Moreover, the buoyancy parameter decreases the thickness of thermal boundary layer. **These findings are published in "Physics Letters A 372, 637-647 (2008)".**

Chapter 1

Introduction

1.1 Literature survey and basic equations

The main purpose of this chapter is to present the literature review on the existing analysis of boundary layer equations and stretching flows. Moreover the basic ideas of solutions techniques, namely, the homotopy analysis method and Padé approximant are explained.

1.2 Literature review on stretching flows

The introduction of boundary layer theory by Prandtl [1] in the early 1904s has given great impetus to modern fluid mechanics. Many problems in fluid mechanics have been solved using this theory and the comparison of obtained results agree very well with experiments. The seminal work of Sakiadis [2, 3] dealt with the boundary layer viscous flow over a continuous solid surface moving with constant velocity. Since then there have been many works on viscous aspects of the problem. The analysis of heat and mass transfer in a stretching problem with constant temperature on the surface was performed by Crane [4] and Gupta and Gupta [5]. For non-Newtonian fluids, an extension of this theory is quite intricate [6 – 8]. This is due to the diversity of these fluids in their constitutive behaviour. The viscous and elastic properties are present in such problems. Thus most studies in Newtonian boundary layers deal with single model. However, inspite of these limitations richer behaviour is expected for non-Newtonian fluids in comparison with the Newtonian fluids [7]. For steady flow, no exact solution is available

for blowing in non-Newtonian fluid past an infinite porous plate [9]. Also, for non-Newtonian fluids boundary layers are found at large Reynolds numbers, while for non-linear fluids they even form at small Reynolds numbers [7, 8]. One of the most striking characteristics of viscoelastic boundary layers is that boundary layers of varying natures may develop [7] which sometimes exhibit intricate multiple deck structures with different effects that dominate in different decks [10]. In [11, 12], applications of dilute polymer solutions, the viscoelastic flow occurs on a stretched sheet. Such fluids of second order on a stretched sheet have been investigated by Rajagopal et al. [12]. Therein (see [12]) the momentum boundary layer equation was solved numerically. In [13], Troy et al. discussed the uniqueness of the momentum boundary layer equation. However, Chang [14] and Rao [15] demonstrated the non-uniqueness of the solutions. These works were without the heat transfer phenomena. Similar flow analysis in the absence of heat transfer in the flow of non-Newtonian fluid of Walters' liquid B has been considered by Siddappa and Abel [16]. Also the Stokes' problem for a viscoelastic fluid was studied by Soundalgekar [17]. This in turn was further looked at by Siddappa and Khapate [18] for second order viscoelastic fluids.

The above studies utilized the boundary layer concept due to Prandtl. These are valid for small viscosity or high Reynolds number and simplifies the analysis of the Navier-Stokes equations. Beard and Walters [19] endeavoured to obtain the governing equations for the boundary layer flow for a prototype viscoelastic fluid which was called liquid B. Such viscoelastic nature was found in polymer fluids which also exhibit elastic properties. Andersson [20] provided an exact solution of MHD flow of a Walters liquid B over a stretched sheet. The non-Newtonian behaviour of a power-law fluid was investigated by Acrivos et al. [21] and Schowalter [22] whereas Srivastava [23] attempted to understand differential-type fluids. The solution for the boundary layer flow past a stretched wall with speed proportional to the distance along the wall was investigated by Danberg and Fansler [24]. Further, Abel et al. [25], Ariel [26] and Datti et al. [27] conducted researches on MHD boundary layer viscoelastic fluids. Seddeek [28] looked at non-reactive species. There have been continuous focus on similar problems of second-grade/second-order, and, Maxwell fluids [29 – 35]. Cortell [36] also looked at MHD flow and mass transfer of viscoelastic fluids in porous media with chemically reactive species. An increase in the concentration profiles was reported when magnetic field parameter increases. In

[36], it was stated that the effect of the reaction-order parameter increases the fluid concentration with its increase. When a destructive chemical reaction was present-an opposite effect was seen with a generative chemical reaction on the flow problem. The results of [36] were extended in Cortell [37]. Chakrabarti and Gupta [38] investigated the flows of heat and mass transfer over a stretching sheet while Gorla [39] presented applications in electro-chemistry. The study of transport of mass and momentum of chemically reactive species in the flow over a linear stretching surface was presented by Andersson et al. [40]. Moreover, Takhar et al. [41] researched flow and mass transfer characteristics of a viscous electrically conducting fluid over a stretched sheet with non-zero slot velocity. An extension of this was provided by Akyildiz et al. [42]. This was to the subclass of non-Newtonian, second grade fluids immersed in a porous medium on a stretching sheet. These authors augmented the missing boundary condition.

The stagnation-point flow of such fluids display the incompleteness of the current boundary layer theory for viscoelastic fluids. Indeed for Newtonian fluid this flow results in an exact solution which is valid at any Reynolds number [43] while the second grade model [44] does not give rise to an exact solution. In fact Rajeswari and Rathna [45] relied a boundary layer approximations to obtain an estimate of the wall shear stress for stagnation-point flow of a second grade fluid. In order to provide solutions to the governing equation, they [45] utilized the Karman-Pohlhausen momentum integral method [43]. They concluded that the wall shear stress becomes larger with higher fluid elasticity. Davies [46] by using a similar approach corroborated the results of [43]. Beard and Walters [19] in their seminal study of stagnation point flows of a second grade fluid used boundary layer theory together with similarity and made reductions of the governing PDEs to a single nonlinear fourth order ODE. There was insufficient physical boundary conditions and they [19] transformed their singular perturbation problem [47] into a regular one by reducing the equation to a system of two third order ODEs. This was showed numerically. They concluded that the main effect of fluid elasticity is to increase the wall shear stress as in [45]. However, contrary to [45] and [46], they [19] predicted an overshoot in the velocity inside the boundary layer as a consequence of the fluid's elasticity. No experiments as yet validate these theoretical results.

Many investigators over the last few decades have been stimulated to validate the prediction of [19] that in stagnation point flow of a viscoelastic fluid the velocity inside the boundary layer

may exceed that outside this layer. It has been hinted, Frater [48], that this overshoot of velocity can be as a consequence of looking for a straightforward perturbation solution of the problem in terms of the elasticity number. Teipel [49], Garg and Rajagopal [50] and Pakdemirli and Suhubi [51] have shown that the perturbation approach may not acceptable results for viscoelastic fluids. This was nicely demonstrated by Ariel [52]. Notwithstanding, Ariel [52] endeavoured to solve the original fourth order ODE instead of the perturbed system by utilizing an accurate hybrid approach. This necessitated the augmentation of the boundary conditions to four. He imposed an extra condition at the wall. It turns out that the findings of [52] is quite disparate from those of [19] especially for $k > 0.1$. In another work dealing with the fourth order ODE, Serth [53] showed that the wall shear stress computed by means of the orthogonal collocation-point approach is distinct from that deduced from perturbations. Moreover, Garg and Rajagopal [50] have shown that the elasticity number k signature should be reversed in order to imply with thermodynamical constraints [54, 55]. As a matter of fact, they [50] found no overshoot in the velocity for arbitrary k. Ariel [56] showed that by using his hybrid method and sign reversal in the elasticity number, he can obtain results for large values of k, while for same sign as used in [19] his method gives the results up to $k = 0.326$.

The works cited thus far as regards to the overshoot of the velocity in the boundary layer suggests that this problem is by no means closed. The method of solution has significant on the results obtained. These studies were on the second grade model which is a simple reasonable rheological model for slow flows having small levels of elasticity. However, there are several cases for which one has large elasticity number [57]. This is compounded by the sign and magnitude of the parameters as we have mentioned above. So the results derived at even small elasticity number is questionable as is in the foregoing discussion.

Due to the mentioned limitations, it is appropriate to look at more realistic constitutive equations such as Maxwell, Oldroyd-B, Phan-Thien Tanner and Giesukus [44] to further investigate stagnation-point flows of viscoelastic fluids. These rheological models have been tried in other geometries though. We mention a few studies. Sadeghy and Sharifi [58] and Sadeghy et al [59] have examined Blasius and Sakiadis flows of second grade and upper-convected Maxwell models. They observed differences between the predictions relating to wall shear stress and that of boundary layer thickness. The study of elastic boundary layer formed above stretching

sheets were looked at in terms of an Oldroyd-B model [60]. Furthermore, Renardy [62] and Hagen and Renardy [61] provided a general formulation for the boundary layer flows of Maxwell, Phan-Thien Tanner and the Giesukus models. It was shown by these authors that of the three rheological model tested, the derivation from Newtonian behaviour is more significant of the fluid adheres to the upper-convected Maxwell model [61, 62].

The flow and heat transfer together with the effect of the fluids elasticity on an incompressible homogeneous second grade fluid past a stretched sheet were studied in [32]. The effects of viscous dissipation and strain energy stored in the fluid were taken into account in the energy equation. These effects are vital for heat transfer analyses. On the one hand if the viscosity of the fluid is high, the dissipation term becomes relevant and, on the other hand due to the fluids elasticity there is change in the heat transfer characteristics and temperature distributions. Lawrence and Rao [63] published on heat transfer for viscoelastic flows on a stretched sheet devoid of viscous dissipation although such flows generate heat by means of viscous dissipation. Another important aspect is to take into account temperature dependent heat source present in the boundary layer. A work on momentum and heat transfer in such fluid with both internal heat generation and viscous dissipation was presented by Bujurke et al. [64]. The extension of the problem [12] was analyzed with heat transfer by Dandapat and Gupta [65] in which an exact solution was given which agrees with the results of [12]. An extension of [65] was given in the work of Cortell [29, 32] which dealt with heat transfer in an incompressible second order/grade fluid as caused by a stretched sheet. This was a view of examining the influence of the viscoelastic parameter on the temperature distributions. These results were in agreement of [65]. The analysis of heat transfer in a viscoelastic/second grade fluids was also discussed by Rollins and Vajravelu [66], Char [67], Bhattacharya et al. [68] and Vajravelu and Rollins [69]. Stretching and stagnation point flows with and without partial slip effect were looked in studies [70 – 75] and several refs. therein.

Viscoelastic boundary layer flows and heat transfer with temperature dependent heat source/sink are available [76 – 83]. Heat transfer on a vertical sheet in a heat generating fluid was analyzed by Vajravelu and Nayfeh [84]. The effect of variable viscosity on forced convection flow past a horizontal flat plate in a porous space was studied by Postelnicu et al. [85]. This author [86] also looked at free convection boundary layer on a vertical permeable plate in porous medium

with internal space dependent heat generation. Again similar results were given in Postelnicu et al. [87]. The study of blowing/suction effects in hydromagnetic heat transfer by mixed convection on an inclined stretching surface with heat generation in both space and temperature heat source was given in Abo-Eldahab and El Aziz [88].

1.3 Basic equations

The equations of magnetohydrodynamics that describe the flow and heat transfer characteristics are given as follows.

(a) Maxwell's equations

$$\begin{aligned} \operatorname{div}\mathbf{E} &= 0, \ \operatorname{div}\mathbf{B} = 0, \\ \operatorname{curl}\mathbf{E} &= -\frac{\partial \mathbf{B}}{\partial t}, \ \operatorname{curl}\mathbf{B} = \mu_m \mathbf{J}. \end{aligned} \tag{1.1}$$

These equations hold only when the displacement current is negligible.

(b) Ohms' law

$$\mathbf{J} = \sigma\left(\mathbf{E} + \mathbf{V} \times \mathbf{B}\right). \tag{1.2}$$

(c) The incompressibility condition

$$\operatorname{div}\mathbf{V} = 0. \tag{1.3}$$

(d) The momentum equation

$$\rho\frac{d\mathbf{V}}{dt} = \operatorname{div}\tau + \rho\mathbf{b}. \tag{1.4}$$

(e) The energy equation

$$\rho c_p \frac{dT}{dt} = \tau.\mathbf{L} - \operatorname{div}\mathbf{q}. \tag{1.5}$$

(e) The concentration equation

$$\frac{dC}{dt} = D\left(\operatorname{div} C\right) - k_n C^n. \tag{1.6}$$

1.4 Boundary layer flow/equations

A major impetus to the study of fluid mechanics was initiated L. Prandtl in the year 1904. He was instrumental in classifying the essence and influence of viscosity in flows at high Reynolds numbers and he showed how the Navier-Stokes equations could be simplified to provide approximate solutions under this situation. A boundary layer flow deals with that portion of a fluid flow, near a solid surface, where shear stresses are of significances and the inviscid-flow assumption is not a reliable assumption. A solid surface has interaction with a viscous fluid flow. This is due to the no-slip condition which is a physical requirement that the fluid and solid have equal velocities at their interface. Therefore a fluid flow is retarded by a fixed solid surface and a finite slow-moving boundary layer is formed. A requirement that the boundary layer be thin is for the Reynolds number of the body to be large, i.e. 10^3 or greater. Under the said conditions, the flow outside the boundary layer is largely inviscid and plays the role of a driving mechanism for the layer.

The discovery of the boundary layer equations can be considered as one of the more important advances in fluids. The use of an order of magnitude analysis results in the governing Navier–Stokes equations of viscous fluid flow to be immensely simplified within the boundary layer. Indeed, the partial differential equations (PDE) becomes parabolic. This greatly enhances the solution procedure for the equations. The flow is divided into an inviscid portion (which is easy to solve by a number of approaches) and the boundary layer (which is governed by an easier to solve PDE). Navier–Stokes equations for an incompressible two-dimensional flow are

$$u\frac{\partial u}{\partial x}+v\frac{\partial u}{\partial y}=-\frac{1}{\rho}\frac{\partial \widetilde{p}}{\partial x}+\nu\left(\frac{\partial^2 u}{\partial x^2}+\frac{\partial^2 u}{\partial y^2}\right), \tag{1.7}$$

$$u\frac{\partial v}{\partial x}+v\frac{\partial v}{\partial y}=-\frac{1}{\rho}\frac{\partial \widetilde{p}}{\partial y}+\nu\left(\frac{\partial^2 v}{\partial x^2}+\frac{\partial^2 v}{\partial y^2}\right), \tag{1.8}$$

$$\frac{\partial u}{\partial x}+\frac{\partial v}{\partial y}=0. \tag{1.9}$$

In above expressions ν is the kinematic viscosity, ρ is the density of the fluid, $\widetilde{p}$ is the pressure, x and y are the horizontal and vertical coordinates and u and v the velocity components parallel to x and y axes. A wall is considered $y = 0$. The non-dimensional quantities are defined as

$$x^* = \frac{x}{L}, \quad y^* = \frac{y}{\delta_1}, \quad u^* = \frac{u}{U}, \quad v^* = \frac{v}{U}\frac{L}{\delta_1}, \quad p^* = \frac{p}{\rho U^2}. \tag{1.10}$$

Here L indicates the horizontal length scale and δ_1 the boundary layer thickness. Equations (1.7) to (1.9) in non-dimensional variables are

$$u^*\frac{\partial u^*}{\partial x^*} + v^*\frac{\partial u^*}{\partial y^*} = -\frac{\partial \widetilde{p}^*}{\partial x^*} + \frac{\nu}{UL}\frac{\partial^2 u^*}{\partial x^{*2}} + \frac{\nu}{UL}\left(\frac{L}{\delta_1}\right)^2\frac{\partial^2 u^*}{\partial y^{*2}}, \tag{1.11}$$

$$u^*\frac{\partial v^*}{\partial x^*} + v^*\frac{\partial v^*}{\partial y^*} = -\left(\frac{L}{\delta_1}\right)^2\frac{\partial \widetilde{p}^*}{\partial y^*} + \frac{\nu}{UL}\frac{\partial^2 v^*}{\partial x^{*2}} + \frac{\nu}{UL}\left(\frac{L}{\delta_1}\right)^2\frac{\partial^2 v^*}{\partial y^{*2}}, \tag{1.12}$$

$$\frac{\partial u^*}{\partial x^*} + \frac{\partial v^*}{\partial y^*} = 0, \tag{1.13}$$

in which the Reynold number is written as

$$R = \frac{UL}{\nu}. \tag{1.14}$$

The inertial and viscous forces are of the same order and hence

$$\frac{\nu}{UL}\left(\frac{L}{\delta_1}\right)^2 = O(1) \tag{1.15}$$

or

$$\delta_1 = O\left(R^{-1/2}L\right). \tag{1.16}$$

Dropping asterisks and utilizing above equation one obtains

$$u\frac{\partial u}{\partial x} + v\frac{\partial u}{\partial y} = -\frac{\partial \widetilde{p}}{\partial x} + \frac{1}{R}\frac{\partial^2 u}{\partial x^2} + \frac{\partial^2 u}{\partial y^2}, \tag{1.17}$$

$$\frac{1}{R}\left(u\frac{\partial v}{\partial x} + v\frac{\partial v}{\partial y}\right) = -\frac{\partial \widetilde{p}}{\partial y} + \frac{1}{R^2}\left(\frac{\partial^2 v}{\partial x^2} + \frac{\partial^2 v}{\partial y^2}\right), \tag{1.18}$$

$$\frac{\partial u}{\partial x} + \frac{\partial v}{\partial y} = 0. \tag{1.19}$$

For $R \to \infty$ we have

$$u\frac{\partial u}{\partial x}+v\frac{\partial u}{\partial y}=-\frac{\partial \widetilde{p}}{\partial x}+\frac{\partial^2 u}{\partial y^2}, \tag{1.20}$$

$$-\frac{\partial \widetilde{p}}{\partial y}=0, \tag{1.21}$$

$$\frac{\partial u}{\partial x}+\frac{\partial v}{\partial y}=0, \tag{1.22}$$

in which Eq. (1.21) shows that pressure is constant across the boundary layer. In dimensional form, Eqs. (1.20) to (1.22) become

$$u\frac{\partial u}{\partial x}+v\frac{\partial u}{\partial y}=-\frac{1}{\rho}\frac{\partial \widetilde{p}}{\partial x}+\nu\frac{\partial^2 u}{\partial y^2}, \tag{1.23}$$

$$-\frac{1}{\rho}\frac{\partial \widetilde{p}}{\partial y}=0, \tag{1.24}$$

$$\frac{\partial u}{\partial x}+\frac{\partial v}{\partial y}=0. \tag{1.25}$$

1.5 Constitutive equation

It is well established fact now that non-Newtonian fluids cannot be described by a single relationship between stress and rate of strain. This is quite distinct feature of non-Newtonian fluids from the Newtonian ones. In fact such difficulty arises because of diversity of non-Newtonian fluids in nature. In view of this several models of non-Newtonian fluids have been suggested. In this thesis, we will study the flows of second grade, Maxwell and micropolar fluids.

1.5.1 Boundary layer equation in a second grade fluid

The Cauchy stress tensor $\mathbf{T}$ in a second grade fluid is represented by the following relation [9].

$$\mathbf{T}=-\widetilde{p}\mathbf{I}+\mathbf{F}, \tag{1.26}$$

where an extra stress tensor $\mathbf{F}$ is

$$\mathbf{F}=\mu\mathbf{A}_1+\alpha_1\mathbf{A}_2+\alpha_2\mathbf{A}_1^2. \tag{1.27}$$

In above equation μ is the dynamic viscosity, $\widetilde{p}$ the pressure, $\mathbf{I}$ the identity tensor and α_1 and α_2 the material moduli. The first two Rivilin-Ericksen tensors $\mathbf{A}_1$ and $\mathbf{A}_2$ are given by

$$\begin{aligned} \mathbf{A}_1 &= \mathbf{L}+\mathbf{L}^{\mathrm{T}}, \\ \mathbf{A}_2 &= \frac{d\mathbf{A}_1}{dt}+\mathbf{A}_1\mathbf{L}+\mathbf{L}^{\mathrm{T}}\mathbf{A}_1, \end{aligned} \tag{1.28}$$

where $\mathbf{L}=\operatorname{grad}\mathbf{V}$ and $\mathbf{L}^{\mathrm{T}}=(\operatorname{grad}\mathbf{V})^{\mathrm{T}}$ and d/dt signifies the material derivative.

For two-dimensional flow, the velocity is expressed as

$$\mathbf{V}=[u(x,y),v(x,y),0]\,. \tag{1.29}$$

Employing above definition of velocity, one can write

$$\mathbf{A}_1=\begin{bmatrix} 2\frac{\partial u}{\partial x} & \frac{\partial u}{\partial y}+\frac{\partial v}{\partial x} & 0 \\ \frac{\partial v}{\partial x}+\frac{\partial u}{\partial y} & 2\frac{\partial v}{\partial y} & 0 \\ 0 & 0 & 0 \end{bmatrix}, \tag{1.30}$$

$$\mathrm{A}_2=\begin{bmatrix} 2u\frac{\partial^2 u}{\partial x^2}+2v\frac{\partial^2 u}{\partial x\partial y}+4\left(\frac{\partial u}{\partial x}\right)^2 & u\frac{\partial^2 u}{\partial x\partial y}+u\frac{\partial^2 u}{\partial x^2}+v\frac{\partial^2 u}{\partial y^2}+3\frac{\partial v}{\partial x}\frac{\partial v}{\partial y} & 0 \\ +2\left(\frac{\partial v}{\partial x}\right)^2+2\frac{\partial u}{\partial y}\frac{\partial v}{\partial x} & +3\frac{\partial u}{\partial x}\frac{\partial u}{\partial y}+\frac{\partial u}{\partial y}\frac{\partial v}{\partial y}+\frac{\partial u}{\partial x}\frac{\partial v}{\partial x}+v\frac{\partial^2 v}{\partial x\partial y} & \\ u\frac{\partial^2 u}{\partial x\partial y}+u\frac{\partial^2 v}{\partial x^2}+v\frac{\partial^2 u}{\partial y^2}+3\frac{\partial v}{\partial x}\frac{\partial v}{\partial y} & 2v\frac{\partial^2 v}{\partial y^2}+2u\frac{\partial^2 v}{\partial x\partial y}+4\left(\frac{\partial v}{\partial y}\right)^2 & 0 \\ +3\frac{\partial u}{\partial x}\frac{\partial u}{\partial y}+\frac{\partial u}{\partial y}\frac{\partial v}{\partial y}+\frac{\partial u}{\partial x}\frac{\partial v}{\partial x}+v\frac{\partial^2 v}{\partial x\partial y} & +2\left(\frac{\partial u}{\partial y}\right)^2+2\frac{\partial u}{\partial y}\frac{\partial v}{\partial x} & \\ 0 & 0 & 0 \end{bmatrix}, \tag{1.31}$$

$$\mathbf{A}_1^2=\begin{bmatrix} 4\left(\frac{\partial u}{\partial x}\right)^2+\left(\frac{\partial u}{\partial y}\frac{\partial v}{\partial x}\right)^2 & 2\frac{\partial u}{\partial x}\frac{\partial u}{\partial y}+2\frac{\partial u}{\partial x}\frac{\partial v}{\partial x} & 0 \\ & +2\frac{\partial u}{\partial y}\frac{\partial v}{\partial y}+2\frac{\partial v}{\partial x}\frac{\partial v}{\partial y} & \\ 2\frac{\partial u}{\partial x}\frac{\partial u}{\partial y}+2\frac{\partial u}{\partial x}\frac{\partial v}{\partial x} & 4\left(\frac{\partial v}{\partial x}\right)^2+\left(\frac{\partial u}{\partial y}\frac{\partial v}{\partial x}\right)^2 & 0 \\ +2\frac{\partial u}{\partial y}\frac{\partial v}{\partial y}+2\frac{\partial v}{\partial x}\frac{\partial v}{\partial y} & & \\ 0 & 0 & 0 \end{bmatrix} \tag{1.32}$$

and now Eq. (1.27) yields

$$\mathbf{F}=\begin{bmatrix} \begin{array}{c} 2\mu\frac{\partial u}{\partial x}+\alpha_1\left\{2u\frac{\partial^2 u}{\partial x^2}\right. \\ +2v\frac{\partial^2 u}{\partial x\partial y}+4\left(\frac{\partial u}{\partial x}\right)^2 \\ \left.+2\left(\frac{\partial v}{\partial x}\right)^2+2\frac{\partial u}{\partial y}\frac{\partial v}{\partial x}\right\} \\ +\alpha_2\left(\left(\frac{\partial u}{\partial x}\right)^2+\left(\frac{\partial u}{\partial y}\frac{\partial v}{\partial x}\right)\right) \end{array} & \begin{array}{c} \mu\left(\frac{\partial u}{\partial y}+\frac{\partial v}{\partial x}\right)+\alpha_1\left\{u\frac{\partial^2 u}{\partial x\partial y}+u\frac{\partial^2 u}{\partial x^2}\right. \\ +v\frac{\partial^2 u}{\partial y^2}+3\frac{\partial v}{\partial x}\frac{\partial v}{\partial y}+3\frac{\partial u}{\partial x}\frac{\partial u}{\partial y} \\ \left.+\frac{\partial u}{\partial y}\frac{\partial v}{\partial y}+\frac{\partial u}{\partial x}\frac{\partial v}{\partial x}+v\frac{\partial^2 v}{\partial x\partial y}\right\} \\ +\alpha_2\left(\frac{\partial u}{\partial x}\frac{\partial u}{\partial y}+\frac{\partial u}{\partial y}\frac{\partial v}{\partial y}\right) \end{array} & 0 \\ \begin{array}{c} \mu\left(\frac{\partial u}{\partial y}+\frac{\partial v}{\partial x}\right)+\alpha_1\left\{u\frac{\partial^2 u}{\partial x\partial y}+u\frac{\partial^2 v}{\partial x^2}\right. \\ +v\frac{\partial^2 u}{\partial y^2}+3\frac{\partial v}{\partial x}\frac{\partial v}{\partial y}+3\frac{\partial u}{\partial x}\frac{\partial u}{\partial y} \\ \left.+\frac{\partial u}{\partial y}\frac{\partial v}{\partial y}+\frac{\partial u}{\partial x}\frac{\partial v}{\partial x}+v\frac{\partial^2 u}{\partial x\partial y}\right\} \\ +\alpha_2\left(\frac{\partial u}{\partial x}\frac{\partial u}{\partial y}+\frac{\partial u}{\partial y}\frac{\partial v}{\partial y}\right) \end{array} & \begin{array}{c} 2\mu\frac{\partial u}{\partial x}+\alpha_1\left\{2u\frac{\partial^2 v}{\partial y^2}\right. \\ +2v\frac{\partial^2 v}{\partial x\partial y}+4\left(\frac{\partial u}{\partial y}\right)^2 \\ \left.+4\left(\frac{\partial v}{\partial y}\right)^2+2\frac{\partial u}{\partial y}\frac{\partial v}{\partial x}\right\} \\ +\alpha_2\left(\left(\frac{\partial u}{\partial x}\right)^2+\left(\frac{\partial u}{\partial y}\frac{\partial v}{\partial x}\right)\right) \end{array} & 0 \\ 0 & 0 & 0 \end{bmatrix} \tag{1.33}$$

Substitution of Eqs. (1.26) and (1.33) into momentum equation (1.4) yields the following scalar equations

$$\begin{aligned} u\frac{\partial u}{\partial x}+v\frac{\partial u}{\partial y} &= -\frac{1}{\rho}\frac{\partial \widetilde{p}}{\partial x}+\nu\left(\frac{\partial^2 u}{\partial x^2}+\frac{\partial^2 u}{\partial y^2}\right)+\frac{\alpha_1}{\rho}\left[\begin{array}{c} \frac{\partial u}{\partial x}\left(13\frac{\partial^2 u}{\partial x^2}+\frac{\partial^2 u}{\partial y^2}\right)+u\left(\frac{\partial^3 u}{\partial x^3}+\frac{\partial^3 u}{\partial x\partial y^2}\right) \\ +v\left(\frac{\partial^3 v}{\partial y^3}+\frac{\partial^3 u}{\partial x^2\partial y}\right)+2\frac{\partial v}{\partial x}\left(2\frac{\partial^2 u}{\partial x^2}+\frac{\partial^2 u}{\partial x\partial y}\right) \\ +3\frac{\partial u}{\partial y}\left(\frac{\partial^2 u}{\partial x\partial y}+\frac{\partial^2 v}{\partial x^2}\right) \end{array}\right] \\ &+\frac{2\alpha_2}{\rho}\left[4\frac{\partial u}{\partial x}\frac{\partial^2 u}{\partial x^2}+\frac{\partial u}{\partial y}\left(\frac{\partial^2 u}{\partial x\partial y}+\frac{\partial^2 v}{\partial x^2}\right)+\frac{\partial v}{\partial x}\left(\frac{\partial^2 u}{\partial x\partial y}+\frac{\partial^2 v}{\partial x^2}\right)\right], \end{aligned} \tag{1.34}$$

$$\begin{aligned} u\frac{\partial v}{\partial x}+v\frac{\partial v}{\partial y} &= -\frac{1}{\rho}\frac{\partial \widetilde{p}}{\partial y}+\nu\left(\frac{\partial^2 v}{\partial x^2}+\frac{\partial^2 v}{\partial y^2}\right)+\frac{\alpha_1}{\rho}\left[\begin{array}{c} \frac{\partial v}{\partial y}\left(\frac{\partial^2 v}{\partial x^2}+13\frac{\partial^2 v}{\partial y^2}\right)+u\left(\frac{\partial^3 v}{\partial x^3}+\frac{\partial^3 v}{\partial x\partial y^2}\right) \\ +v\left(\frac{\partial^3 v}{\partial y^3}+\frac{\partial^3 v}{\partial x^2\partial y}\right)+2\frac{\partial u}{\partial y}\left(\frac{\partial^2 u}{\partial y^2}+\frac{\partial^2 v}{\partial x\partial y}\right) \\ +3\frac{\partial v}{\partial x}\left(\frac{\partial^2 v}{\partial x\partial y}+\frac{\partial^2 u}{\partial y^2}\right) \end{array}\right] \\ &+\frac{2\alpha_2}{\rho}\left[4\frac{\partial v}{\partial y}\frac{\partial^2 v}{\partial y^2}+\frac{\partial u}{\partial y}\left(\frac{\partial^2 v}{\partial x\partial y}+\frac{\partial^2 u}{\partial y^2}\right)+\frac{\partial v}{\partial x}\left(\frac{\partial^2 v}{\partial x\partial y}+\frac{\partial^2 u}{\partial y^2}\right)\right], \end{aligned} \tag{1.35}$$

Using [1]

$$u=O(1),\quad v=O(\delta),\quad x=O(1),\quad y=O(\delta), \tag{1.36}$$

$$\frac{T_{xx}}{\rho} = O(1), \quad \frac{T_{xy}}{\rho} = O(\delta), \quad \frac{T_{yy}}{\rho} = O(\delta^2) \tag{1.37}$$

equation (1.35) is identical to Eq. (1.24) and Eq. (1.34) reduces to

$$u\frac{\partial u}{\partial x}+v\frac{\partial u}{\partial y} = -\frac{1}{\rho}\frac{\partial \widetilde{p}}{\partial x}+\nu\frac{\partial^2 u}{\partial y^2}+\frac{\alpha_1}{\rho}\left[\frac{\partial u}{\partial x}\frac{\partial^2 u}{\partial y^2}+u\frac{\partial^3 u}{\partial x \partial y^2}+3\frac{\partial u}{\partial y}\frac{\partial^2 v}{\partial y^2}+v\frac{\partial^3 v}{\partial y^3}\right]+\frac{2\alpha_2}{\rho}\frac{\partial u}{\partial y}\frac{\partial^2 v}{\partial y^2}, \tag{1.38}$$

where [55]

$$\mu \geq 0, \ \alpha_1 \geq 0, \ \alpha_1 + \alpha_2 = 0. \tag{1.39}$$

and now Eq. (1.38) can be written as

$$u\frac{\partial u}{\partial x}+v\frac{\partial u}{\partial y} = -\frac{1}{\rho}\frac{\partial \widetilde{p}}{\partial x}+\nu\frac{\partial^2 u}{\partial y^2}+\frac{\alpha_1}{\rho}\left[\frac{\partial u}{\partial x}\frac{\partial^2 u}{\partial y^2}+u\frac{\partial^3 u}{\partial x \partial y^2}+\frac{\partial u}{\partial y}\frac{\partial^2 v}{\partial y^2}+v\frac{\partial^3 u}{\partial y^3}\right]. \tag{1.40}$$

1.5.2 Boundary layer equation in a Maxwell fluid

The Cauchy stress tensor here is defined by Eq. (1.26). However, the expression of $\mathbf{F}$ in Maxwell fluid satisfies

$$\mathbf{F} + \lambda_1 \frac{\delta \mathbf{F}}{\delta t} = \mu \mathbf{A}_1, \tag{1.41}$$

in which λ_1 is the relaxation time and $\delta/\delta t$ is the upper convected derivative given by

$$\frac{\delta \mathbf{F}}{\delta t} = \frac{d\mathbf{F}}{dt} - \mathbf{L}\mathbf{F} - \mathbf{F}\mathbf{L}^{\top} \tag{1.42}$$

where

$$\mathbf{F} = \begin{bmatrix} F_{xx} & F_{xy} & F_{xz} \\ F_{yx} & F_{yy} & F_{yz} \\ F_{zx} & F_{zy} & F_{zz} \end{bmatrix}. \tag{1.43}$$

The momentum equation for two-dimensional flow gives

$$\rho\left(u\frac{\partial u}{\partial x}+v\frac{\partial u}{\partial y}\right) = -\frac{\partial \widetilde{p}}{\partial x}+\frac{\partial F_{xx}}{\partial x}+\frac{\partial F_{xy}}{\partial y}, \tag{1.44}$$

$$\rho\left(u\frac{\partial v}{\partial x}+v\frac{\partial v}{\partial y}\right) = -\frac{\partial \widetilde{p}}{\partial y}+\frac{\partial F_{yx}}{\partial x}+\frac{\partial F_{yy}}{\partial y}. \tag{1.45}$$

From Eq. (1.29) we write

$$\mathbf{LF} = \begin{bmatrix} F_{xx}\frac{\partial u}{\partial x} + F_{yx}\frac{\partial u}{\partial y} & F_{xy}\frac{\partial u}{\partial x} + F_{yy}\frac{\partial u}{\partial y} & 0 \\ F_{xx}\frac{\partial v}{\partial x} + F_{yx}\frac{\partial v}{\partial y} & F_{xy}\frac{\partial v}{\partial x} + F_{yy}\frac{\partial v}{\partial y} & 0 \\ 0 & 0 & 0 \end{bmatrix}, \tag{1.46}$$

$$\mathbf{FL}^{\top} = \begin{bmatrix} F_{xx}\frac{\partial u}{\partial x} + F_{xy}\frac{\partial u}{\partial y} & F_{xx}\frac{\partial v}{\partial x} + F_{xy}\frac{\partial v}{\partial y} & 0 \\ F_{yx}\frac{\partial u}{\partial x} + F_{yy}\frac{\partial u}{\partial y} & F_{xy}\frac{\partial v}{\partial x} + F_{yy}\frac{\partial v}{\partial y} & 0 \\ 0 & 0 & 0 \end{bmatrix}, \tag{1.47}$$

$$(\mathbf{V}\cdot\nabla)\mathbf{F} = \begin{bmatrix} u\frac{\partial F_{xx}}{\partial x} + v\frac{\partial F_{xx}}{\partial y} & u\frac{\partial F_{xy}}{\partial x} + v\frac{\partial F_{xy}}{\partial y} & 0 \\ u\frac{\partial F_{yx}}{\partial x} + v\frac{\partial F_{yx}}{\partial y} & u\frac{\partial F_{yy}}{\partial x} + v\frac{\partial F_{yy}}{\partial y} & 0 \\ 0 & 0 & 0 \end{bmatrix} \tag{1.48}$$

and now Eq. (1.44) yields

$$F_{xx} + \lambda_1\left[u\frac{\partial F_{xx}}{\partial x} + v\frac{\partial F_{xy}}{\partial y} - F_{xx}\frac{\partial u}{\partial x} - F_{xy}\frac{\partial u}{\partial y} - F_{xx}\frac{\partial u}{\partial x} - F_{xy}\frac{\partial u}{\partial y}\right] = 2\mu\frac{\partial u}{\partial x}, \tag{1.49}$$

$$F_{xy} + \lambda_1\left[u\frac{\partial F_{xy}}{\partial x} + v\frac{\partial F_{xy}}{\partial y} - F_{xy}\frac{\partial u}{\partial x} - F_{yy} - F_{xx}\frac{\partial v}{\partial x} - F_{xy}\frac{\partial v}{\partial y}\right] = \mu\left(\frac{\partial u}{\partial y} + \frac{\partial v}{\partial x}\right), \tag{1.50}$$

$$F_{yy} + \lambda_1\left[u\frac{\partial F_{yy}}{\partial x} + v\frac{\partial F_{yy}}{\partial y} - F_{xy}\frac{\partial v}{\partial x} - F_{yy}\frac{\partial v}{\partial y} - F_{yx}\frac{\partial v}{\partial x} - F_{yy}\frac{\partial v}{\partial y}\right] = 2\mu\frac{\partial v}{\partial x}. \tag{1.51}$$

Invoking Eqs (1.36) and (1.37) one can write

$$u\frac{\partial u}{\partial x} + v\frac{\partial u}{\partial y} + \lambda_1\left[u^2\frac{\partial^2 u}{\partial x^2} + v^2\frac{\partial^2 u}{\partial y^2} + 2uv\frac{\partial^2 u}{\partial x\partial y}\right] = -\frac{1}{\rho}\frac{\partial \widetilde{p}}{\partial x} + \nu\frac{\partial^2 u}{\partial y^2}. \tag{1.52}$$

1.5.3 Micropolar fluid

For micropolar fluid, the momentum equation (1.4) along with the law of angular momentum in the absence of body forces and body couple are given by

$$\rho\frac{d\mathbf{V}}{dt} = -\nabla\widetilde{p} + (\mu + k)\,\nabla^2\mathbf{V} + k\nabla\times\mathbf{N}, \tag{1.53}$$

$$\rho j\frac{d\mathbf{N}}{dt} = \gamma_1\nabla\left(\nabla\cdot\mathbf{N}\right) - \gamma_1\nabla\times\left(\nabla\times\mathbf{N}\right) + k\nabla\times\mathbf{V} - 2k\mathbf{N}, \tag{1.54}$$

where V and N are the velocity and micro-rotation vectors, j denotes the gyration parameters of the fluid, γ_1 and k are the spin gradient viscosity and vortex viscosity, respectively. For two-dimensional flow, we take the micro-rotation vector N of the form

$$\mathrm{N} = [0, 0, N_z(x, y)]\,. \tag{1.55}$$

With the help of Eqs. (1.29) and (1.55), the equations (1.53) and (1.54) for steady flow become

$$u\frac{\partial u}{\partial x} + v\frac{\partial u}{\partial y} = -\frac{1}{\rho}\frac{\partial \widetilde{p}}{\partial x} + \left(\frac{\mu + k}{\rho}\right)\left(\frac{\partial^2 u}{\partial x^2} + \frac{\partial^2 u}{\partial y^2}\right) + \frac{k}{\rho}\frac{\partial N_z}{\partial y}, \tag{1.56}$$

$$u\frac{\partial v}{\partial x} + v\frac{\partial v}{\partial y} = -\frac{1}{\rho}\frac{\partial \widetilde{p}}{\partial y} + \left(\frac{\mu + k}{\rho}\right)\left(\frac{\partial^2 v}{\partial x^2} + \frac{\partial^2 v}{\partial y^2}\right) - \frac{k}{\rho}\frac{\partial N_z}{\partial x}, \tag{1.57}$$

$$u\frac{\partial N_z}{\partial x} + v\frac{\partial N_z}{\partial y} = \frac{\gamma_1}{\rho j}\left(\frac{\partial^2 N_z}{\partial x^2} + \frac{\partial^2 N_z}{\partial y^2}\right) + \frac{k}{\rho j}\left(\frac{\partial v}{\partial x} - \frac{\partial v}{\partial y}\right) - \frac{2k}{\rho j}N_z, \tag{1.58}$$

in which the Eq. (1.58) suggests that $O(N_z) \sim O\left(\frac{\partial u}{\partial y}\right) \sim O\left(\frac{\partial v}{\partial x}\right)$.

Using Eqs. (1.36) and (1.37), the Eqs. (1.56) – (1.58) give

$$u\frac{\partial u}{\partial x} + v\frac{\partial u}{\partial y} = -\frac{1}{\rho}\frac{\partial \widetilde{p}}{\partial x} + \left(\nu + \frac{k}{\rho}\right)\frac{\partial^2 u}{\partial y^2} + \frac{k}{\rho}\frac{\partial N}{\partial y}, \tag{1.59}$$

$$u\frac{\partial N_z}{\partial x} + v\frac{\partial N_z}{\partial y} = \frac{\gamma}{\rho j}\frac{\partial^2 N_z}{\partial y^2} - \frac{k}{\rho j}\left(2N_z + \frac{\partial u}{\partial y}\right). \tag{1.60}$$

1.6 Solution methods

1.6.1 Homotopy analysis method

Perturbation methods have been extensively utilized by engineers and scientists in obtaining solutions especially for non-linear problems. Such methods require small (large) parameters so that approximate solutions can be expressed in term of series. It is not necessary that many problems involve such a small parameter. Therefore it is important to have an analytic method which does not require a small (large) parameters. Bearing this in mind, Liao [90 – 98] developed the homotopy analysis method (HAM) which is independent of the small parameter assumption. A few recent investigations in the literature that contain HAM solutions is men-

tioned in the refs. [99 – 124]. In order to describe the basic idea of homotopy analysis method, we consider the following (nonlinear) differential equation

$$\mathcal{N}[w(x)] = 0, \tag{1.61}$$

where $\mathcal{N}$ is the nonlinear operator, w is an unknown dependent function and x denotes the independent variable. For simplicity, we ignore all the boundary or initial conditions which can be treated similarly. We can construct the zero-order deformation equation as

$$(1-p)\,\mathcal{L}[\widehat{w}(x;p) - w_0(x)] = p\hbar\mathcal{N}[\widehat{w}(x;p)], \tag{1.62}$$

where $p \in [0,1]$ is called the embedding parameter, $\hbar$ is the non-zero-auxiliary parameter, $\mathcal{L}$ is the auxiliary linear operator, $w_0(x)$ is the initial approximation which satisfy all the boundary conditions. It is vital that one has freedom to choose the initial approximation and auxiliary linear operator. When $p = 0$ and $p = 1$

$$\widehat{w}(x;0) - w_0(x) = 0 \text{ and } \widehat{w}(x;1) - w(x) = 0 \tag{1.63}$$

respectively. Thus as p increases from 0 to 1, the solution $\widehat{w}(x;p)$ varies from initial approximation $w_0(x)$ to the desired solution $w(x)$. Expanding $\widehat{w}(x;p)$ in the Taylor series with respect to p, one has

$$\widehat{w}(x;p) = w_0(x) + \sum_{m=1}^{\infty} w_m(x)\,p^m, \qquad w_m(x) = \frac{1}{m!}\frac{\partial^m \widehat{w}(x,p)}{\partial p^m}\bigg|_{p=0}. \tag{1.64}$$

The mth order deformation equation is

$$\mathcal{L}[w_m(\eta) - \chi_m w_{m-1}(\eta)] = \hbar\mathcal{R}_m(w_{m-1}), \tag{1.65}$$

where

$$\mathcal{R}_m(w_{m-1}) = \frac{1}{(m-1)!}\frac{\partial^{m-1}\widehat{w}(x,p)}{\partial p^{m-1}}\bigg|_{p=0}, \tag{1.66}$$

$$\chi_m = \begin{cases} 0, & m \leq 1, \\ 1, & m > 1. \end{cases} \tag{1.67}$$

Equation (1.65) can be easily solved by using a symbolic computation software such as MAPLE or MATHEMATICA. If the auxiliary linear operator, the initial approximation and the auxiliary parameter $\hbar$ is properly chosen, the series (1.64) converges at $p = 1$ and one has

$$w(x) = w_0(x) + \sum_{m=1}^{\infty} w_m(x), \tag{1.68}$$

which must be one of the solutions of the original nonlinear Eq. (1.61). There are many different ways to deduce the higher order deformation equations. However, according to the fundamental theorem in calculus [125] the term $w_m(x)$ in the series (1.64) is unique. Note that the HAM contains an auxiliary parameters $\hbar$,which provides us with a simple way to control and adjust the convergence of the series solution (1.68).

Remark: Since Homotopy analysis method (HAM) provides us a great freedom to choose any suitable linear operator and initial guess as mentioned by Liao [90] in his book. In HAM, we have to choose any operator which satisfies all the boundary conditions. Hence, we can choose fourth order and third order linear operators. Why we choose third order operator?. This operator not only satisfies all the prescribed boundary conditions but it also enhances the rate of convergence of the solution when compared to the fourth order linear operator. This is in fact one of the beauty and soundness of the homotopy analysis method. One can choose any linear operator corresponding to the given situation, even in the less number of boundary conditions too. Moreover we are having an auxiliary parameter introduced in the mth order problem, which is used to control and adjust the convergence region for the solution for different values of the parameters. Similarly, we can choose any initial guess via different options available to us. Obviously, our initial guess will be the best if it enhances the rate of convergence.

1.6.2 Homotopy-Padé approximation

The homotopy analysis method is based on such an assumption that the series (1.64) of $\widehat{w}(x;p)$ converges at $p = 1$ for the illustrative problem. Besides, the convergence region and rate of solution series given by the homotopy analysis method depend upon the auxiliary parameter $\hbar$.

Therefore, the auxiliary parameter $\hbar$ provides us with a convenient way to adjust and control the convergence region and rate of solution series.

There exist some techniques to accelerate the convergence of given series. Among them, the so-called Padé technique is widely applied for a given series. For a series of the form

$$\sum_{n=0}^{+\infty} c_n x^n, \tag{1.69}$$

the Padé approximant $[m, n]$ is

$$\frac{\sum_{k=0}^{m} a_{m,k} x^k}{\sum_{k=0}^{n} b_{m,k} x^k}, \tag{1.70}$$

where $a_{m,k}$ and $b_{m,k}$ can be found by the coefficients c_i $(i = 0, 1, 2, 3, ...m + n)$. In many cases the traditional Padé technique can greatly increase the convergence region and rate of a given series.

Note that the homotopy-Padé technique [126] was proposed by combining the traditional Padé technique and homotopy analysis method. In order to ensure the convergence of the series (1.64) at $p = 1$, we first use the traditional $[m, n]$ Padé technique in an embedding parameter p to get $[m, n]$ Padé approximant in the form

$$\frac{\sum_{k=0}^{m} A_{m,k}(x) p^k}{\sum_{k=0}^{n} B_{m,k}(x) p^k}, \tag{1.71}$$

in which the first several approximations $w_0(x)$, $w_1(x)$, . ..$w_{m+n}(x)$ help us in finding the coefficients $A_{m,k}(x)$ and $B_{m,k}(x)$. Putting $p = 1$ in Eq. (1.71) one obtains

$$\frac{\sum_{k=0}^{m} A_{m,k}(x)}{\sum_{k=0}^{n} B_{m,k}(x)}. \tag{1.72}$$

Generally, the $[m,m]$ homotopy-Padé approximation is

$$\frac{\sum_{k=0}^{m^2+m+1} A_1^{m,k}(x)}{\sum_{k=0}^{m^2+m+1} B_1^{m,k}(x)}, \tag{1.73}$$

where $A_1^{m,k}(r)$ and $B_1^{m,k}(r)$ are the coefficients. It is very interesting that these coefficients are independent of the auxiliary parameter $\hbar$. We find through the comparison of Eqs. (1.70) and (1.73) that in accuracy the $[m,m]$ homotopy-Padé approximation is equivalent to the traditional $[m^2+m+1, m^2+m+1]$ Padé approximant. In a similar manner, the so-called homotopy-Padé techn.ique can be utilized in accelerating the convergence of the related series.

1.6.3 Numerical Scheme: Finite Difference Method

In order to find the numerical solution of nonlinear differential equations, the continuous variables are replaced by the discrete variables. This is accomplished by replacing derivative in the equations by finite difference relations. Here, we replace the time derivatives by its forward difference and the space derivative is replaced by central difference approximation. The result is a system of algebraic equations which can easily be solved by the Gaussian elimination method.

Let us consider the x-axis and t in finite intervals at a distance Δx and Δt apart. Let u be a function of coordinates x and t and the subscripts i and j represents $x-$coordinate and time. Thus $u(x,t)$ can be represented by $u(i\Delta x, j\Delta t) = u_{i,j}$. The finite difference approximations to derivatives can be obtained from Taylor's series expansions. For example, the Taylor's series expansion of $u_{i,j}$ about the grid points (i,j) gives

$$u_{i+1,j} = u_{i,j} + \left(\frac{\partial u}{\partial x}\right)_{i,j} \Delta x + \left(\frac{\partial^2 u}{\partial x^2}\right)_{i,j} \frac{(\Delta x)^2}{2} + \ldots \tag{1.74}$$

$$u_{i-1,j} = u_{i,j} - \left(\frac{\partial u}{\partial x}\right)_{i,j} \Delta x + \left(\frac{\partial^2 u}{\partial x^2}\right)_{i,j} \frac{(\Delta x)^2}{2} - \ldots. \tag{1.75}$$

Subtracting Eq. (1.75) from Eq. (1.74) and then rearranging we obtain

$$\left(\frac{\partial u}{\partial x}\right)_{i,j} = \frac{u_{i+1,j} - u_{i-1,j}}{2\Delta x} - \left(\frac{\partial^3 u}{\partial x^3}\right)_{i,j} \frac{(\Delta x)^2}{6} + \ldots$$

or

$$\left(\frac{\partial u}{\partial x}\right)_{i,j} \simeq \frac{u_{i+1,j} - u_{i-1,j}}{2\Delta x}. \tag{1.76}$$

Since the first term truncated involves Δx^2, the truncation error is second order. Similarly, the second and third-order derivatives are

$$\left(\frac{\partial^2 u}{\partial x^2}\right)_{i,j} \simeq \frac{u_{i+1,j} - 2u_{i,j} + u_{i-1,j}}{\Delta x^2} \tag{1.77}$$

$$\left(\frac{\partial^3 u}{\partial x^3}\right)_{i,j} \simeq \frac{u_{i+2,j} - 2u_{i+1,j} + 2u_{i-1,j} - u_{i-2,j}}{2\Delta x^3}, \tag{1.78}$$

which are again correct to second-order. Similar expansions can be written for t derivatives

$$\left(\frac{\partial u}{\partial t}\right)_{i,j} \simeq \frac{u_{i,j+1} - u_{i,j}}{\Delta t} + O(\Delta t).$$

Chapter 2

MHD flow of a second grade fluid over an oscillatory stretching surface

This chapter looks at the unsteady magnetohydrodynamic (MHD) two-dimensional boundary layer flow of a second grade fluid caused by an oscillatory stretching surface. An infinite elastic sheet is stretched back and forth in its own plane. The resulting equations from conservation laws of mass and momentum are reduced to a non-linear partial differential equation by invoking similarity transformations. Both analytic and numerical solutions of the governing partial differential equation are developed. Analytic solution of the nonlinear problem is derived by a newly developed analytic technique, namely homotopy analysis method (HAM). Numerical solution is presented by using the finite difference scheme, in which a coordinate transformation is employed to transform the semi-infinite physical space to a bounded computational domain. The results obtained by means of both methods are then compared and show an excellent agreement. The effects of various parameters like viscoelastic parameter, the Hartman number and the relative frequency amplitude of the oscillatory sheet to the stretching rate on the velocity field are plotted and analyzed. The values of wall shear stress for these parameters are also tabulated and discussed.

2.1 Flow analysis

Let us consider the unsteady MHD two-dimensional laminar flow of an incompressible second grade fluid over an oscillatory stretching sheet coinciding with the plane $\overline{y} = 0$, the flow being confined to the semi-infinite space $\overline{y} > 0$. The elastic sheet is stretched back and forth periodically with velocity $u_w = c\overline{x}\sin\omega t$ (c is the maximum stretching rate, $\overline{x}$ is the coordinate along the sheet and ω is the frequency) parallel to the $\overline{x}$-axis, as shown in Fig. 2.1. A constant magnetic field of strength B_0 is applied perpendicular to the stretching surface. The induced magnetic field is neglected under the assumption of small magnetic Reynolds number. Invoking boundary layer assumptions and in the absence of pressure gradient, the unsteady basic boundary layer equations governing the MHD flow of second grade fluid are:

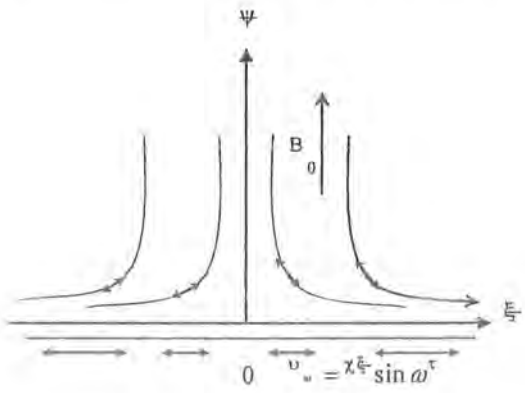

Fig. 2.1. Geometry of the problem and coordinate system

$$\frac{\partial u}{\partial \overline{x}} + \frac{\partial v}{\partial \overline{y}} = 0, \tag{2.1}$$

$$\frac{\partial u}{\partial t} + u\frac{\partial u}{\partial \overline{x}} + v\frac{\partial u}{\partial \overline{y}} = \nu\frac{\partial^2 u}{\partial \overline{y}^2} + \frac{\alpha_1}{\rho}\left[\frac{\partial^3 u}{\partial t \partial \overline{y}^2} + \frac{\partial}{\partial \overline{x}}\left(u\frac{\partial^2 u}{\partial \overline{y}^2}\right) + \frac{\partial u}{\partial \overline{y}}\frac{\partial^2 v}{\partial \overline{y}^2} + v\frac{\partial^3 u}{\partial \overline{y}^3}\right] - \frac{\sigma B_0^2}{\rho}u. \tag{2.2}$$

In the above equations (u, v) are the velocity components in $(\overline{x}, \overline{y})$ directions respectively, ν is the kinematic viscosity of fluid, ρ is the fluid density, σ is the electrical conductivity of the fluid and α_1 is the viscoelastic parameter of the fluid.

The subjected boundary conditions are

$$u = u_w = c\overline{x}\sin\omega t, \quad v = 0 \quad \text{at} \quad \overline{y} = 0, \quad t > 0, \tag{2.3}$$

$$u(\overline{y}, 0) = 0 \quad \text{at} \quad t \leq 0, \quad u = 0, \quad \frac{\partial u}{\partial \overline{y}} = 0 \quad \text{as} \quad \overline{y} \to \infty, \tag{2.4}$$

in which both c and ω have the dimension $(\text{time})^{-1}$. Note that the system can also be solved by using the cosine function $(\cos\omega t)$ instead of $\sin\omega t$. The second condition in (2.4) is the augmented condition since the flow is in an unbounded domain, which has been discussed by Garg and Rajagopal [127].

We write

$$S \equiv \frac{\omega}{c} \tag{2.5}$$

which denotes the ratio of the oscillation frequency of the sheet to its stretching rate.

Any particle path on the sheet is

$$\overline{x} = \overline{x}_0 \exp\left(\frac{1}{S}\cos\omega t\right). \tag{2.6}$$

The boundary conditions (2.3) and (2.4) suggest the following similarity transformations

$$y = \sqrt{\frac{c}{\nu}}\overline{y}, \quad \tau = t\omega, \quad u = c\overline{x}f_y(y,\tau), \quad v = -\sqrt{\nu c}f(y,\tau). \tag{2.7}$$

Using above transformations, the continuity equation (2.1) is identically satisfied and the governing equation (2.2) becomes

$$Sf_{y\tau} + f_y^2 - ff_{yy} + M^2 f_y = f_{yyy} + K\left(Sf_{yyy\tau} + 2f_y f_{yyy} - f_{yy}^2 - ff_{yyyy}\right). \tag{2.8}$$

The boundary conditions (2.3) and (2.4) are

$$f_y(0,\tau) = \sin\tau, \quad f(0,\tau) = 0, \quad f_y(\infty,\tau) = 0 \quad \text{and} \quad f_{yy}(\infty,\tau) = 0, \tag{2.9}$$

in which $M^2 = \sigma B_0^2/c\rho$ is the Hartman number or the magnetic parameter and $K = c\alpha_1/\nu\rho$ is the non-dimensional viscoelastic parameter. Here $K = 0$ corresponds to the case of a viscous fluid.

A physical quantity of interest is the skin-friction coefficient C_f, which is defined as

$$C_f = \frac{\tau_w}{\rho u_w^2}, \tag{2.10}$$

where τ_w is wall skin friction given by

$$\tau_w = \mu \left(\frac{\partial u}{\partial \overline{y}} \right)_{\overline{y}=0} + k_0 \left(\frac{\partial^2 u}{\partial t \partial \overline{y}} + u \frac{\partial^2 u}{\partial \overline{x} \partial \overline{y}} + v \frac{\partial^2 u}{\partial \overline{y}^2} - 2 \frac{\partial u}{\partial \overline{y}} \frac{\partial v}{\partial \overline{y}} \right)_{\overline{y}=0}. \tag{2.11}$$

Using the variables (2.7), we get

$$\mathrm{Re}_x^{1/2} C_f = \left[f_{yy} + K \left(3 f_y f_{yy} + S f_{yy\tau} - f f_{yyy} \right) \right]_{y=0}, \tag{2.12}$$

where $\mathrm{Re}_x = u_w \overline{x} / \nu$ is the local Reynolds number.

2.2 Homotopy analysis method

Liao [90] proposed a new approximate analytical solution technique, called the Homotopy analysis method (HAM), especially for non-linear problems, which can overcome the foregoing restrictions of perturbation techniques. Different from perturbation methods, the validity of the HAM is independent on whether there exist small/large parameters in considered non-linear problems.

2.2.1 Homotopy analytic solution

In this part, we solve Eqs. (2.8) and (2.9) by means of homotopy analysis method (HAM). According to the boundary conditions (2.9) the velocity distribution $f(y, \tau)$ can be expressed by the set of base functions

$$\left\{ y^k \sin(j\tau) \exp(-ny) \,\middle|\, k \geq 0, j \geq 0, n \geq 0 \right\}$$

in the following form

$$f(y, \tau) = a_{0,0}^0 + \sum_{n=0}^{\infty} \sum_{k=0}^{\infty} \sum_{j=0}^{\infty} a_{n,k}^j y^k \sin(j\tau) \exp(-ny), \tag{2.13}$$

in which $a_{n,k}^{j}$ are the coefficients. These provide us with the so-called *rule of solution expressions* (see Liao [90]). With the help of these solution expressions and Eq. (2.9), it is straightforward to choose the initial approximations $f_0(y,\tau)$ for $f(y,\tau)$ as

$$f_0(y,\tau) = \sin\tau\,(1-\exp(-y)), \tag{2.14}$$

and the linear operator

$$\mathcal{L}_f(f) = \frac{\partial^3 f}{\partial y^3} - \frac{\partial f}{\partial y}, \tag{2.15}$$

satisfying the following properties

$$\mathcal{L}_f\left[C_1 + C_2\exp(-y) + C_3\exp(y)\right] = 0, \tag{2.16}$$

where C_i $(i=1,2,3)$ are arbitrary constants.

Let $p \in [0,1]$ denotes an embedding parameter and $\hbar_f$ is a non-zero auxiliary parameter. We construct the zeroth-order deformation problem as

$$(1-p)\,\mathcal{L}_f\left[\widehat{f}(y,\tau;p) - f_0(y,\tau)\right] = p\hbar_f\mathcal{N}_f\left[\widehat{f}(y,\tau;p)\right], \tag{2.17}$$

$$\begin{aligned}
\widehat{f}(0,\tau;p) &= 0, & \left.\frac{\partial\widehat{f}(y,\tau;p)}{\partial y}\right|_{y=0} &= \sin\tau,\\
\left.\frac{\partial\widehat{f}(y,\tau;p)}{\partial y}\right|_{y=\infty} &= 0, & \left.\frac{\partial^2\widehat{f}(y,\tau;p)}{\partial y^2}\right|_{y=\infty} &= 0,
\end{aligned} \tag{2.18}$$

where the non-linear operator $\mathcal{N}_f$ is defined by

$$\begin{aligned}
\mathcal{N}_f\left[\widehat{f}(y,\tau;p)\right] &= \frac{\partial^3\widehat{f}(y,\tau;p)}{\partial y^3} - S\frac{\partial^2\widehat{f}(y,\tau;p)}{\partial y\partial\tau} + \widehat{f}(y,\tau;p)\frac{\partial^2\widehat{f}(y,\tau;p)}{\partial y^2} - \left(\frac{\partial\widehat{f}(y,\tau;p)}{\partial y}\right)^2\\
&\quad -M^2\frac{\partial\widehat{f}(y,\tau;p)}{\partial y} + K\left\{\begin{array}{c} S\frac{\partial^4\widehat{f}(y,\tau;p)}{\partial^3 y\partial\tau} + 2\frac{\partial\widehat{f}(y,\tau;p)}{\partial y}\frac{\partial^3\widehat{f}(y,\tau;p)}{\partial y^3}\\ -\left(\frac{\partial^2\widehat{f}(y,\tau;p)}{\partial y^2}\right)^2 - \widehat{f}(y,\tau;p)\frac{\partial^4\widehat{f}(y,\tau;p)}{\partial y^4}\end{array}\right\}.
\end{aligned} \tag{2.19}$$

When $p=0$ and $p=1$, the above zeroth-order deformation problem has the following solutions,

respectively

$$\widehat{f}(y,\tau;0) = f_0(y,\tau) \qquad \text{and} \qquad \widehat{f}(y,\tau;1) = f(y,\tau). \tag{2.20}$$

Thus, as p increases from 0 to 1, $\widehat{f}(y,\tau;p)$ varies from $f_0(y,\tau)$ to the solution $f(y,\tau)$ of the original equation (2.8). By Taylor's theorem and the relations (2.20), one can write

$$\widehat{f}(y,\tau;p) = f_0(y,\tau) + \sum_{m=1}^{\infty} f_m(y,\tau)\, p^m, \tag{2.21}$$

$$f_m(y,\tau) = \frac{1}{m!} \frac{\partial^m \widehat{f}(y,\tau;p)}{\partial p^m}\bigg|_{p=0}. \tag{2.22}$$

Substituting the expansion (2.21) into the differential equation (2.17) and the corresponding boundary conditions (2.18), and equating coefficient of equal powers of p lead to the boundary-value problems for $f_m(y,\tau)$ $(m = 0,1,2.....)$. Note that Eq. (2.17)) contains the auxiliary parameter $\hbar_f$. The convergence of the series given in Eq. (2.21) strongly depends upon this parameter $\hbar_f$. Therefore $\hbar_f$ should be properly chosen so that the above series (2.21) is convergent at $p = 1$. Hence, using Eq. (2.20), we have the solution series

$$f(y,\tau) = f_0(y,\tau) + \sum_{m=1}^{\infty} f_m(y,\tau). \tag{2.23}$$

We differentiate the zeroth-order equation m times with respect to embedding parameter p, then setting $p = 0$, and finally dividing by $m!$, we have the following mth-order deformation equation $(m \geq 1)$

$$\mathcal{L}_f\left[f_m(y,\tau) - \chi_m f_{m-1}(y,\tau)\right] = \hbar_f \mathcal{R}_m^f(y,\tau), \tag{2.24}$$

with boundary equations

$$f_m(0,\tau;p) = 0, \qquad \frac{\partial f_m(y,\tau;0)}{\partial y}\bigg|_{y=0} = \frac{\partial f_m(y,\tau;0)}{\partial y}\bigg|_{y=\infty} = \frac{\partial^2 f_m(y,\tau;0)}{\partial y^2}\bigg|_{y=\infty} = 0, \tag{2.25}$$

where

$$\mathcal{R}_m^f(y,\tau) = \frac{\partial^3 f_{m-1}}{\partial y^3} - S\frac{\partial^2 f_{m-1}}{\partial y \partial \tau} - M^2\frac{\partial f_{m-1}}{\partial y} + \sum_{k=0}^{m-1}\left(f_{m-1-k}\frac{\partial^2 f_j}{\partial y^2} - \frac{\partial f_{m-1-k}}{\partial y}\frac{\partial f_j}{\partial y}\right) \quad (2.26)$$
$$+KS\frac{\partial^4 f_{m-1}}{\partial y^3 \partial \tau} + K\sum_{k=0}^{m-1}\left[2\frac{\partial f_{m-1-k}}{\partial y}\frac{\partial^3 f_j}{\partial y^3} - \frac{\partial^2 f_{m-1-k}}{\partial y^2}\frac{\partial^2 f_j}{\partial y^2} - f_{m-1-k}\frac{\partial^4 f_j}{\partial y^4}\right],$$

and

$$\chi_m = \begin{cases} 0, & m \leq 1, \\ 1, & m > 1. \end{cases} \quad (2.27)$$

Note that, we obtain a linear non-homogeneous system equation in the form of high-order deformation equation, which is easy to solve using MATHEMATICA or other softwares. The general solution of Eq. (2.24) with $f_m^\star(y,\tau)$ denoting the special solution can be written as

$$f_m(y,\xi) = f_m^\star(y,\xi) + C_1 + C_2\exp(-y) + C_3\exp(y), \quad (2.28)$$

where the integral constants C_1, C_2 and C_3 are determined by the boundary conditions (2.18) and given by

$$C_2 = \left.\frac{\partial f_m^\star(y,\xi)}{\partial y}\right|_{y=0}, \quad C_1 = -C_2 - f_m^\star(0,\xi), \quad C_3 = 0. \quad (2.29)$$

2.2.2 Convergence of the HAM solution

Liao [90] proved that, as long as a solution series given by the homotopy analysis method converges, it must be one of the solutions. Therefore, it is important to ensure that the solution series are convergent. The solution series (2.23) contains the non-zero auxiliary parameter $\hbar_f$, which can be chosen properly by plotting the so-called $\hbar$-curves to ensure the convergence of the solution series and rate of approximation of the HAM solution, as proposed by Liao [90]. To find the admissible values of $\hbar_f$, $\hbar$-curves of $f''(0,0)$ are shown in Fig. (2.2) for 15th-order of approximation for two groups of different parameters values: $S = 0.2$, $M = 1$, $K = 0.3$ and $S = 0.5$, $M = 2$, $K = 0.5$, respectively. From this Fig., it can be seen that $\hbar$-curve has a parallel line segment that corresponds to a region $-1.2 \leq \hbar_f \leq -0.2$ for $S = 0.2$, $M = 1$, $K = 0.3$ and $-0.45 \leq \hbar_f \leq -0.1$ for $S = 0.5$, $M = 2$, $K = 0.5$, respectively. To ensure the convergence of the HAM solution, the values of the $\hbar_f$ should be chosen from these regions. The region for

the values of $\hbar_f$ is dependent on the values of involving parameters. We can see that for the different values of the parameters, we get different $\hbar$-curves (for the admissible values of $\hbar_f$). It is evident from our calculations that the solution series (2.23) converges in the whole region of y if it is convergent at $y = 0$ when the proper values of $\hbar_f$ is chosen. Table 2.1 shows the convergence of the HAM solutions $f''(0,\tau)$ for several different times ($\tau = 0, 0.5\pi, 0.75\pi, 1.5\pi$) at different orders of approximation when $S = 0.3$, $M = 1.2$ and $K = 0.2$. For different times τ different $\hbar$-values are chosen from the admissible ranges of the corresponding $\hbar$-curves. It is shown that with the increase of the order of approximation a convergent solution can be reached.

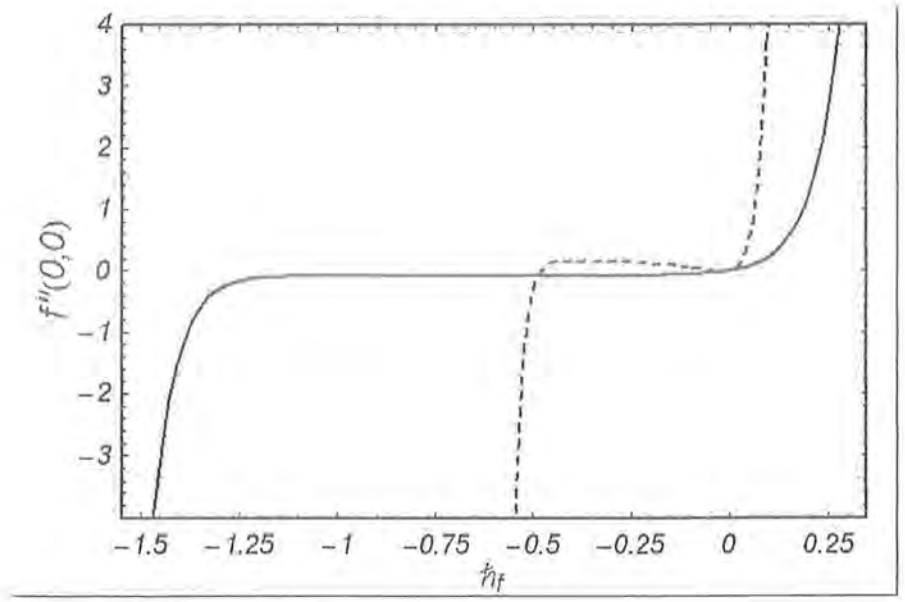

Fig. 2.2. The $\hbar$-curve of $f''(0,0)$ at the 15th-order of approximation: Solid line with $S = 0.2$, $M = 1$ and $K = 0.3$ and Dashed line with $S = 0.5$, $M = 2$ and $K = 0.5$.

Order of approximations	$\tau = 0$ $\hbar_f = -0.7$	$\tau = 0.5\pi$ $\hbar_f = -0.5$	$\tau = 0.75\pi$ $\hbar_f = -0.4$	$\tau = 1.5\pi$ $\hbar_f = -0.45$
1	−0.08400	−1.31005	−0.82134	0.91913
3	−0.09735	−1.41491	−0.91400	0.83429
5	−0.10051	−1.42701	−0.93798	0.80239
10	−0.10197	−1.42876	−0.94599	0.78789
12	−0.10205	−1.42878	−0.94620	0.78716
15	−0.10209	−1.42878	−0.94627	0.78683
18	−0.10209	−1.42878	−0.94628	0.78679
20	−0.10209	−1.42878	−0.94628	0.78679
30	−0.10209	−1.42878	−0.94628	0.78679

Table 2.1. The convergence of the HAM solution of $f''(0,\tau)$ for different order of approximations with $S = 0.3$, $K = 0.2$, $M = 1.2$ and $\tau = 0, 0.5\pi, 0.75\pi$ and 1.5π, respectively.

2.3 Numerical method

The non-linear boundary-value problem consisting of Eqs. (2.8) and (2.9) is also solved by means of the finite difference method. For this purpose, the coordinate transformation $\eta = 1/(y+1)$ is applied for transforming the semi-infinite physical domain $y \in [0, \infty]$ to a finite calculation domain $\eta \in [0, 1]$, i.e.,

$$y = \frac{1}{\eta} - 1, \qquad \frac{\partial}{\partial y} = -\eta^2 \frac{\partial}{\partial \eta}, \qquad \frac{\partial^2}{\partial y^2} = \eta^4 \frac{\partial^2}{\partial \eta^2} + 2\eta^3 \frac{\partial}{\partial \eta}, \qquad \frac{\partial^2}{\partial y \partial \tau} = -\eta^2 \frac{\partial^2}{\partial \eta \partial \tau},$$

$$\frac{\partial^3}{\partial y^3} = -\eta^6 \frac{\partial^3}{\partial \eta^3} - 6\eta^5 \frac{\partial^2}{\partial \eta^2} - 6\eta^4 \frac{\partial}{\partial \eta}, \qquad \frac{\partial^4}{\partial y^3 \partial \tau} = -\eta^6 \frac{\partial^4}{\partial \eta^3 \partial \tau} - 6\eta^5 \frac{\partial^3}{\partial \eta^2 \partial \tau} - 6\eta^4 \frac{\partial^2}{\partial \eta \partial \tau},$$

$$\frac{\partial^4}{\partial y^4} = \eta^8 \frac{\partial^4}{\partial \eta^4} + 12\eta^7 \frac{\partial^3}{\partial \eta^3} + 35\eta^6 \frac{\partial^2}{\partial \eta^2} + 24\eta^5 \frac{\partial}{\partial \eta}.$$

With these transformations, the differential equation (2.8) in terms of η can be rewritten in the forms

$$\begin{aligned} & S\left(1-6K\eta^2\right)\frac{\partial^2 f}{\partial\tau\partial\eta}-SK\eta^4\frac{\partial^4 f}{\partial\eta^3\partial\tau}-6SK\eta^3\frac{\partial^3 f}{\partial\eta^2\partial\tau} \\ = & \left(\eta^2-8K\eta^4\right)\left(\frac{\partial f}{\partial\eta}\right)^2+\left(6\eta^2-M^2+36Kf\eta^4-2f\eta\right)\frac{\partial f}{\partial\eta}+\eta^4\frac{\partial^3 f}{\partial\eta^3}, \\ & +\left(6\eta^3-f\eta^2+36Kf\eta^4\right)\frac{\partial^2 f}{\partial\eta^2}-8K\eta^5\frac{\partial f}{\partial\eta}\frac{\partial^2 f}{\partial\eta^2}+K\eta^6\left(\frac{\partial^2 f}{\partial\eta^2}\right)^2, \\ & -2K\eta^6\frac{\partial f}{\partial\eta}\frac{\partial^3 f}{\partial\eta^3}+12K\eta^5 f\frac{\partial^3 f}{\partial\eta^3}+K\eta^6 f\frac{\partial^4 f}{\partial\eta^4}. \end{aligned} \tag{2.30}$$

The boundary conditions (2.9) in terms of η can be rewritten as

$$f_\eta=0, \qquad f_{\eta\eta}=0 \qquad \text{at} \qquad \eta=0, \tag{2.31}$$

$$f=0, \quad f_\eta=-\sin\tau, \qquad \text{at} \quad \eta=1. \tag{2.32}$$

Because the equation (2.30) is a differential equation, we can discretise it for L uniformly distributed discrete points in $\eta=\left(\eta_1,\eta_2,\eta_3.....\eta_{\{L\}}\right)\in(0,1)$ with a space grid size of $\Delta\eta=1/(L+1)$ and the time levels $t=\left(t^1,t^2,.....\right)$. Hence the discrete values $(f_1^n,f_2^n,.....f_L^n)$ at these grid points for the time step $t^n=n\Delta t$ (Δt is the time step size) can be numerically solved together with the boundary conditions at $\eta=\eta_0=0$ and $\eta=\eta_{\{L+1\}}=1$, (2.31) and (2.32), as the initial conditions are given. We start our simulations from a motionless velocity field as

$$f\left(\eta,\tau=0\right)=0.$$

We will see that a periodic motion will be immediately reached within the first period. We construct a semi-implicit time difference for f and assure that only linear equations for the new time step $(n+1)$ need to be solved

$$
\begin{aligned}
& S\left(1-6K\eta^2\right)\frac{1}{\Delta t}\left(\frac{\partial f^{(n+1)}}{\partial \eta}-\frac{\partial f^{(n)}}{\partial \eta}\right)-SK\eta^4\frac{1}{\Delta t}\left(\frac{\partial^3 f^{(n+1)}}{\partial \eta^3}-\frac{\partial^3 f^{(n)}}{\partial \eta^3}\right) \\
& -6SK\eta^3\frac{1}{\Delta t}\left(\frac{\partial^2 f^{(n+1)}}{\partial \eta^2}-\frac{\partial^2 f^{(n)}}{\partial \eta^2}\right) \\
= \; & \left(\eta^2-8K\eta^4\right)\left(\frac{\partial f^{(n)}}{\partial \eta}\right)^2+\left(6\eta^2-M^2\right)\frac{\partial f^{(n+1)}}{\partial \eta}+\left(36K\eta^4-2\eta\right)f^{(n)}\frac{\partial f^{(n)}}{\partial \eta}+6\eta^3\frac{\partial^2 f^{(n+1)}}{\partial \eta^2} \\
& +\left(36K\eta^4-\eta^2\right)f^{(n)}\frac{\partial^2 f^{(n)}}{\partial \eta^2}-8K\eta^5\frac{\partial f^{(n)}}{\partial \eta}\frac{\partial^2 f^{(n)}}{\partial \eta^2}+K\eta^6\left(\frac{\partial^2 f^{(n)}}{\partial \eta^2}\right)^2+\eta^4\frac{\partial^3 f^{(n+1)}}{\partial \eta^3}, \\
& -2K\eta^6\frac{\partial f^{(n)}}{\partial \eta}\frac{\partial^3 f^{(n)}}{\partial \eta^3}+12K\eta^5 f^{(n)}\frac{\partial^3 f^{(n)}}{\partial \eta^3}+K\eta^6 f^{(n)}\frac{\partial^4 f^{(n)}}{\partial \eta^4}. \qquad (2.33)
\end{aligned}
$$

It should be noted that other different time differences are also possible. By means of the finite-difference method we can obtain a linear equation system for each time step, which can be solved e.g. by Gaussian elimination.

2.4 Results and discussion

We compute the velocity field by solving Eq. (2.8) with the boundary conditions (2.9) both analytically and numerically. To obtain the analytic series solutions we have used the new analytic technique, namely, the homotopy analysis method (HAM). For the numerical solution, first we solve the initial boundary-value problem in the computational space $\eta \in [0, 1]$ and then the numerical solutions are transformed to the physical space with y-coordinate $y \in [0, \infty)$. The velocity field f' $(= f_y)$ is plotted to observe the influence of the various involving parameters, for example, the viscoelastic parameter K, the Hartman number or magnetic parameter M and the non-dimensional relative amplitude of frequency to the stretching rate S for the time series of the first five periods $\tau \in [0, 10\pi]$ and the transverse profiles. Furthermore, we calculate and show the values of the skin-friction coefficient $\mathrm{Re}_x^{1/2} C_f$ both graphically and in tabular form.

For the HAM solution, the higher the order of approximation is, the more accurate is the HAM solution. If the HAM solution does nearly not change any longer with the increase of the order of approximation, the HAM solution can be considered as the exact solution. For the problem investigated it is the case with the 20th-order of approximation (see Table 2.1). We

can also obtain the accuracy/error of the HAM solution by comparing the HAM solution with the convergent numerical solution as displayed in Figs. 2.3 and 2.4.

Figs. 2.3-2.5 are depicted just to compare the homotopy analysis solution and the numerical solution with fixed $S = 1$, $M = 5$, $K = 0.1$ and two different times $\tau = 0.5\pi$ and $\tau = 1.5\pi$. Figs. 2.3 and 2.4 show the comparison between the HAM solutions with the 5th and 25th-order of approximation and the numerical solution, respectively. The results show that the HAM solution with the 5th-order of approximation is obviously deviated from the numerical solution, as displayed in Fig. 2.3. As the order of approximation of the HAM solution is increased, the excellent agreement of HAM solution to the numerical solution for both at $\tau = 0.5\pi$ and $\tau = 1.5\pi$ is demonstrated, as we can see from Fig. 2.4 by comparing the HAM solution with the 25th-order approximation with the numerical solution. Fig. 2.5 gives the comparison of the velocity field f' of the HAM solution with three different orders of approximation at $\tau = 0.5\pi$ and $\tau = 1.5\pi$. It is also observed that the analytic solution obtained by the homotopy analysis method has good agreement for higher order of approximation, for example, with 15th and 25th-orders of approximation, whilst the HAM solution with the 5th-order of approximation has a visible deviation from the higher-order solutions. Obviously, the higher order of approximation the HAM solution has, the closer to the exact solution is the analytic solution.

In the following discussions we will present only numerical solutions. Fig. 2.6 shows the time series of the velocity field f' at the four different distances from the oscillatory sheet for the first five periods $\tau \in [0, 10\pi]$ with fixed values of $S = 2$, $M = 10$ and $K = 0.1$, 0.4, respectively. It can be seen from Fig. 2.6(a) ($K = 0.1$) that the amplitude of the flow near the oscillatory surface is larger as compared to that far away from the surface. As the distance increases from the surface, the amplitude of the flow motion is decreased and almost vanishes (approached to zero) for larger distance from the sheet. From Fig. 2.6(b), we observe the similar phenomenon for the value of $K = 0.4$. However, for $K = 0.4$ the amplitude of the flow motion is larger as compared with the analysis at $K = 0.1$. That indicates as increased effective viscosity with the increase of the non-Newtonian parameter K.

Fig. 2.7 illustrates the effects of the non-dimensional relative amplitude of frequency to the stretching rate S, the viscoelastic parameter K and the magnetic parameter M on the time series of the velocity field f' at a fixed distance $y = 0.25$ from the surface, respectively. Fig.

2.7(a) shows that with the increase of S the amplitude of the flow increases slightly and a phase shift occurs which increases with the increase of S. The influence of the viscoelastic parameter K on the time series of the velocity f' can be seen from Fig. 2.7(b) with fixed values of $S = 2$ and $M = 10$. We see that the amplitude of the flow motion is increased by increasing the viscoelastic parameter K due to the increased effective viscosity. Similarly to the effects of S, a phase difference occurs for different values of K. Fig. 2.7(c) shows the time series of the velocity profile f' for the different values of the magnetic parameter M with fixed values of $S = 1$ and $K = 0.2$. As expected, the amplitude of the flow decreases with the increase of the magnetic parameter M. This is because for the investigated problem the magnetic force acts as a resistance to the flow. Only slight phase difference occurs among the time series for different values of M in comparison with those for different values of S and K.

Fig. 2.8 gives the effects of the viscoelastic parameter K on the transverse profiles of the velocity f' for the different times of $\tau = 8.5\pi, 9\pi, 9.5\pi$ and 10π in the fifth period $\tau \in [8\pi, 10\pi]$ for which a periodic motion has been reached. Fig. 2.8(a) shows that at $\tau = 8.5\pi$, $f' = 1$ at the surface $y = 0$ equating the sheet velocity and $f' \to 0$ far away from the sheet. It can also be seen that at this point of time, there is no oscillation in the velocity profile and the velocity field f' is increased as the values of K increases, i.e. the boundary layer becomes thick with the increase of K. Fig. 2.8(b) gives the velocity profile f' at time point $\tau = 9\pi$. At this time point the velocity field f' is zero at the surface $y = 0$ and far away from the wall it again approaches to zero. It is also evident that near the wall, there exist some oscillation in the velocity profile and the amplitude of the flow increases as K increases. This oscillation in the transverse profile is an evidence of a phase shift in the viscoelastic fluid ($K \neq 0$) against the viscous fluid ($K = 0$). The velocity profiles for others two time points within the fifth period are displayed in Figs. 2.8c-d. For the viscous fluid, the flow in the whole domain is almost in phase with the sheet oscillation, as shown from the solid lines displayed in Figs. 2.8a-d (for $K = 0$). The boundary layer thickness increases by increasing the viscoelastic parameter K, as we can see from Fig. 2.8.

Fig. 2.9 illustrates the influence of the magnetic parameter M on the transverse profiles of the velocity field f' for the different times of $\tau = 8.5\pi, 9\pi, 9.5\pi$ and 10π. It can be seen that the influence of the magnetic field reduces the boundary layer thickness. As expected, the magnetic

force is a resistance to the flow, hence reduces the velocity magnitude. Similar effects have also been shown in previous papers of MHD flows, e.g. [46 – 49]. Although for $\tau = 9\pi$ (Fig. 2.9b) and $\tau = 10\pi$ (Fig. 2.9d), there exist still velocity oscillations in the transverse profiles, their amplitudes are fairly small (in comparison with those in Fig. 2.8 (b,d)). It means that for different values of M, the phase difference is almost invisible, which is in the agreement to the results shown in Fig. 2.7(c).

Fig. 2.10 shows the effects of the non-dimensional relative amplitude of frequency to the stretching rate S on the velocity f' for the different times of $\tau \in [8.5\pi, 9\pi, 9.5\pi, 10\pi]$ in the fifth period. Fig. 2.10(a) is plotted for the variations of S on the velocity f' at time $\tau = 8.5\pi$ at the surface. It is noted that the velocity is equal to the sheet velocity $f' = 1$ at the surface $y = 0$ and far away from the wall it is zero. The velocity f' increases only slightly with the increase of S. Fig. 2.10(b) shows the influence of S on the velocity f' at time $\tau = 9\pi$. It can be seen that for very small values of $S = 0.1$ at this time point, the velocity in the whole transverse section takes its value at the plate almost to zero ($f' \to 0$), i.e., for small values of S no phase difference occurs with the increase of the distance from the plate and the flow in the whole flow domain is in phase with the sheet motion. However, with the increase of S, a phase difference occurs and increases, as shown also in Fig. 2.7(a). The velocity profiles for others two time points within the fifth period are plotted in Figs. 2.10c-d and the similar observations are found as in Figs. 2.10a-b, respectively.

Fig. 2.11 gives the variations of the viscoelastic parameter K, the relative amplitude of frequency to the stretching rate and the magnetic parameter M on the skin friction coefficient $\mathrm{Re}_x^{1/2} C_f$ for the time series in the first five periods $\tau \in [0, 10\pi]$. Fig. 2.11(a) illustrates the influence of the viscoelastic parameter K on the skin friction coefficient $\mathrm{Re}_x^{1/2} C_f$ with fixed $S = 5$ and $M = 12$. It is noted that the skin friction coefficient varies also periodically due to the oscillatory surface motion. The oscillation amplitude of skin friction coefficient $\mathrm{Re}_x^{1/2} C_f$ increases as the values of K are increased. Fig. 2.11(b) shows the effects of S on the skin friction coefficient $\mathrm{Re}_x^{1/2} C_f$. It can be seen that the oscillation amplitude of the skin friction coefficient increases as S increases. Fig. 2.11(c) displays the results of the magnetic number M on the skin friction coefficient $\mathrm{Re}_x^{1/2} C_f$ with fixed $S = 1$ and $K = 0.1$. It is observed that the oscillation amplitude of the skin friction coefficient $\mathrm{Re}_x^{1/2} C_f$ is increased by increasing the

values of M.

Table 2.2 shows the numerical values of the skin friction coefficient $\mathrm{Re}_x^{1/2} C_f$ for different values of K, S and M at the different periods of time series. The results show that the values of the skin friction coefficient for the three different time points $\tau = 1.5\pi, 5.5\pi$ and 9.5π are almost identical. It means that the periodic motion may be reached within the first period when the initial conditions are set up. The change of the skin friction coefficient from positive to negative with the increase of K indicates the large phase difference with the increase of K, as shown in Fig. 2.11(a) (but for slightly different parameters). It can also be seen that the values of the skin friction coefficient $\mathrm{Re}_x^{1/2} C_f$ are increased as the relative frequency to the stretching rate S or/and the magnetic field M are increased. A change in the sign of skin-friction does not appear for different values of S and M cause mainly the change on the values of the skin-friction, less on the phase difference.

2.5 Concluding remarks

In the present investigation, the boundary layer flow of the MHD viscoelastic fluid over an oscillatory stretching sheet has been discussed. The obtained flow equation is solved both analytically using homotopy analysis method and numerically by means of the finite difference method. The comparison between both solutions is given and found in excellent agreement for the HAM solution with higher-order approximation. It demonstrates the convergence of the presented HAM solution for the investigated problem. The influence of the different parameters on the transverse profiles and the time series of velocity is illustrated and discussed. The numerical results give a view towards understanding the response characteristics of the second grade viscoelastic fluid

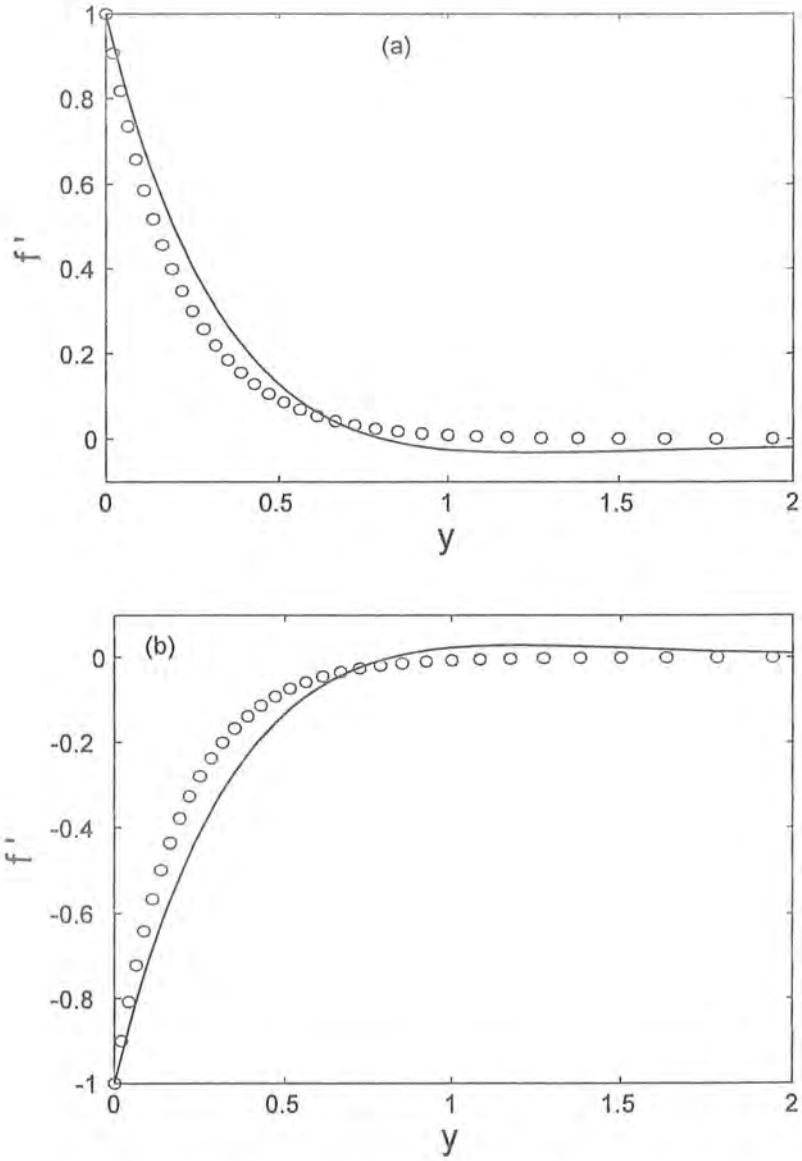

Fig. 2.3. Comparison of $f'(y,\tau)$ obtained from the HAM solution at the 5th-order of approximation (solid lines) and the numerical solution (open circles) with $S = 1$, $M = 5$ and $K = 0.1$ for two different times (a) $\tau = 0.5\pi$ and (b) $\tau = 1.5\pi$, respectively.

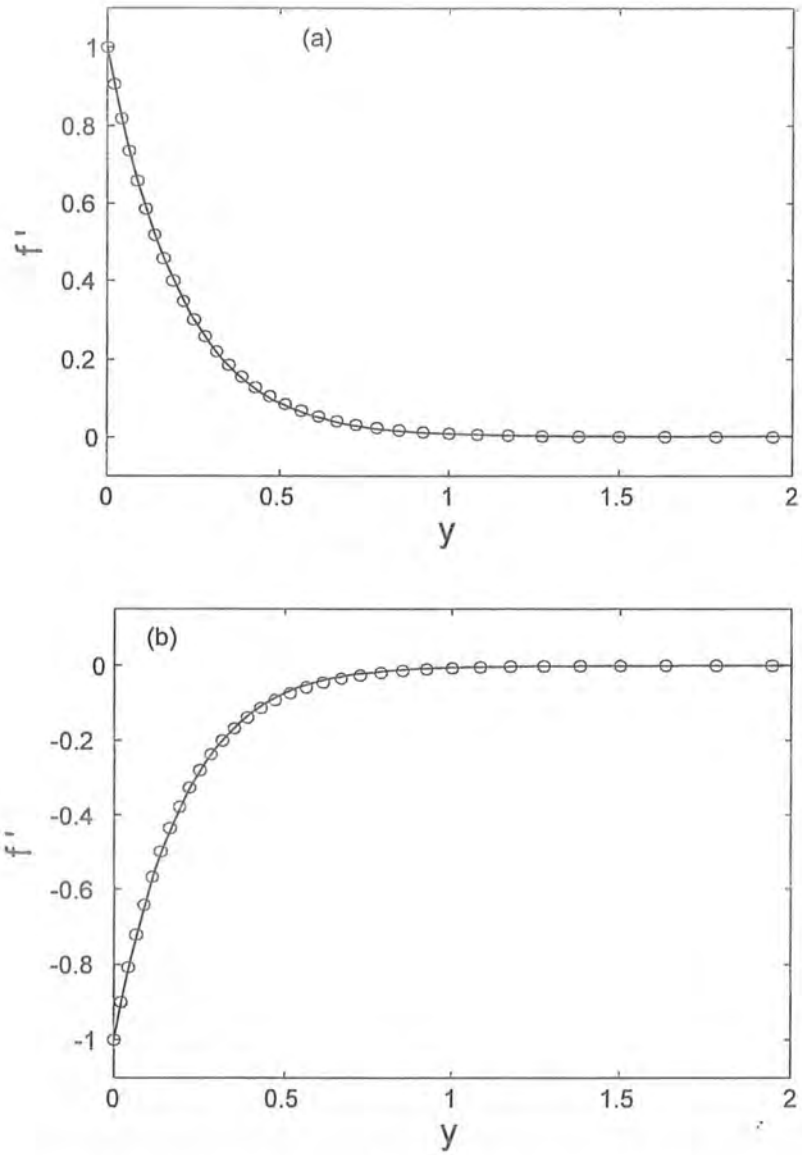

Fig. 2.4. Comparison of $f'(y,\tau)$ obtained from the HAM solution at the 25th-order of approximation (solid lines) and the numerical solution (open circles) with $S = 1$, $M = 5$ and $K = 0.1$ for two different times (a) $\tau = 0.5\pi$ and (b) $\tau = 1.5\pi$, respectively.

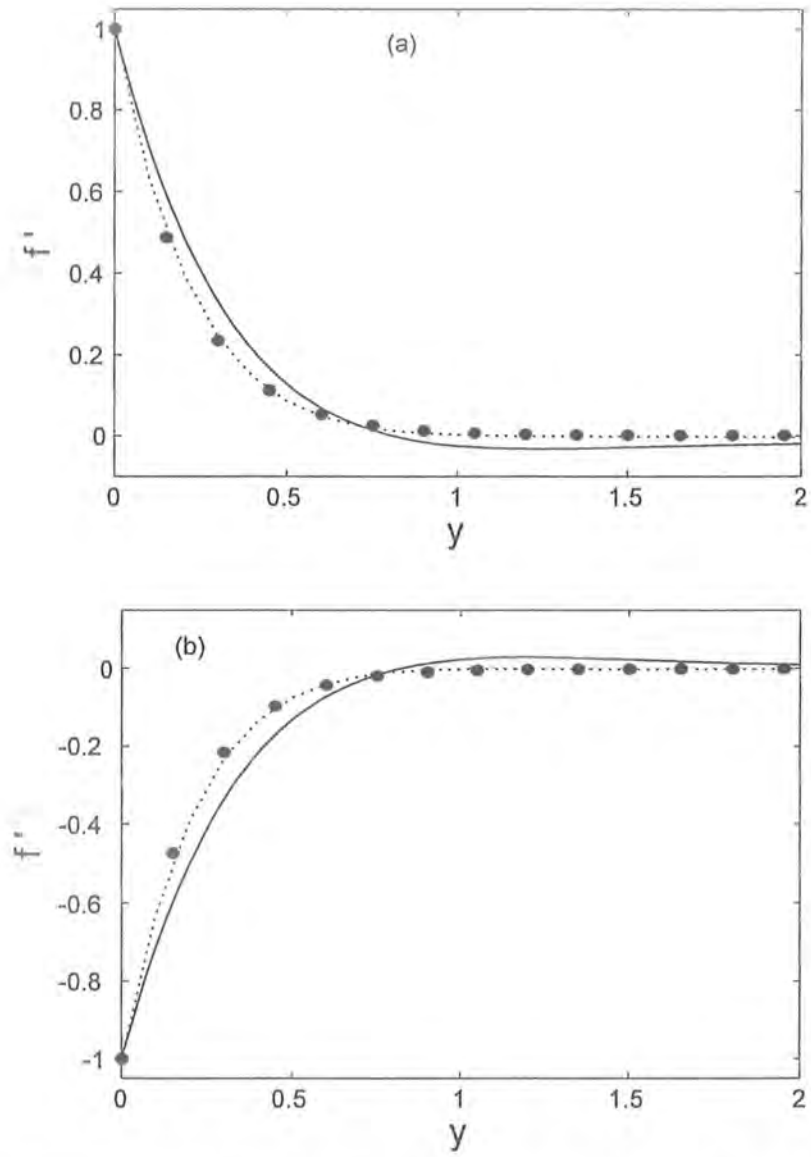

Fig. 2.5. Approximation of $f'(y,\tau)$ with $S = 1$, $M = 5$ and $K = 0.1$. Solid line: 5th-order approximation; Dashed line: 15th-order approximation; Filled circle: 25th-order approximation for two different times (a) $\tau = 0.5\pi$ and (b) $\tau = 1.5\pi$.

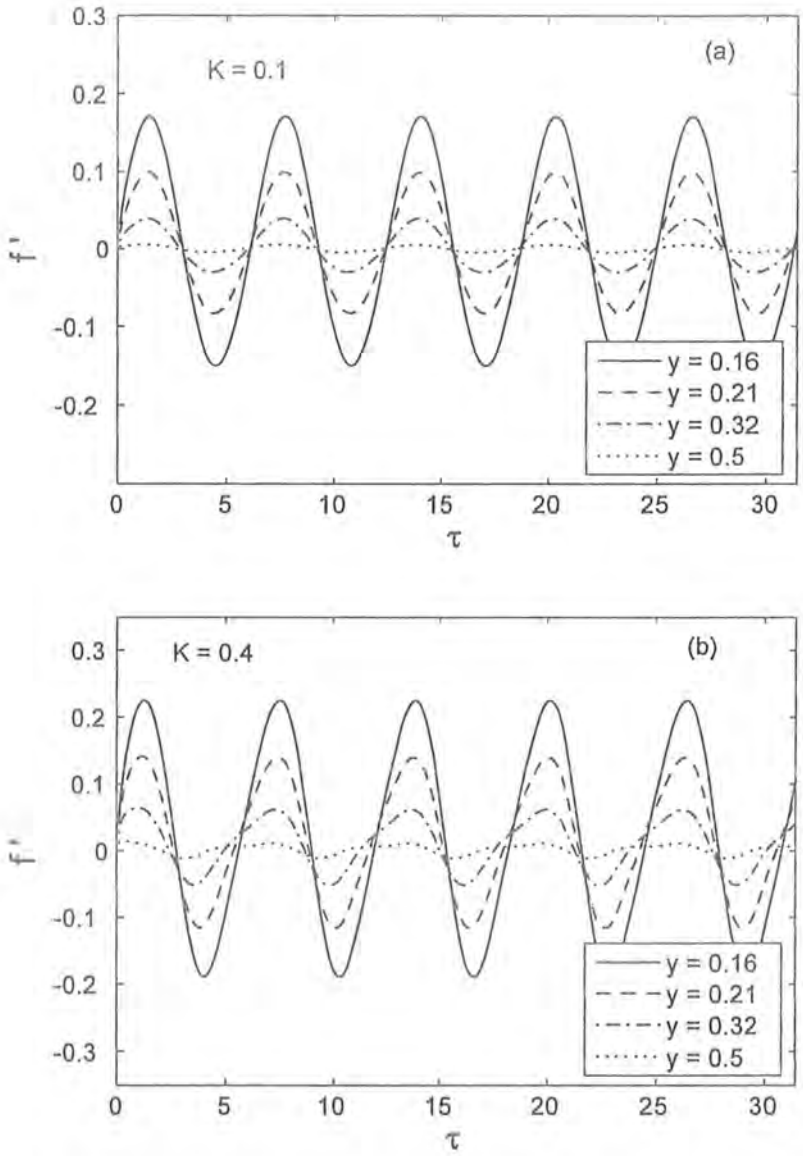

Fig. 2.6. Time series of the flow of the velocity field f' at the four different distances from the surface for the time period $\tau \in [0, 10\pi]$ with $S = 2$, $M = 10$: (a) $K = 0.1$, (b) $K = 0.4$.

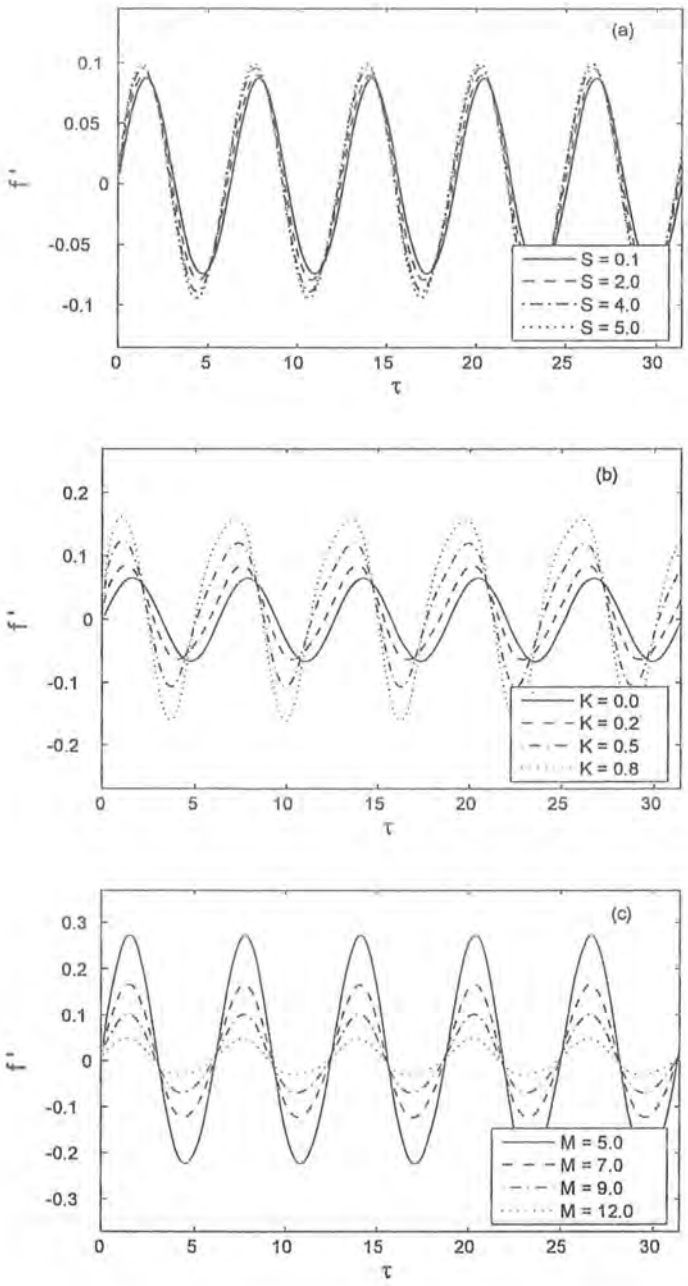

Fig. 2.7. Time series of the velocity field f' in the first five periods $\tau \in [0, 10\pi]$ at a fixed distance to the sheet, $y = 0.25$: (a) effects of S with $K = 0.2$, $M = 10$, (b) effects of viscoelastic parameter K with $S = 2$, $M = 10$ and (c) effects of the magnetic parameter M with $S = 1$, $K = 0.2$.

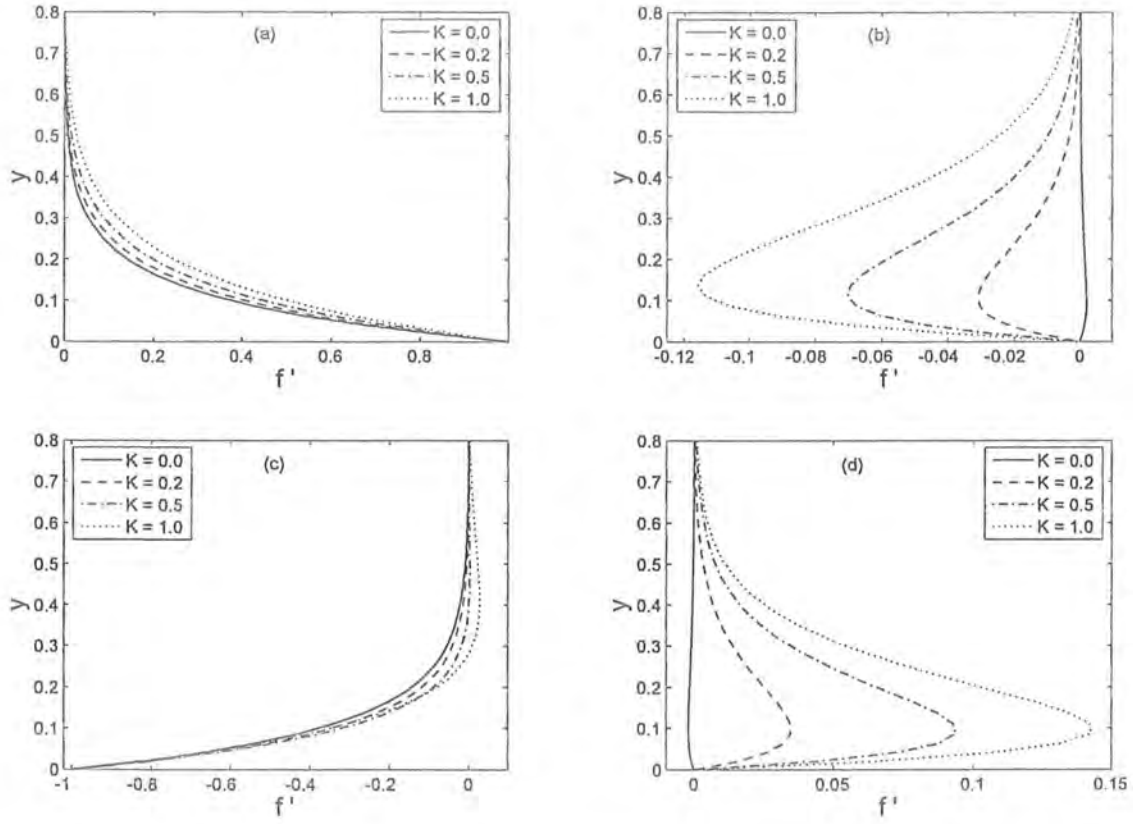

Fig. 2.8. Transverse profiles of the velocity field f' at the four different values of K for the fifth period $\tau \in [8\pi, 10\pi]$ for which a periodic velocity field has been reached: (a) $\tau = 8.5\pi$, (b) $\tau = 9\pi$, (c) $\tau = 9.5\pi$ and (d) $\tau = 10\pi$ with $S = 2$ and $M = 10$.

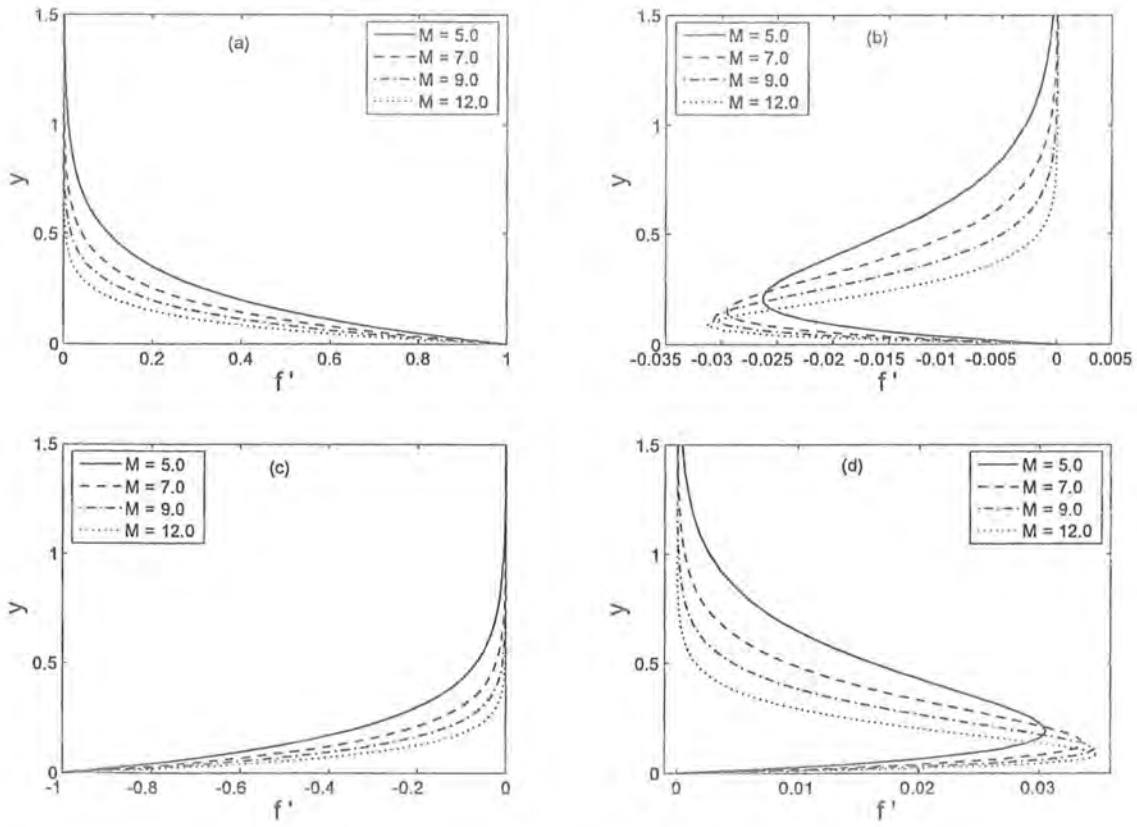

Fig. 2.9. Transverse profiles of the velocity field f' at the four different values of M for the fifth period $\tau \in [8\pi, 10\pi]$ for which a periodic velocity field has been reached: (a) $\tau = 8.5\pi$, (b) $\tau = 9\pi$, (c) $\tau = 9.5\pi$ and (d) $\tau = 10\pi$ with $S = 1$ and $K = 0.2$.

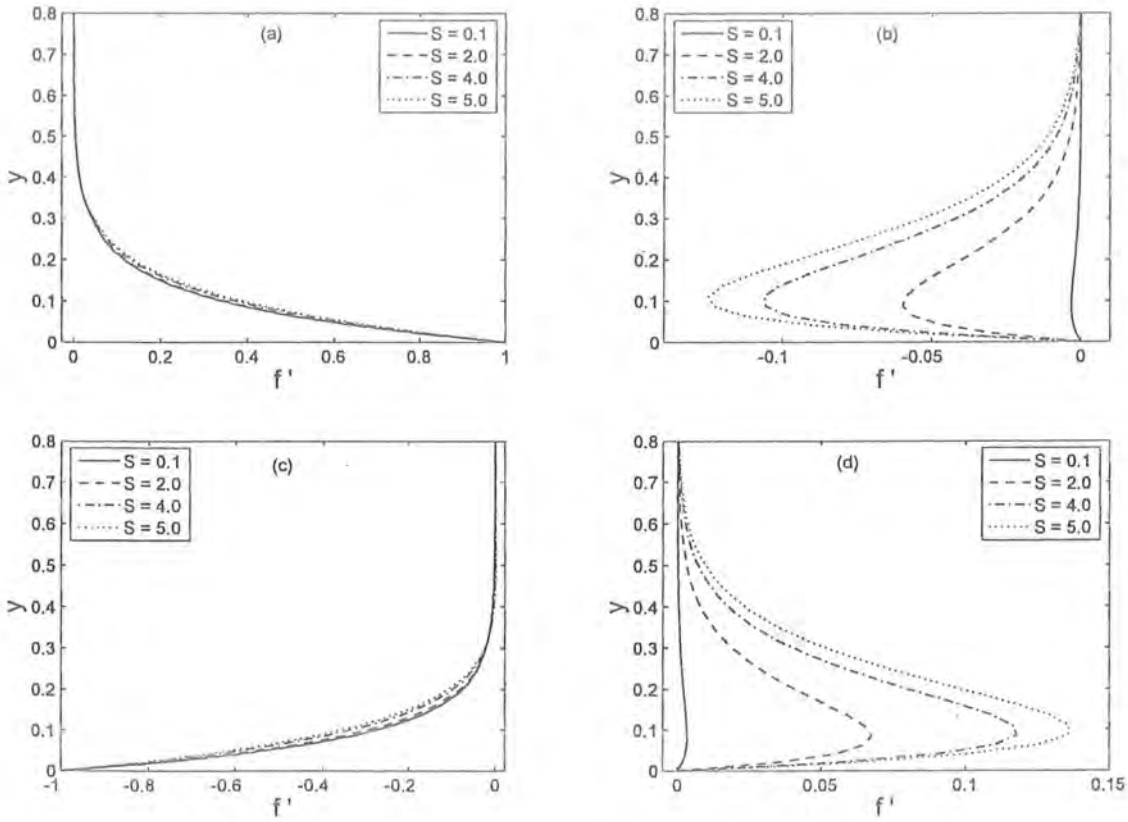

Fig. 2.10. Transverse profiles of the velocity field f' at the four different values of S for the fifth period $\tau \in [8\pi, 10\pi]$ for which a periodic velocity field has been reached: (a) $\tau = 8.5\pi$, (b) $\tau = 9\pi$, (c) $\tau = 9.5\pi$ and (d) $\tau = 10\pi$ with $K = 0.2$ and $M = 12$.

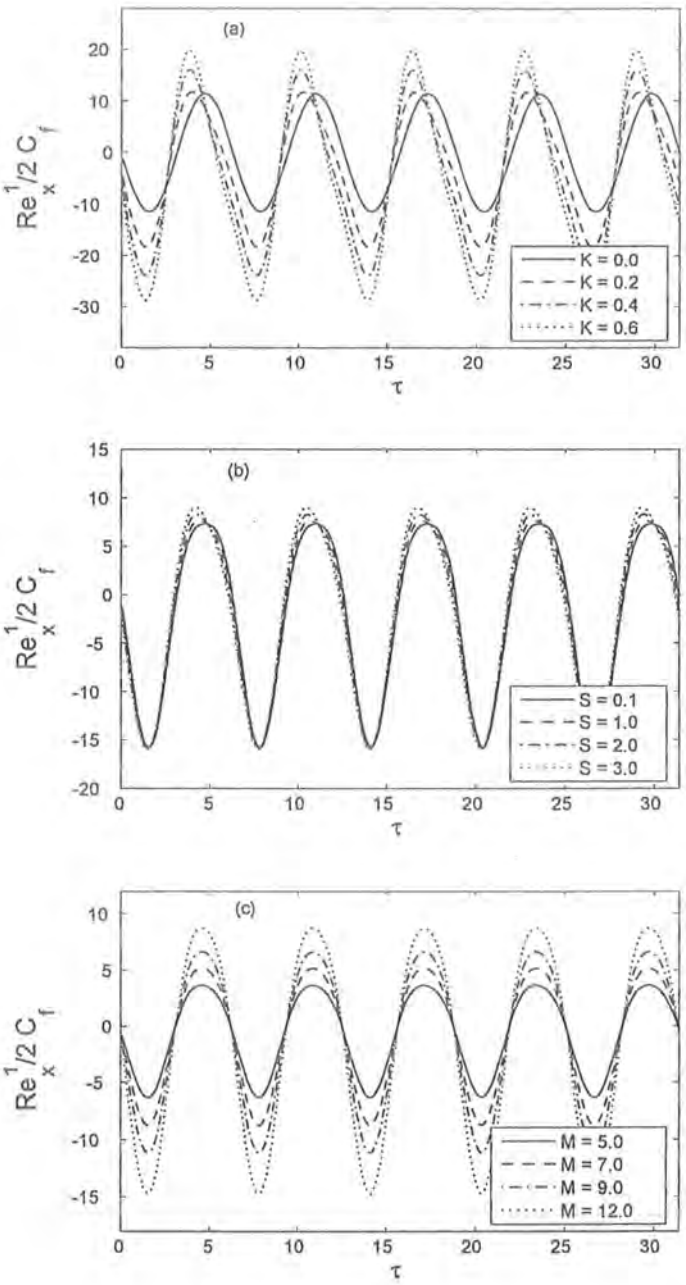

Fig. 2.11. Time series of the skin-friction coefficient $\mathrm{Re}_x^{1/2} C_f$ in the first five periods $\tau \in [0, 10\pi]$: (a) effects of K with $S = 5$, $M = 12$, (b) effects of S with $K = 0.1$, $M = 12$ and (c) effects of M with $K = 0.1$, $S = 1$.

K	S	M	$\tau = 1.5\pi$	$\tau = 5.5\pi$	$\tau = 9.5\pi$
0.0	1.0	12.0	11.678656	11.678707	11.678656
0.2			5.523296	5.523371	5.523257
0.5			−3.899067	−3.899268	−3.899162
0.8			−11.674383	−11.676506	−11.676116
1.0			−15.617454	−15.624607	−15.624963
0.2	0.5		5.322161	5.322193	5.322173
	1.0		5.523296	5.523371	5.523257
	2.0		6.087060	6.087031	6.087156
	3.0		6.769261	6.768992	6.769294
	4.0		7.497932	7.496924	7.496870
	5.0		8.232954	8.229085	8.228996
	1.0	5.0	2.323502	2.323551	2.323548
		7.0	3.278018	3.278005	3.278123
		9.0	4.197624	4.197771	4.197733
		12.0	5.523296	5.523371	5.523257
		15.0	6.791323	6.791301	6.791278

Table 2.2. Values of the skin-friction coefficient $\mathrm{Re}_x^{1/2} C_f$ for different values of K, S and M for three different time points $\tau = 1.5\pi$, 5.5π and 9.5π.

Chapter 3

Momentum and heat transfer over a continuously moving surface with a parallel free stream in a viscoelastic fluid

This chapter concerns with the flow and heat transfer characteristics for a continuous moving surface in a viscoelastic fluid. Constitutive equations of viscoelastic fluid obey the elastico-viscous model. Expressions of velocity and temperature are developed by employing homotopy analysis method (HAM). The criterion to the convergence of the series solutions is properly checked. The features of the analytic solutions as function of the problems are discussed with the help of graphs. In addition the values of skin friction coefficient and the local Nusselt number have been computed and discussed.

3.1 Mathematical formulation

We consider the steady laminar boundary layer flow of a viscoelastic fluid over a surface moving with constant velocity u_w in the same direction as that of the uniform free stream velocity u_∞ (see Fig. 3.1). It is assumed that the wall and the free stream temperature T_w and T_∞

are constants with $T_w > T_\infty$ (heated wall). We take into account of frictional heating due to viscous dissipation as the fluid considered for analysis is of non-Newtonian type. However, in order to get similarity equations, we ignore the effect of elastic stresses on the energy balance. Under the assumption of boundary layer equations and in the presence of viscous dissipation term, the boundary layer equations are given by [89, 128],

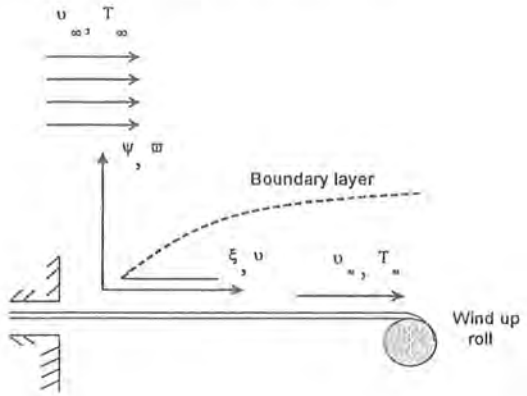

Fig. 3.1. Physical model and coordinate system

$$\frac{\partial u}{\partial x} + \frac{\partial v}{\partial y} = 0, \tag{3.1}$$

$$u\frac{\partial u}{\partial x} + v\frac{\partial u}{\partial y} = \nu\frac{\partial^2 u}{\partial y^2} - k_0\left(u\frac{\partial^3 u}{\partial x \partial y^2} + \frac{\partial u}{\partial x}\frac{\partial^2 u}{\partial y^2} - \frac{\partial u}{\partial y}\frac{\partial^2 u}{\partial x \partial y} + v\frac{\partial^3 u}{\partial y^3}\right), \tag{3.2}$$

$$u\frac{\partial T}{\partial x} + v\frac{\partial T}{\partial y} = \frac{\alpha}{\rho c_p}\frac{\partial^2 T}{\partial y^2} + \frac{\nu}{c_p}\left(\frac{\partial u}{\partial y}\right)^2. \tag{3.3}$$

The boundary conditions of these equations are

$$u = u_w, \quad v = 0, \quad T = T_w \quad \text{at} \quad y = 0, \tag{3.4}$$

$$u \to u_\infty, \quad \frac{\partial u}{\partial y} \to 0, \quad T \to T_\infty \quad \text{as} \quad y \to \infty, \tag{3.5}$$

where x and y are the Cartesian coordinates along and normal to the plate, respectively, u and v are the velocity components along x- and y-axes, respectively, ρ is the fluid density, ν is the kinematic viscosity, T is the fluid temperature, α is the thermal diffusivity, c_p is the specific

heat at constant pressure and k_0 is the viscoelastic parameter.

We look for a solution of Eqs. (3.1) – (3.3) of the form

$$\begin{aligned} \psi &= \sqrt{2x\nu U}\, f(\eta), \qquad \theta(\eta) = T - T_\infty / T_w - T_\infty, \qquad \eta = \sqrt{\frac{U}{2x\nu}}\, y, \\ u &= U f'(\eta), \qquad\qquad v = -\sqrt{\frac{U\nu}{2x}}\left[f(\eta) - \eta f'(\eta)\right] \end{aligned} \tag{3.6}$$

where $U = u_w + u_\infty$. Furthermore, the velocity components u and v in term of stream function ψ are defined as:

$$u = \frac{\partial \psi}{\partial y}, \qquad v = -\frac{\partial \psi}{\partial x}.$$

Substituting (3.6) into Eqs. (3.2) and (3.3), we get the following ordinary differential equations

$$f''' + ff'' - \frac{K}{2}\left(f''^2 - 2f'f''' - ff''''\right) = 0, \tag{3.7}$$

$$\frac{1}{\mathrm{Pr}}\theta'' + f\theta' + 2Ecf''^2 = 0 \tag{3.8}$$

and the boundary conditions (3.4) and (3.5) become

$$f(0) = 0, \qquad f'(0) = \epsilon, \qquad \theta(0) = 1, \tag{3.9}$$

$$f'(\infty) = 1 - \epsilon, \qquad f''(\infty) = 0, \qquad \theta(\infty) = 0. \tag{3.10}$$

Here ϵ is a constant parameter, Pr is the Prandtl number, Ec is the Eckert number and K (≥ 0) is the dimensionless viscoelastic parameter, which are defined as

$$\epsilon = \frac{u_w}{U}, \qquad \mathrm{Pr} = \frac{\mu c_p}{\alpha}, \qquad K = \frac{k_0 U}{x\nu}, \qquad Ec = \frac{U^2}{c_p\left(T_w - T_\infty\right)}. \tag{3.11}$$

The viscoelastic parameter K can be interpret as a local Deborah number of the flow (see Bird et al. [57]) as it compares fluid's natural time, k_0, to the flow characteristics (or residence) time, x/U, and at $x = 0$, there is no fluid velocity one cannot expect any influence of K on the velocity particularly at $x = 0$. It should also be noticed that $Ec > 0$ because the wall is heated ($T_w > T_\infty$) and $Ec = 0$ corresponds to the case when the viscous dissipation term in the

energy equation (3.3) is neglected. Further, we notice that $\epsilon = 0$ corresponds to the flow over a stationary surface caused by the free stream velocity, while $\epsilon = 1$ corresponds to a moving plate in an ambient fluid, respectively. The case $0 < \epsilon < 1$ is when the plate and the fluid are moving in the same direction. If $\epsilon < 0$, the free stream is directed towards the positive x-direction, while the plate moves towards the negative x-direction. On the other hand, if $\epsilon > 1$, the free stream is directed towards the negative x-direction, while the plate moves towards the positive x-direction. It is worth mentioning to this end that when $K = 0$ (viscous fluid) and $Ec = 0$, Eqs. (3.7) and (3.8) along with the boundary conditions (3.9) and (3.10) reduce to those given by Afzal et al. [129]. However, in this chapter we consider only the case of $\epsilon \leq 1$, i.e. the direction of the free stream is fixed (towards the positive x-direction).

Physical quantities of interest are the skin friction coefficient C_f and the local Nusselt number Nu_x, which are defined as

$$C_f = \frac{\tau_w}{\rho U^2}, \qquad Nu_x = \frac{x q_w}{\alpha (T_w - T_\infty)}, \tag{3.12}$$

where τ_w and q_w are the wall skin friction and the heat transfer from the plate, which are given by

$$\tau_w = \mu \left(\frac{\partial u}{\partial y}\right)_{y=0} - k_0 \left(u \frac{\partial^2 u}{\partial x \partial y} + v \frac{\partial^2 u}{\partial y^2} - 2 \frac{\partial u}{\partial y} \frac{\partial v}{\partial y}\right)_{y=0}, \qquad q_w = -\alpha \left(\frac{\partial T}{\partial y}\right)_{y=0}. \tag{3.13}$$

Using variables (3.6), we get

$$(2\,\mathrm{Re}_x)^{1/2} C_f = f''(0), \qquad (2/\mathrm{Re}_x)^{1/2} Nu_x = -\theta'(0), \tag{3.14}$$

where $\mathrm{Re}_x = Ux/\upsilon$ is the local Reynolds number.

The analytical series solution of the non-linear system consisting of Eqs. (3.7) and (3.8) with boundary conditions (3.9) and (3.10) is obtained using the homotopy analysis method (HAM).

3.2 Homotopy analysis solutions

The velocity distribution $f(\eta)$ and the temperature profile $\theta(\eta)$ can be expressed by the set of base functions

$$\left\{ \eta^k \exp\left(-n\eta\right) \middle| \, k \geq 0, n \geq 0 \right\} \tag{3.15}$$

in the form

$$f\left(\eta\right) = a_{0,0}^{0} + \sum_{n=0}^{\infty} \sum_{k=0}^{\infty} a_{m,n}^{k} \eta^k \exp\left(-n\eta\right), \tag{3.16}$$

$$\theta\left(\eta\right) = \sum_{n=0}^{\infty} \sum_{k=0}^{\infty} b_{m,n}^{k} \eta^k \exp\left(-n\eta\right), \tag{3.17}$$

where $a_{m,n}^{k}$ and $b_{m,n}^{k}$ are the coefficients. Based on the *rule of solution expressions* by (3.16) and (3.17) and Eqs. (3.9) and (3.10), it is straightforward to choose

$$f_0\left(\eta\right) = \left(1-\epsilon\right)\eta - \left(1-2\epsilon\right)\left(1-\exp(-\eta)\right), \quad \text{for} \quad \epsilon \neq 1/2, \tag{3.18}$$

$$\theta_0(\eta) = \exp(-\eta) \tag{3.19}$$

as our initial approximations of $f\left(\eta\right)$ and $\phi(\eta)$. Besides that we select the auxiliary linear operators $\mathcal{L}_f$ and $\mathcal{L}_\theta$ as

$$\mathcal{L}_f\left(f\right) = \frac{d^3 f}{d\eta^3} - \frac{df}{d\eta}, \tag{3.20}$$

$$\mathcal{L}_\theta\left(f\right) = \frac{d^2 f}{d\eta^2} - f \tag{3.21}$$

which satisfy the following properties:

$$\mathcal{L}_f\left[C_1 + C_2 \exp(\eta) + C_3 \exp(-\eta)\right] = 0, \tag{3.22}$$

$$\mathcal{L}_\theta\left[C_4 \exp(\eta) + C_5 \exp(-\eta)\right] = 0 \tag{3.23}$$

in which C_i, $i = 1-5$ are arbitrary constants. If $p\left(\in [0,1]\right)$ and $\hbar_f$, $\hbar_\theta$ indicate the embedding and non-zero auxiliary parameters, respectively then the zeroth-order deformation problems

are

$$(1-p)\,\mathcal{L}_f\left[\widehat{f}(\eta;p)-f_0(\eta)\right]=p\hbar_f H(\eta)\mathcal{N}_f\left[\widehat{f}(\eta;p)\right], \tag{3.24}$$

$$\widehat{f}(0;p)=0,\quad \widehat{f}'(0;p)=\epsilon,\quad \widehat{f}'(\infty;p)=1-\epsilon,\quad \widehat{f}''(\infty;p)=0, \tag{3.25}$$

$$(1-p)\,\mathcal{L}_\theta\left[\widehat{\theta}(\eta;p)-\theta_0(\eta)\right]=p\hbar_\theta H(\eta)\mathcal{N}_\theta\left[\widehat{\theta}(\eta;p),\widehat{f}(\eta;p)\right], \tag{3.26}$$

$$\widehat{\theta}(0;p)=1,\qquad \widehat{\theta}(\infty;p)=0, \tag{3.27}$$

in which the non-linear operators $\mathcal{N}_f$ and $\mathcal{N}_\theta$ are of the following forms:

$$\mathcal{N}_f\left[\widehat{f}(\eta;p)\right]=\frac{\partial^3\widehat{f}(\eta;p)}{\partial\eta^3}+\widehat{f}(\eta;p)\frac{\partial^2\widehat{f}(\eta;p)}{\partial\eta^2}-\frac{K}{2}\left(\begin{array}{c}\left(\frac{\partial^2\widehat{f}(\eta,p)}{\partial\eta^2}\right)^2-2\frac{\partial\widehat{f}(\eta,p)}{\partial\eta}\frac{\partial^3\widehat{f}(\eta,p)}{\partial\eta^3}\\ -\widehat{f}(\eta,p)\frac{\partial^4\widehat{f}(\eta,p)}{\partial\eta^4}\end{array}\right), \tag{3.28}$$

$$\mathcal{N}_\theta\left[\widehat{\theta}(\eta;p),\widehat{f}(\eta;p)\right]=\frac{\partial^2\widehat{\theta}(\eta;p)}{\partial\eta^2}+\Pr\widehat{f}(\eta;p)\frac{\partial\widehat{\theta}(\eta;p)}{\partial\eta}+\Pr Ec\left(\frac{\partial^2\widehat{f}(\eta,p)}{\partial\eta^2}\right)^2 \tag{3.29}$$

and $H(\eta)$ is the base function. For the present flow problem we take $H(\eta)=1$.

Obviously for $p=0$ and $p=1$, the above zeroth-order deformation equations have the solutions

$$\widehat{f}(\eta;0)=f_0(\eta),\quad \widehat{f}(\eta;1)=f(\eta),\qquad \widehat{\theta}(\eta;0)=\theta_0(\eta),\quad \widehat{\theta}(\eta;1)=\theta(\eta). \tag{3.30}$$

As p increases from 0 to 1, $\widehat{f}(\eta;p)$ and $\widehat{\theta}(\eta;p)$ vary from $f_0(\eta)$ and $\theta_0(\eta)$ to the exact solutions $f(\eta)$ and $\theta(\eta)$. Due to Taylors theorem and Eq. (3.30), we have

$$\widehat{f}(\eta;p)=f_0(\eta)+\sum_{m=1}^{\infty}f_m(\eta)\,p^m, \tag{3.31}$$

$$\widehat{\theta}(\eta;p)=\theta_0(\eta)+\sum_{m=1}^{\infty}\theta_m(\eta)\,p^m, \tag{3.32}$$

where

$$f_m(\eta)=\frac{1}{m!}\frac{\partial^m\widehat{f}(\eta;p)}{\partial p^m}\bigg|_{p=0},\qquad \theta_m(\eta)=\frac{1}{m!}\frac{\partial^m\widehat{\theta}(\eta;p)}{\partial p^m}\bigg|_{p=0}, \tag{3.33}$$

respectively. The convergence of the series in Eqs. (3.31) and (3.32) is dependent upon $\hbar_f$

and $\hbar_\theta$. Assume that $\hbar_f$ and $\hbar_\theta$ are selected such that the series in Eqs. (3.31) and (3.32) are convergent at $p = 1$, then due to Eq. (3.30) one can write

$$f(\eta) = f_0(\eta) + \sum_{m=1}^{\infty} f_m(\eta), \tag{3.34}$$

$$\theta(\eta) = \theta_0(\eta) + \sum_{m=1}^{\infty} \theta_m(\eta). \tag{3.35}$$

In order to obtain the mth order deformation problems, we differentiating the Eqs. (3.24) and (3.26) m times with respect to p, then set $p = 0$, in the resulting equations and divide them by $m!$, we obtain

$$\mathcal{L}_f[f_m(\eta) - \chi_m f_{m-1}(\eta)] = \hbar_f \mathcal{R}_m^f(\eta), \tag{3.36}$$

$$\mathcal{L}_\theta[\theta_m(\eta) - \chi_m \theta_{m-1}(\eta)] = \hbar_\theta \mathcal{R}_m^\theta(\eta), \tag{3.37}$$

$$f_m(0) = f_m'(0) = f_m'(\infty) = f_m''(\infty) = 0, \tag{3.38}$$

$$\theta_m(0) = \theta_m(\infty) = 0, \tag{3.39}$$

where

$$\mathcal{R}_m^f(\eta) = f_{m-1}'''(\eta) + \sum_{k=0}^{m-1}\left[f_{m-1-k}f_k'' - \frac{K}{2}\left(f_{m-1-k}''f_k'' - 2f_{m-1-k}'f_k''' - f_{m-1-k}f_k''''\right)\right], \tag{3.40}$$

$$\mathcal{R}_m^\theta(\eta) = \theta_{m-1}''(\eta) + \Pr\sum_{k=0}^{m-1}\left[\theta_{m-1-k}'f_k + Ecf_{m-1-k}''f_k''\right], \tag{3.41}$$

and

$$\chi_m = \begin{cases} 0, & m \le 1 \\ 1, & m > 1 \end{cases} \tag{3.42}$$

The general solutions of equations $(3.35) - (3.37)$ are given by

$$\begin{aligned} f_m(\eta) &= f_m^*(\eta) + C_1 + C_2\exp(\eta) + C_3\exp(-\eta), \\ \theta_m(\eta) &= \theta_m^*(\eta) + C_4\exp(\eta) + C_5\exp(-\eta), \end{aligned} \tag{3.43}$$

in which $f_m^*(\eta)$ and $\theta_m^*(\eta)$ denote the special solutions of Eqs. (3.36) and (3.37), and the

integral constants C_1, C_2, C_3, C_4 and C_5 are determined by the boundary conditions (3.38) and (3.39)

$$C_2 = C_5 = 0, \quad C_3 = \left.\frac{\partial f_m^*(\eta)}{\partial \eta}\right|_{\eta=0}, \quad C_1 = -C_3 - f_m^*(0), \quad C_4 = -\theta_m^*(0). \tag{3.44}$$

In this way, it is easy to solve the linear non-homogeneous Eqs. (3.36) and (3.37) by using Mathematica one after the other in the order $m = 1, 2, 3....$

3.3 Convergence of the homotopy solution

Our analytical series solutions are given by Eqs. (3.34) and (3.35). The convergence and rate of approximation of the series (3.34) and (3.35) are dependent upon $\hbar_f$ and $\hbar_\theta$. According to Liao [90] one can choose the proper values of $\hbar_f$ and $\hbar_\theta$ by plotting the $\hbar$-curves which ensure that the solution series (3.34) and (3.35) converge. For this purpose the $\hbar$-curves are plotted for 15th-order of approximations of the functions f and θ in Fig. 3.2(a,b) at different values of interesting parameters K, ϵ, Pr and Ec. Fig. 3.2(a) is drawn for the range of the admissible values of $\hbar_f$ and $\hbar_\theta$ when $K = \epsilon = \Pr = Ec = 0.2$. It can be seen from this Fig. that the range for the values of $\hbar_f$ are $-1.4 \leq \hbar_f \leq -0.2$ and for $\hbar_\theta$ are $-1.7 \leq \hbar_\theta \leq -0.2$. Fig. 3.2(b) gives the $\hbar$-curves when $K = 0.5$, $\epsilon = 0.7$ and $\Pr = 0.5 = Ec$, and from this Fig., the range for admissible values of $\hbar_f$ are $-2 \leq \hbar_f \leq -0.1$ and for $\hbar_\theta$ are $-1.9 \leq \hbar_\theta \leq -0.2$. It is evident from our calculations that the series (3.34) and (3.35) converge in the whole region of η when $\hbar_f = \hbar_\theta = -1$. In order to show the convergence of the HAM solutions for $-f''(0)$ and $-\theta'(0)$ at different order of approximations, we prepared Table 3.1.

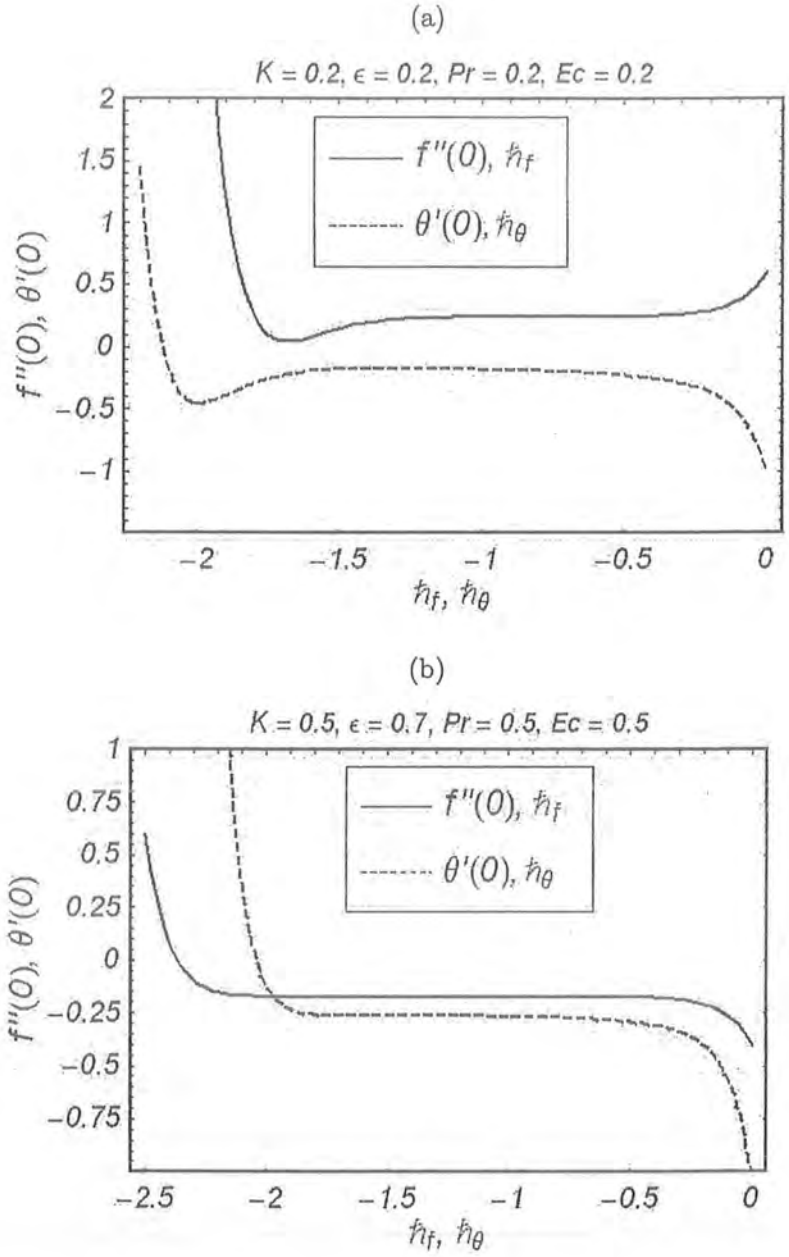

Fig. 3.2. The $\hbar$-curves of $f''(0)$ and $\theta'(0)$ at the 15th-order of approximations.

order of approximations	$-f''(0)$	$-\theta'(0)$
1	0.7000	0.6000
5	0.6418	0.4633
10	0.6522	0.4503
14	0.6517	0.4487
20	0.6517	0.4485
25	0.6517	0.4485
30	0.6517	0.4485

Table 3.1. Convergence of the HAM solutions for different order of approximations when $K = 0.5$, $\epsilon = 1 = \Pr$, $Ec = 0.5$ and $\hbar_f = \hbar_\theta = -0.8$.

3.4 Results and discussion

This section deals with the variations of some physical parameters on the velocity and temperature profiles. For this purpose, the Figs. $3.3 - 3.11$ have been plotted just to see the influence of viscoelastic parameter K, the constant velocity ratio ϵ, the Prandtl number Pr and the Eckert number Ec on the velocity f', the temperature θ, the skin friction coefficient ad the local Nusselt number, respectively. The values of the skin friction coefficient $\mathrm{Re}_x^{1/2} C_f$ and the local Nusselt number $\mathrm{Re}_x^{-1/2} Nu_x$ are tabulated in case of viscous ($K = 0$) and viscoelastic ($K \neq 0$) fluids in Tables $3.2 - 3.4$, respectively.

The variation of the viscoelastic parameter K and the velocity ratio ϵ on the velocity component f' and the skin friction coefficient $\mathrm{Re}_x^{1/2} C_f$ can be seen through Figs. $3.3 - 3.6$. Figs. 3.3 and 3.4 indicate the influence of K on the velocity f' when $\epsilon = 0$ and $\epsilon = 1$. It is found from these Figs. that the velocity f' increases by increasing the viscoelastic parameter K. The boundary layer thickness decreases when K increases in case of $\epsilon = 0.2$ and is quite opposite in case of $\epsilon = 1$. Fig. 3.5 displays the effects of ϵ on the velocity f'. It is noted that initially f' increases but after $\eta = 1$, it decreases when ϵ increases. Fig. 3.6 illustrates the variation of K against ϵ on the skin friction coefficient $\mathrm{Re}_x^{1/2} C_f$. The skin friction coefficient increases when the viscoelastic parameter K increases.

Figs. 3.7−3.11 have been drawn just to see the effects of K, ϵ, Pr and Ec on the temperature profile θ and the local Nusselt number $\mathrm{Re}_x^{-1/2} Nu_x$. Fig. 3.7 shows the influence of K on the temperature θ. It is observed that the temperature θ is a decreasing function of K. The thermal boundary layer decreases as K increases. Fig. 3.8 depicts the effects of ϵ on the temperature θ. It is noted that initially θ decreases but after $\epsilon > 0.7$, it increases. The thermal boundary layer thickness increases by increasing ϵ. Fig. 3.9 elucidates the variations of the Prandtl number Pr on the temperature θ. It shows that θ decreases when Pr increases and the thermal boundary layer thickness also decreases. The influence of the Eckert number Ec on the temperature field θ is shown in Fig. 3.10. It is observed that θ is an increasing function of Ec. The boundary layer thickness also increases when Ec increases. It is further noted that Fig. 3.10 has quite opposite results when compared with Fig. 3.9. Fig. 3.11 indicates the variations of the ϵ versus the Prandtl number Pr on the local Nusselt number $\mathrm{Re}_x^{-1/2} Nu_x$. The local Nusselt number increases by increasing ϵ.

Tables 3.2 − 3.4 are prepared in order to see the variations of the skin friction coefficient $\mathrm{Re}_x^{1/2} C_f$ and the local Nusselt number $\mathrm{Re}_x^{-1/2} Nu_x$ for some values of interesting parameters in viscous ($K = 0$ and $\epsilon = 0$) and viscoelastic fluid ($K \neq 0$) when $\epsilon = 0.2$ and $\epsilon = 1$, respectively using Homotopy-Pade approximation $[m, m]$. Table 3.2 shows the values of the local Nusselt number $-\theta'(0)$ for some values of Pr in case of viscous fluid ($K = 0$) and $\epsilon = 0$. It is found that the magnitude of the local Nusselt number increases with an increase in Pr. The comparison between the present results with the numerical results of reference [130] is given and a good agreement is noted. It is also observed that the values of skin friction coefficient $f''(0) = 0.333$ has a good agreement with (Ref. [130] $f''(0) = 0.332$) for $K = 0$ and $\epsilon = 0$, and the present results for $f''(0) = 0.33299$ are comparable with the results of (Ref. [131] $f''(0) = 0.33197$) for viscous fluid ($K = 0 = \epsilon = M = \xi$ and $j = 1 = N$).

Tables 3.3 and 3.4 are made to see the values of the skin friction coefficient $\mathrm{Re}_x^{1/2} C_f$ and the local Nusselt number $\mathrm{Re}_x^{-1/2} Nu_x$ for some values of K, Pr and Ec for viscoelastic fluid ($K \neq 0$) in case of $\epsilon = 0.2$ and $\epsilon = 1$, respectively. It is noted from Table 3.3 that both the skin friction coefficient $\mathrm{Re}_x^{1/2} C_f$ and the local Nusselt number $\mathrm{Re}_x^{-1/2} Nu_x$ are decreased by increasing K when $\epsilon = 0.2$. It is also found that the magnitude of the skin friction coefficient $\mathrm{Re}_x^{1/2} C_f$ increases and the local Nusselt number $\mathrm{Re}_x^{-1/2} Nu_x$ decreases as K increases when

$\epsilon = 1$. But this change in both the skin friction coefficient and the Nusselt number are larger in case of $\epsilon = 1$ when compared with $\epsilon = 0.2$. Table 3.4 shows the values of the local Nusselt number $\mathrm{Re}_x^{-1/2} Nu_x$ for some values of Pr and Ec when $\epsilon = 0.2$ and $\epsilon = 1$. It is observed that the local Nusselt number increases by increasing Pr in both cases of $\epsilon = 0.2$ and $\epsilon = 1$. It can also be seen that the local Nusselt number $\mathrm{Re}_x^{-1/2} Nu_x$ decreases when Ec increases for when $\epsilon = 0.2$ and $\epsilon = 1$, respectively. However in case of $\epsilon = 1$, the change in the local Nusselt number is larger for $Ec < 0.5$, and for $Ec \geq 0.5$ this change in the local Nusselt number is small.

3.5 Final remarks

In this chapter, the analytic solution of the highly non-linear problem is constructed. The effects of various sundry parameters on the velocity, temperature, skin friction coefficient and the local Nusselt number are analyzed. From the presented analysis, the following observations may be made:

- The velocity f' increases and the temperature θ decreases by increasing viscoelastic parameter K.
- The constant velocity ratio ϵ has opposite results on f' and θ.
- By increasing K, the skin friction coefficient decreases for $\epsilon = 0.2$ and increases for $\epsilon = 1$. But the local Nusselt number decreases for both $\epsilon = 0.2$ and $\epsilon = 1$.
- The behaviours of Pr and Ec on the temperature field θ are opposite.
- The thermal boundary layer thickness increases for large values of ϵ.
- The local Nusselt number increases as Pr increases and decreases when Ec increases.
- The present results has a good agreement with the numerical results [130] when $\epsilon = K = 0$.

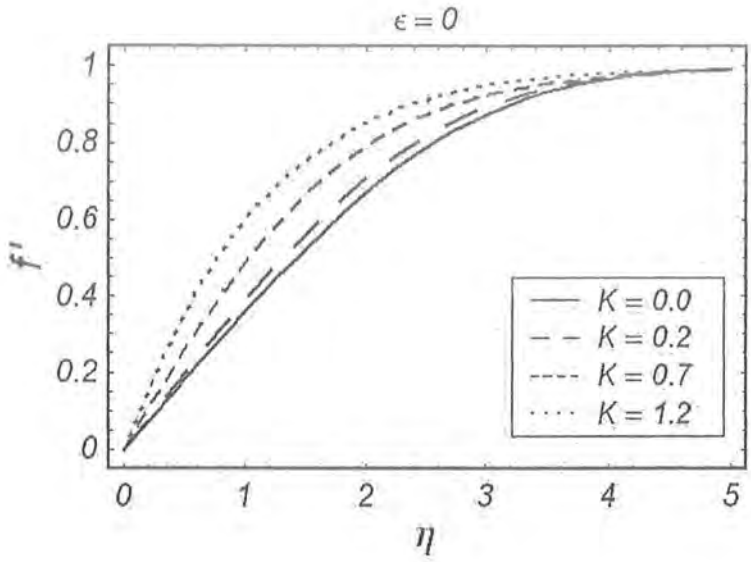

Fig. 3.3. The influences of second grade/viscoelastic parameter K on the velocity component f' in case of stationary plate $\epsilon = 0$.

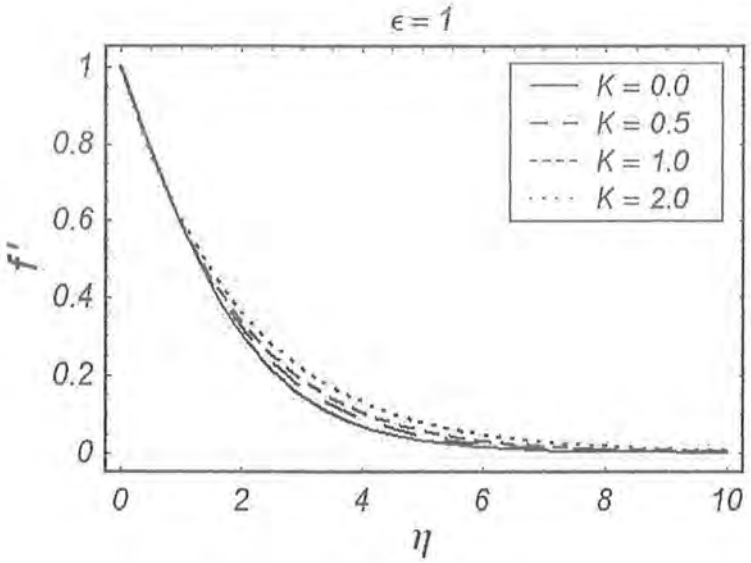

Fig. 3.4. The influences of viscoelastic parameter K on the velocity component f' in case of moving plate $\epsilon = 1$.

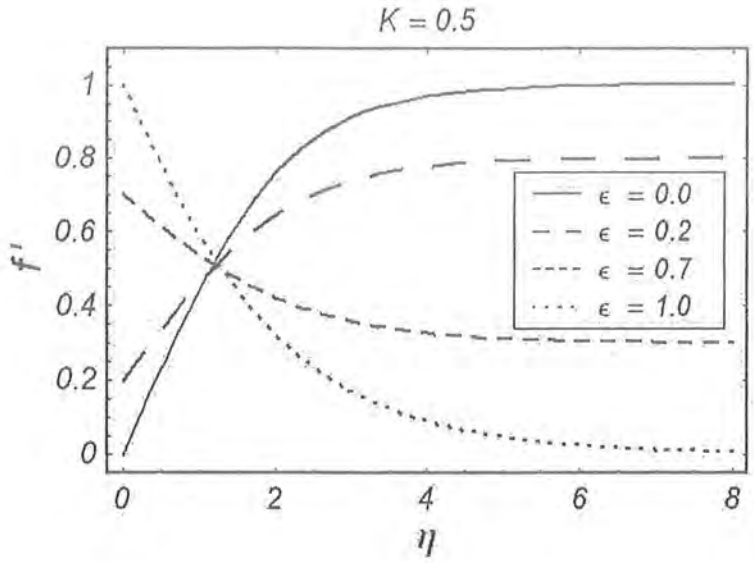

Fig. 3.5. The influences of parameter ϵ on the velocity component f' keeping $K = 0.5$ fixed.

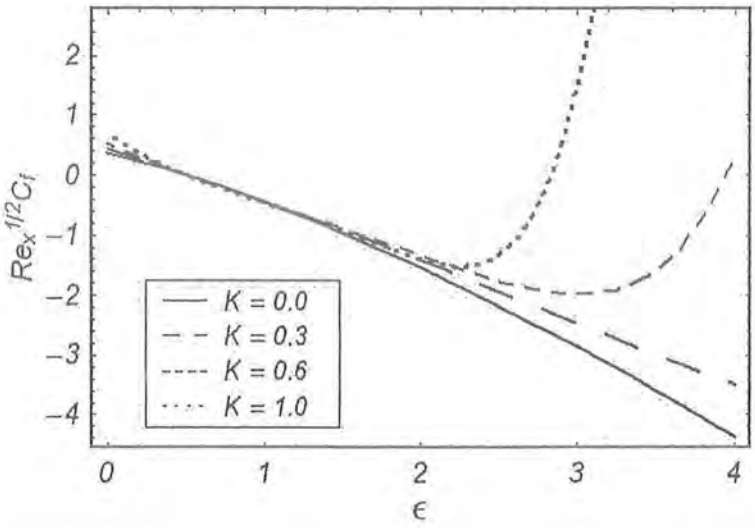

Fig. 3.6. The influences of viscoelastic parameter K on the skin friction coefficient $\mathrm{Re}_x^{1/2} C_f$ verses the parameter ϵ.

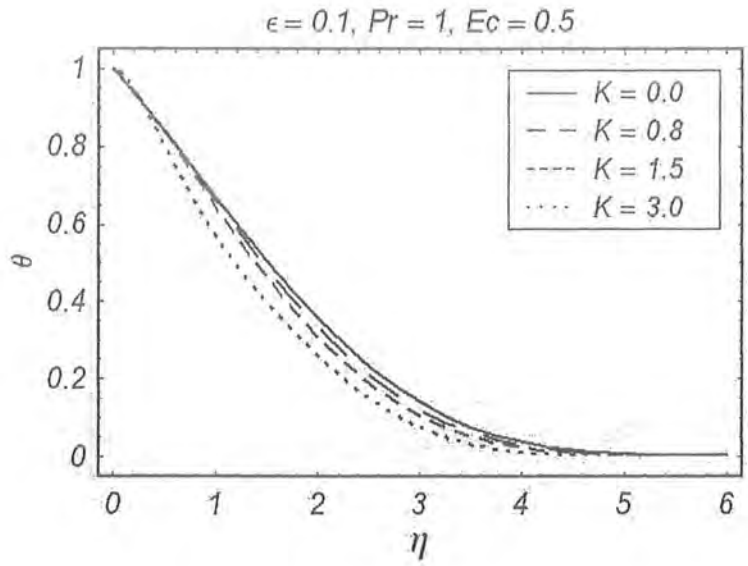

Fig. 3.7. The influences of viscoelastic parameter K on the temperature field θ in case of moving plate $\epsilon = 0.1$.

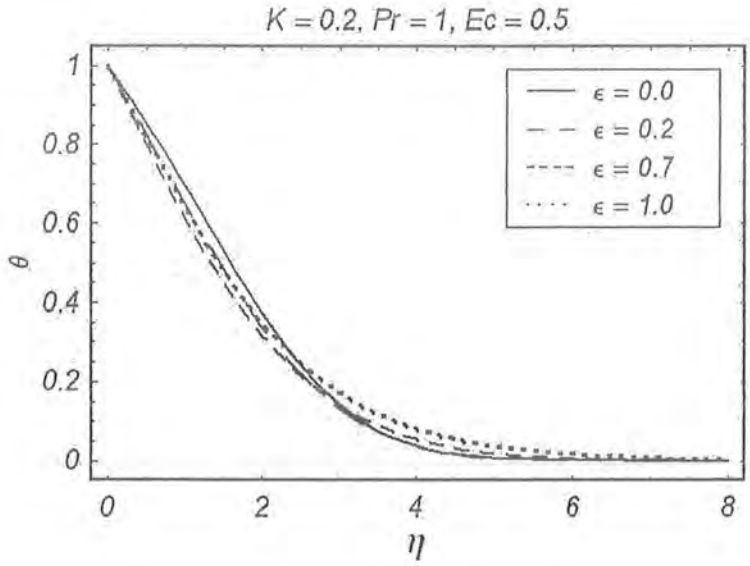

Fig. 3.8. The influences of parameter ϵ on the temperature field θ keeping $K = 0.2$ fixed.

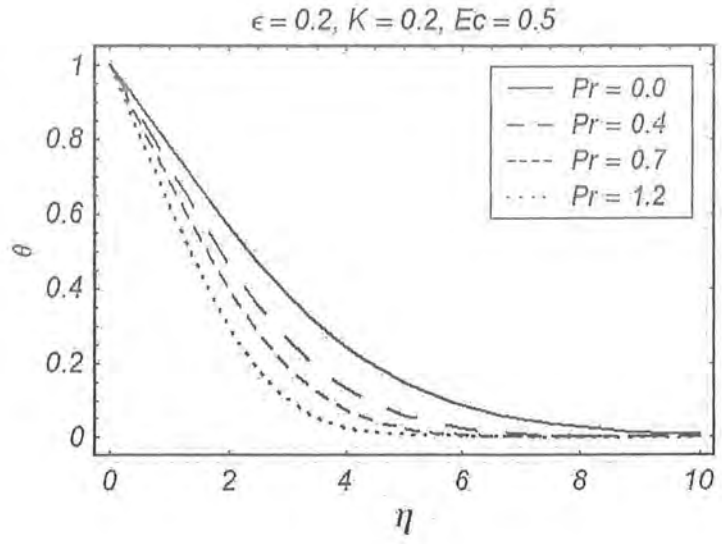

Fig. 3.9. The influences of the Prandtl number Pr on the temperature field θ keeping $\epsilon = 0.2$ fixed.

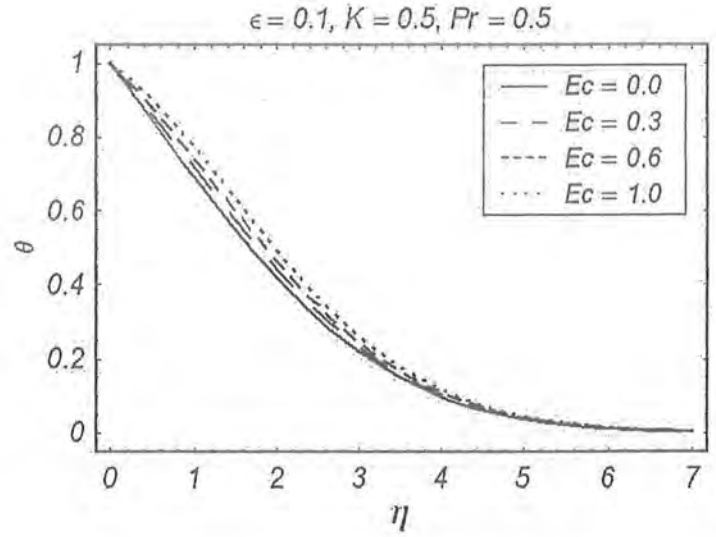

Fig. 3.10. The influences of the Eckert number Ec on the temperature field θ keeping $\epsilon = 0.1$ fixed.

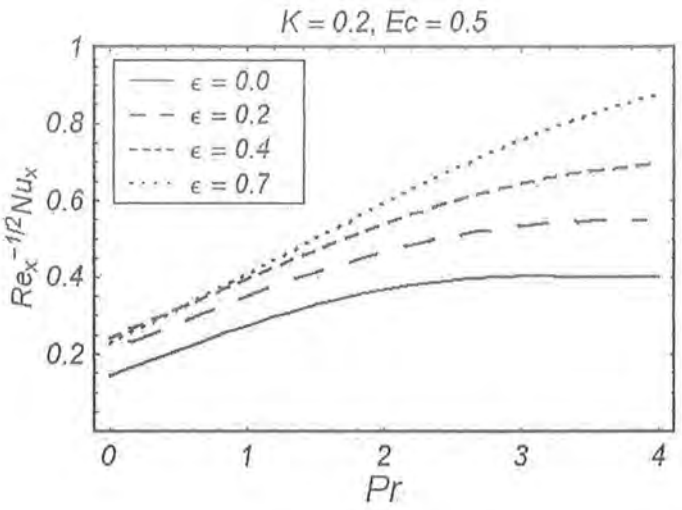

Fig. 3.11. The influences of the parameter ϵ on the local Nusselt number $\mathrm{Re}_x^{-1/2} Nu_x$ verses the Prandtl number Pr.

Homotopy-Pade App.	Pr	Ref. [130]	Present results
[25, 25]	0.01	−0.0519	−0.0519
[15, 15]	0.1	−0.140	−0.141
[10, 10]	0.7	−0.293	−0.293
[10, 10]	1.0	−0.332	−0.333
[25, 25]	10.0	−0.728	−0.728

Table 3.2. Values of local Nusselt number $\theta'(0)$ for some values of Pr when $\epsilon = K = 0$ using homotopy-Pade approximation $[m, m]$.

		$\epsilon = 0.2$		$\epsilon = 1$	
Homotopy-Pade App. $[m, m]$	K	$\mathrm{Re}_x^{1/2} C_f$	$\mathrm{Re}_x^{-1/2} Nu_x$	$\mathrm{Re}_x^{1/2} C_f$	$\mathrm{Re}_x^{-1/2} Nu_x$
$[15, 15]$	0.0	0.3070	0.4659	-0.6276	0.4707
$[15, 15]$	0.2	0.2847	0.4637	-0.6360	0.4629
$[15, 15]$	0.5	0.2571	0.4605	-0.6517	0.4485
$[20, 20]$	0.7	0.2417	0.4584	-0.6648	0.4362
$[20, 20]$	1.0	0.2221	0.4560	-0.6905	0.4112

Table 3.3. Values of skin friction coefficient $\mathrm{Re}_x^{1/2} C_f$ and local Nusselt number $\mathrm{Re}_x^{-1/2} Nu_x$ for some values of K when $\mathrm{Pr} = 1$ and $Ec = 0.5$ using homotopy-Pade approximation $[m, m]$.

			$\epsilon = 0.2$	$\epsilon = 1$
Homotopy-Pade App. $[m, m]$	Pr	Ec	$\mathrm{Re}_x^{-1/2} Nu_x$	$\mathrm{Re}_x^{-1/2} Nu_x$
$[15, 15]$	0.0	0.5	0.03226	0.03226
$[15, 15]$	0.2		0.2437	0.1435
$[15, 15]$	0.5		0.3540	0.2841
$[15, 15]$	0.7		0.4027	0.3580
$[15, 15]$	1.0		0.4605	0.4485
$[15, 15]$	3.0		0.7111	0.8039
$[15, 15]$	1.0	0.0	0.4991	0.6174
$[15, 15]$		0.2	0.4836	0.5498
$[15, 15]$		0.5	0.4605	0.4485
$[15, 15]$		0.7	0.4450	0.3809
$[15, 15]$		1.0	0.4219	0.2796

Table 3.4. Values of local Nusselt number $\mathrm{Re}_x^{-1/2} Nu_x$ for some values of Pr and Ec when $K = 0.5$ using homotopy-Pade approximation $[m, m]$.

Chapter 4

Unsteady flow of a second grade fluid film over a stretching surface

This chapter deals with the flow analysis in a thin liquid film of second grade fluid over an unsteady stretching sheet. The governing non-linear partial differential equation has been reduced first to the non-linear ordinary differential equation. The developed non-linear ordinary differential equation is solved analytically using homotopy analysis method (HAM). An expression of analytic solution is derived in the form of a series. The convergence of the obtained series is analyzed through numerical computations. The effects of various parameters on the velocity components are shown through graphs and discussed. The values of the skin-friction coefficient for different emerging parameters are also tabulated.

4.1 Governing problem

We consider the unsteady, incompressible and two-dimensional flow of a second grade fluid thin liquid film of uniform thickness $h(t)$ lies on the horizontal sheet (as shown in Fig. 4.1). The fluid motion within the film is induced by stretching of the elastic sheet. The x-axis is taken along the stretching sheet with the slot as the origin and the y-axis is normal to the sheet in the outward direction toward the fluid.

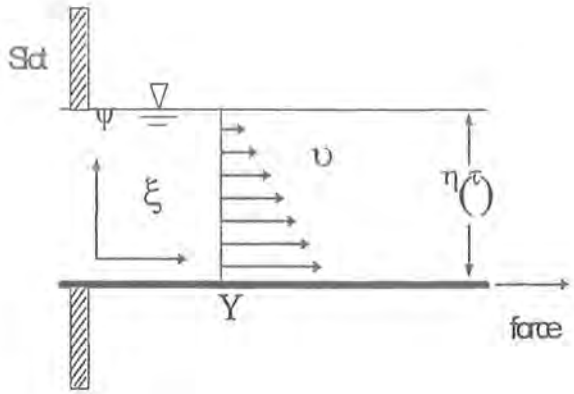

Fig. 4.1. Flow geometry

The unsteady boundary layer equations are:

$$\frac{\partial u}{\partial x}+\frac{\partial v}{\partial y}=0, \tag{4.1}$$

$$\frac{\partial u}{\partial t}+u\frac{\partial u}{\partial x}+v\frac{\partial u}{\partial y}=\nu\frac{\partial^2 u}{\partial y^2}+\frac{\alpha_1}{\rho}\left[\frac{\partial^3 u}{\partial t\partial y^2}+u\frac{\partial^3 u}{\partial x\partial y^2}+\frac{\partial u}{\partial x}\frac{\partial^2 u}{\partial y^2}+\frac{\partial u}{\partial y}\frac{\partial^2 v}{\partial y^2}+v\frac{\partial^3 u}{\partial y^3}\right], \tag{4.2}$$

in which ν is the kinematic viscosity, ρ is the fluid density and α_1 is the material parameter of second grade fluid, u and v are the velocity components in x- and y-directions, respectively. By taking $\alpha_1 = 0$, we recover the problem of Wang [132].

The relevant boundary conditions for the flow problem are [133 – 137]

$$u = U_1(x,t), \quad v = 0 \quad \text{at} \quad y = 0, \tag{4.3}$$

$$\frac{\partial u}{\partial y} = 0, \quad v = \frac{dh}{dt} \quad \text{at} \quad y = h, \tag{4.4}$$

where $U_1(x,t)$ is the surface velocity of the stretching sheet and the flow is caused by stretching the elastic surface at $y = 0$ such that the continuous sheet moves in the x-direction with the velocity

$$U_1(x,t) = \frac{cx}{1-at}. \tag{4.5}$$

Here a and c are positive constants with dimension (time)$^{-1}$. The expression (4.5) for the sheet velocity $U_1(x,t)$ reflects that the elastic sheet, which is fixed at the origin, is stretched by applying a force in the positive x-direction. The effective stretching rate $c/(1-at)$ increases with time since $a > 0$. Note that the Eq. (4.5) on which the analysis is based holds only for time $t < 1/a$.

We define the following dimensionless transformations [135]

$$\eta = \sqrt{\frac{c}{\nu}}(1-at)^{-\frac{1}{2}}y, \qquad \psi = \sqrt{c\nu}x(1-at)^{-\frac{1}{2}}f(\eta), \tag{4.6}$$

and the stream function $\psi(x,y)$ as

$$u = \frac{\partial\psi}{\partial y} = \frac{cx}{1-at}f'(\eta), \tag{4.7}$$

$$v = -\frac{\partial\psi}{\partial x} = -\sqrt{\frac{c\nu}{1-at}}f(\eta). \tag{4.8}$$

The continuity equation (4.1) is automatically satisfied and from Eqs. (4.2) – (4.8) one can write

$$f''' - f'^2 + ff'' - B\left(f' + \frac{1}{2}\eta f''\right) + K\left(2ff''' + B(2f''' + \frac{1}{2}\eta f'''') - f''^2 - ff''''\right) = 0, \tag{4.9}$$

$$\begin{aligned} f &= 0, \quad f' = 1, \quad \text{at} \quad \eta = 0, \\ f &= \frac{1}{2}B\delta, \quad f'' = 0 \quad \text{at} \quad \eta = \delta. \end{aligned} \tag{4.10}$$

Here $B = a/c$ is the unsteadiness parameter, $K = c\alpha_1/\mu(1-at)$ is the dimensionless local second grade parameter and the primes indicate the differentiation with respect to η. Moreover, δ is the dimensionless film thickness and denotes the value of η at the free surface so that Eq. (4.6) gives [135]

$$\delta = \sqrt{\frac{c}{\nu(1-at)}}h(t), \tag{4.11}$$

$$\frac{dh(t)}{dt} = -\frac{a\delta}{2}\sqrt{\frac{\nu}{c}}(1-at)^{-1/2}. \tag{4.12}$$

Note that $h(t)$ decreases monotonically when time increases and δ is a constant depending only upon B [134]. Such scenarios have been discussed in detail in the references [134 – 137]. The shear stress τ_w on the surface of the thin liquid film sheet is

$$\tau_w = \left[\mu\frac{\partial u}{\partial y} + \alpha_1\left(\frac{\partial^2 u}{\partial y \partial t} + 2\frac{\partial u}{\partial x}\frac{\partial u}{\partial y} + u\frac{\partial^2 u}{\partial x \partial y} + v\frac{\partial^2 u}{\partial y^2}\right)\right]_{y=0}, \tag{4.13}$$

and the local skin-friction coefficient or frictional drag coefficient is

$$C_f = \frac{\tau_w}{\rho U_1^2} \quad \text{and} \quad \alpha_1 = \widetilde{\alpha_1}(1 - at). \tag{4.14}$$

In dimensionless form we have

$$R_{e_x}^{1/2} C_f = \left[f''(\eta) + K\left(3f'(\eta)f''(\eta) - f(\eta)f'''(\eta) + \frac{B}{2}\left(3f''(\eta) + \eta f'''(\eta)\right)\right)\right]_{\eta=0}, \tag{4.15}$$

where $R_{e_x}^{1/2} = cx^2/\nu(1 - at)$ is the local Reynolds number.

We will solve Eqs. (4.9) and (4.10) analytically using HAM in the next section.

4.2 Analytical solution

To seek the series solution using homotopy analysis method (HAM), the velocity distribution $f(\eta)$ can be expressed by the set of base functions

$$\left\{\eta^k \middle| k \geq 0\right\} \tag{4.16}$$

in the form

$$f(\eta) = \sum_{n=0}^{\infty}\sum_{k=0}^{\infty} a_{m,n}\eta^k, \tag{4.17}$$

where $a_{m,n}$ are the coefficients. Based on the *rule of solution expressions* by Eqs. (4.10) and Eq. (4.17), the initial approximation $f_0(\eta)$ of the velocity $f(\eta)$ and auxiliary linear operator $\mathcal{L}(f)$ are selected as follows:

$$f_0(\eta) = \eta - \frac{2 - B}{4\delta^2}(3\delta - \eta)\eta^2, \tag{4.18}$$

$$\mathcal{L}(f) = \frac{d^3 f}{d\eta^3}, \tag{4.19}$$

where

$$\mathcal{L}\left[C_1\eta^2 + C_2\eta + C_3\right] = 0 \tag{4.20}$$

and C_i, $(i = 1, 2, 3)$ are arbitrary constants. Denoting $p \in [0, 1]$ as an embedding parameter and $\hbar_f$ a non-zero auxiliary parameter, the zeroth-order deformation problem is

$$(1-p)\,\mathcal{L}\left[\widehat{f}(\eta;p) - f_0(\eta)\right] = p\hbar_f \mathcal{N}_f\left[\widehat{f}(\eta;p)\right], \tag{4.21}$$

$$\widehat{f}(0;p) = 0, \quad \widehat{f}'(0;p) = 1, \quad \widehat{f}(\delta;p) = \frac{B\delta}{2}, \quad \widehat{f}''(\delta;p) = 0, \tag{4.22}$$

where we define a nonlinear operator $\mathcal{N}_f$ as

$$\begin{aligned} \mathcal{N}_f\left[\widehat{f}(\eta;p)\right] &= \frac{\partial^3 \widehat{f}(\eta;p)}{\partial\eta^3} - \left(\frac{\partial \widehat{f}(\eta;p)}{\partial\eta}\right)^2 + \widehat{f}(\eta;p)\frac{\partial^2 \widehat{f}(\eta;p)}{\partial\eta^2} - B\frac{\partial \widehat{f}(\eta;p)}{\partial\eta} \\ &\quad -\frac{1}{2}B\eta\frac{\partial^2 \widehat{f}(\eta;p)}{\partial\eta^2} + K\left\{\begin{array}{c} -\left(\frac{\partial^2 \widehat{f}(\eta;p)}{\partial\eta^2}\right)^2 - B\left(2\frac{\partial^3 \widehat{f}(\eta;p)}{\partial\eta^3} + \frac{1}{2}\eta\frac{\partial^4 \widehat{f}(\eta;p)}{\partial\eta^4}\right) \\ +2\frac{\partial \widehat{f}(\eta;p)}{\partial\eta}\frac{\partial^3 \widehat{f}(\eta;p)}{\partial\eta^3} - \frac{\partial \widehat{f}(\eta;p)}{\partial\eta}\frac{\partial^4 \widehat{f}(\eta;p)}{\partial\eta^4} \end{array}\right\}. \end{aligned} \tag{4.23}$$

The above zeroth-order deformation equations for $p = 0$ and $p = 1$ have the solutions

$$\widehat{f}(\eta;0) = f_0(\eta), \quad \widehat{f}(\eta;1) = f(\eta). \tag{4.24}$$

When p increases from 0 to 1, $\widehat{f}(\eta;p)$ varies from $f_0(\eta)$ to the exact solution $f(\eta)$. By Taylors theorem and Eq. (4.24), we have

$$\widehat{f}(\eta;p) = f_0(\eta) + \sum_{m=1}^{\infty} f_m(\eta)\,p^m, \tag{4.25}$$

where

$$f_m(\eta) = \frac{1}{m!}\frac{\partial^m \widehat{f}(\eta;p)}{\partial p^m}\bigg|_{p=0}, \tag{4.26}$$

respectively. The convergence of the series in Eq. (4.25) is dependent upon $\hbar_f$. Assume that $\hbar_f$ is selected such that the series in Eq. (4.25) is convergent at $p = 1$, then due to Eq. (4.24)

one can write

$$f(\eta) = f_0(\eta) + \sum_{m=1}^{\infty} f_m(\eta), \tag{4.27}$$

In order to obtain the mth order deformation problems, we differentiate the Eq. (4.21) m times with respect to p, then set $p = 0$, in the resulting equations and divide them by $m!$, we obtain

$$\mathcal{L}_f\left[f_m(\eta) - \chi_m f_{m-1}(\eta)\right] = \hbar_f \mathcal{R}_m^f(\eta), \tag{4.28}$$

$$f_m(0) = f_m'(0) = f_m(\delta) = f_m''(\delta) = 0, \tag{4.29}$$

where

$$\begin{aligned} \mathcal{R}_m^f(\eta) &= f_{m-1}''' - B\left(f_{m-1}' + \frac{1}{2}\eta f_{m-1}''\right) + BK\left(2f_{m-1}''' + \frac{1}{2}\eta f_{m-1}''''\right) \\ &+ \sum_{k=0}^{m-1}\left[f_{m-1-k}f_k'' - f_{m-1-k}'f_k' + B\left(2f_{m-1-k}f_k''' - f_{m-1-k}''f_k'' - f_{m-1-k}f_k''''\right)\right], \end{aligned} \tag{4.30}$$

and

$$\chi_m = \begin{cases} 0, & m \leq 1 \\ 1, & m > 1 \end{cases}. \tag{4.31}$$

The general solution of equation (4.28) is given by

$$f_m(\eta) = f_m^*(\eta) + C_1\eta^2 + C_2\eta + C_3, \tag{4.32}$$

in which $f_m^*(\eta)$ denote the special solution of Eq. (4.32), and the integral constants C_1, C_2 and C_3 are determined by the boundary conditions (4.29). In this way, it is easy to solve the linear non-homogeneous Eq. (4.32) by using Mathematica one after the other in the order $m = 1, 2, 3....$successively, and at the Mth-order approximation, we have the analytic series solution of $f(\eta)$ as

$$f(\eta) \approx \sum_{m=0}^{M} f_m(\eta). \tag{4.33}$$

To ensure that $f(\eta)$ can be expressed by (4.17) and that each coefficient $a_{m,n}$ can be modified as the order of approximation M goes to infinity.

4.3 Convergence of the HAM solution

The solution of the considered problem is analytically determined and given in Eq. (4.27). In this section we show the convergence of the obtained solution numerically. Note that our series solution contains the auxiliary parameter $\hbar_f$, which provides us with a simple way to control and adjust the convergence of the series. Following Liao [90], one can check the range of the admissible values of $\hbar_f$ by drawing the so-called $\hbar$-curves. For the present analysis the $\hbar$-curves are plotted for 30th-order of approximations in Fig. 4.2. It is evident from Fig. 4.2 that the admissible range for the values of $\hbar_f$ is $-1.2 \leq \hbar_f \leq -0.3$. It is also noted that the interval for the admissible values of $\hbar_f$ increases by increasing the order of approximation. It is found that the series (4.27) converges in the whole region of η when $\hbar_f = -0.8$. Table 4.1 shows the convergence of the HAM solution for different order of approximations at $K = 0.2$, $B = 0.5$ and $\delta = 1$.

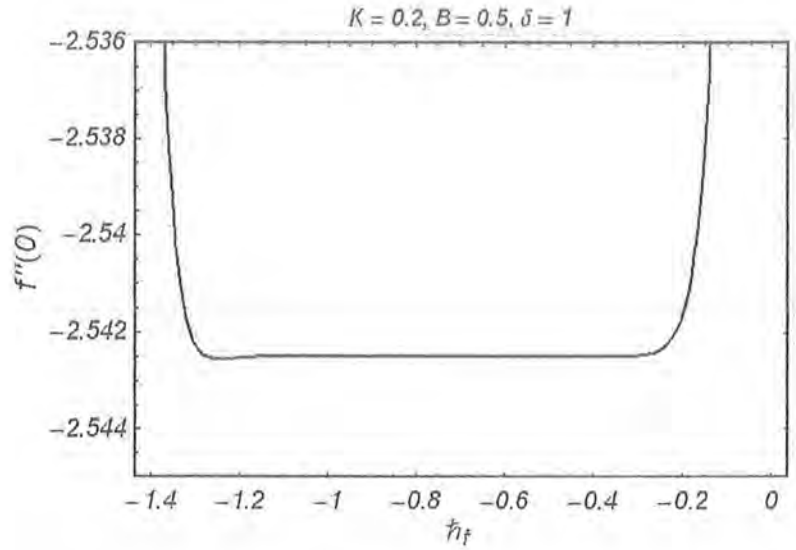

Fig. 4.2. The $\hbar$-curve of $f''(0)$ at the 30th-order of approximations.

order of approximations	$-f''(0)$
1	2.5390714
3	2.5421682
5	2.5425275
8	2.5425162
9	2.5425161
15	2.5425161
20	2.5425161
30	2.5425161
40	2.5425161

Table 4.1. Convergence of HAM solution for different order of approximations.

4.4 Results and discussion

In this section, Figs. 4.3 and 4.4 are prepared in order to see the effects of second grade parameter K and unsteadiness parameter B on the velocity components f and f' by keeping the dimensionless film thickness fixed as $\delta = 1$. Also the variation of the skin friction coefficient $R_{e_x}^{1/2} C_f$ for the various values of the involving parameters K, δ and B is given in Table 4.2.

In order to see the effects of the second grade parameter K on the velocity profiles f and f', we plot Figs. 4.3(a,b). Fig. 4.3(a) depicts that the velocity f is a decreasing function of K. However, Fig. 4.3(b) shows that the velocity f' initially increases as K increases but after approximately $\eta = 0.8$, it decreases for large values of K. The change in f' is small in comparison to f. It is also noted that the velocity component f has maximum values in the middle for $(0 \leq \eta \leq 1)$. The boundary layer thickness increases when K increases. Figs. 4.4(a,b) give the influence of unsteadiness parameter B on the velocity profiles f and f'. It is noted from these Figs. that both the velocities f and f' are the increasing functions of the dimensionless unsteadiness parameter B. The boundary layer thickness also increases for large values of B.

Table 4.2 is made just to see the variation of skin-friction coefficient $R_{e_x}^{1/2}C_f$ for various values of K and B and keeping $\delta = 1$ fixed. It is observed that the magnitude of the skin-friction coefficient $R_{e_x}^{1/2}C_f$ is increased by increasing K. This table also indicates that the magnitude of the skin-friction coefficient decreases when the unsteadiness parameter $B < 2$. For $B = 2$ the skin friction coefficient $R_{e_x}^{1/2}C_f$ is equal to zero and for $B > 2$, it increases.

4.5 Concluding remarks

Here we propose homotopy analysis method (HAM) to discuss the flow over an unsteady stretching surface. The series solution of the highly non-linear problem is established. The auxiliary parameter $\hbar_f$ provides us with a convenient way to adjust and control convergence region and rate of solution series. Moreover the effects of pertinent parameters are analyzed on the velocity and skin friction. The corresponding HAM results for a viscous fluid which are yet not available in the literature can be obtained as a limiting case when $K = 0$.

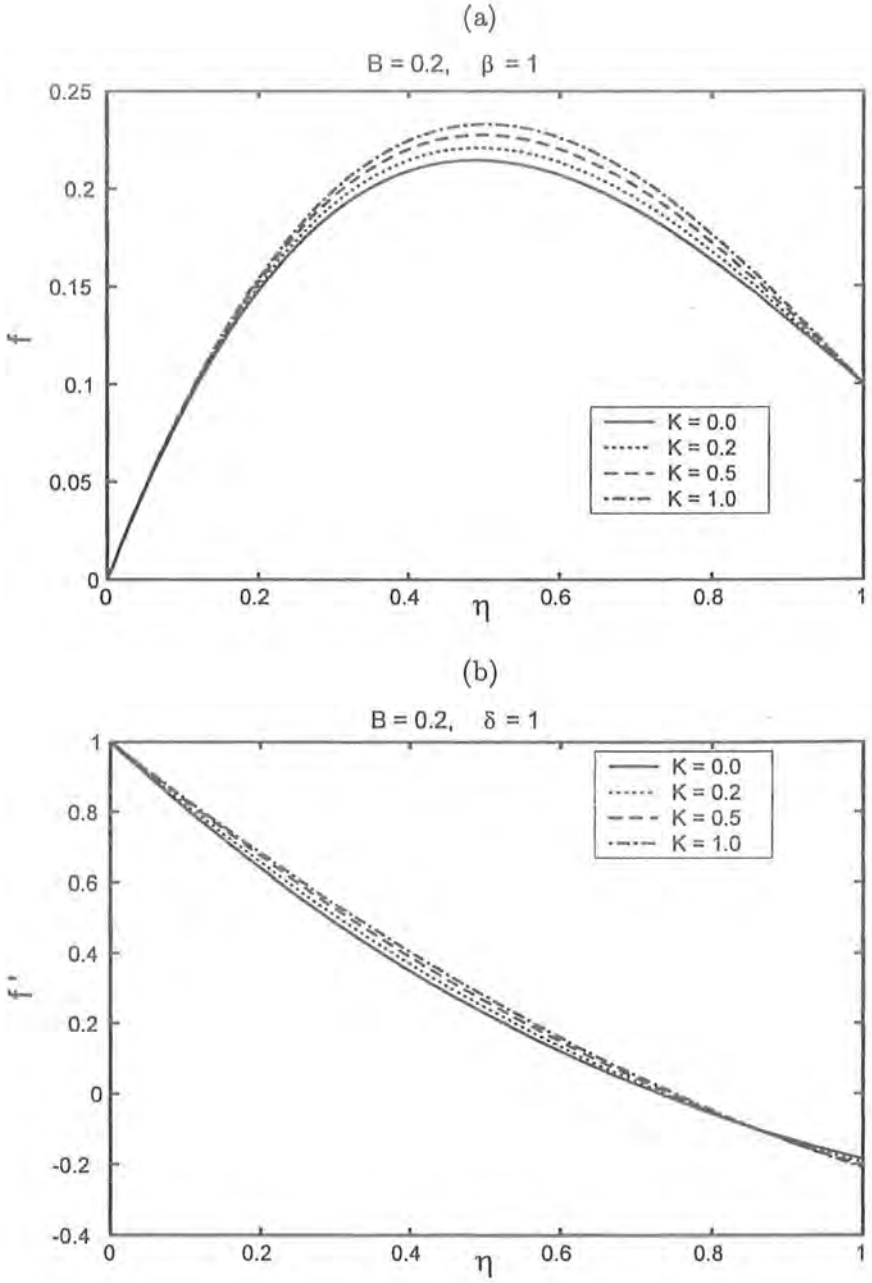

Fig. 4.3. Influence of second grade parameter K on the velocity components f and f' at $\hbar = -0.8$.

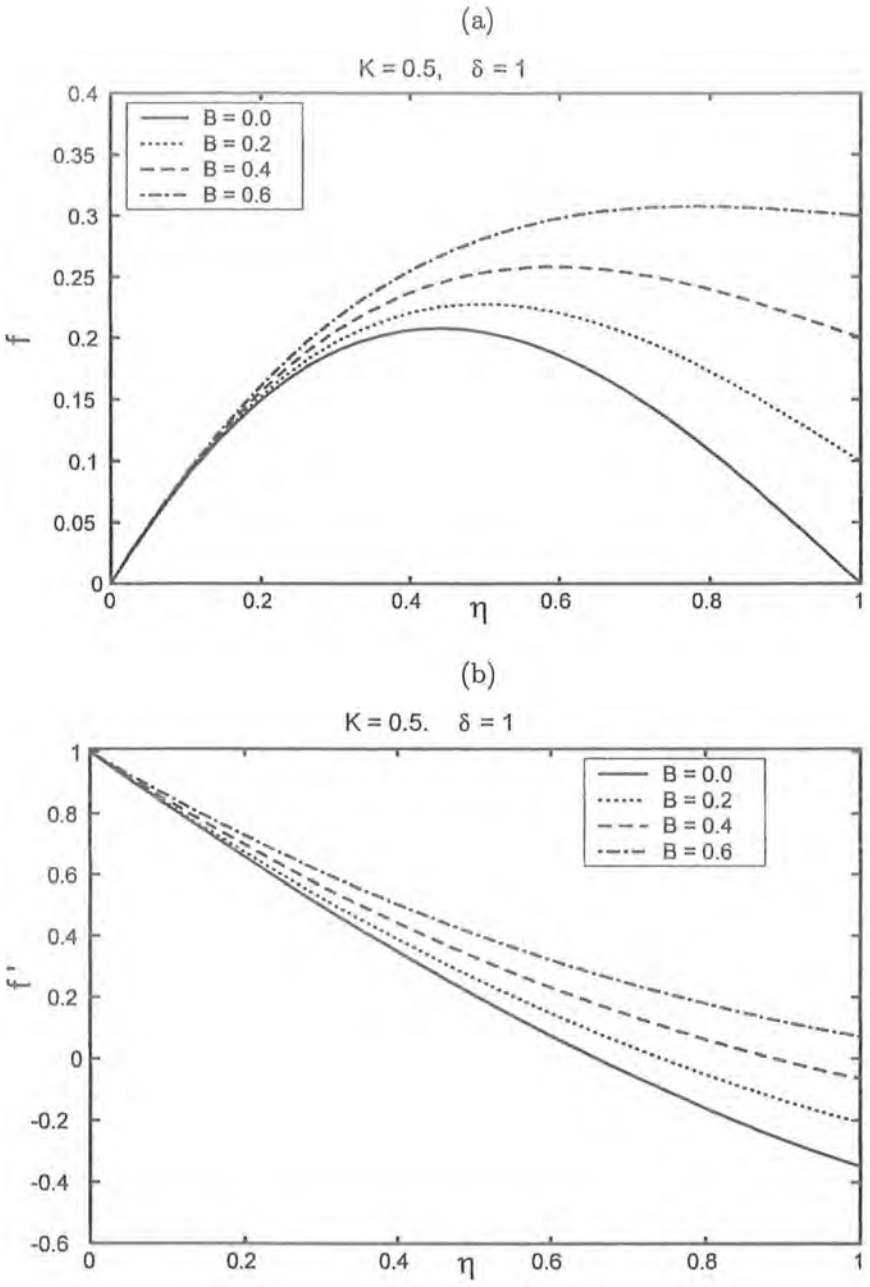

Fig. 4.4. Influence of unsteadiness parameter B on the velocity components f and f' at $\hbar = -0.8$.

K	B	δ	$R_{e_x}^{1/2} C_f$
0.0	0.5	1.0	−2.44408
0.2			−4.44940
0.5			−7.57410
0.7			−9.69713
1.0			−12.91349
2.0			−23.75668
0.5	0.0		−5.31440
	0.2		−5.01055
	0.5		−4.44940
	1.0		−3.25871
	1.5		−1.77117
	2.0		0.00000
	3.0		4.36925
	5.0		16.35201

Table 4.2: Values of skin-friction coefficient $R_{e_x}^{1/2} C_f$ for different values of parameters K, B and δ at $\eta = 0$.

Chapter 5

Series solution for MHD flow of a second grade fluid over a shrinking surface

Analytical solution describing the magnetohydrodynamic (MHD) boundary layer flow of a second grade fluid over a shrinking sheet is described in this chapter. Both exact and series solutions have been determined. For the series solution, the governing non-linear problem is solved using homotopy analysis method (HAM). The convergence of the obtained solution is analyzed explicitly. Graphical results for the velocity field are presented and discussed for the embedded parameters in the flow. The influence of the involved pertinent parameters on the skin-friction coefficient is also analyzed.

5.1 Mathematical statement of the problem

Consider an incompressible second grade fluid past a horizontal shrinking sheet at $y = 0$. The x- and y- axes are taken along and perpendicular to the sheet respectively (as shown in Fig. 5.1). The flow is confined to $y > 0$. A constant magnetic field of strength B_0 acts in the direction parallel to the y-axis. The induced magnetic field is negligible when the magnetic Reynolds number is small [83, 138 – 143]. Since no external electric field is applied and the effect of polarization of the ionized fluid is negligible, we can assume that the electric filed

$E = 0$. The boundary layer equations governing the MHD flow of a second grade fluid are:

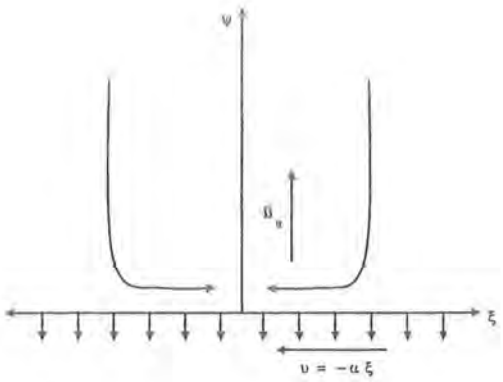

Fig. 5.1. Geometry of the problem

$$\frac{\partial u}{\partial x} + \frac{\partial v}{\partial y} = 0 \tag{5.1}$$

$$u\frac{\partial u}{\partial x} + v\frac{\partial u}{\partial y} = \nu\frac{\partial^2 u}{\partial y^2} + \frac{\alpha_1}{\rho}\left(u\frac{\partial^3 u}{\partial x \partial y^2} + \frac{\partial u}{\partial x}\frac{\partial^2 u}{\partial y^2} + \frac{\partial u}{\partial y}\frac{\partial^2 v}{\partial y^2} + v\frac{\partial^3 u}{\partial y^3}\right) - \frac{\sigma B_0^2}{\rho}u, \tag{5.2}$$

where ν is the kinematic viscosity, σ is the electrical conductivity, ρ is the fluid density, α_1 is the second grade parameter and u and v are x- and y-components of velocity, respectively.

The boundary conditions of the considered system are

$$u = -cx, \quad v = -V \quad \text{at} \quad y = 0, \tag{5.3}$$

$$u \to 0, \quad \frac{\partial u}{\partial y} \to 0 \quad \text{as} \quad y \to \infty, \tag{5.4}$$

where $c > 0$ is the shrinking constant, V (> 0) is the suction velocity. In order to solve the problem completely in unbounded domains, it is possible to augment the boundary conditions by assuming certain asymptotic structures for the solutions at infinity. Here, the second condition in Eq. (5.4) is the augmented condition (see reference [127]). Later Vajravelu and Roper [144], Cortell [32] and others have used this condition for flow problems over a stretching sheet.

The formulation of the boundary value problem is now completed. In order to solve this problem, it is convenient to non-dimensionalize the governing equations and conditions. This can be accomplished by using the following transformations:

$$u = cxf'(\eta), \qquad v = -\sqrt{c\nu}\, f(\eta), \qquad \eta = \sqrt{\frac{c}{\nu}}y. \tag{5.5}$$

The Eq. (5.1) is now identically satisfied and after performing the mathematical operations, the resulting dimensionless problem can be written as:

$$f''' - M^2 f' - f'^2 + ff'' + K\left(2f'f''' - f''^2 - ff^{iv}\right) = 0, \tag{5.6}$$

$$f = A, \quad f' = -1 \quad \text{at} \quad \eta = 0, \tag{5.7}$$

$$f' \to 0, \quad f'' \to 0 \quad \text{as} \quad \eta \to \infty, \tag{5.8}$$

where $A = V/\sqrt{c\nu}$, $M^2 = \sigma {B_0}^2/\rho c$ and $K = c\alpha_1/\nu\rho \neq 0$ and a prime indicates differentiation with respect to η.

The exact solution of Eqs. (5.6), (5.7) and (5.8) is of the form

$$f(\eta) = A - \frac{1}{b}\left(1 - e^{-b\eta}\right). \tag{5.9}$$

Substituting Eq. (5.9) into Eq. (5.6) we get the following cubic equation in b as

$$b^3 KA - (K-1)b^2 - Ab - M^2 + 1 = 0, \tag{5.10}$$

which has one real and two complex roots. The real root is given by

$$b = \frac{1}{6KA}\left(\frac{2(K-1) + 2^{4/3}\left((1-K)^2 + 3KA^2\right)}{\Gamma} + 2^{2/3}\Gamma\right),$$

in which

$$\Gamma = \left[\begin{array}{c} -2\left(1-K\right)^3 - 9(1-K)KA^2 - 27K^2(1-M^2)A^2 \\ +\sqrt{-4\left((1-K)^2+3KA^2\right)^3 + \left(2\left(1-K\right)^3 + 9(1-K)KA^2 + 27K^2(1-M^2)A^2\right)^2} \end{array} \right]^{1/3},$$

and the solution (5.9) is valid for all non-zero values of K. We have just shown the values of f in the Table 5.3 for K upto 20 in order to compare with HAM. However, we can select $K > 20$. Also, the existing solution (5.9) is unique.

The shear stress $\widetilde{\tau}_w$ at the surface is defined as

$$\widetilde{\tau}_w|_{y=0} = \left[\mu\frac{\partial u}{\partial y} + \alpha_1\left(u\frac{\partial^2 u}{\partial x \partial y} + v\frac{\partial^2 u}{\partial y^2} + 2\frac{\partial u}{\partial x}\frac{\partial u}{\partial y}\right)\right]\Big|_{y=0}. \tag{5.11}$$

The above equation in dimensionless form becomes

$$\tau_w = \frac{\widetilde{\tau}_w}{c^{3/2}x\sqrt{\mu\rho}} = \left[f'' + K\left(3f'f'' - ff'''\right)\right]\Big|_{\eta=0} = f''(0). \tag{5.12}$$

The problem consisting of Eq. (5.6) alongwith the boundary conditions (5.7) and (5.8) can also be solved analytically by using HAM in the next section.

5.2 Analytic solution by homotopy analysis method

For the series solution of Eqs. (5.6) – (5.8), we express the velocity distribution $f(\eta)$ by the set of base functions

$$\left\{\eta^k \exp\left(-n\eta\right)\Big|\, k \geq 0, n \geq 0\right\} \tag{5.13}$$

in the form

$$f\left(\eta\right) = a_{0,0}^0 + \sum_{n=0}^{\infty}\sum_{k=0}^{\infty} a_{m,n}^k \eta^k \exp\left(-n\eta\right), \tag{5.14}$$

where $a_{m,n}^k$ are the coefficients. Based on the *rule of solution expressions* (5.14) and the boundary conditions (5.7) and (5.8), it is straightforward to choose the initial guess $f_0\left(\eta\right)$ for $f\left(\eta\right)$ as

$$f_0\left(\eta\right) = A - 1 + \exp(-\eta), \tag{5.15}$$

and the auxiliary linear operator $\mathcal{L}_f$ is

$$\mathcal{L}_f(f) = \frac{d^3 f}{d\eta^3} - \frac{df}{d\eta}. \tag{5.16}$$

Note that the operator $\mathcal{L}_f$ satisfies following properties:

$$\mathcal{L}_f\left[C_1 + C_2 \exp(\eta) + C_3 \exp(-\eta)\right] = 0 \tag{5.17}$$

in which C_i $(i = 1 - 3)$ are the arbitrary constants. If $p\,(\in [0,1])$ is an embedding parameter and $\hbar_f$ indicate the non-zero auxiliary parameters, respectively then we have the following zeroth-order deformation problem

$$(1-p)\,\mathcal{L}_f\left[\widehat{f}(\eta;p) - f_0(\eta)\right] = p\hbar_f \mathcal{N}_f\left[\widehat{f}(\eta;p)\right], \tag{5.18}$$

with the following boundary conditions

$$\widehat{f}(\eta;p)\Big|_{\eta=0} = A, \qquad \frac{\partial \widehat{f}(\eta;p)}{\partial \eta}\bigg|_{\eta=0} = -1, \qquad \frac{\partial \widehat{f}(\eta;p)}{\partial \eta}\bigg|_{\eta=\infty} = 0, \tag{5.19}$$

where the non-linear operator $\mathcal{N}_f$ is

$$\begin{aligned}\mathcal{N}_f\left[\widehat{f}(\eta;p)\right] &= \frac{\partial^3 \widehat{f}(\eta,p)}{\partial \eta^3} - M^2 \frac{\partial \widehat{f}(\eta,p)}{\partial \eta} - \left(\frac{\partial \widehat{f}(\eta,p)}{\partial \eta}\right)^2 + \widehat{f}(\eta,p)\frac{\partial^2 \widehat{f}(\eta,p)}{\partial \eta^2} \\ &+K\left\{2\frac{\partial \widehat{f}(\eta;p)}{\partial \eta}\frac{\partial^3 \widehat{f}(\eta;p)}{\partial \eta^3} - \left(\frac{\partial^2 \widehat{f}(\eta;p)}{\partial \eta^2}\right)^2 - \widehat{f}(\eta;p)\frac{\partial^4 \widehat{f}(\eta;p)}{\partial \eta^4}\right\}.\end{aligned} \tag{5.20}$$

When $p = 0$ and $p = 1$, the above zeroth-order deformation Eq. (5.18) has the solution

$$\widehat{f}(\eta;0) = f_0(\eta), \qquad \widehat{f}(\eta;1) = f(\eta). \tag{5.21}$$

As p increases from 0 to 1, $\widehat{f}(\eta;p)$ varies from $f_0(\eta)$ to the solution $f(\eta)$ of the original equation (5.6). By Taylor's theorem and the relation (5.21) we have

$$\widehat{f}(\eta;p) = f_0(\eta) + \sum_{m=1}^{\infty} f_m(\eta)\, p^m, \tag{5.22}$$

where

$$f_m(\eta) = \frac{1}{m!}\frac{\partial^m \widehat{f}(\eta;p)}{\partial p^m}\bigg|_{p=0}. \tag{5.23}$$

Note that Eq. (5.18) contains the nonzero auxiliary parameter $\hbar_f$. The convergence of the series (5.22) is dependent upon $\hbar_f$. Assuming that $\hbar_f$ is chosen in such a way that the series in Eq. (5.22) is convergent at $p = 1$. Hence using Eq. (5.21), we have the solution series

$$f(\eta) = f_0(\eta) + \sum_{m=1}^{\infty} f_m(\eta). \tag{5.24}$$

We differentiate the zeroth-order deformation Eq. (5.18) m times with respect to p, then setting $p = 0$, and finally dividing by $m!$, the mth-order deformation problem becomes

$$\mathcal{L}_f\left[f_m(\eta) - \chi_m f_{m-1}(\eta)\right] = \hbar_f \mathcal{R}_m^f(\eta), \tag{5.25}$$

$$f_m(0) = f_m'(0) = f_m'(\infty) = 0, \tag{5.26}$$

where

$$\mathcal{R}_m^f(\eta) = f_{m-1}'''(\eta) - M^2 f_{m-1}'(\eta) + \sum_{k=0}^{m-1}\left[\begin{array}{c} f_{m-1-k}f_k'' - f_{m-1-k}'f_k' \\ +K\left(2f_{m-1-k}'f_k'' - f_{m-1-k}''f_k'' - f_{m-1-k}f_k^{iv}\right)\end{array}\right], \tag{5.27}$$

and

$$\chi_m = \begin{cases} 0, & m \le 1 \\ 1, & m > 1 \end{cases}. \tag{5.28}$$

The general solution of Eq. (5.25) which contain the $f_m^{\star}(\eta)$ as the special solutions can be written as

$$f_m(\eta) = f_m^{\star}(\eta) + C_1 + C_2\exp(\eta) + C_3\exp(-\eta), \tag{5.29}$$

where the integral constants are determined by the boundary conditions (5.26)

$$C_2 = 0, \quad C_3 = \left.\frac{\partial f_m^*(\eta)}{\partial \eta}\right|_{\eta=0}, \quad C_1 = -C_3 - f_m^*(0). \tag{5.30}$$

In this way, it is easy to solve the linear non-homogeneous Eq. (5.25) by using Mathematica one after the other in the order $m = 1, 2, 3.....$

5.3 Convergence of the series solution

The explicit, analytic expression given by Eq. (5.24) contains the auxiliary parameter $\hbar_f$, which gives the convergence region and rate of approximation for the homotopy analysis method. The auxiliary parameter $\hbar_f$ depends upon the physical parameters of the flow problem. In Fig. 5.2, the $\hbar$-curves are plotted for different values of M, A and K at 30th-order of approximation. Fig. 5.2(a) gives the admissible range of $\hbar_f$ for different values of M $(= 1.2, 1.5, 1.8)$ keeping A and K fixed. The variations of A and K for the range of $\hbar_f$ can be seen in Figs. 5.2(b) and 5.2(c), respectively. Fig. 5.2 indicates the range for the admissible values of the parameter $\hbar_f$ which is $-1.6 \leq \hbar_f < -0.1$. The series (5.24) converges in the whole region of η when $\hbar_f = -0.8$. It is further noted from Fig. 5.2 that the interval for admissible values of $\hbar_f$ increases by increasing order of approximation. Fig. 5.3 gives the comparison between the HAM solution (5.24) and exact solution given in Eq. (5.9). Table 5.2 is displayed to show the convergence of the HAM solution with increasing order of approximation. Table 5.2 gives the comparison between HAM solution and shows a good agreement with exact an solution.

Order of approximation	1	5	10	15	20	25	Exact solution
$f''(0)$	1.5	1.5879	1.59416	1.59443	1.59443	1.59443	1.59443

Table 5.1: Convergence of the HAM solution and comparison with the exact solution.

(a)

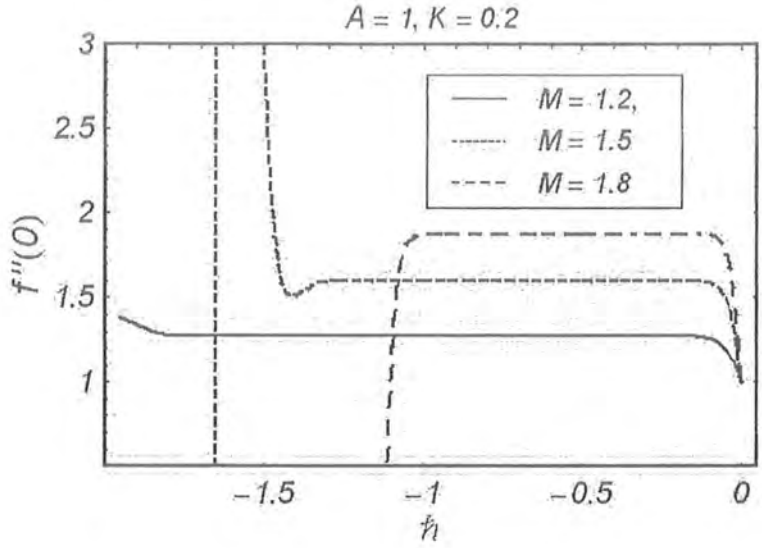
A = 1, K = 0.2
M = 1.2,
M = 1.5
M = 1.8
f''(0)
ħ
3
2.5
2
1.5
1
-1.5
-1
-0.5
0

(b)

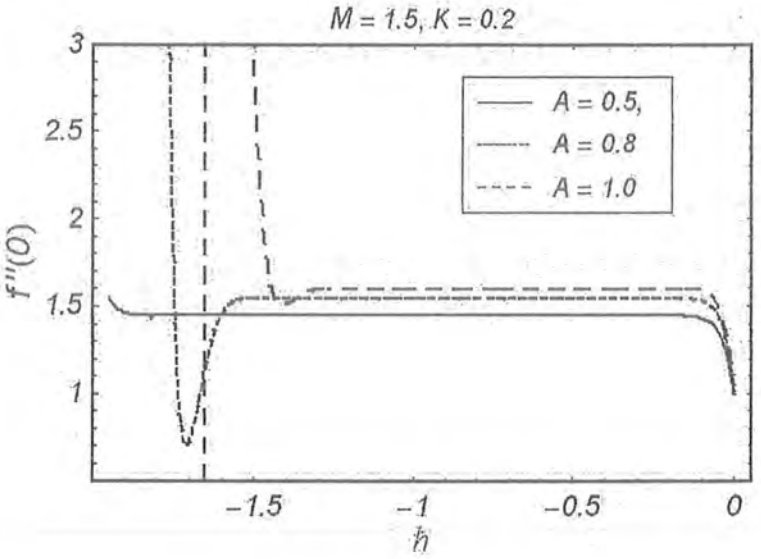
M = 1.5, K = 0.2
A = 0.5,
A = 0.8
A = 1.0
f''(0)
ħ
3
2.5
2
1.5
1
-1.5
-1
-0.5
0

(c)

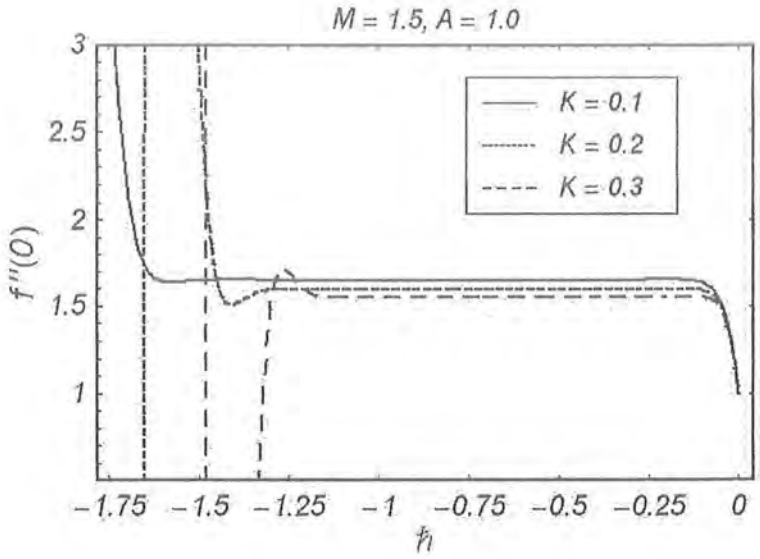

Fig. 5.2. The $\hbar$-curves of $f''(0)$ at the 30th-order of approximations.

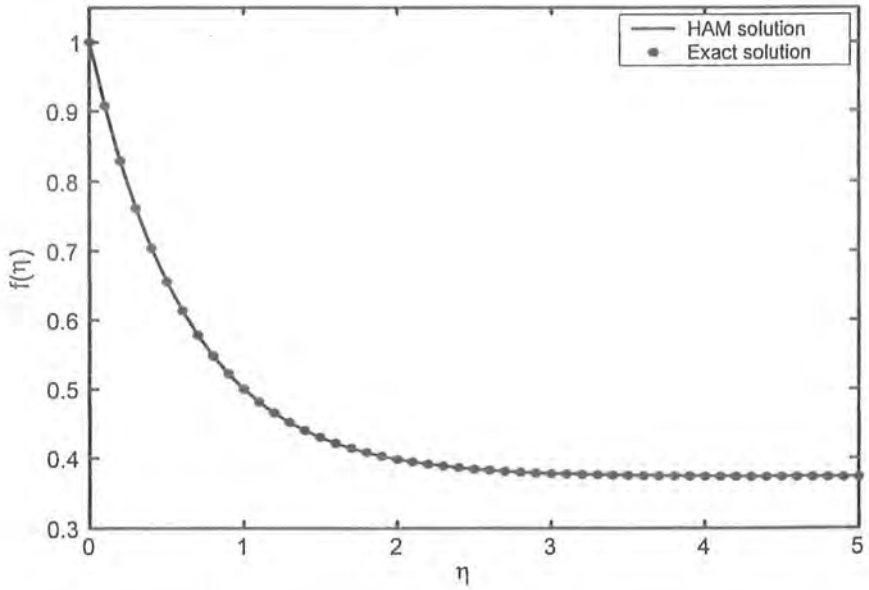

Fig. 5.3. Comparison between the HAM and the exact solutions with $K = 0.2$, $A = 1$ and $M = 1.5$.

η	HAM solution [5.24]	Exact solution [5.9]
0.0	1.0	1.0
0.2	0.818731	0.818731
0.5	0.606531	0.606531
1.0	0.367879	0.367879
2.0	0.135335	0.135335
3.0	0.0497871	0.0497871
5.0	0.00673795	0.00673795
10.0	0.0000453999	0.0000453999

Table 5.2: Comparison of the velocity f for HAM solution and exact solution for different values of η.

5.4 Results and discussion

The main results of interest here are the influence of suction velocity at the wall A, the Hartman number M and the second grade parameter K on the velocity profiles f and f'. In order to analyze these important characteristics of the problem, we plot Figs. $5.4 - 5.9$. The variations of these parameters on the velocity and the shear stress at the wall (the skin-friction coefficient) are also tabulated in Tables 5.3 and 5.4, respectively.

Figs. 5.4 and 5.5 represent the variations of velocity components f and f' for various values of suction parameter A. It is noted from these Figs. that the magnitude of both f and f' decreases when the suction parameter A increases and this decrement is larger in case of f. Moreover, the thickness of the boundary layer decreases with the increase in A. This is in keeping with the fact that suction causes reduction in the boundary layer thickness.

In order to illustrate the influence of Hartman number M on the velocity f and f', we prepared Figs. 5.6 and 5.7, respectively. As expected, by increasing the magnitude of M reduces the velocity profiles f and f'. This is due to the effect of magnetic force against the flow direction. It can be seen that with the increase of M, the magnitude of f increases more rapidly when compared with f'. Figs. 5.6 and 5.7 further depict that there is a decrease in the

thickness of the boundary layer due to an increase in M.

The flow dependence of a second grade fluid or the material parameter K on the velocity components f and f' can be clearly observed from Figs. 5.8 and 5.9. From these Figs. it can be read off that increasing of K decreases the magnitude of f and f'. These Figs. also indicate that large values of K cause the velocity f and f' to become flatter. It may also be noted from Fig. 5.9 that the boundary layer thickness decreases when K increases. Also, the magnitude of f is larger than f' when K increases.

Table 5.1 shows the values of the skin-friction coefficient $f''(0)$. It is interesting to note here that the values of $f''(0)$ correspond to the exact solution at the 15th order of approximation. Table 5.2 provides a comparison of the values of the velocity component f for HAM and exact solutions for various values of η and keeping other parameters fixed. An excellent agreement is noted here.

Tables 5.3 and 5.4 have been made just to see the influences of second grade parameter K, the Hartman number M and the suction velocity A on the velocity f and the skin-friction coefficient ($\tau_w = f''(0)$), respectively. Table 5.3 shows the variations of K, M and A on the velocity f for both HAM and exact solutions given by Eqs. (5.24) and (5.9), respectively. It is found that f decreases as the second grade parameter K increases and, increases for large values of M and A. Table 5.4 elucidates the variation of K, M and A on the skin friction coefficient or the shear stress at the wall τ_w (or $f''(0)$). It is observed that the magnitude of the skin friction first decreases and after $K = 0.5$, it increases for large values of K (≤ 10). The skin friction increases when both M and A increases. It is further noted that the agreement between HAM and exact solution is quite good.

5.5 Concluding remarks

In this work the MHD second grade fluid flow due to a porous shrinking sheet is considered. The series solution is obtained and the convergence is shown. The effects of the sundry parameters are discussed through graphs. Comparison between HAM and exact solutions are given. Such kind of analytic solution for MHD flow of a second grade fluid over a shrinking sheet is presented first time in the literature. The following observations have been made:

- The magnitude of f and f' is decreased by increasing A, M and K, respectively.
- The boundary layer thickness is decreased as A, M and K increases.
- The magnitude of f is larger when compared with f'.
- The HAM results for MHD viscous fluid can be obtained by setting $K = 0$.
- The HAM results are identical to the exact solution (Tables 1 and 2).

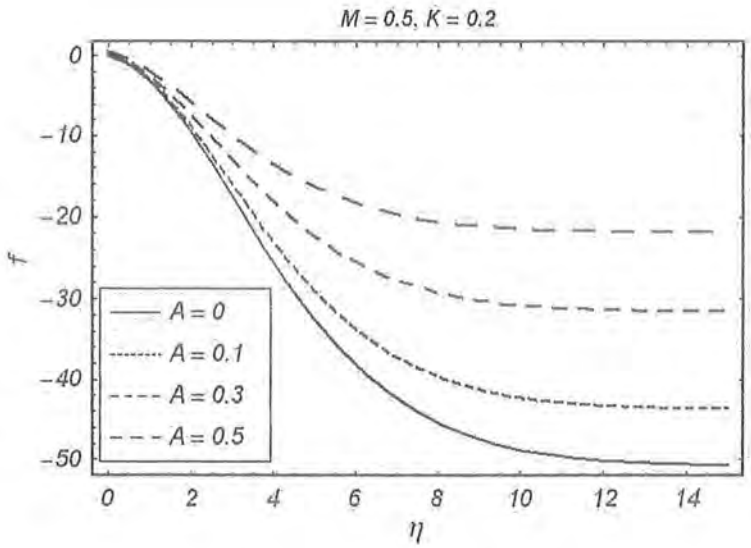

Fig. 5.4. The variations of the suction parameter A on the velocity component f.

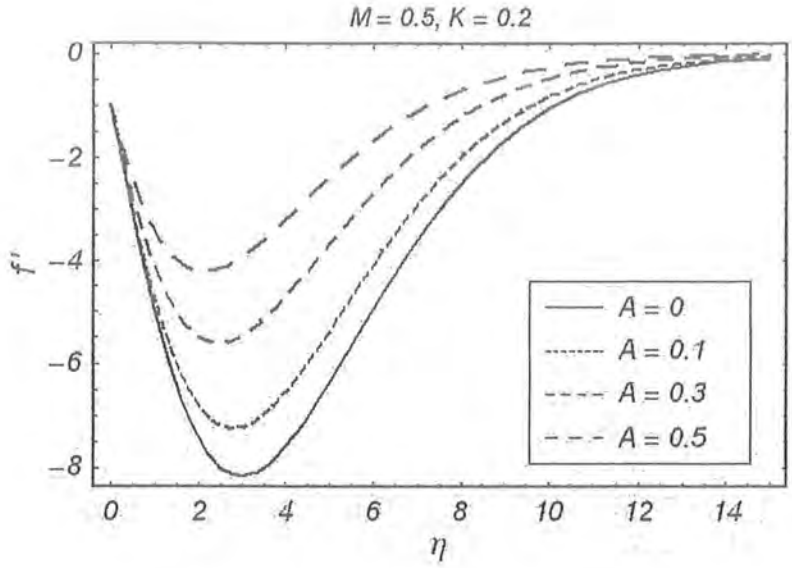

Fig. 5.5. The variations of the suction parameter A on the velocity component f'.

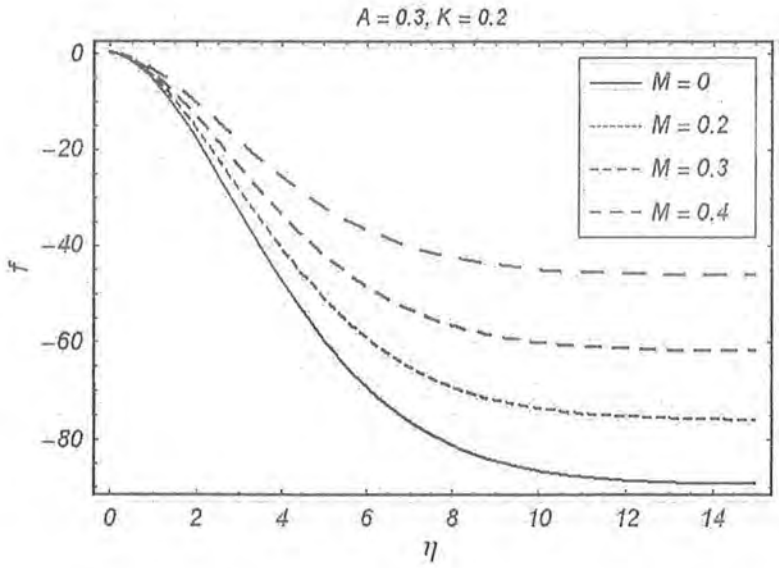

Fig. 5.6. The variations of the Hartman number or the magnetic field M on the velocity component f.

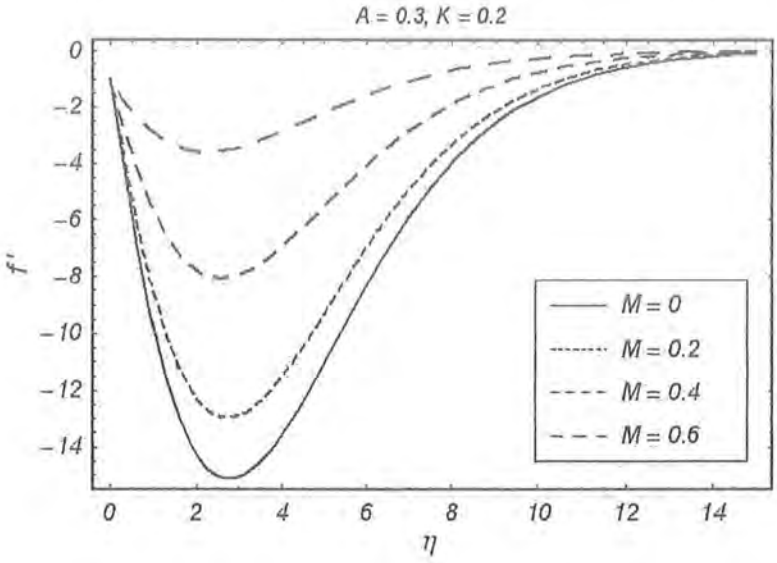

Fig. 5.7. The variations of the Hartman number or the magnetic field M on the velocity component f'.

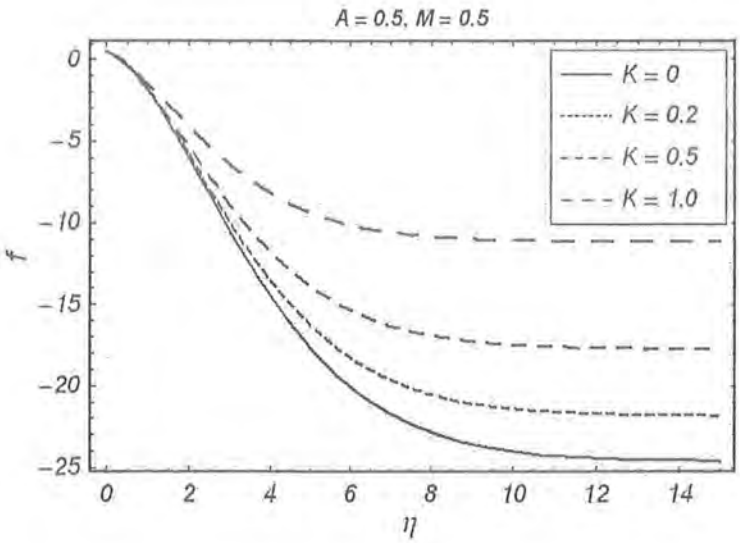

Fig. 5.8. The variations of second grade parameter K on the velocity component f.

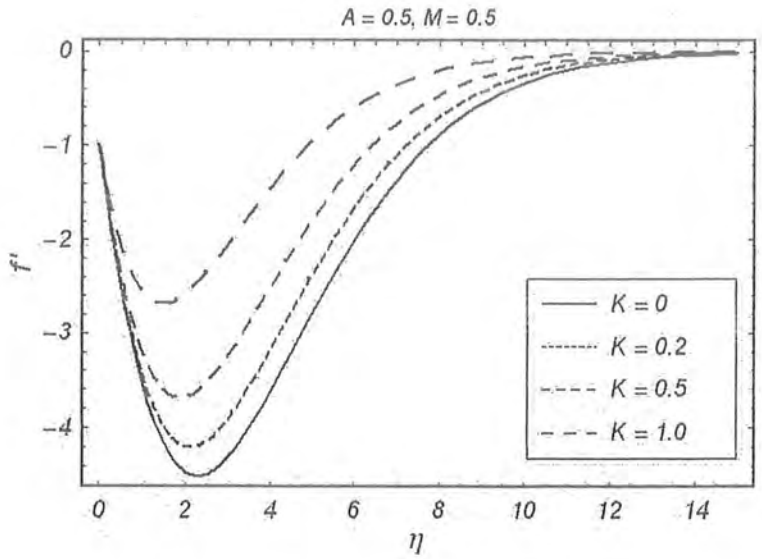

Fig. 5.9. The variations of second grade parameter K on the velocity component f'.

K	M	A	HAM solution [5.24]	Exact solution [5.9]
0.1	1.5	1.0	0.829654	0.829654
0.2			0.828747	0.828753
0.5			0.826977	0.826944
0.7			0.826439	0.826136
1.0			0.825786	0.825734
2.0			0.823493	0.823478
5.0			0.821473	0.821484
10.0			0.820394	0.820393
20.0			0.819669	0.819669
0.5	1.0		0.818731	0.818731
	1.2		0.822586	0.822585
	1.5		0.826977	0.826944
	2.0		0.832040	0.832758
	3.0		0.842011	0.842021
	4.0		0.849647	0.849604
	5.0		0.856786	0.856129
	20.0		− − −	0.907408
	1.5	0.0	−0.071811	−0.071812
		0.2	0.027922	0.027922
		0.5	0.327404	0.327402
		1.0	0.826977	0.826944
		1.5	1.326691	1.326690
		2.0	1.826531	1.826530
		3.0	2.826341	2.826340
		5.0	4.826151	4.826150
		10.0	9.825981	9.825990

Table 5.3: Comparison of the velocity f between the HAM and the exact solutions for different values of K, M and A.

K	M	A	HAM solution [5.24]	Exact solution [5.9]
0.1	1.5	1.0	1.427490	1.427450
0.2			1.146130	1.146210
0.5			0.358841	0.358816
1.0			−0.855190	−0.855289
1.5			−2.007020	−2.007130
2.0			−3.120720	−3.123660
3.0			−5.594256	−5.594730
5.0			−9.502730	−9.509060
10.0			−19.752400	−19.768000
0.5	1.0		0.0	0.0
	1.2		0.136592	0.136510
	1.5		0.358841	0.358816
	2.0		0.780263	0.780140
	3.0		1.794175	1.794080
	5.0		4.366281	4.366020
	1.5	0.1	−0.658248	−0.658203
		0.2	−0.533468	−0.533490
		0.5	−0.184517	−0.184580
		1.0	0.358844	0.358816
		1.5	0.881981	0.882960
		2.0	1.396990	1.398320
		3.0	2.416510	2.416960
		5.0	4.435196	4.435010

Table 5.4: Comparison of the skin friction coefficient $f''(0)$ between the HAM and the exact solutions for different values of K, M and A.

Chapter 6

Mixed convection in the stagnation-point flow of a Maxwell fluid towards a vertical stretching surface

In this chapter we investigate the steady mixed convection boundary layer flow of an incompressible Maxwell fluid near the two-dimensional stagnation-point flow over a vertical stretching surface. It is assumed that the stretching velocity and the surface temperature vary linearly with the distance from the stagnation-point. The governing non-linear partial differential equations have been reduced into the coupled non-linear ordinary differential equations by the similarity transformations. Analytical and numerical solutions of the derived system of equations are developed. The homotopy analysis method (HAM) and finite difference scheme are employed in constructing the analytical and numerical solutions, respectively. Comparison between the analytical and numerical solutions is given and found in an excellent agreement. Both cases of assisting and opposing flows are considered. The influence of the various interesting parameters on the flow and heat transfer are analyzed and discussed through graphs in detail. The values of the local Nusselt number for different physical parameters are also tabulated. Comparison of the present results with known numerical results of viscous fluid is shown and noted a very

good agreement.

6.1 Physical model and governing equations

Here we examine the steady, two-dimensional stagnation-point flow of an incompressible Maxwell fluid adjacent a vertical stretching surface which coincides with the plane $y = 0$ of a Cartesian system of coordinate Oxy ($y = 0$) with the x-axis along the sheet (see Fig. 6.1). The Maxwell fluid occupies the half plane ($y > 0$). Two equal and opposite forces are applied along the x-axis so that the surface is stretched keeping the origin fixed. It is assumed that the velocity $u_w(x) = cx$, where c (> 0) is the constant or the stretching rate and the temperature $T_w(x)$ of the stretching sheet is proportional to the distance x from the stagnation-point, where $T_w(x) > T_\infty$ with T_∞ being the uniform temperature of the ambient fluid. The velocity of the flow external to the boundary layer is $u_e(x) = ax$, where a (> 0) is the constant. Under these assumptions along with the Boussinesq and boundary layer approximations, the governing equations for Maxwell fluid are [35, 89]:

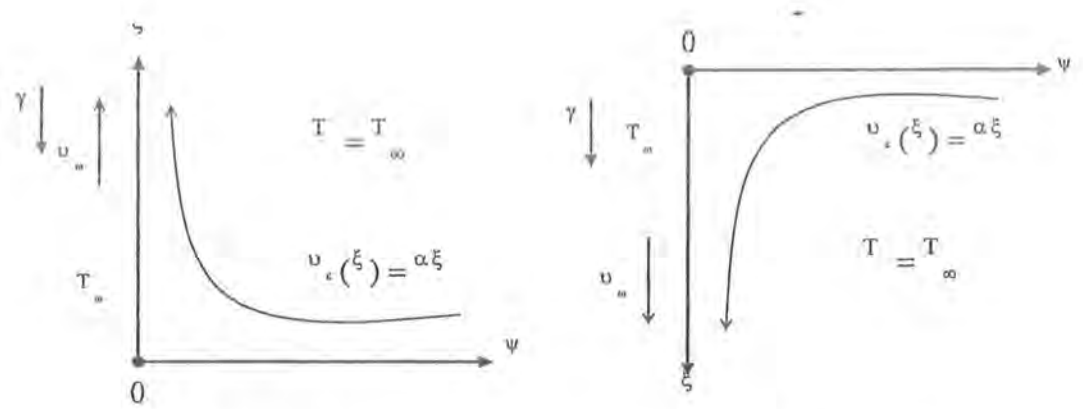

(a) Assisting flow (b) Opposing flow

Fig. 6.1. Geometry of flow and coordinate system

$$\frac{\partial u}{\partial x} + \frac{\partial v}{\partial y} = 0, \tag{6.1}$$

$$u\frac{\partial u}{\partial x}+v\frac{\partial u}{\partial y}+\lambda_1\left[u^2\frac{\partial^2 u}{\partial x^2}+v^2\frac{\partial^2 u}{\partial y^2}+2uv\frac{\partial^2 u}{\partial x\partial y}\right]=u_e\frac{du_e}{dx}+\nu\frac{\partial^2 u}{\partial y^2}\pm g_c\beta_T\left(T-T_\infty\right), \quad (6.2)$$

$$\frac{\partial \widetilde{p}}{\partial y}=O(\delta_1), \quad (6.3)$$

$$\rho c_p\left(u\frac{\partial T}{\partial x}+v\frac{\partial T}{\partial y}\right)=\alpha\frac{\partial^2 T}{\partial y^2}, \quad (6.4)$$

where u, v are the velocity components in the $x-$ and y-directions, respectively, ν is the kinematic viscosity of fluid, $\widetilde{p}$ is the pressure, ρ is the density of fluid, λ_1 is the relaxation time, g_c is the gravitational acceleration, β_T is the thermal expansion coefficient, c_p is the specific heat, α is the thermal diffusivity, T is the temperature and δ_1 being the boundary layer thickness. Here the "+" sign in Eq. (6.2) corresponds to the assisting flow while the "−" sign corresponds to the opposing flow, respectively.

The appropriate boundary conditions are

$$u = u_w(x)=cx, \quad v=0, \quad T=T_w(x)=T_\infty+b_1x \quad \text{at} \quad y=0, \quad (6.5)$$

$$u = u_e(x)=ax, \quad T=T_\infty \quad \text{as} \quad y\to\infty \quad (6.6)$$

in which b_1 is the positive constant.

To examine the flow regime, the following similarity variables are introduced

$$\eta=\sqrt{\frac{c}{\nu}}y, \quad u=cxf'(\eta), \quad v=-\sqrt{\nu c}f(\eta), \quad \theta(\eta)=\frac{T-T_\infty}{T_w-T_\infty}. \quad (6.7)$$

Using above equation, the continuity Eq. (6.1) is satisfied automatically and Eqs. (6.2) and (6.4) with boundary conditions (6.5) and (6.6)are

$$f'''-f'^2+ff''+\frac{a^2}{c^2}\pm\lambda\theta+\beta\left(2ff'f''-f^2f'''\right)=0, \quad (6.8)$$

$$\theta''+\mathrm{Pr}\left(f\theta'-\theta f'\right)=0, \quad (6.9)$$

$$f = 0, \quad f'=1, \quad \theta=1 \quad \text{at} \quad \eta=0 \quad (6.10)$$

$$f' = \frac{a}{c}, \quad \theta=0 \quad \text{as} \quad \eta\to\infty \quad (6.11)$$

Here primes denote differentiation with respect to η and the Deborah number $\beta = \lambda_1 c$, the Prandtl number $\Pr = \mu c_p/\alpha$ and the constant λ (≥ 0) is the buoyancy or mixed convection parameter defined as

$$\lambda = \frac{Gr_x}{\mathrm{Re}_x^2} \tag{6.12}$$

with $Gr_x = g\beta_T (T_w - T_\infty) x^3/\nu^2$ is the local Grashof number and $\mathrm{Re}_x = u_w x/\nu$ is the local Reynolds number. When $\lambda = 0$ and $a/c = 1$, the solution of Eq. (6.8) subject to boundary condition (6.10) and (6.11) is

$$f(\eta) = \eta. \tag{6.13}$$

The physical quantity of interest is the local Nusselt number Nu_x defined by

$$Nu_x = \frac{x q_w}{\alpha (T_w - T_\infty)}, \tag{6.14}$$

where q_w is the heat transfer from the plate i.e.

$$q_w = -\alpha \left(\frac{\partial T}{\partial y}\right)_{y=0}. \tag{6.15}$$

Using variables (6.7), we get

$$\mathrm{Re}_x^{-1/2} Nu_x = -\theta'(0). \tag{6.16}$$

In the next two sections, we will present the analytical and numerical solution of Eqs. (6.8) – (6.11).

6.2 Homotopy analysis of the governing problem

In this section, we solve Eqs. (6.8) and (6.9) by means of homotopy analysis method and discuss the convergence of the HAM solution.

6.2.1 Homotopy analysis solution

For the series solutions of Eqs. (6.8) and (6.9) using homotopy analysis method (HAM), it is obvious that the velocity and the temperature profiles $f(\eta)$ and $\theta(\eta)$ can be expressed by the set of base functions

$$\left\{ \eta^k \exp\left(-n\eta\right) \middle| \, k \geq 0, n \geq 0 \right\} \tag{6.17}$$

in the form

$$f\left(\eta\right) = a_{0,0}^{0} + \sum_{n=0}^{\infty} \sum_{k=0}^{\infty} a_{m,n}^{k} \eta^k \exp\left(-n\eta\right), \tag{6.18}$$

$$\theta\left(\eta\right) = \sum_{n=0}^{\infty} \sum_{k=0}^{\infty} b_{m,n}^{k} \eta^k \exp\left(-n\eta\right), \tag{6.19}$$

where $a_{m,n}^{k}$ and $b_{m,n}^{k}$ are the coefficients. These provide us with *solution expressions* of $f(\eta)$ and $\theta(\eta)$, respectively. With the help of boundary conditions (6.10) and (6.11) and the *solution expressions*, one can choose $f_0\left(\eta\right)$ and $\theta_0\left(\eta\right)$ as

$$f_0\left(\eta\right) = \frac{a}{c}\eta + \left(1 - \frac{a}{c}\right)\left(1 - \exp(-\eta)\right), \tag{6.20}$$

$$\theta_0\left(\eta\right) = \exp(-\eta) \tag{6.21}$$

as the initial guess approximations of $f(\eta)$ and $\theta(\eta)$ and

$$\mathcal{L}_f(f) = \frac{d^3 f}{d\eta^3} - \frac{df}{d\eta}, \tag{6.22}$$

$$\mathcal{L}_\theta(f) = \frac{d^2 f}{d\eta^2} - f, \tag{6.23}$$

are the auxiliary linear operators having the following properties

$$\mathcal{L}_f\left[C_1 + C_2 \exp(\eta) + C_3 \exp(-\eta)\right] = 0, \tag{6.24}$$

$$\mathcal{L}_\theta\left[C_4 \exp(\eta) + C_5 \exp(-\eta)\right] = 0, \tag{6.25}$$

respectively, and C_i $(i = 1 - 5)$ are arbitrary constants. If $\hbar_f$ and $\hbar_\theta$ denote the non-zero auxiliary parameters then the zeroth-order deformation problems are constructed as follows:

$$\left(1 - p\right)\mathcal{L}_f\left[\widehat{f}\left(\eta; p\right) - f_0\left(\eta\right)\right] = p\hbar_f \mathcal{N}_f\left[\widehat{f}\left(\eta; p\right), \widehat{\theta}\left(\eta; p\right)\right], \tag{6.26}$$

$$(1-p)\,\mathcal{L}_\theta\left[\widehat{\theta}(\eta;p)-\theta_0(\eta)\right]=p\hbar_\theta\mathcal{N}_\theta\left[\widehat{f}(\eta;p),\widehat{\theta}(\eta;p)\right], \tag{6.27}$$

$$\widehat{f}(0;p)=0,\qquad \left.\frac{d\widehat{f}(\eta;p)}{d\eta}\right|_{\eta=0}=1,\qquad \left.\frac{d\widehat{f}(\eta;p)}{d\eta}\right|_{\eta=\infty}=\frac{a}{c}, \tag{6.28}$$

$$\widehat{\theta}(0;p)=1,\quad \widehat{\theta}(\infty;p)=0, \tag{6.29}$$

where $p\in[0,1]$ is an embedding parameter and the nonlinear operators $\mathcal{N}_f$ and $\mathcal{N}_\theta$ are

$$\begin{aligned}\mathcal{N}_f\left[\widehat{f}(\eta;p),\widehat{\theta}(\eta;p)\right] &= \frac{\partial^3\widehat{f}(\eta,p)}{\partial\eta^3}-\left(\frac{\partial\widehat{f}(\eta,p)}{\partial\eta}\right)^2+\widehat{f}(\eta,p)\frac{\partial^2\widehat{f}(\eta,p)}{\partial\eta^2}+\frac{a^2}{c^2}\pm\lambda\widehat{\theta}(\eta;p)\\ &\quad+\beta\left\{2\widehat{f}(\eta,p)\frac{\partial\widehat{f}(\eta,p)}{\partial\eta}\frac{\partial^2\widehat{f}(\eta,p)}{\partial\eta^2}-\left(\widehat{f}(\eta,p)\right)^2\frac{\partial^3\widehat{f}(\eta,p)}{\partial\eta^3}\right\},\end{aligned} \tag{6.30}$$

$$\mathcal{N}_\theta\left[\widehat{f}(\eta;p),\widehat{\theta}(\eta;p)\right]=\frac{\partial^2\widehat{\theta}(\eta;p)}{\partial\eta^2}+\Pr\left(\widehat{f}(\eta;p)\frac{\partial\widehat{\theta}(\eta;p)}{\partial\eta}-\frac{\partial\widehat{f}(\eta;p)}{\partial\eta}\widehat{\theta}(\eta;p)\right). \tag{6.31}$$

For $p=0$ and $p=1$, the above zeroth-order deformation Eqs. (6.26) and (6.27) have the solutions

$$\widehat{f}(\eta;0)=f_0(\eta),\qquad \widehat{f}(\eta;1)=f(\eta), \tag{6.32}$$

$$\widehat{\theta}(\eta;0)=\theta_0(\eta),\qquad \widehat{\theta}(\eta;1)=\theta(\eta). \tag{6.33}$$

Expanding $\widehat{f}(\eta;p)$ and $\widehat{\theta}(\eta;p)$ in Taylor's series with respect to p, we have

$$\widehat{f}(\eta;p)=f_0(\eta)+\sum_{m=1}^{\infty}f_m(\eta)\,p^m, \tag{6.34}$$

$$\widehat{\theta}(\eta;p)=\theta_0(\eta)+\sum_{m=1}^{\infty}\theta_m(\eta)\,p^m, \tag{6.35}$$

where

$$f_m(\eta)=\frac{1}{m!}\left.\frac{\partial^m\widehat{f}(\eta;p)}{\partial p^m}\right|_{p=0},\qquad \theta_m(\eta)=\frac{1}{m!}\left.\frac{\partial^m\widehat{\theta}(\eta;p)}{\partial p^m}\right|_{p=0}. \tag{6.36}$$

Note that the zeroth-order deformation Eqs. (6.26) and (6.27) contain two auxiliary parameters $\hbar_f$ and $\hbar_\theta$. The convergence of the series (6.26) and (6.27) depend on these parameters. Assuming that $\hbar_f$ and $\hbar_\theta$ are selected such that the above series are convergent at $p=1$, then

using Eqs. (6.32) and (6.33), the series solutions are

$$f(\eta) = f_0(\eta) + \sum_{m=1}^{\infty} f_m(\eta), \tag{6.37}$$

$$\theta(\eta) = \theta_0(\eta) + \sum_{m=1}^{\infty} \theta_m(\eta). \tag{6.38}$$

Differentiate the zeroth-order deformation equations (6.26) and (6.27) m times with respect to p, then setting $p = 0$, and finally dividing them by $m!$, we obtain the mth-order deformations equations

$$\mathcal{L}_f[f_m(\eta) - \chi_m f_{m-1}(\eta)] = \hbar_f \mathcal{R}_m^f(\eta), \tag{6.39}$$

$$\mathcal{L}_\theta[\theta_m(\eta) - \chi_m \theta_{m-1}(\eta)] = \hbar_\theta \mathcal{R}_m^\theta(\eta), \tag{6.40}$$

$$f_m(0) = \left.\frac{df_m(\eta;0)}{d\eta}\right|_{\eta=0} = \left.\frac{df_m(\eta;0)}{d\eta}\right|_{\eta=\infty} = 0, \tag{6.41}$$

$$\theta_m(0) = \theta_m(\infty) = 0, \tag{6.42}$$

where

$$\mathcal{R}_m^f(\eta) = f_{m-1}'''(\eta) + (1-\chi_m)\frac{a^2}{c^2} \pm \lambda\theta_{m-1}(\eta) + \sum_{k=0}^{m-1}\left[\begin{array}{c} f_{m-1-k}f_k'' - f_{m-1-k}'f_k' \\ +\beta f_{m-1-k}\sum_{l=0}^{k}\left\{2f_{k-l}'f_l'' - f_{k-l}f_l'''\right\} \end{array}\right], \tag{6.43}$$

$$\mathcal{R}_m^\theta(\eta) = \theta_{m-1}''(\eta) + \Pr\sum_{k=0}^{m-1}\left[\theta_{m-1-k}'f_k - \theta_{m-1-k}f_k'\right], \tag{6.44}$$

$$\chi_m = \begin{cases} 0, & m \le 1, \\ 1, & m > 1. \end{cases} \tag{6.45}$$

If we let $f_m^\star(\eta)$ and $\theta_m^\star(\eta)$ as the special solutions of Eqs. (6.39) and (6.40) then from Eqs. (6.39) and (6.40), the general solutions are given by

$$f_m(\eta) = f_m^*(\eta) + C_1 + C_2\exp(\eta) + C_3\exp(-\eta), \tag{6.46}$$

$$\theta_m(\eta) = \theta_m^*(\eta) + C_4 \exp(\eta) + C_5 \exp(-\eta), \tag{6.47}$$

where the integral constants C_i $(i = 1 - 5)$ are determined by the boundary conditions (6.41) and (6.42) as

$$C_2 = C_5 = 0, \quad C_3 = \left.\frac{\partial f_m^*(\eta)}{\partial \eta}\right|_{\eta=0}, \quad C_1 = -C_3 - f_m^*(0), \quad C_4 = -\theta_m^*(0). \tag{6.48}$$

In this way, it is easy to solve the linear non-homogeneous Eqs. (6.39) and (6.40) by using Mathematica one after the other in the order $m = 1, 2, 3.....$

6.2.2 Convergence of the HAM solution

As proved by Liao [90] that, as long as a solution series given by the homotopy analysis method converge, it must be one of the solutions. Therefore, it is important to ensure that the solutions series are convergent. The series solutions (6.37) and (6.38) contain the non-zero auxiliary parameters $\hbar_f$ and $\hbar_\theta$, which can be chosen properly by plotting the so-called $\hbar$-curves to ensure the convergence of the solutions series and rate of approximation of the HAM solution. To see the range for admissible values of $\hbar_f$ and $\hbar_\theta$, $\hbar$-curves of $f''(0)$ and $\theta'(0)$ are shown in Fig. 6.2 for 15th-order of approximation when $a/c = 0.3$, $\mathrm{Pr} = 0.5$, $\lambda = 0.2$ and $\beta = 0.2$ for both cases of assisting and opposing flows. From this figure, it can be seen that $\hbar$-curves have a parallel lines segment that correspond to the regions $-2.2 \leq \hbar_f \leq -0.2$ and $-1.8 \leq \hbar_\theta \leq -0.3$ (for assisting flow) and $-2 \leq \hbar_f \leq -0.3$ and $-1.8 \leq \hbar_\theta \leq -0.2$ (for opposing flow), respectively. To assure the convergence of the HAM solution, the values of $\hbar_f$ and $\hbar_\theta$ should be chosen from these regions. The region for the values of $\hbar_f$ and $\hbar_\theta$ is dependent on the values of involving parameters. Our calculations depict that the solutions series (6.37) and (6.38) converge in the whole region of η if it is convergent at $\eta = 0$ when the proper values of $\hbar_f$ and $\hbar_\theta$ are chosen.

(a)

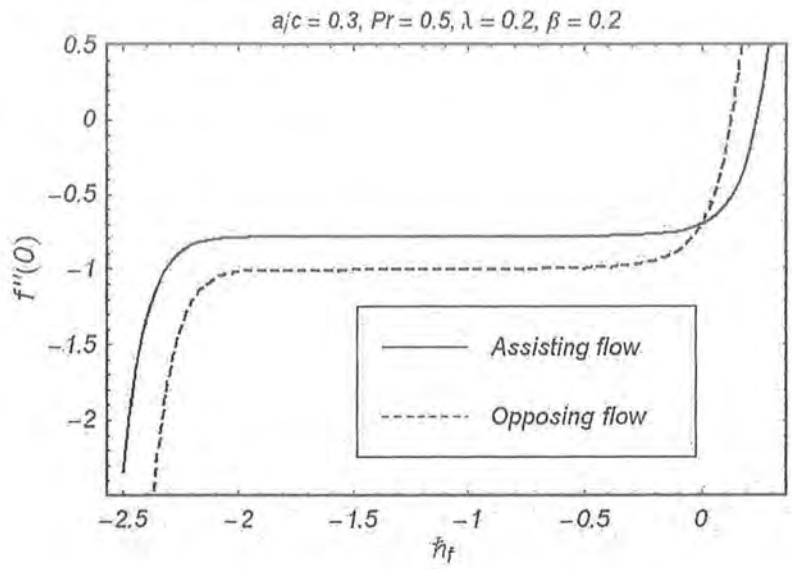

(b)

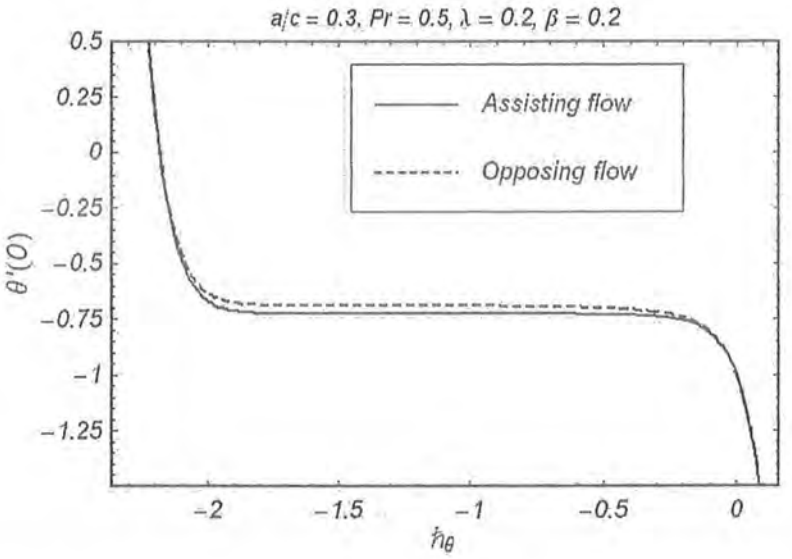

Fig. 6.2. The $\hbar$-curves of $f''(0)$ and $\theta'(0)$ at the 15th-order of approximation with $a/c = 0.3$, $\mathrm{Pr} = 0.5$, $\lambda = 0.2$ and $\beta = 0.2$.

6.3 Numerical method

Besides the HAM solution, the boundary-layer problem consisting of Eqs. (6.8) – (6.11) are also solved numerically.

Usually, there exist two methods numerically handling flow problems in a semi-infinite domain. The one is by a coordinate transformation, e.g. $\xi = 1/(\eta + 1)$, to transform the semi-infinite physical domain, $\eta \in [0, \infty)$, to a finite calculation domain, $\xi \in [0, 1]$. For the present problem, due to the boundary condition $f' = a/c$ at $\eta \to \infty$, which yields $f \to \infty$ at $\eta \to \infty$ in case of $a \neq 0$, a numerical simulation up to $\to \infty$ is impossible. Therefore, we will not employ the method of coordinate transformation.

The other method is by truncating the semi-infinite domain to obtain approximate solutions. The semi-infinite domain $\eta \in [0, \infty)$ is replaced by a finite domain $\eta \in [0, L]$ and the boundary conditions at infinity $\eta \to \infty$ are enforced at $\eta = L$. The extent of the domain L is chosen in such a manner that any increase in the domain does not significantly alter the solution.

We intend to find direct numerical solutions of the differential system (6.8) – (6.11) by means of a suitable numerical technique for a finite calculation domain $\eta \in [0, L]$. Because the differential equation (6.8) is nonlinear in f, we cannot solve this boundary value problem by the direct finite-difference method. In solving such nonlinear equation, iterative methods are commonly used.

We can define an iterative procedure determining a sequence of functions $f^{(0)}(\eta)$, $f^{(1)}(\eta)$, $f^{(2)}(\eta)$,..... and $\theta^{(0)}(\eta)$, $\theta^{(1)}(\eta)$, $\theta^{(2)}(\eta)$,.....in the following manner: $f^{(0)}(\eta)$ and $\theta^{(0)}(\eta)$ are chosen arbitrarily, then $f^{(1)}(\eta)$, $f^{(2)}(\eta)$,..... and $\theta^{(1)}(\eta)$, $\theta^{(2)}(\eta)$,.....are calculated successively from the following iteration steps

$$f^{(n+1)'''} - f^{(n)\prime} f^{(n+1)\prime} + f^{(n)} f^{(n+1)''} + \frac{a^2}{c^2} \pm \lambda\theta^{(n)} + \beta\left(2f^{(n)} f^{(n)\prime} f^{(n+1)''} - f^{(n)2} f^{(n+1)'''}\right) = 0, \tag{6.49}$$

$$\theta^{(n+1)''} + \mathrm{Pr}\left(f^{(n)}\theta^{(n+1)\prime} - f^{(n)\prime}\theta^{(n+1)}\right) = 0 \tag{6.50}$$

with the boundary conditions

$$f^{(n+1)} = 0, \quad f^{(n+1)\prime} = 1, \quad \theta^{(n+1)} = 1 \quad \text{at} \quad \eta = 0,$$

$$f^{(n+1)\prime} = \frac{a}{c}, \qquad \theta^{(n+1)} = 0 \quad \text{at} \quad \eta = L, \tag{6.51}$$

which yield two linear differential boundary value problems for each iteration step $n+1$ and can be numerically solved by a direct different method. It is easy to confirm that if the indices (n) and $(n+1)$ are withdrawn, the differential equations (6.49) and (6.50) as well as the boundary conditions (6.51) are consistent with the original differential equations (6.8) and (6.9) as well as the boundary conditions(6.10) and (6.11) (if $L \to \infty$).

The iteration steps are carried out until convergent solutions are reached. The effectiveness of the method is often influenced considerably by the form of the arrangement for the iteration steps (n) and $(n+1)$ in Eqs. (6.49) and (6.50), which are not sole, and by the choice of the starting functions $f^{(0)}(\eta)$ and $\theta^{(0)}(\eta)$; the method is generally more effective the closer $f^{(0)}(\eta)$ and $\theta^{(0)}(\eta)$ are to the solutions $f(\eta)$, $\theta(\eta)$, respectively.

Usually, in order to achieve a better convergence, the so-called method of successive under-relaxation is used. We solve the Eqs. (6.49) and (6.50) for the iterative step $(n+1)$ to obtain an estimated value of $f^{(n+1)}$, $\widetilde{f}^{(n+1)}$, and an estimated value of $\theta^{(n+1)}$, $\widetilde{\theta}^{(n+1)}$, then $f^{(n+1)}$ and $\theta^{(n+1)}$ are defined by the formulas

$$\left.\begin{aligned} f^{(n+1)} &= f^{(n)} + \tau\left(\widetilde{f}^{(n+1)} - f^{(n)}\right), \\ \theta^{(n+1)} &= \theta^{(n)} + \tau\left(\widetilde{\theta}^{(n+1)} - \theta^{(n)}\right) \end{aligned}\right\} \; 0 < \tau \leq 1, \tag{6.52}$$

where $\tau \in (0,1]$ is a real under-relaxation parameter. We should choose τ so small that convergent iteration is reached. The iteration should be carried out until the relative differences of the computed $f^{(n)}$, $f^{(n+1)}$ as well as $\theta^{(n)}$, $\theta^{(n+1)}$ between two consecutive iterative steps (n) and $(n+1)$ are smaller than a given error chosen to be 10^{-10}.

6.4 Discussion of the results

We calculated the velocity and temperature profiles by solving equations (6.8) and (6.9) with boundary conditions (6.10) and (6.11) both analytically (using the analytic technique homotopy analysis method (HAM)) and numerically (using finite difference scheme). The velocity filed $f'(\eta)$ and the temperature profile $\theta(\eta)$ are plotted to see the influence of the various interesting parameters, for example, the Deborah number β, the Prandtl number Pr, the buoyancy/mixed

convection parameter λ and a/c in both cases of assisting and opposing flows, respectively. The effects of various parameters on the local Nusselt number $\mathrm{Re}_x^{-1/2} Nu_x$ are also discussed through graphs. The values of $f''(0)$ and the local Nusselt number $\mathrm{Re}_x^{-1/2} Nu_x$ are given for different involving parameters in tabular form for viscous ($\beta = 0$) and non-Newtonian ($\beta \neq 0$) fluids in both cases of assisting and opposing flows.

Fig. 6.3 compares the homotopy analytic solutions to the numerical solutions for the velocity field $f'(\eta)$ and the temperature profile $\theta(\eta)$ when $\beta = 0.5$, $\lambda = 0.5$, $a/c = 0.5$ and $\mathrm{Pr} = 1$ in both cases of assisting and opposing flows. It is noted that the homotopy analysis method (HAM) has an excellent agreement with numerical solution is a sufficiently high order of approximation in the HAM solution is employed. As shown in Fig. 6.3, for the investigated case, the homotopy analytic solution for the velocity $f'(\eta)$ and temperature profile $\theta(\eta)$ has an excellent agreement to the numerical solution in both cases of assisting and opposing flows, if the 15th and 10th-order of approximations are employed in the HAM solution, respectively.

In the following discussions we will present only the numerical solutions.

Figs. 6.4 and 6.5 are illustrated to observe the effects of the Deborah number β, the Prandtl number Pr, the buoyancy/mixed convection parameter λ and a/c on the velocity component $f'(\eta)$ for both the assisting and opposing flows, respectively. Generally, if $a/c = 1$, indicating the velocity $f'(\eta)$ at the wall is equal to that far apart from the wall, a deviation of the velocity from $f' = 1$ occurs only within the boundary layer near the wall. As may be expected, for the assisting flow, $f' > 1$ in boundary layer, because the thermal expansion caused by the high wall temperature assists the flow. On the contrary, for the opposing flow, $f' < 1$ in this boundary layer due to the resistance of the thermal expansion to the flow. Such flow behaviors can be seen in Figs. 6.4a,b and 6.5a. As shown in these Figs., the magnitude of the flow deviation from $f' = 1$ in the boundary layer depends on the values of the material parameters. With the increase of the Deborah number β or the relaxation time, the velocity deviation decreases, as displayed in Fig. 6.4a. It may be expected that for $\beta \to \infty$, $f' = 1$ in the whole flow domain. Fig. 6.4(b) shows that increasing the Prandtl number Pr causes the decrease of the flow deviation from $f' = 1$. This is because increasing the Prandtl number Pr indicates the increase of the fluid heat capacity or the decrease of the thermal diffusivity, hence causes a diminution of the influence of the thermal expansion to the flow. For both assisting and

opposing flows as β and Pr increases, the boundary layer thickness decreases.

The buoyancy or mixed convection parameter λ represents the ability of the fluid thermal expansion or the coupling of the temperature field to the velocity field. Increasing λ will amplify the effect of the temperature variation on the velocity field, increase the buoyancy force, and hence cause the increase of the velocity deviation and the increase of the boundary layer thickness, as shown in Fig. 6.5a. When $a/c \neq 1$, the flow velocity f' changes from $f' = 1$ at the wall to $f' = a/c$ far away from the wall, as we can see from Fig. 6.5b. In the transition region/the boundary layer the assisting flow possesses larger velocity values than for the opposing flow. It is interesting to note that the boundary layer thickness is decreased when a/c is increased. According to studies [145, 146], it can be explained as follows: for a fixed values of c corresponding to the stretching of the surface, an increase in a implies an increase in straining motion near the stagnation region resulting in increased acceleration of the external stream and this leads to thinning of the boundary layer by increasing a/c.

The influence of the Deborah number β, the Prandtl number Pr, the buoyancy/mixed convection parameter λ and a/c on the temperature field $\theta(\eta)$ can be seen from Figs. 6.6 and 6.7. Comparison of Figs. 6.6a and 6.7b with Figs. 6.4a and 6.5b shows that the temperature field is much less intensive to the variations of the Deborah number β and the buoyancy or mixed convection parameter λ. The obvious dependence of the temperature field on a/c and the Prandtl number Pr can be identified from Figs. 6.6b and 6.7a. With the increase of a/c and Pr, the boundary layer thickness of the temperature decreases, similar to that for the velocity boundary layer. Generally, the difference between the assisting and opposing flows is still visible, but not so obvious as in the velocity field.

The local Nusselt number $Nu_x \operatorname{Re}_x^{1/2}$ is the physical quantity of interest in practical applications. This describes the heat transfer from the wall, respectively. Fig. 6.8 is illustrated to show the effects of the Deborah number β and the Prandtl number Pr on $Nu_x \operatorname{Re}_x^{1/2}$ with the different values of the buoyancy parameter λ for both cases of assisting and opposing flows, respectively. It can be seen from Fig. 6.8 that the local Nusselt number (or the heat transfer near the wall) for the assisting flow is larger than that of the opposing flow. The wall heat transfer increases with the increase of the Deborah number β for the opposing flow. The assisting flow behaves on the contrary, increasing β decreases the heat transfer near the wall, as displayed in

Fig. 6.8a. Furthermore, for both the assisting and opposing flows, the Nusselt number increases substantially by increasing the Prandtl number Pr (Fig. 6.8b).

In Table 6.1 the values of $f''(0)$ obtained by other different authors are compared to our results obtained by the homotopy analysis method and the numerical simulation for the case of a viscous fluid ($\beta = 0$) in the absence of the buoyancy force $\lambda = 0$ (i.e. no heat transfer). It demonstrates an excellent agreement of our (HAM and numerical) results with the existing simple results in the references [145 – 147] in such a simple flow case.

Table 6.2 gives the numerical values of the local Nusselt number $Nu_x \operatorname{Re}_x^{1/2}$ for different values of β and Pr for the non-Newtonian fluid ($\beta \neq 0$) investigated here in presence of buoyancy force $\lambda = 1$. The local Nusselt number $Nu_x \operatorname{Re}_x^{1/2}$ increases with an increase of Pr for both the assisting and opposing flows, but decreases for the assisting flow and increases for the opposing flow with the increase of β. The results are consistent with the previous graphic representations.

Table 6.3 shows a comparison of the values of $f''(0)$ and the local Nusselt number $Nu_x \operatorname{Re}_x^{1/2}$ of the present numerical results with the existing numerical results presented in [146] also for a viscous fluid ($\beta = 0$) as in Table 6.1 but in the presence of the buoyancy force ($\lambda = 1$). We can see that both results have a good agreement. It is also noted that the magnitude of $f''(0)$ decreases when Pr increases, however, the magnitude of $Nu_x \operatorname{Re}_x^{1/2}$ increases with the increase of Pr in both assisting and opposing flows, as we have observed in the previous graphics.

6.5 Final remarks

In the present study, the stagnation-point flow of an upper-convected Maxwell fluid in the presence of the buoyancy force due to the heat transfer is investigated by means of both the homotopy analysis method and the finite difference scheme with an iterative technique. The comparison of the solutions shows an excellent agreement of the results obtained from both the methods. The numerical results for various material parameters are displayed and discussed. For a Newtonian fluid, the results are reduced to the existing results obtained by other authors.

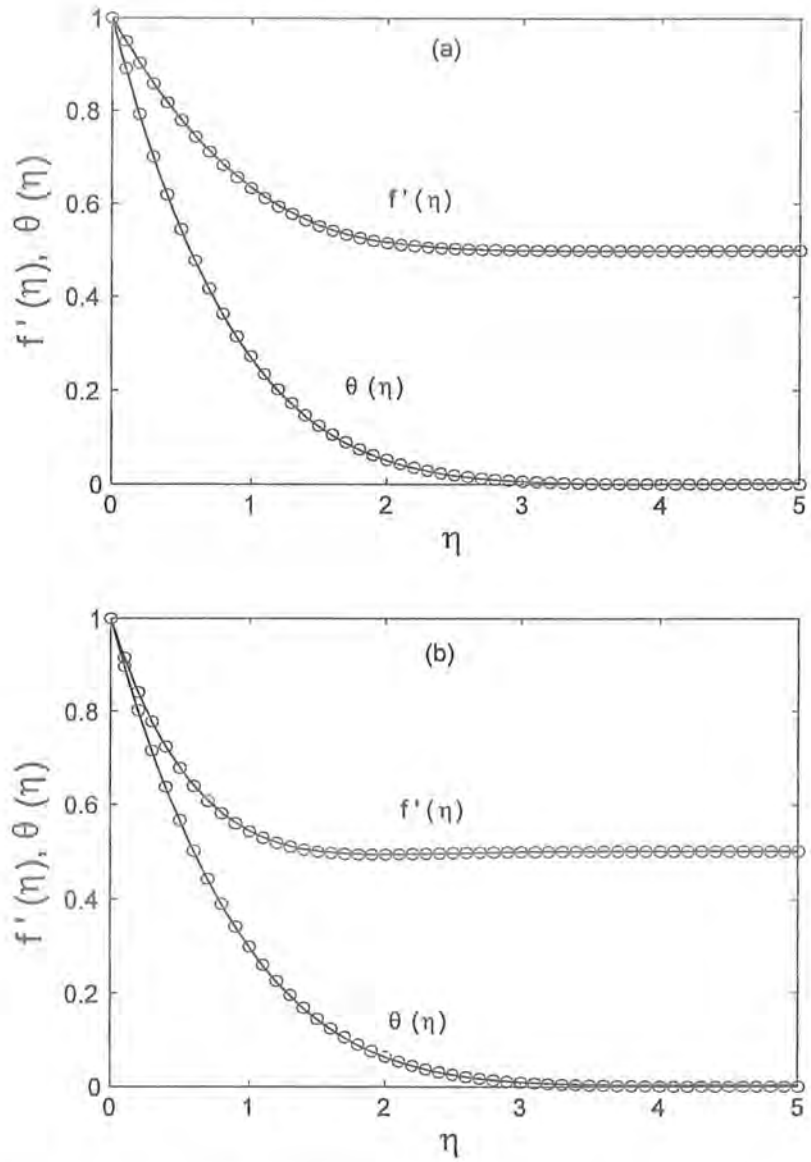

Fig. 6.3. Comparison of $f'(\eta)$ and $\theta(\eta)$ obtained from the HAM solution (solid lines: for $f'(\eta)$ at the 15th and for $\theta(\eta)$ at the 10th-order of approximation) and the numerical solution (open circles) with $\beta = 0.5$, $\lambda = 0.5$, $a/c = 0.5$ and $\mathrm{Pr} = 1$ (a) for assisting flow case and (b) for opposing flow case, respectively.

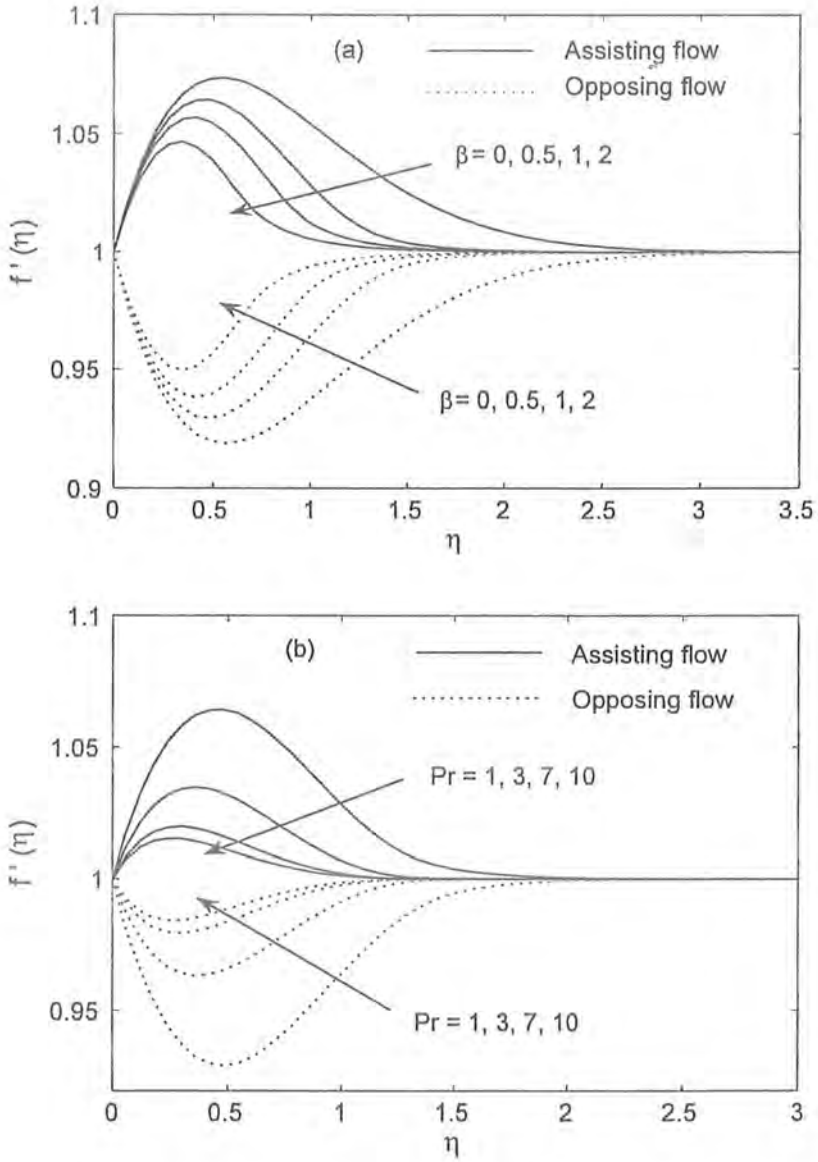

Fig. 6.4. Velocity profile $f'(\eta)$ verses η: (a) effects of the Deborah number β when $a/c = 1$, $\lambda = 1$ and $\mathrm{Pr} = 1$ and (b) effects of the Prandtl number Pr when $a/c = 1$, $\lambda = 1$ and $\beta = 0.5$.

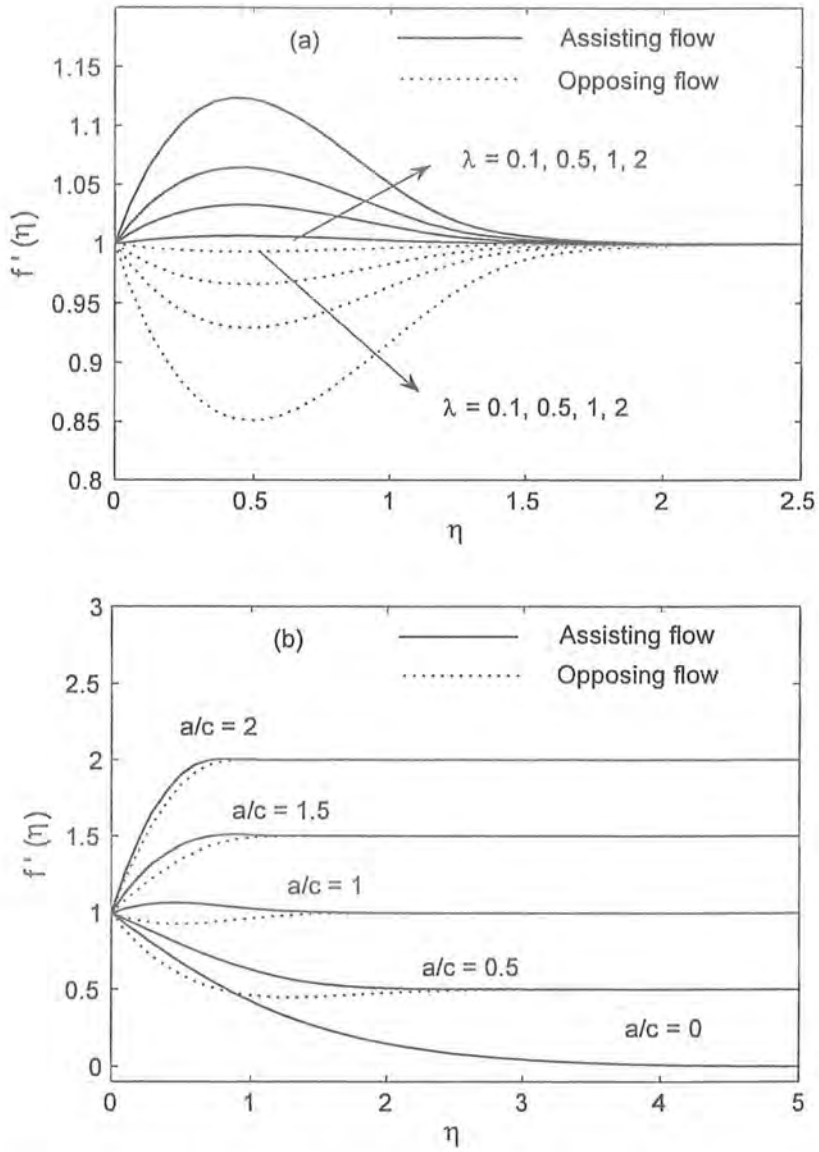

Fig. 6.5. Velocity profile $f'(\eta)$ verses η: (a) effects of the mixed convection parameter λ when $a/c = 1$, $\beta = 0.5$ and $\mathrm{Pr} = 1$ and (b) effects of a/c when $\mathrm{Pr} = 1$, $\lambda = 1$ and $\beta = 0.5$.

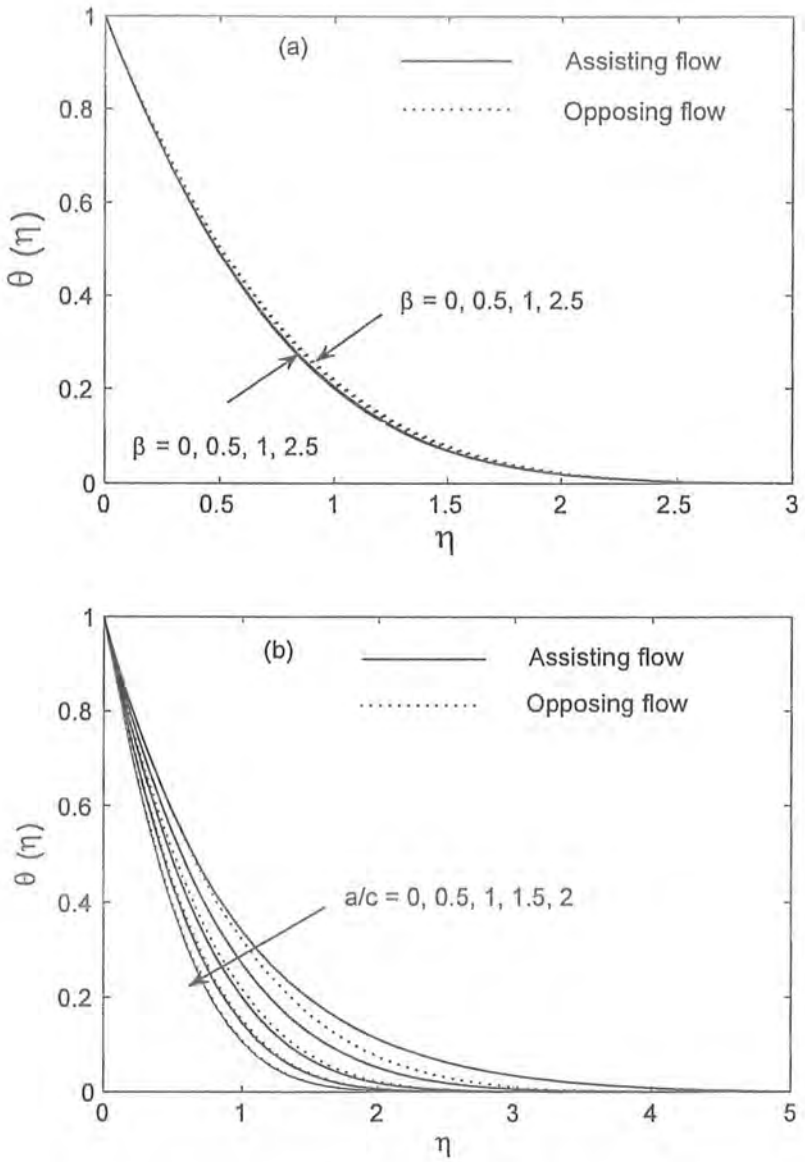

Fig. 6.6. Temperature profile $\theta(\eta)$ verses η: (a) effects of the Deborah number β when $a/c = 1$, $\lambda = 1$ and $\mathrm{Pr} = 1$ and (b) effects of a/c when $\mathrm{Pr} = 1$, $\lambda = 1$ and $\beta = 0.5$.

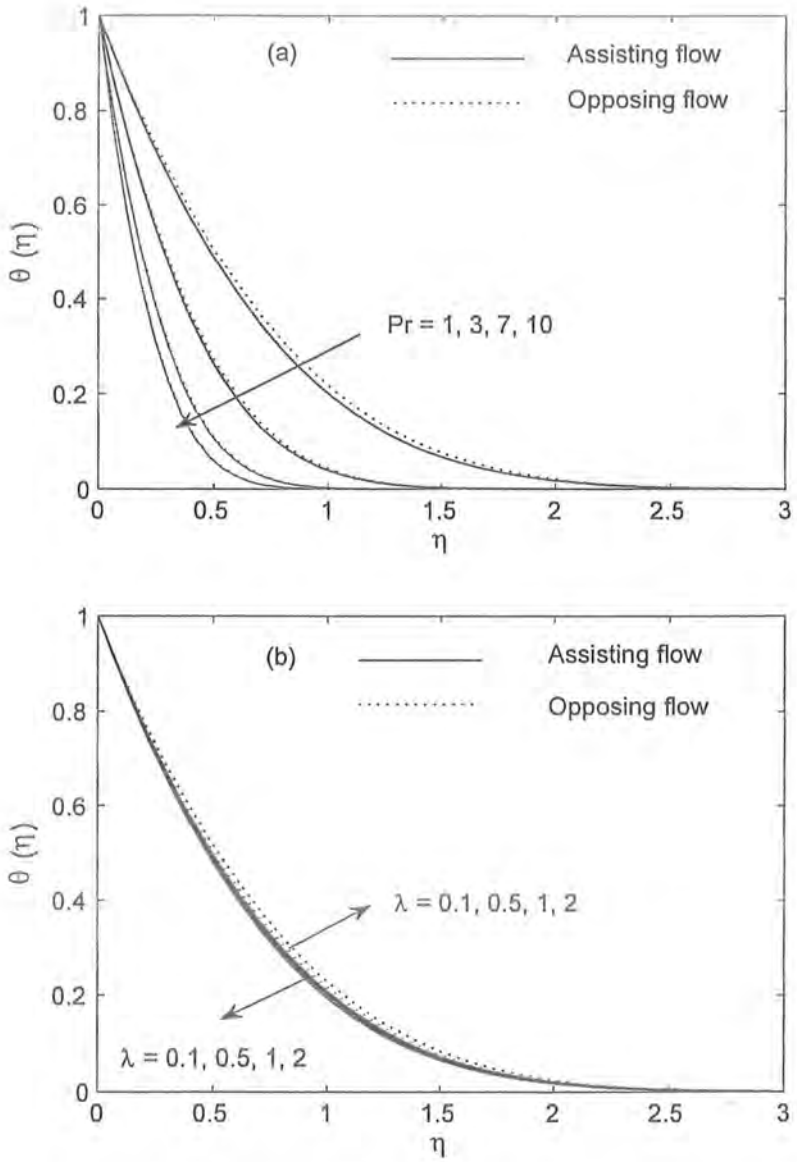

Fig. 6.7. Temperature profile $\theta(\eta)$ verses η: (a) effects of the Prandtl number Pr when $a/c = 1$, $\lambda = 1$ and $\beta = 0.5$ and (b) effects of mixed convection parameter λ when $\mathrm{Pr} = 1$, $a/c = 1$ and $\beta = 0.5$.

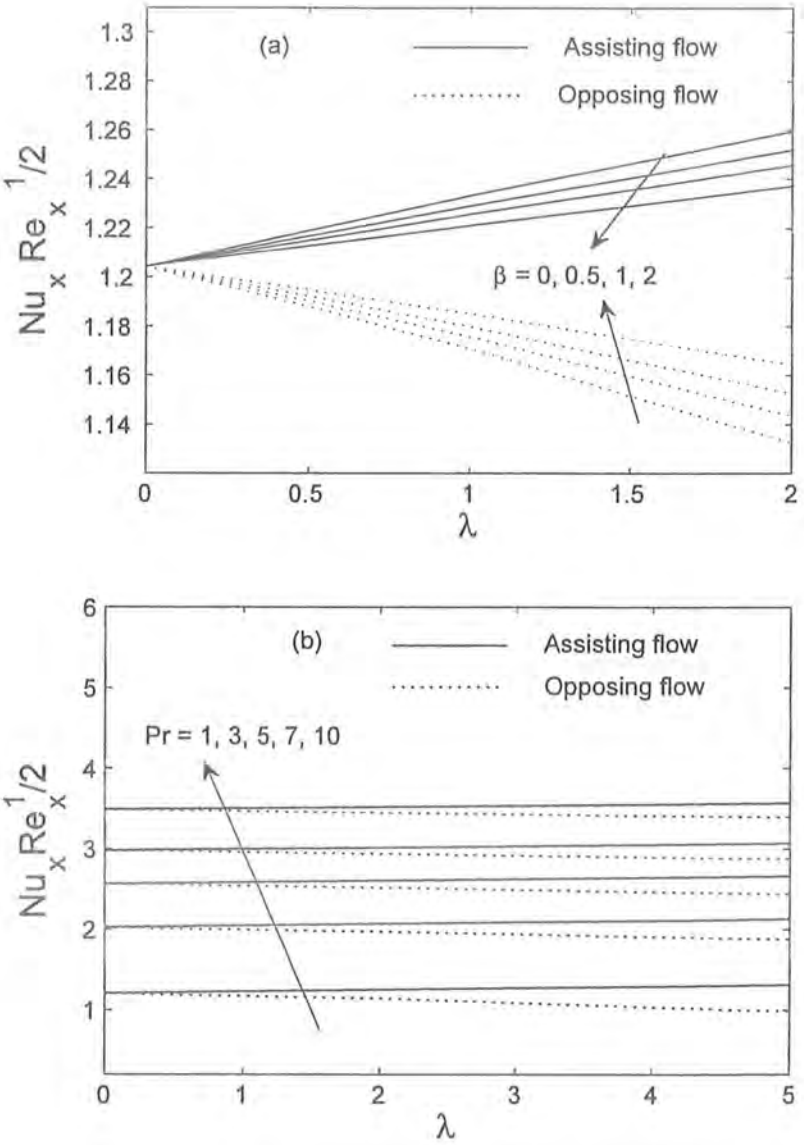

Fig. 6.8. Variation of the local Nusselt number $Nu_x \operatorname{Re}_x^{1/2}$ verses λ: (a) effects of the Deborah number β when $a/c = 1$ and $\Pr = 1$ and (b) effects of the Prandtl number Pr when $\beta = 0.5$, $a/c = 1$.

a/c	Mahapatra and Gupta [145]	Nazar et al. [147]	Ishak et al. [146]	Present solutions	
				HAM	Numerical
0.1	−0.9694	−0.9694	−0.9694	−0.9694	−0.9694
0.2	−0.9181	−0.9181	−0.9181	−0.9181	−0.9181
0.5	−0.6673	−0.6673	−0.6673	−0.6673	−0.6673
2.0	2.0175	2.0176	2.0175	2.0175	2.0175
3.0	4.7293	4.7296	4.7294	4.7293	4.7294

Table 6.1. Values of $f''(0)$ for different values of a/c when the buoyancy force term $\lambda\theta$ is absent in case of viscous fluid ($\beta = 0$).

		Assisting flow	Opposing flow
β	Pr	$Nu_x\,\mathrm{Re}_x^{-1/2}$	$Nu_x\,\mathrm{Re}_x^{-1/2}$
0.0		1.2578	1.1953
0.2		1.2562	1.1972
0.5		1.2537	1.2002
1.0		1.2503	1.2042
1.5		1.2476	1.2073
2.0		1.2457	1.2096
0.5	1	1.2727	1.2196
	7	3.2973	3.2564
	20	5.5093	5.4792
	40	7.718	7.6952
	60	9.3888	9.3693
	80	10.7802	10.7644
	100	11.9945	11.9790

Table 6.2. Values of the local Nusselt number $Nu_x\,\mathrm{Re}_x^{1/2}$ for various values of β and Pr when $\lambda = 1 = a/c$ in both the cases of assisting and opposing flows.

	Buoyancy assisting flow		Buoyancy opposing flow	
Pr	$C_f\,\mathrm{Re}_x^{1/2}$	$Nu_x\,\mathrm{Re}_x^{-1/2}$	$C_f\,\mathrm{Re}_x^{1/2}$	$Nu_x\,\mathrm{Re}_x^{-1/2}$
0.72	0.3645	1.0931	−0.3852	1.0293
	(0.3645)	(1.0931)	(−0.3852)	(1.0293)
6.8	0.1804	3.2902	−0.1833	3.2466
	(0.1804)	(3.2902)	(−0.1832)	(3.2466)
20	0.1175	5.6230	−0.1183	5.5924
	(0.1175)	(5.6230)	(−0.1183)	(5.5923)
40	0.0874	7.9464	−0.0876	7.9228
	(0.0873)	(7.9463)	(−0.0876)	(7.9227)
60	0.0729	9.7327	−0.0731	9.7126
	(0.0729)	(9.7327)	(−0.0731)	(9.7126)
80	0.0641	11.2414	−0.0643	11.2233
	(0.0640)	(11.2413)	(−0.0642)	(11.2235)
100	0.0577	12.5725	−0.0578	12.5565
	(0.0578)	(12.5726)	(−0.0579)	(12.5564)

Table 6.3. Values of $f''(0)$ and the local Nusselt number $Nu_x\,\mathrm{Re}_x^{1/2}$ for various values of Pr when $a/c = 1 = \lambda$ in case of viscous fluid ($\beta = 0$). The values in the brackets are from Ishak et al. [146].

Chapter 7

Effects of MHD and mass transfer on the flow of a Maxwell fluid past a porous shrinking sheet with chemical reaction species

This chapter concerns with the mass transfer of the steady two-dimensional and magnetohydrodynamic (MHD) boundary layer flow of a Maxwell fluid past a porous shrinking sheet in the presence of chemical reaction. By similarity transformations, the resulting nonlinear partial differential equations are reduced to the system of nonlinear ordinary differential equations. Expressions of velocity and the concentration fields are obtained by using the homotopy analysis method (HAM). Convergence of the developed series solutions is explicitly analyzed. The influences of sundry parameters on the velocity and the concentration fields are noted and discussed in detail. Values of the skin friction coefficient and the surface mass transfer for various interesting parameters are also tabulated.

7.1 Problem statement

We investigate the steady, incompressible, MHD flow of two-dimensional upper-convected Maxwell (UCM) fluid over a porous shrinking sheet with suction. The sheet coincides with the plane $y = 0$ and the flow being in the region $y > 0$. The x and y axes are taken along and perpendicular to the sheet, respectively (Fig. 7.1). A constant magnetic field of strength B_0 acts along the y-axis. The induced magnetic field is negligible, which is a valid assumption on a laboratory scale under the assumption of small magnetic Reynolds number. External electric field is taken zero. The mass transfer is the flow along a sheet that contains a species A slightly soluble in the fluid B. Let C_w be the concentration at the sheet surface and the solubility of A in B and concentration of A far away from the sheet is C_∞. Also the reaction of a species A with B be the first order homogeneous chemical reaction of rate constant k_1. The concentration of dissolved A is considered small enough. Through boundary layer approximations, the governing equations for velocity and concentration fields are:

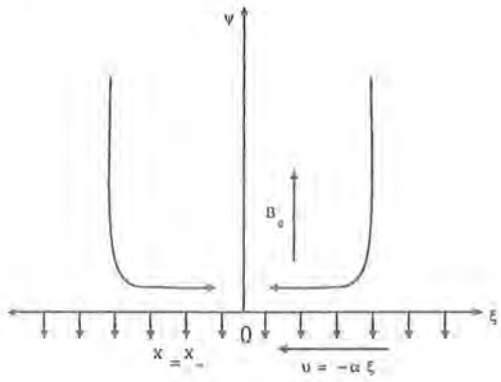

Fig. 7.1. Geometry of the problem and coordinate system

$$\frac{\partial u}{\partial x} + \frac{\partial u}{\partial y} = 0, \tag{7.1}$$

$$u\frac{\partial u}{\partial x} + v\frac{\partial u}{\partial y} + \lambda_1\left[u^2\frac{\partial^2 u}{\partial x^2} + v^2\frac{\partial^2 u}{\partial y^2} + 2uv\frac{\partial^2 u}{\partial x \partial y}\right] = \nu\frac{\partial^2 u}{\partial y^2} - \frac{\sigma B_0^2}{\rho}u, \tag{7.2}$$

$$\frac{\partial \widetilde{p}}{\partial y} = O(\delta_1), \tag{7.3}$$

$$u\frac{\partial C}{\partial x}+v\frac{\partial C}{\partial y}=D\frac{\partial^2 C}{\partial y^2}-k_1C. \tag{7.4}$$

In above equations (u,v) are the velocity components in the (x,y) directions, respectively, ν is the kinematic viscosity of fluid, ρ is the density of the fluid, λ_1 is the relaxation time, σ is the electrical conductivity of the fluid, $\widetilde{p}$ is the pressure, C is the concentration of the species of the fluid, D is the diffusion coefficient of the diffusing species in the fluid and δ_1 being the boundary layer thickness.

The appropriate boundary conditions are

$$u(x,y)=-cx, \quad v(x,y)=-V, \quad C(x,y)=C_w \quad \text{at} \quad y=0, \tag{7.5}$$

$$u(x,y)\to 0, \quad C(x,y)\to C_\infty \quad \text{as} \quad y\to\infty, \tag{7.6}$$

in which $c>0$ is the rate of shrinking and $V>0$ is the suction velocity at the surface.

To simplify the problem, we introduce the following non-dimensional quantities

$$\eta=\sqrt{\frac{c}{\nu}}y, \quad u=cxf'(\eta), \quad v=-\sqrt{\nu c}f(\eta), \quad \phi=C-C_\infty/C_w-C_\infty. \tag{7.7}$$

Using Eq. (7.7), the incompressibility condition (7.1) is satisfied automatically and Eqs. (7.2)–(7.6) reduce to

$$f'''-M^2f'-f'^2+ff''+\beta\left(2ff'f''-f^2f'''\right)=0, \tag{7.8}$$

$$\phi''+Scf\phi'-Sc\gamma\phi=0, \tag{7.9}$$

$$f=A, \quad f'=-1 \quad \phi=1 \quad \text{at} \quad \eta=0, \tag{7.10}$$

$$f'=0, \quad \phi=0 \quad \text{as} \quad \eta\to\infty, \tag{7.11}$$

where prime denotes the differentiation with respect to η. The dimensionless suction parameter A, the Hartman number or the magnetic parameter M, the Deborah number β, the Schmidt number Sc and the chemical reaction parameter γ are given by

$$A=\frac{V}{\sqrt{\nu c}}, \quad M^2=\frac{\sigma B_0^2}{\rho c}, \quad \beta=\lambda_1 c, \quad Sc=\frac{\nu}{D}, \quad \gamma=\frac{k_1}{c}.$$

It is worthmentioning to note that the chemical reaction parameter γ can be real number ($\gamma > 0$ indicates destructive chemical reaction and $\gamma < 0$ denotes generative chemical reaction and we can take $\gamma = 0$ for a non-reactive species) [36].

The skin friction coefficient C_f and the surface mass transfer ϕ' at the wall are defined by

$$C_f = \frac{\tau_w}{\rho u_w^2}, \qquad \phi'(0) = \left(\frac{\partial \phi}{\partial y}\right)_{\eta=0} \leq 0, \tag{7.12}$$

where the wall skin friction τ_w is

$$\tau_w = \mu \left(\frac{\partial u}{\partial y}\right)_{y=0} - \lambda_1 \left(2uv\frac{\partial u}{\partial x} + v^2\frac{\partial u}{\partial y}\right)_{y=0}. \tag{7.13}$$

Using variables (7.7), we get

$$\mathrm{Re}_x^{1/2}\, C_f = \left[f''(\eta) - \beta\left(f^2(\eta)f''(\eta) - 2f(\eta)\right)f'^2(\eta)\right]\Big|_{\eta=0}, \tag{7.14}$$

where $\mathrm{Re}_x^{1/2} = u_w x/\nu$ is the local Reynolds number. In the next section we will present the analytic solution of Eqs. (7.8) – (7.11) using homotopy analysis method (HAM).

7.2 Homotopy analysis solutions

For the series solutions of Eqs. (7.8) and (7.9) we express the velocity distribution $f(\eta)$ and the concentration field $\phi(\eta)$ by the set of base functions

$$\left\{\eta^k \exp\left(-n\eta\right)\Big| \, k \geq 0, n \geq 0\right\} \tag{7.15}$$

in the form

$$f\left(\eta\right) = a_{0,0}^0 + \sum_{n=0}^{\infty}\sum_{k=0}^{\infty} a_{m,n}^k \eta^k \exp\left(-n\eta\right), \tag{7.16}$$

$$\phi\left(\eta\right) = \sum_{n=0}^{\infty}\sum_{k=0}^{\infty} b_{m,n}^k \eta^k \exp\left(-n\eta\right), \tag{7.17}$$

where $a_{m,n}^k$ and $b_{m,n}^k$ are the coefficients. Based on the *rule of solution expressions* and the boundary conditions (7.10) and (7.11), one can choose

$$f_0(\eta) = A - 1 + \exp(-\eta), \tag{7.18}$$

$$\phi_0(\eta) = \exp(-\eta), \tag{7.19}$$

as our initial approximations of $f(\eta)$ and $\phi(\eta)$. Besides that we select

$$\mathcal{L}_f(f) = \frac{d^3 f}{d\eta^3} - \frac{df}{d\eta}, \tag{7.20}$$

$$\mathcal{L}_\phi(f) = \frac{d^2 f}{d\eta^2} - f, \tag{7.21}$$

as our auxiliary linear operators which have the following properties:

$$\mathcal{L}_f[C_1 + C_2 \exp(\eta) + C_3 \exp(-\eta)] = 0, \tag{7.22}$$

$$\mathcal{L}_\phi[C_4 \exp(\eta) + C_5 \exp(-\eta)] = 0 \tag{7.23}$$

in which C_i $(i = 1 - 5)$ are the arbitrary constants. If $p\,(\in [0,1])$ is an embedding parameter and $\hbar_f$, $\hbar_\phi$ indicate the non-zero auxiliary parameters, respectively then we construct the following zeroth-order deformation problems

$$(1-p)\,\mathcal{L}_f\left[\widehat{f}(\eta;p) - f_0(\eta)\right] = p\hbar_f \mathcal{N}_f\left[\widehat{f}(\eta;p)\right], \tag{7.24}$$

$$(1-p)\,\mathcal{L}_\phi\left[\widehat{\phi}(\eta;p) - \phi_0(\eta)\right] = p\hbar_\phi \mathcal{N}_\phi\left[\widehat{\phi}(\eta;p), \widehat{f}(\eta;p)\right], \tag{7.25}$$

subject to the boundary conditions

$$\widehat{f}(\eta;p)\Big|_{\eta=0} = A, \qquad \frac{\partial \widehat{f}(\eta;p)}{\partial \eta}\Big|_{\eta=0} = -1, \qquad \frac{\partial \widehat{f}(\eta;p)}{\partial \eta}\Big|_{\eta=\infty} = 0, \tag{7.26}$$

$$\widehat{\phi}(\eta;p)\Big|_{\eta=0} = 1, \qquad \widehat{\phi}(\eta;p)\Big|_{\eta=\infty} = 0, \tag{7.27}$$

in which the non-linear operators $\mathcal{N}_f$ and $\mathcal{N}_\phi$ are

$$\mathcal{N}_f\left[\widehat{f}(\eta;p)\right] = \frac{\partial^3\widehat{f}(\eta;p)}{\partial\eta^3} + \widehat{f}(\eta;p)\frac{\partial^2\widehat{f}(\eta;p)}{\partial\eta^2} - \left(\frac{\partial\widehat{f}(\eta;p)}{\partial\eta}\right)^2 - M^2\frac{\partial\widehat{f}(\eta;p)}{\partial\eta}$$
$$+\beta\left(2\widehat{f}(\eta;p)\frac{\partial\widehat{f}(\eta;p)}{\partial\eta}\frac{\partial^2\widehat{f}(\eta;p)}{\partial\eta^2} - \widehat{f}(\eta;p)\,\widehat{f}(\eta;p)\frac{\partial^3\widehat{f}(\eta;p)}{\partial\eta^3}\right), \quad (7.28)$$

$$\mathcal{N}_\phi\left[\widehat{\phi}(\eta;p), \widehat{f}(\eta;p)\right] = \frac{\partial^2\widehat{\phi}(\eta;p)}{\partial\eta^2} + Sc\widehat{f}(\eta;p)\frac{\partial\widehat{\phi}(\eta;p)}{\partial\eta} - Sc\gamma\widehat{\phi}(\eta;p). \quad (7.29)$$

Obviously, when $p = 0$ and $p = 1$, the above zeroth-order deformation Eqs. (7.24) and (7.25) have the solutions

$$\widehat{f}(\eta;0) = f_0(\eta), \qquad \widehat{f}(\eta;1) = f(\eta), \quad (7.30)$$

$$\widehat{\phi}(\eta;0) = \phi_0(\eta), \qquad \widehat{\phi}(\eta;1) = \phi(\eta). \quad (7.31)$$

Expanding $\widehat{f}(\eta;p)$ and $\widehat{\phi}(\eta;p)$ in Taylor's theorem with respect to p, we have

$$\widehat{f}(\eta;p) = f_0(\eta) + \sum_{m=1}^{\infty} f_m(\eta)\,p^m, \quad (7.32)$$

$$\widehat{\phi}(\eta;p) = \phi_0(\eta) + \sum_{m=1}^{\infty} \phi_m(\eta)\,p^m, \quad (7.33)$$

where

$$f_m(\eta) = \frac{1}{m!}\frac{\partial^m\widehat{f}(\eta;p)}{\partial p^m}\bigg|_{p=0}, \qquad \phi_m(\eta) = \frac{1}{m!}\frac{\partial^m\widehat{\phi}(\eta;p)}{\partial p^m}\bigg|_{p=0}. \quad (7.34)$$

Note that Eqs. (7.24) and (7.25) contain two nonzero auxiliary parameters $\hbar_f$ and $\hbar_\phi$. The convergence of the series (7.32) and (7.33) is dependent upon $\hbar_f$ and $\hbar_\phi$. Assuming that $\hbar_f$ and $\hbar_\phi$ are chosen in such a way that the series in Eqs. (7.32) and (7.33) are convergent at $p = 1$, then due to Eqs. (7.30) and (7.31) one can write

$$f(\eta) = f_0(\eta) + \sum_{m=1}^{\infty} f_m(\eta), \quad (7.35)$$

$$\phi(\eta) = \phi_0(\eta) + \sum_{m=1}^{\infty} \phi_m(\eta). \quad (7.36)$$

Differentiating the zeroth-order deformation Eqs. (7.24) and (7.25) m times with respect to p, then setting $p = 0$, and finally dividing by $m!$, the mth-order deformation problems are

$$\mathcal{L}_f \left[f_m(\eta) - \chi_m f_{m-1}(\eta) \right] = \hbar_f \mathcal{R}_m^f(\eta), \tag{7.37}$$

$$\mathcal{L}_\phi \left[\phi_m(\eta) - \chi_m \phi_{m-1}(\eta) \right] = \hbar_\phi \mathcal{R}_m^\phi(\eta), \tag{7.38}$$

$$f_m(0) = f_m'(0) = f_m'(\infty) = 0, \quad \text{and} \quad \phi_m(0) = \phi_m(\infty) = 0, \tag{7.39}$$

where

$$\begin{aligned} \mathcal{R}_m^f(\eta) &= f_{m-1}'''(\eta) - M^2 f_{m-1}' + \sum_{k=0}^{m-1} \left[f_{m-1-k} f_k'' - f_{m-1-k}' f_k' \right] \\ &\quad + \beta \sum_{k=0}^{m-1} f_{m-1-k} \sum_{l=0}^{k} \left[2 f_{k-l}' f_l'' - f_{k-l} f_l''' \right], \end{aligned} \tag{7.40}$$

$$\mathcal{R}_m^\phi(\eta) = \phi_{m-1}''(\eta) - Sc\gamma \phi_{m-1} + Sc \sum_{k=0}^{m-1} \phi_{m-1-k}' f_k, \tag{7.41}$$

and

$$\chi_m = \begin{cases} 0, & m \leq 1 \\ 1, & m > 1 \end{cases}. \tag{7.42}$$

The general solutions of Eqs. (7.37) – (7.39) which contain the $f_m^\star(\eta)$ and $\theta_m^\star(\eta)$ as the special solutions are

$$f_m(\eta) = f_m^\star(\eta) + C_1 + C_2 \exp(\eta) + C_3 \exp(-\eta), \tag{7.43}$$

$$\phi_m(\eta) = \phi_m^\star(\eta) + C_4 \exp(\eta) + C_5 \exp(-\eta), \tag{7.44}$$

where

$$C_2 = C_5 = 0, \quad C_3 = \left. \frac{\partial f_m^\star(\eta)}{\partial \eta} \right|_{\eta=0}, \quad C_1 = -C_3 - f_m^\star(0), \quad C_4 = -\phi_m^\star(0). \tag{7.45}$$

In this way, it is easy to solve the linear non-homogeneous Eqs. (7.37) and (7.38) by using Mathematica one after the other in the order $m = 1, 2, 3.....$

7.3 Convergence of the HAM solutions

Our analytic solutions (7.35) and (7.36) contain the non-zero auxiliary parameters $\hbar_f$ and $\hbar_\phi$ which determine the convergence and rate of approximation of the HAM solution [90]. To see the range for admissible values of $\hbar_f$ and $\hbar_\phi$ of the functions $f''(0)$ and $\phi'(0)$, the so-called $\hbar$-curves are plotted for 15th-order of approximation in Fig. 7.2. From Fig. 7.2, it is clearly seen that $\hbar$-curves have a parallel line segment that correspond to a region for admissible values of $\hbar_f$ for f is $-2.1 \leq \hbar_f \leq -0.2$ and the range for the values of $\hbar_\phi$ for ϕ is $-2 \leq \hbar_\phi \leq -0.3$ when $A = 0.5$, $M = 1$, $\beta = 0.2$ and $Sc = 0.5 = \gamma$. It is evident from our calculations that the solutions series (7.35) and (7.36) converge in the whole region of η when $\hbar_f = \hbar_\phi = -1$. Table 7.1 shows the convergence of the HAM solutions for $f''(0)$ and $-\phi'(0)$ at different order of approximations when $A = 1$, $M = 1.5$, $Sc = \gamma = 1$ and $\beta = 0.2$.

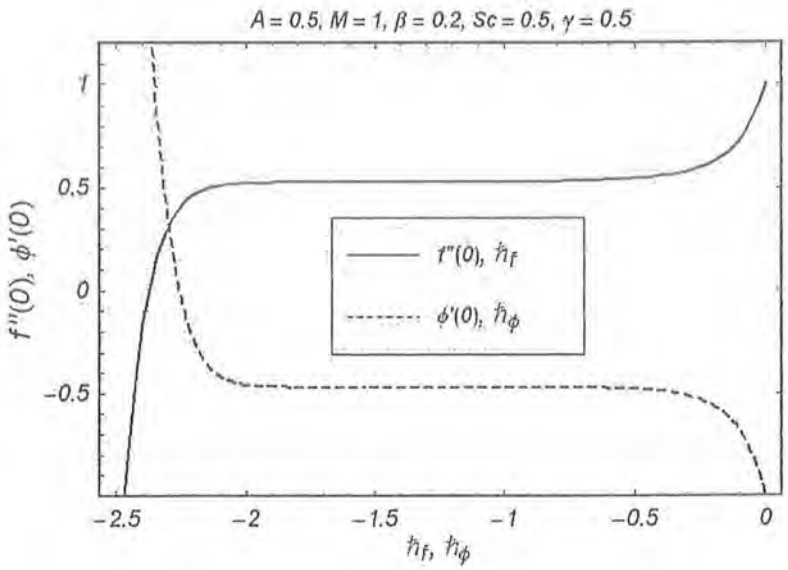

Fig. 7.2. The $\hbar$-curves of $f''(0)$ and $\phi'(0)$ at the 15th-order of approximations.

order of approximation	$f''(0)$	$-\phi'(0)$
1	1.402500	1.233333
5	1.719884	1.431262
10	1.732064	1.436541
14	1.732260	1.436517
18	1.732268	1.436517
20	1.732268	1.436517
30	1.732268	1.436517
40	1.732268	1.436517
50	1.732268	1.436517
60	1.732268	1.436517

Table 7.1. Convergence of the HAM solutions for different order of approximations when $A = 1$, $M = 1.5$, $Sc = \gamma = 1$ and $\beta = 0.2$.

7.4 Results and discussion

In order to see the influence of the various parameters, for example the suction parameter A, the Hartman number M, the Deborah number β, the Schmidt number Sc and the chemical reaction parameter γ on the velocity f' and the concentration field ϕ, we have prepared Figs. $7.3 - 7.15$. The values of the skin-friction coefficient $\mathrm{Re}_x^{1/2} C_f$, the surface mass transfer $\phi'(0)$ and the gradient of mass transfer $-\phi'(\eta)$ for several values of the emerging parameters are also given in Tables 7.2 and 7.3, respectively.

Figs. $7.3-7.5$ are made to show the effects of the suction parameter A, the Hartman number M and the Deborah number β on the velocity component f'. Fig. 7.3 gives the variations of A on the velocity f'. It is found that the magnitude of the velocity decreases when A increases. The change in f' is larger near the wall when compared to far away from the surface. For the shrinking sheet, the vorticity of the sheet is not confined within a boundary layer and the flow is unlikely to exist unless adequate suction on the sheet is imposed. Thus suction occurs when the fluid condenses on the surface. Therefore we can say that physically the suction plays

very important role to flow the fluid smoothly in case of shrinking sheet. The boundary layer thickness also decreases by increasing A. Fig. 7.4 displays the distributions of the velocity f' for several values of the Hartman number M. It is noted that the magnitude of the velocity f' decreases for large values of M. However, this change in the velocity near the surface is maximum and far away from the surface, this change is small and finally approaches to zero. As expected the boundary layer thickness is decreased when M increases. The influence of the Deborah number β on the velocity f' can be seen from Fig. 7.5. It is observed that f' has the similar results for the large values of β (Fig. 7.3). This change in the velocity is larger in case of suction. The boundary layer thickness also decreases as the Deborah number β increases.

Figs. $7.6 - 7.15$ illustrate the variations of the suction parameter A, the Hartman number M, the Deborah number β, the chemical reaction parameter γ and the Schmidt number Sc on the concentration field ϕ and the gradient of the mass transfer $-\phi'(\eta)$. Fig. 7.6 elucidates the effects of A on the concentration field ϕ. It can be seen that ϕ is a decreasing function of A and the concentration boundary layer also decreases when A increases. Fig. 7.7 depicts the distributions of the concentration field ϕ for various values of the Hartman number M. From this Fig., we observe that ϕ is decreased for large values of the magnetic parameter M. The concentration boundary layer also decreases when M increases. Fig. 7.8 gives the effects of β on the concentration field ϕ for a non-reactive species $\gamma = 0$. We can see that without reactive species the concentration field ϕ is decreased as β increases.

Figs. 7.9 and 7.10 show the distributions of the concentration field ϕ for several values of the Deborah number β in the case of destructive ($\gamma > 0$) and generative ($\gamma < 0$) chemical reactions, respectively. It is noted from Fig. 7.9 that the concentration field ϕ is a decreasing function of β. The concentration field ϕ also decreases for large values of β in case of generative chemical reaction ($\gamma < 0$) as shown in Fig. 7.10. But the magnitude of ϕ is larger in case of ($\gamma < 0$) when compared with the case of destructive chemical reaction ($\gamma > 0$). It is also found that the concentration field is decreased for several values of β in all cases ($\gamma = 0, \gamma > 0$ and $\gamma < 0$). Fig. 7.11 displays the influence of the generative chemical reaction parameter ($\gamma < 0$) on ϕ. It can be seen that the fluid concentration increases with an increase in the generative chemical reaction parameter. Fig. 7.12 illustrates the variations of the destructive chemical reaction parameter ($\gamma > 0$) on the concentration profile ϕ. From this Fig. the

fluid concentration ϕ has the opposite behavior for ($\gamma > 0$) when compared with the case of generative chemical reaction parameter ($\gamma < 0$). However the change in concentration field is larger for the generative chemical reaction (Fig. 7.11). The concentration boundary layer is decreased in case of destructive chemical reaction. The variations of the Schmidt number Sc on the concentration field ϕ can be seen from Fig. 7.13. As expected, the concentration field ϕ is decreased by increasing Sc. The concentration boundary layer also decreases for large values of Sc. Fig. 7.14 shows the effects of destructive/generative chemical reaction parameter γ on the gradient of mass transfer $-\phi'(\eta)$. We can say that initially the gradient of mass transfer increases for large values of destructive chemical reaction ($\gamma > 0$) but after $\eta = 2$, it has reverse flow and finally approaches to zero, while the gradient of concentration profile has the opposite behavior in the case of generative chemical reaction ($\gamma < 0$). Fig. 7.15 elucidates the change in the gradient of mass transfer $-\phi'(\eta)$ for several values of β in case of destructive ($\gamma > 0$) and generative ($\gamma < 0$) chemical reactions. It is noted from this Fig. that $-\phi'(\eta)$ has the similar behavior for large values of β as in Fig. 7.14. The magnitude of $-\phi'(\eta)$ is smaller in Fig. 7.15 when compared with Fig. 7.14.

Tables 7.2 and 7.3 are prepared to show the values of the skin-friction coefficient $\mathrm{Re}_x^{1/2} C_f$, the surface mass transfer $\phi'(0)$ and the gradient of mass transfer $\phi'(\eta)$ for some values of A, M, β, Sc and γ (for destructive chemical reaction $\gamma > 0$), respectively. The influence of A, M and β on the skin friction coefficient $\mathrm{Re}_x^{1/2} C_f$ and surface mass transfer $-\phi'(0)$ are given in Table 7.2 for destructive chemical reaction $\gamma = 1$. From Table 7.2 we observe that, the magnitude of the skin friction coefficient $\mathrm{Re}_x^{1/2} C_f$ increases for large values of A, M and β. It is also noted that the magnitude of $-\phi'(0)$ is increased by increasing A and M, while it decreases for large values of β. Table 7.3 gives the values of the surface mass transfer $-\phi'(0)$ and the gradient of mass transfer $-\phi'(\eta)$ for several values of Sc and γ (for $\gamma > 0$) with $A = 1$, $M = 1.2$ and $\beta = 0.2$. It is found that the magnitude of $-\phi'(0)$ increases as both Sc and γ increase, respectively. The values of the gradient of mass transfer $-\phi'(\eta)$ for different values of Sc and γ at $\eta = 0.2$ and 0.6 is shown. The magnitude of the gradient of mass transfer $-\phi'(\eta)$ is increased as both Sc and γ increases with $\eta = 0.2$ and 0.6. But the magnitude of $-\phi'(\eta)$ is larger at $\eta = 0.2$.

7.5 Conclusions

Here we investigate the mass transfer in the MHD flow of an upper-convected Maxwell (UCM) fluid over a porous shrinking sheet with chemical reaction species. The nonlinear system of ordinary differential equations is solved analytically using homotopy analysis method (HAM). The velocity f and the concentration field ϕ are obtained in the form of series. The effects of the different emerging parameters on the velocity f' and the concentration field ϕ are shown through some graphs. The values of the skin friction coefficient, the surface mass transfer and the gradient of mass transfer are also given in tabular form. From this analysis, we have made the following observations.

- The velocity field f' increases by increasing A, M and β.
- The concentration field ϕ decreases when A, M, β and Sc increases in both cases of destructive/generative chemical reactions.
- The concentration field ϕ has opposite results for destructive ($\gamma > 0$) and generative ($\gamma < 0$) chemical reactions.
- The gradient of mass transfer $-\phi'(\eta)$ has opposite behavior for destructive/generative chemical reaction when β is increased.
- The magnitude of the skin friction coefficient $\mathrm{Re}_x^{1/2} C_f$ increases for large values of A, M and β.
- The magnitudes of the surface mass transfer $-\phi'(0)$ and the gradient of mass transfer $-\phi'(\eta)$ are increased by increasing A, M, Sc and γ. However the magnitude of $-\phi'(0)$ decreases as β increases.

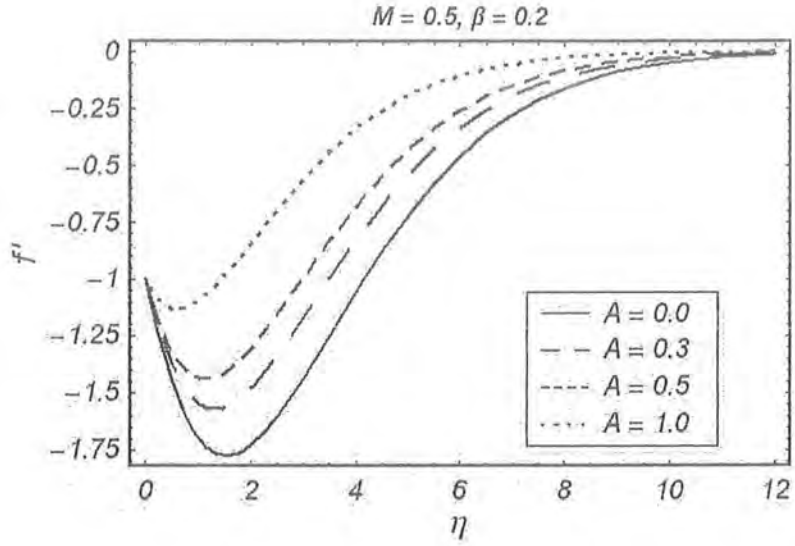

Fig. 7.3. The variations of the suction parameter A on the velocity field f'.

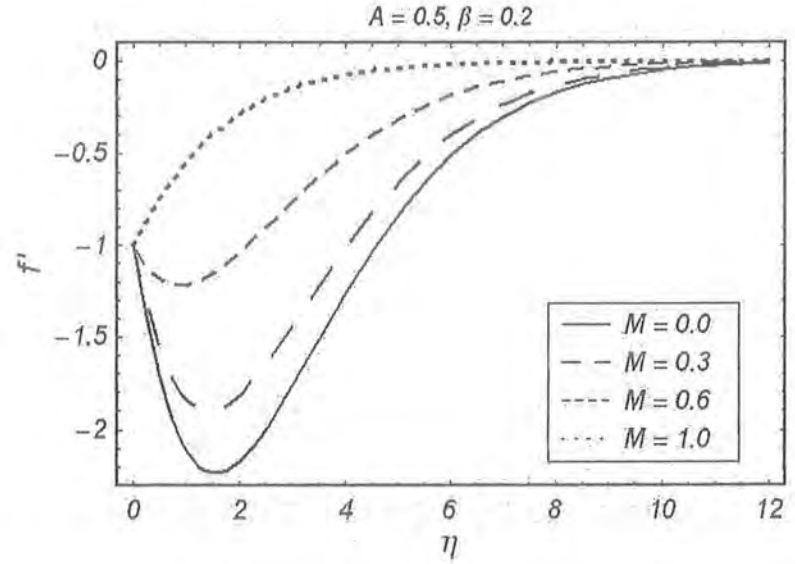

Fig. 7.4. The variations of the Hartman number M on the velocity field f'.

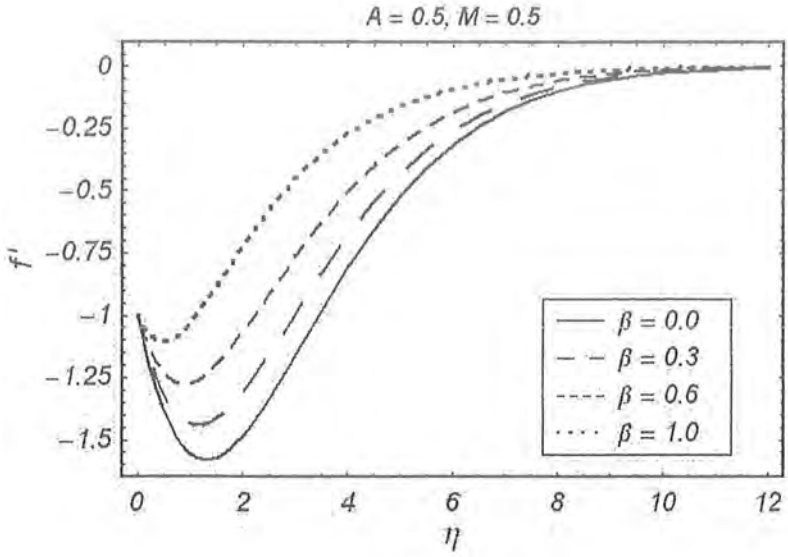

Fig. 7.5. The variations of the Deborah number β on the velocity field f'.

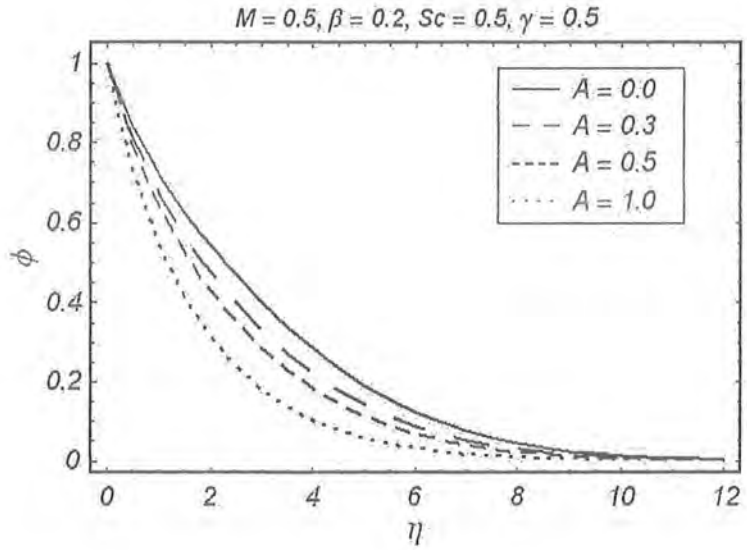

Fig. 7.6. The variations of the suction parameter A on the concentration field ϕ.

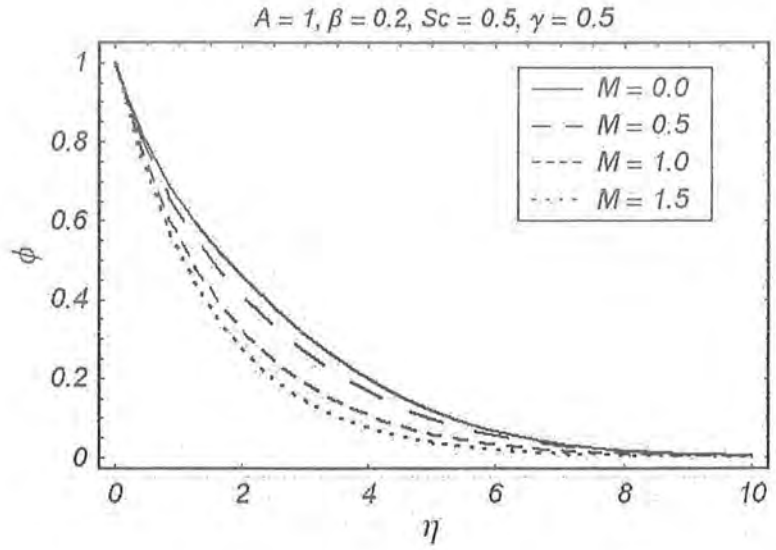

Fig. 7.7. The variations of the Hartman number M on the concentration field ϕ.

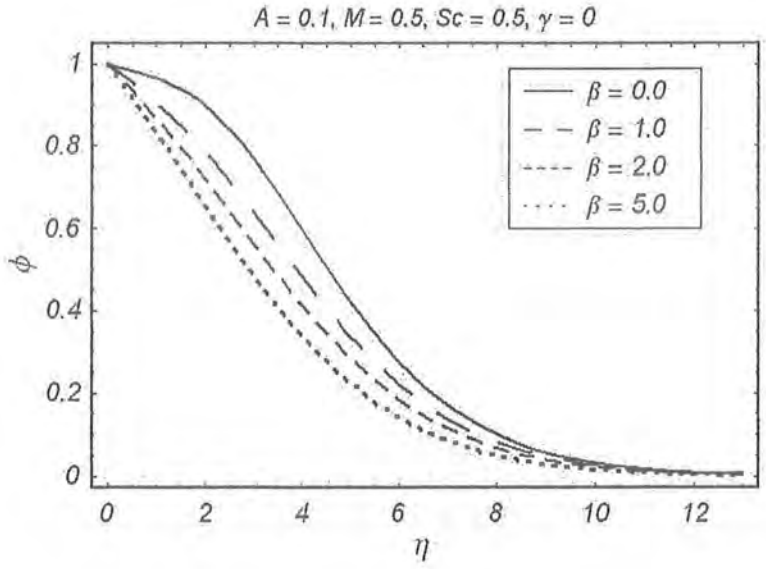

Fig. 7.8. The variations of the Deborah number β on the concentration field ϕ with no chemical reaction $\gamma = 0$.

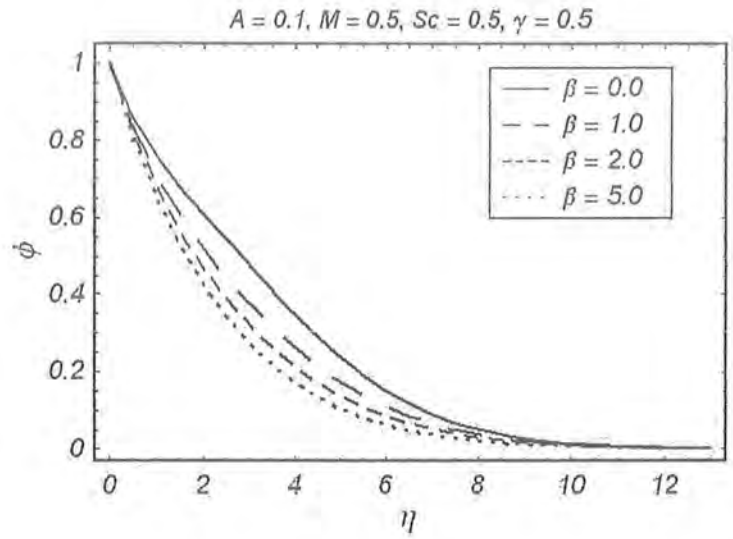

Fig. 7.9. The variations of the Deborah number β on the concentration field ϕ for destructive chemical reaction $\gamma > 0$.

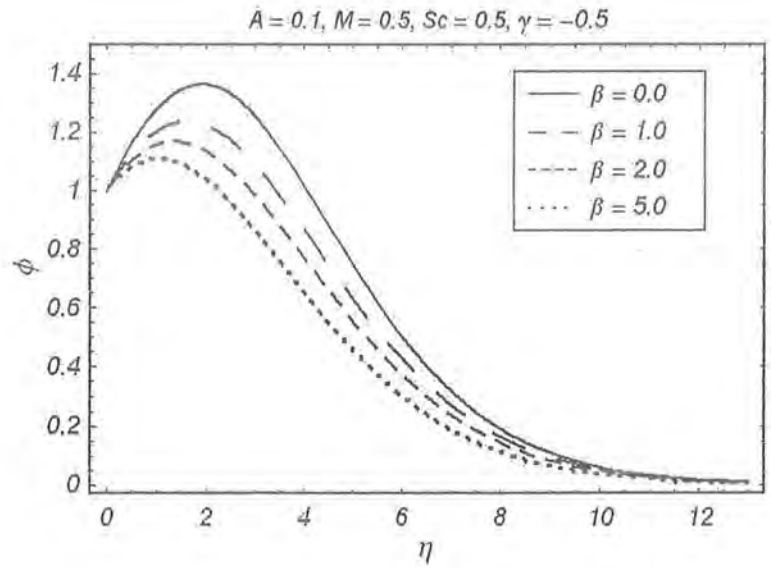

Fig. 7.10. The variations of the Deborah number β on the concentration field ϕ for generative chemical reaction $\gamma < 0$.

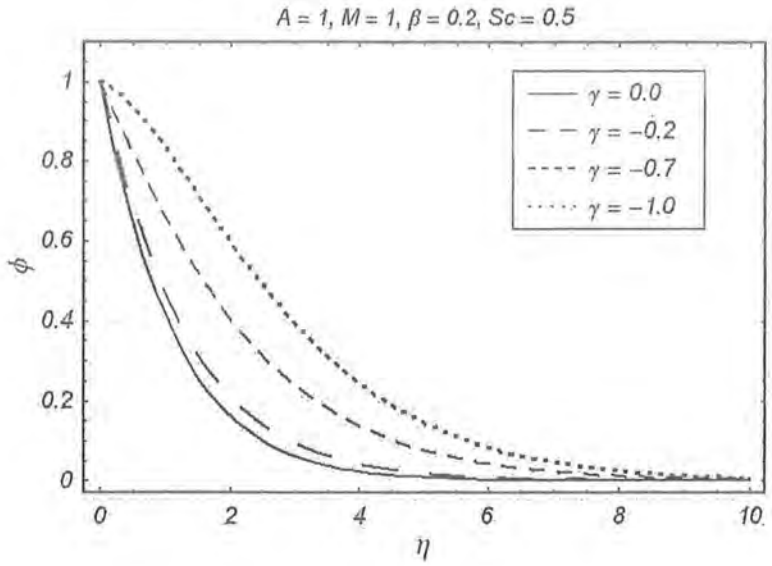

Fig. 7.11. The variations of the generative chemical reaction parameter γ on the concentration field ϕ.

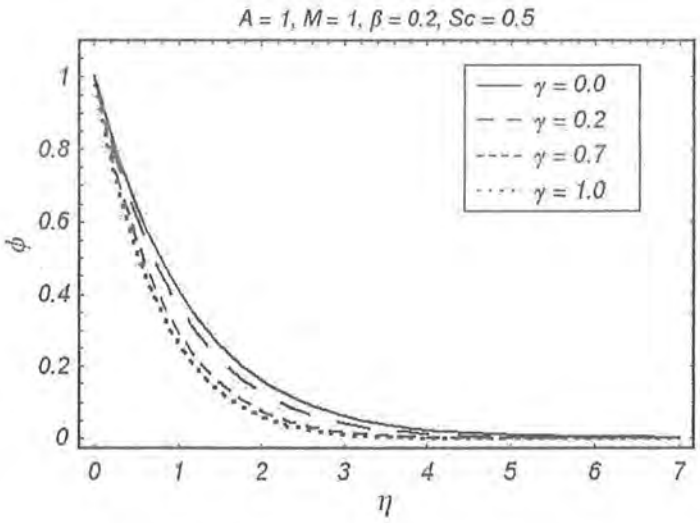

Fig. 7.12. The variations of the destructive chemical reaction parameter γ on the concentration field ϕ.

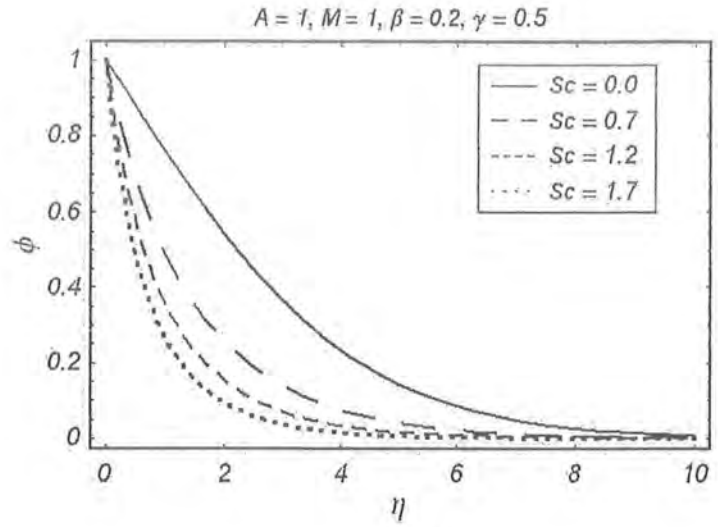

Fig. 7.13. The variations of the Schmidt parameter Sc on the concentration field ϕ.

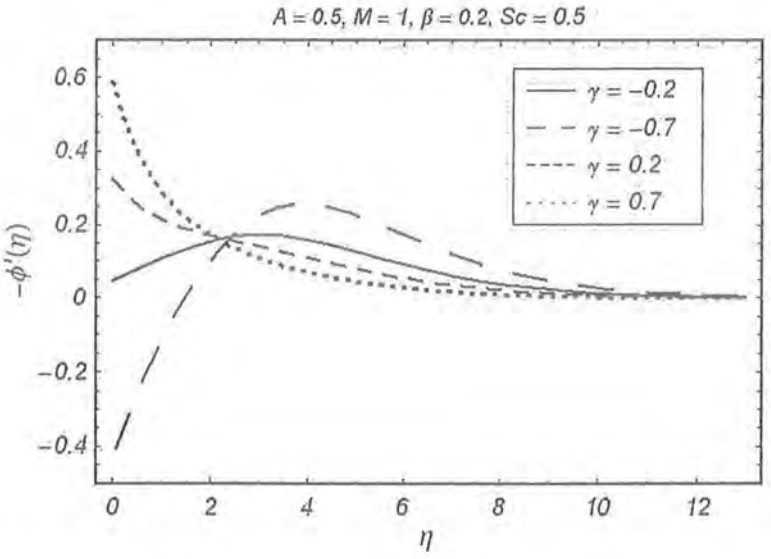

Fig. 7.14. The variations of the chemical reaction parameter γ on the gradient of mass transfer $-\phi'(\eta)$.

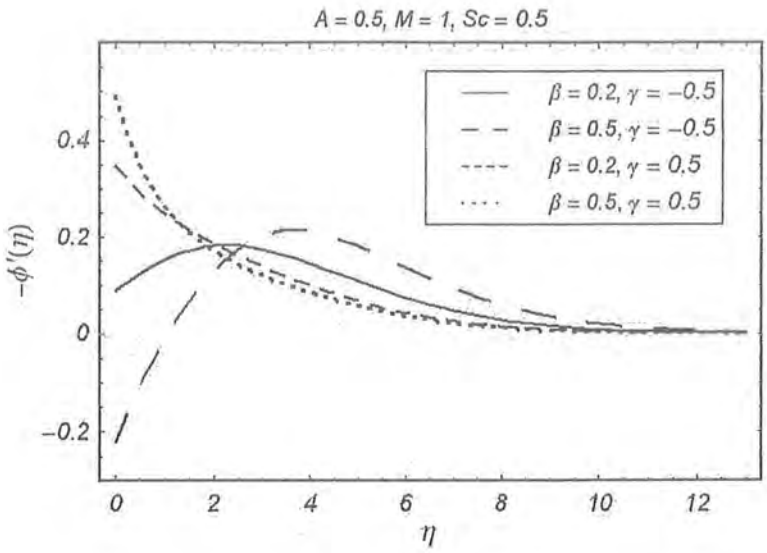

Fig. 7.15. The variations of the Deborah number on the gradient of mass transfer $-\phi'(\eta)$ for destructive/generative chemical reaction.

A	M	β	$\mathrm{Re}_x^{1/2} C_f$	$-\phi'(0)$
0.0	1.5	0.5	1.223676	0.860477
0.2			1.412204	0.949625
0.5			1.646600	1.106254
0.7			1.765886	1.227578
1.0			1.868705	1.438716
0.5	1.0		0.967329	1.060457
	1.2		1.278197	1.083708
	1.5		1.646600	1.106254
	2.0		2.186934	1.131740
	3.0		3.185976	1.163358
	1.5	0.0	1.395644	1.108198
		0.2	1.494254	1.107432
		0.5	1.646600	1.106254
		0.7	1.751294	1.105449
		1.0	1.913348	1.104212
		2.0	2.502933	1.099823

Table 7.2. Values of the skin friction coefficient $\mathrm{Re}_x^{1/2} C_f$ and the surface mass transfer $-\phi'(0)$ for some values of A, M and β with $Sc = \gamma = 1$.

Sc	γ	$-\phi'(0)$	η	Sc	γ	$-\phi'(\eta)$
0.2	1.0	0.505403	0.2	0.2	1.0	0.449991
0.7		1.103298		0.7		0.853461
1.0		1.412999		1.0		1.018820
1.5		1.905535	0.6	0.2		0.361776
2.0		2.386075		0.7		0.535222
5.0		5.254511		1.0		0.566249
1.0	0.1	0.667048	0.2	1.0	0.2	0.645063
	0.7	1.239376			0.7	0.919963
	1.2	1.513555			1.0	1.018821
	1.7	1.731334	0.6		0.2	0.436890
	2.0	1.845883			0.7	0.543046
	3.0	2.173501			1.0	0.566249

Table 7.3. Values of the surface mass transfer $\phi'(0)$ and the gradient of mass transfer $-\phi'(\eta)$ for some values of Sc and γ with $A = 1$, $M = 1.2$ and $\beta = 0.2$.

Chapter 8

MHD stagnation-point flow of a micropolar fluid over stretching surface

The work here is concerned with the two-dimensional magnetohydrodynamic (MHD) stagnation-point flow of an incompressible micropolar fluid over a non-linear stretching surface. The resulting nonlinear system of equations is solved analytically by using homotopy analysis method (HAM). The convergence of the obtained series solutions is explicitly discussed and given in the form of recurrence formulas. The influence of various pertinent parameters on the velocity, micro-rotation and skin-friction are shown in the tables and graphs. Comparison is also made with the corresponding numerical results of viscous ($K_1 = 0$) [148] and hydrodynamic micropolar fluid ($M = 0$) [149] for linear and non-linear stretching sheets. An excellent agreement is found.

8.1 Problem formulation

We consider the steady two-dimensional, incompressible flow of a micropolar fluid near a stagnation-point on the stretching surface in the region $y > 0$. The plane surface is located at $y = 0$ with a fixed end at $x = 0$. We take the non-linear stretching sheet in the XOZ plane (see Fig. 8.1). Two equal and opposite forces are applied along the x-axis. The surface is stretched

in the x-direction such that the x-component of the velocity varies non-linearly along it, i.e. $u_w(x) = cx^n$, where c (> 0) is constant of proportionality and n is a power index. A magnetic field of uniform strength B_0 is applied perpendicular to the surface. The magnetic Reynolds number is taken to be very small enough so that the induced magnetic field can be neglected. It is also assumed that the ambient fluid is moved with a external flow velocity $u_e(x) = ax^n$, where a (> 0) is a constant. In the absence of body couple, the equations governing the flow of an incompressible micropolar fluid are described by:

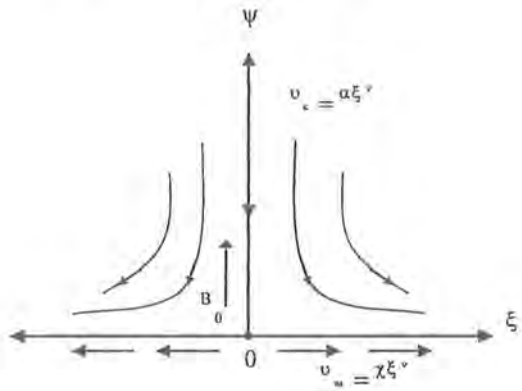

Fig. 8.1. Physical model and coordinate system.

$$\nabla \cdot \mathbf{V} = 0, \tag{8.1}$$

$$\rho \frac{D\mathbf{V}}{Dt} = -\nabla p + (\mu + k)\,\nabla^2 \mathbf{V} + k\nabla \times \mathbf{N} + \mathbf{J} \times \mathbf{B}, \tag{8.2}$$

$$\rho j \frac{D\mathbf{N}}{Dt} = \gamma_1 \nabla\,(\nabla \cdot \mathbf{N}) - \gamma_1 \nabla \times (\nabla \times \mathbf{N}) + k\nabla \times \mathbf{V} - 2k\mathbf{N}, \tag{8.3}$$

where D/Dt is the material derivative, $\mathbf{V}$ and $\mathbf{N}$ represent the velocity and micro-rotation vectors, μ is the dynamic viscosity, ρ and j denote the density and the gyration parameters of the fluid, γ_1 and k are the spin gradient viscosity and vortex viscosity, respectively.

The equations governing the boundary layer flow are:

$$\frac{\partial u}{\partial x} + \frac{\partial v}{\partial y} = 0, \tag{8.4}$$

$$u\frac{\partial u}{\partial x}+v\frac{\partial u}{\partial y}=u_e\frac{du_e}{dx}+\left(\nu+\frac{k}{\rho}\right)\frac{\partial^2 u}{\partial y^2}+\frac{k}{\rho}\frac{\partial N}{\partial y}+\frac{\sigma B_0^2}{\rho}\left(u_e-u\right), \tag{8.5}$$

$$u\frac{\partial N}{\partial x}+v\frac{\partial N}{\partial y}=\frac{\gamma_1}{\rho j}\frac{\partial^2 N}{\partial y^2}-\frac{k}{\rho j}\left(2N+\frac{\partial u}{\partial y}\right), \tag{8.6}$$

where u and v are the components of the velocity in the x- and y-directions, respectively, ν is the kinematic viscosity and σ is the electrical conductivity of the fluid. Here γ_1 is given by [149]

$$\gamma_1=\left(\mu+\frac{k}{2}\right)j \tag{8.7}$$

and $j=\nu/cx^{1-n/2}$ is the reference length. As pointed out by Ahmadi [150], relation (8.7) is invoked to allow Eqs. (8.4) – (8.6) to predict the correct behavior in the limiting case when microstructure effects become negligible and in this case micro-rotation N reduces to the angular velocity.

The boundary conditions of the problem are given by

$$\begin{aligned} u(x,0) &= u_w(x)=cx^n, \quad v(x,0)=0, \quad N(x,0)=-m_0\frac{\partial u}{\partial y}, \\ u(x,y) &\to u_e(x)=ax^n, \quad N(x,y)\to 0 \quad \text{as} \quad y\to\infty, \end{aligned} \tag{8.8}$$

in which m_0 is a constant and $0\le m_0\le 1$. The case $m_0=0$, which indicates $N=0$ at the wall, represents concentrated particle flows in which the microelements close to the wall surface are unable to rotate [151]. This case is also known as the strong concentration of mircoelements [152]. The case $m_0=\frac{1}{2}$ indicates the vanishing of anti-symmetric part of the stress tensor and denotes weak concentration [150] of mircoelements. We shall consider here both cases of $m_0=0$ and $m_0=\frac{1}{2}$. However, it can easily be shown that for $m_0=\frac{1}{2}$ the governing equations can be reduced to the classical problem of steady boundary layer flow of a viscous incompressible fluid near the plane wall. However the most common boundary condition used in the literature is the vanishing of the spin on the boundary, so-called strong interaction. The opposite extreme, the weak interaction, is the vanishing of the momentum stress on the boundary [152]. A third, or compromise in the vanishing of a linear combination of spin, shearing stress and couple stress, involving some friction coefficients, a particular case of which was the condition used by Peddieson [153].

Defining

$$\eta = \sqrt{\frac{c(n+1)}{2\nu}}x^{\frac{n-1}{2}}y, \qquad N = cx^n\sqrt{\frac{c(n+1)}{2\nu}}x^{\frac{n-1}{2}}g(\eta),$$
$$u = cx^n f'(\eta), \qquad v = -\sqrt{\frac{c\nu(n+1)}{2}}x^{\frac{n-1}{2}}\left[f(\eta)+\frac{n-1}{n+1}\eta f'(\eta)\right] \tag{8.9}$$

the incompressibility condition (8.1) is automatically satisfied and Eqs.(8.5) and (8.6) and boundary conditions (8.8) become

$$(1+K_1)f''' + M^2\left(\frac{a}{c}-f'\right) + ff'' + \frac{2n}{n+1}\left(\frac{a^2}{c^2}-f'^2\right) + K_1 g' = 0, \tag{8.10}$$

$$\left(1+\frac{K_1}{2}\right)g'' + fg' - \frac{3n-1}{n+1}f'g - \frac{2K_1}{n+1}(2g+f'') = 0, \tag{8.11}$$

$$\begin{aligned} f &= 0, \quad f'=1, \quad g=-m_0 f'' \quad \text{at} \quad \eta=0, \\ f' &= \frac{a}{c}, \quad g=0 \quad \text{as} \quad \eta\to\infty, \end{aligned} \tag{8.12}$$

where the primes indicate differentiation with respect to η and the local Hartman number M and the material parameter K_1 are

$$M^2 = \frac{2B_0^2\sigma}{c\rho(n+1)x^{n-1}}, \qquad K_1 = \frac{k}{\mu}. \tag{8.13}$$

For the problem under consideration, the wall skin friction τ_w is

$$\tau_w = \left[(\mu+k)\frac{\partial u}{\partial y} + kN\right]_{y=0}. \tag{8.14}$$

Using $u_w(x) = cx^n$ as a characteristic velocity, the skin friction coefficient C_f can be defined as

$$C_f = \frac{\tau_w}{\rho u_w^2}. \tag{8.15}$$

Substitution of Eq. (8.9) into Eq. (8.15) yields

$$C_f\,\mathrm{Re}_x^{\frac{1}{2}} = \left[(1+K_1)f''(0) + K_1 g(0)\right], \tag{8.16}$$

where $\mathrm{Re}_x = 2u_w x/\upsilon(n+1)$ is the local Reynolds number.

For $m_0 = 1/2$, we can take

$$g(\eta) = -\frac{1}{2} f''(\eta), \tag{8.17}$$

and the Eqs. (8.10) and (8.11) can be now reduced to a single equation

$$\left(1 + \frac{K_1}{2}\right) f''' + M^2 \left(\frac{a}{c} - f'\right) + f f'' + \frac{2n}{n+1}\left(\frac{a^2}{c^2} - f'^2\right) = 0. \tag{8.18}$$

The boundary conditions now are

$$f(0) = 0,\ f'(0) = 1,\ f'(\infty) = \frac{a}{c}. \tag{8.19}$$

Writing

$$f(\eta) = (1 + K_1)^{\frac{1}{2}} h(z),\ z = (1 + K_1)^{-\frac{1}{2}} \eta \tag{8.20}$$

the resulting problem takes the following form

$$h''' + M^2 \left(\frac{a}{c} - h'\right) + h h'' + \frac{2n}{n+1}\left(\frac{a^2}{c^2} - h'^2\right) = 0, \tag{8.21}$$

$$h(0) = 0,\ h'(0) = 1,\ h'(\infty) = \frac{a}{c} \tag{8.22}$$

and Eq. (8.16) now is

$$C_f \mathrm{Re}_x^{\frac{1}{2}} = \left(1 + \frac{K_1}{2}\right)^{-\frac{1}{2}} h''(0). \tag{8.23}$$

Note that in above equation prime indicates the differentiation with respect to z. In the next section, we will find the series solution of Eqs. (8.10) – (8.12) by homotopy analysis method (HAM).

8.2 HAM solutions for $f(\eta)$ and $g(\eta)$

For the analytic solutions using HAM, the velocity $f(\eta)$ and the micro-rotation velocity $g(\eta)$ distributions can be expressed by the set of base functions

$$\left\{\eta^k \exp(-n\eta) \middle| k \geq 0, n \geq 0\right\} \tag{8.24}$$

in the form

$$f(\eta) = a_{0,0}^0 + \sum_{m=1}^{\infty}\sum_{n=0}^{\infty}\sum_{k=0}^{\infty} a_{m,n}^k \eta^k \exp(-n\eta), \tag{8.25}$$

$$g(\eta) = b_{0,0}^0 + \sum_{m=1}^{\infty}\sum_{n=0}^{\infty}\sum_{k=0}^{\infty} b_{m,n}^k \eta^k \exp(-n\eta), \tag{8.26}$$

where $a_{m,n}^k$ and $b_{m,n}^k$ are the coefficients. Based on the *rule of solution expressions* by (8.25), (8.26) and the boundary conditions (8.12), we choose

$$f_0(\eta) = (1 - \frac{a}{c})(1 - \exp(-\eta)) + \frac{a}{c}\eta, \tag{8.27}$$

$$g_0(\eta) = m_0 \exp(-\eta), \tag{8.28}$$

as our initial approximations of $f(\eta)$ and $g(\eta)$. We select the auxiliary linear operators $\mathcal{L}_f(f)$ and $\mathcal{L}_g(f)$ as

$$\mathcal{L}_f(f) = \frac{d^3 f}{d\eta^3} - \frac{df}{d\eta}, \tag{8.29}$$

$$\mathcal{L}_g(f) = \frac{d^2 f}{d\eta^2} - f, \tag{8.30}$$

which have the following properties:

$$\mathcal{L}_f[C_1 + C_2 \exp(\eta) + C_3 \exp(-\eta)] = 0, \tag{8.31}$$

$$\mathcal{L}_g[C_4 \exp(\eta) + C_5 \exp(-\eta)] = 0 \tag{8.32}$$

where C_i, $(i = 1 - 5)$ are the arbitrary constants. If $p \in [0, 1]$ is an embedding parameter and $\hbar_f$, $\hbar_g$ are the non-zero auxiliary parameters, respectively then the zeroth-order deformation problems are

$$(1-p)\mathcal{L}_f\left[\widehat{f}(\eta;p) - f_0(\eta)\right] = p\hbar_f \mathcal{N}_f\left[\widehat{f}(\eta;p), \widehat{g}(\eta;p)\right], \tag{8.33}$$

$$\widehat{f}(0;p) = 0, \qquad \widehat{f}'(0;p) = 1, \quad \widehat{f}'(\infty;p) = \frac{a}{c}, \tag{8.34}$$

$$(1-p)\,\mathcal{L}_g\left[\widehat{g}\,(\eta;p)-g_0\,(\eta)\right]=p\hbar_g\mathcal{N}_g\left[\widehat{f}\,(\eta;p),\widehat{g}\,(\eta;p)\right], \tag{8.35}$$

$$\widehat{g}\,(0;p)=-m_0\widehat{f}''\,(0;p), \qquad \widehat{g}\,(\infty;p)=0, \tag{8.36}$$

in which the non-linear operators $\mathcal{N}_f$ and $\mathcal{N}_g$ are given as

$$\begin{aligned}\mathcal{N}_f\left[\widehat{f}\,(\eta;p),\widehat{g}\,(\eta;p)\right] &= (1+K_1)\frac{\partial^3\widehat{f}\,(\eta;p)}{\partial\eta^3}+K_1\frac{\partial\widehat{g}\,(\eta;p)}{\partial\eta}+M^2\left(\frac{a}{c}-\frac{\partial\widehat{f}\,(\eta;p)}{\partial\eta}\right)\\ &\quad+\frac{2n}{n+1}\frac{a^2}{c^2}+\widehat{f}\,(\eta;p)\frac{\partial^2\widehat{f}\,(\eta;p)}{\partial\eta^2}-\frac{2n}{n+1}\left(\frac{\partial\widehat{f}\,(\eta;p)}{\partial\eta}\right)^2,\end{aligned} \tag{8.37}$$

$$\begin{aligned}\mathcal{N}_g\left[\widehat{f}\,(\eta;p),\widehat{g}\,(\eta;p)\right] &= \left(1+\frac{K_1}{2}\right)\frac{\partial^2\widehat{g}\,(\eta;p)}{\partial\eta^2}-\frac{2K_1}{n+1}\left(2\widehat{g}\,(\eta;p)+\frac{\partial^2\widehat{f}\,(\eta;p)}{\partial\eta^2}\right)\\ &\quad+\widehat{f}\,(\eta;p)\frac{\partial\widehat{g}\,(\eta;p)}{\partial\eta}-\frac{3n-1}{n+1}\frac{\partial\widehat{f}\,(\eta;p)}{\partial\eta}\widehat{g}\,(\eta;p).\end{aligned} \tag{8.38}$$

For $p=0$ and $p=1$, the above zeroth-order equations (8.33) and (8.35) have the solutions

$$\widehat{f}\,(\eta;0)=f_0\,(\eta), \qquad \widehat{g}\,(\eta;0)=g_0\,(\eta), \tag{8.39}$$

and

$$\widehat{f}\,(\eta;1)=f\,(\eta), \qquad \widehat{g}\,(\eta;1)=g\,(\eta). \tag{8.40}$$

Expanding $\widehat{f}(\eta)$ and $\widehat{g}(\eta)$ in Taylor series with respect to p, we have

$$\widehat{f}\,(\eta;p)=f_0\,(\eta)+\sum_{m=1}^{\infty}f_m\,(\eta)\,p^m, \tag{8.41}$$

$$\widehat{g}\,(\eta;p)=g_0\,(\eta)+\sum_{m=1}^{\infty}g_m\,(\eta)\,p^m, \tag{8.42}$$

where

$$f_m\,(\eta)=\frac{1}{m!}\frac{\partial^m\widehat{f}\,(\eta;p)}{\partial p^m}\bigg|_{p=0}, \qquad g_m\,(\eta)=\frac{1}{m!}\frac{\partial^m\widehat{g}\,(\eta;p)}{\partial p^m}\bigg|_{p=0}, \tag{8.43}$$

respectively. Equations. (8.33) and (8.35) contain the auxiliary parameters $\hbar_f$ and $\hbar_g$ are chosen in such a way that these series are convergent at $p=1$, we have, using Eq. (8.39), the

solution series of the form

$$f(\eta) = f_0(\eta) + \sum_{m=1}^{\infty} f_m(\eta), \tag{8.44}$$

$$g(\eta) = g_0(\eta) + \sum_{m=1}^{\infty} g_m(\eta). \tag{8.45}$$

Differentiating the zeroth-order equations (8.33) – (8.36) m times with respect to p, then setting $p = 0$, and finally dividing by $m!$ we have the mth-order deformation problems as

$$\mathcal{L}_f[f_m(\eta) - \chi_m f_{m-1}(\eta)] = \hbar_f \mathcal{R}_m^f(\eta), \tag{8.46}$$

$$f_m(0) = f_m'(0) = f_m'(\infty) = 0, \tag{8.47}$$

$$\mathcal{L}_g[g_m(\eta) - \chi_m g_{m-1}(\eta)] = \hbar_g \mathcal{R}_m^g(\eta), \tag{8.48}$$

$$g_m(0) - m_0 f''(0) = g_m(\infty) = 0, \tag{8.49}$$

where

$$\begin{aligned} \mathcal{R}_m^f(\eta) &= (1+K_1) f_{m-1}''' + M^2\left(\frac{a}{c}(1-\chi_m) - f_{m-1}'\right) + K_1 g_{m-1}' \\ &\quad + (1-\chi_m)\frac{2n}{n+1}\frac{a^2}{c^2} + \sum_{k=0}^{m-1}\begin{bmatrix} f_{m-1-k} f_k'' \\ -\frac{2n}{n+1} f_{m-1-k}' f_k' \end{bmatrix}, \end{aligned} \tag{8.50}$$

$$\mathcal{R}_m^g(\eta) = \left(1+\frac{K_1}{2}\right) g_{m-1}'' - \frac{2K_1}{n+1}(2g_{m-1} - f_{m-1}'') - \sum_{k=0}^{m-1}\left[g_{m-1-k}' f_k - \frac{3n-1}{n+1} g_k f_{m-1-k}'\right], \tag{8.51}$$

and

$$\chi_m = \begin{cases} 0, & m \le 1, \\ 1, & m > 1. \end{cases} \tag{8.52}$$

Let $f_m^\star(\eta)$ and $g_m^\star(\eta)$ denote the special solutions of equations (8.46) and (8.48) and using the boundary conditions (8.47) and (8.49) one can write the general solutions given by

$$f_m(\eta) = f_m^\star(\eta) + C_1 + C_2 \exp(\eta) + C_3 \exp(-\eta), \tag{8.53}$$

$$g_m(\eta) = g_m^*(\eta) + C_4 \exp(\eta) + C_5 \exp(-\eta), \tag{8.54}$$

where the integral constants C_i, $(i = 1, 2...5)$ are determined by the boundary conditions (8.47) and (8.49). It is noted that to satisfy the boundary conditions at infinity, we must put C_2 and C_4 equal to zero.

In this way, it is easy to solve the linear non-homogeneous Eqs. (8.46) and (8.48) by using the symbolic software Mathematica one after the other in the order $m = 1, 2, 3.....$

8.3 Convergence of the HAM solutions

The series solutions of the functions f and g are given in Eqs. (8.44) and (8.45). The convergence of these series and rate of approximation for homotopy analysis method strongly depends upon the value of the auxiliary parameters $\hbar_f$ and $\hbar_g$. To see the range of admissible values of $\hbar_f$ and $\hbar_g$, the $\hbar$-curves are plotted in Fig. 8.2(a, b) for the 15th-order of approximation. In Fig. 8.2(a) $\hbar_f$-curve for $f''(0)$ is plotted when $K_1 = 1$, $M = 0.5$, $n = 1$, $m_0 = 0.5$ and $a/c = 0.5$. The admissible range of $\hbar_f$ for the stated value of the parameters is $-0.8 \leq \hbar_f \leq -0.2$. For $g'(0)$, the admissible values of $\hbar_g$ are given in Fig. 8.2(b). The range for values of $\hbar_g$ is $-0.8 \leq \hbar_g \leq -0.1$. Here, it is noted that the series solutions in Eqs. (8.44) and (8.45) converge for all values of the parameters in the whole region of η when $\hbar_f = \hbar_g = \hbar = -0.5$.

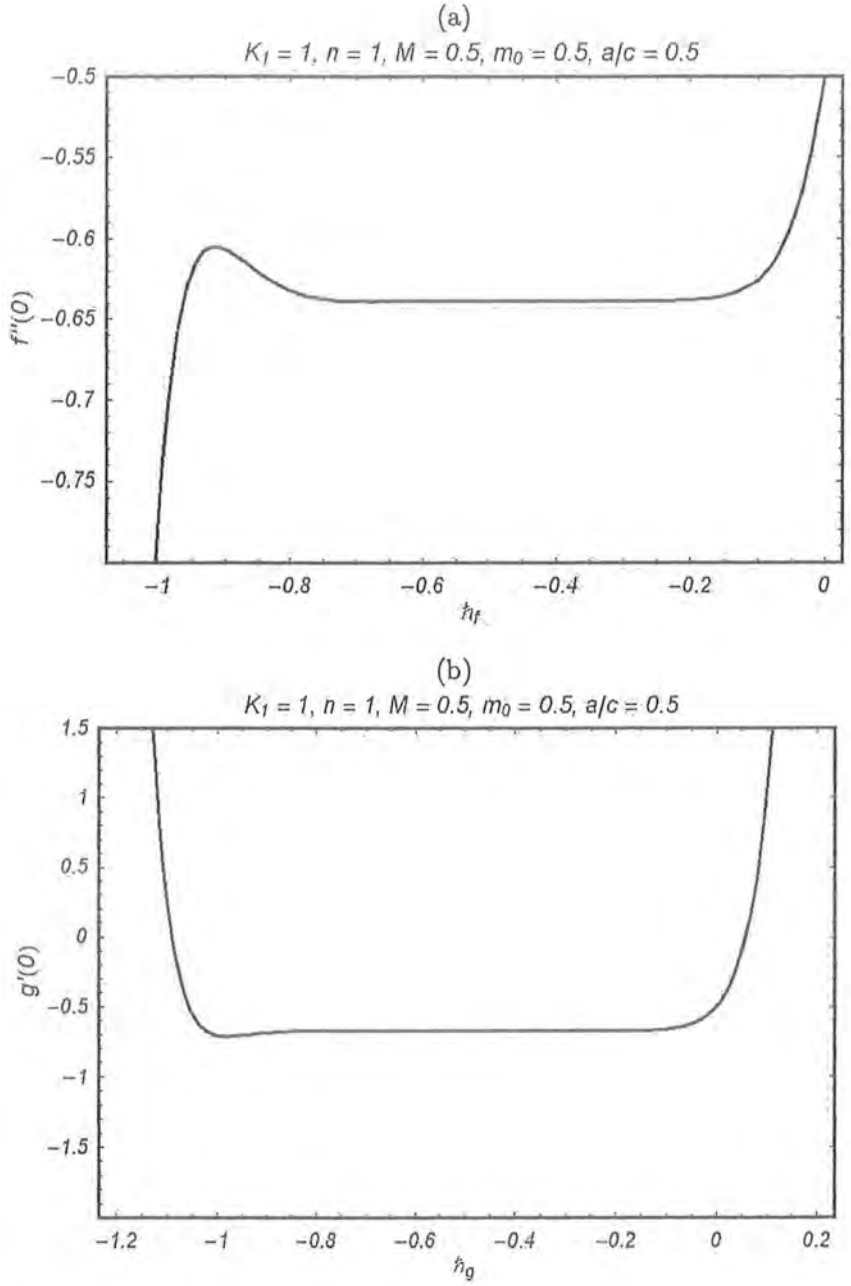

Fig. 8.2: The $\hbar$-curves of $f''(0)$ and $g'(0)$ at the 15th-order of approximations.

8.4 Results and discussion

In this section, Figs. 8.3 – 8.6 have been made to analyze the effects of non-linear stretching parameter n, the material parameter or the vortex viscosity K_1, the magnetic parameter M and the ratio of the external flow rate to the stretching rate a/c on the velocity component f' and the micro-rotation velocity g. The numerical values for the wall shear stress (skin friction coefficient) $C_f \, \mathrm{Re}_x^{1/2}$ in Eq. (8.16) (when $m_0 = 0$) and Eq. (8.23) (when $m_0 = 1/2$) for some different values of the physical parameters n, K_1, M and a/c in case of viscous ($K_1 = 0$) and micropolar fluids for linear ($u_w = cx$) and non-linear ($u_w = cx^n$) stretching velocity are given in Tables 8.1 – 8.5. The comparison of the obtained results with the existing results is also made for viscous ($K_1 = 0$) and hydrodynamic micropolar ($M = 0$) fluids.

Fig. 8.3 shows the effects of non-linear stretching parameter or the power index of stretching rate n on the velocity fields $f'$and microrotation velocity g respectively. It is noted from Fig. 8.3(a) that the velocities f' are decreased when the power index n increases and keeping $M = 0.2$, $a/c = 0.1$, $K_1 = 1$, $m_0 = 0.5$ fixed. The boundary layer thickness in case of f' increases as n increases. Since increase in the non-linearity causes the increase in the friction of the wall with the fluid at $\eta = 0$ therefore the boundary layer thickness increases automatically. The effects of the power index of stretching rate n on the microrotation velocity g is exactly the same as that of f' (see from Fig. 8.3(b)). The effects of vortex-viscosity parameter K_1 on the velocity fields $f'$and microrotation velocity g are depicted in Fig. 8.4. From Fig. 8.4(a), it is observed that the velocity f' increases by increasing micropolar effects. The velocity in viscous fluid is smaller when compared with that of micropolar fluid. It is also clear from Fig. 8.4(b) that the microrotation velocity g increases with an increase in the vortex-viscosity K_1. As K_1 increases, the decrease in viscosity is responsible to decrease f' and g. The boundary layer thickness increases as K_1 increases in case of the velocity f'. Fig. 8.5 depicts the influences of the magnetic parameter M on the fluid velocity f' and the angular velocity of the microrotation g when $n = 5$, $a/c = 0.1$, $K_1 = 1$ and $m_0 = 0.5$. It is a known fact that the application of a uniform magnetic field normal to the flow direction gives rise to a force called Lorentz force. This force has tendency to slow down the velocity of the fluid, as in Fig. 8.5(a). It can be seen from Fig. 8.5(b) that the angular velocity of the microrotation is increased by increasing the magnetic parameter M. It is seen from Fig. 8.6(a,b) that for $a/c > 1$, the flow possesses

boundary layer structure. It is further observed that the boundary layer thickness of the flow decreases with an increase in a/c. Since for fixed value of c, corresponding to the stretching of the surface, increase in a in relation to c such as (a/c) implies increasing in straining motion near the stagnation region resulting in increased acceleration of the external stream, and this leads to the thinning of boundary layer with an increase in a/c. Furthermore it is seen from Fig. 8.6(a) that when $a/c < 1$, the flow has an inverted boundary layer structure. It results from the fact that when $a/c < 1$, the stretching velocity cx^n of the surface exceeds the velocity ax^n of the external stream.

Tables 8.1 and 8.2 show the comparison of the values of the skin-friction coefficient obtained by homotopy-Pade approximation with the numerical results by Nazar et al. [150] for viscous fluid ($K_1 = 0$ and $M = 0$), the micropolar fluid ($K_1 \neq 0$ and $M = 0$) and linear stretching velocity ($m_0 = 0$ and $m_0 = 1/2$) in the absence of magnetic field. It is found that for $a/c < 1$, the skin friction coefficient $C_f \operatorname{Re}_x^{1/2}$ decreases as the vortex-viscosity K_1 increases. For $a/c = 1$, the values of the skin friction coefficient $C_f \operatorname{Re}_x^{1/2}$ are zero for all values of K_1 and, for $a/c > 1$ the skin friction coefficient increases with the increase in K. These tables show excellent agreement with the existing numerical results in reference [149].

Table 8.3 is made in order to compare the present results of non-linear stretching sheet with the obtained numerical results of reference [148] for hydrodynamic viscous fluid in the absence of stagnation-point flow ($K_1 = j = \gamma_1 = M = a.c = 0$). The magnitude of the skin-friction at the wall $-f''(0)$ increases when a power index n of stretching velocity increases and at $n = 10$ the values of $-f''(0) = 1.234875$ is in good agreement with the references [148] and [154]. By varying n, an excellent agreement is noted between present results obtained by homotopy-Pade approximation and the existing numerical results of reference [148].

Table 8.4 gives the values of the skin friction coefficient $C_f \operatorname{Re}_x^{1/2}$ for different values of n in the case of hydrodynamic micropolar fluid by considering $a/c = 0.1$, $m_0 = 0$ and $a/c = 0.1$, $m_0 = 1/2$. The magnitude of the skin-friction coefficient $C_f \operatorname{Re}_x^{1/2}$ increases with the increase in n both for $m_0 = 0$ and $m_0 = 1/2$. However this increment is larger in case of $m_0 = 0$ when compared with the case $m_0 = 1/2$. Table 8.5 is prepared to give the values of skin-friction coefficient $C_f \operatorname{Re}_x^{1/2}$ by keeping $a/c = 0.1$ fixed for micropolar fluid ($K = 1$) and varying the values of n and M in case of $m_0 = 0$ and $m_0 = 1/2$, respectively. As expected, the magnitude

of the skin-friction coefficient $C_f \, \mathrm{Re}_x^{1/2}$ increases by increasing the power index of the stretching rate n and the magnetic parameter M for both the cases $m_0 = 0$ and $m_0 = 1/2$. It is also found that this change in the magnitude of the skin friction coefficient is larger in case of $m_0 = 0$.

8.5 Final remarks

In this chapter, the series solutions of highly non-linear problem describing the MHD flow of a micropolar fluid over a non-linear stretching surface is developed. A powerful easy to use technique is employed in obtaining the series solutions. The recurrence formulas which are not easy to obtain are presented. Finally, the flow quantities have been discussed through graphs and tables. The physical results are interesting. An excellent agreement of the present results with existing limiting results is shown.

(a)

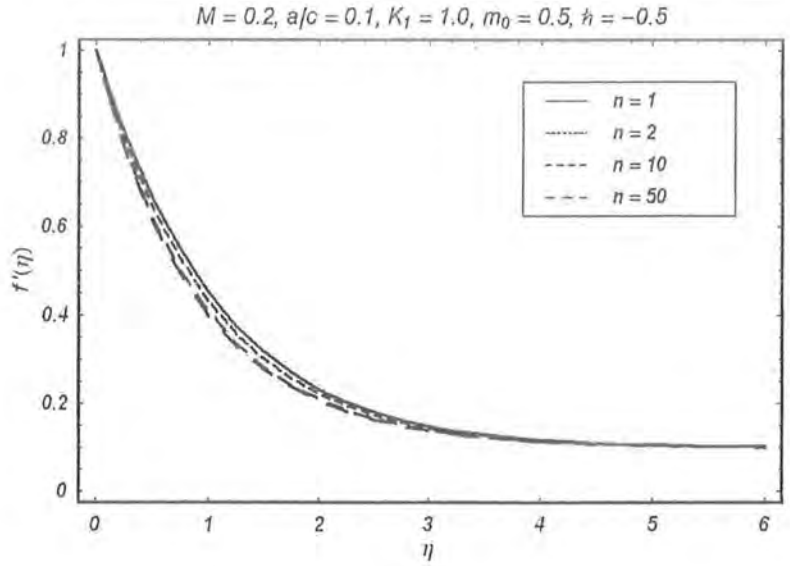

(b)

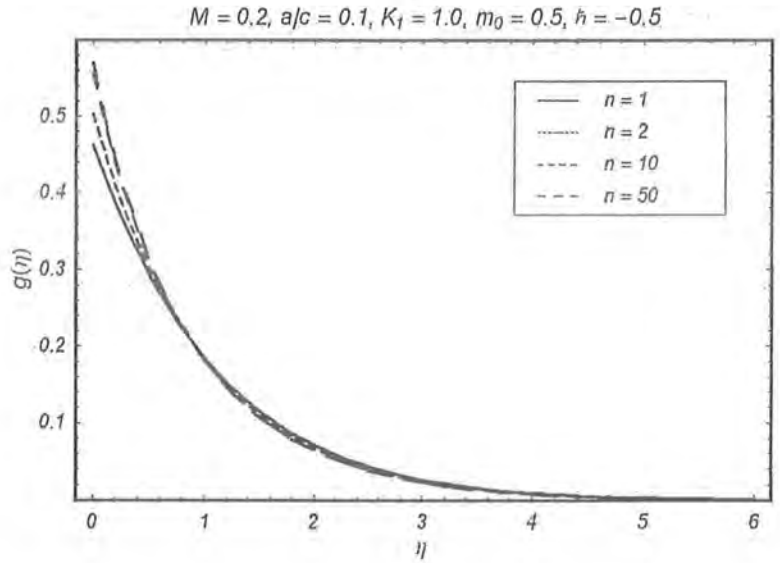

Fig. 8.3(a,b): Influence of non-linear stretching parameter n on the velocity component f' and the micro-rotation velocity g.

(a)

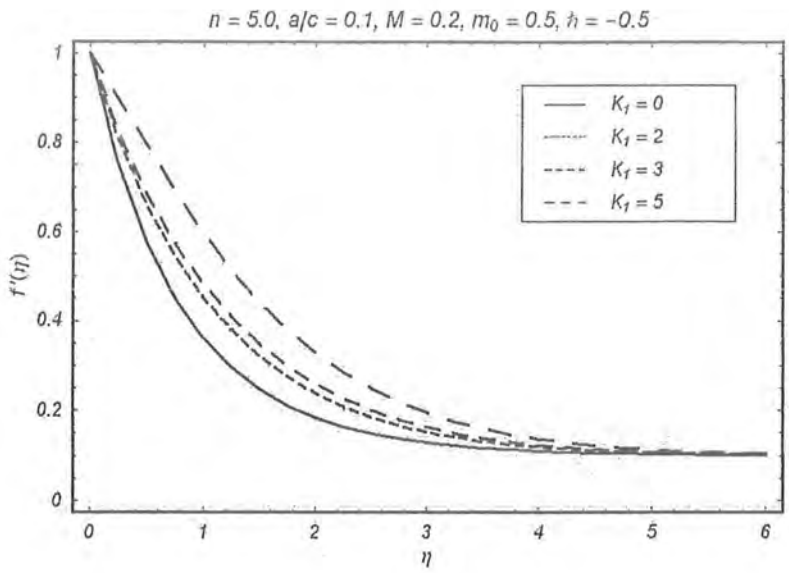

(b)

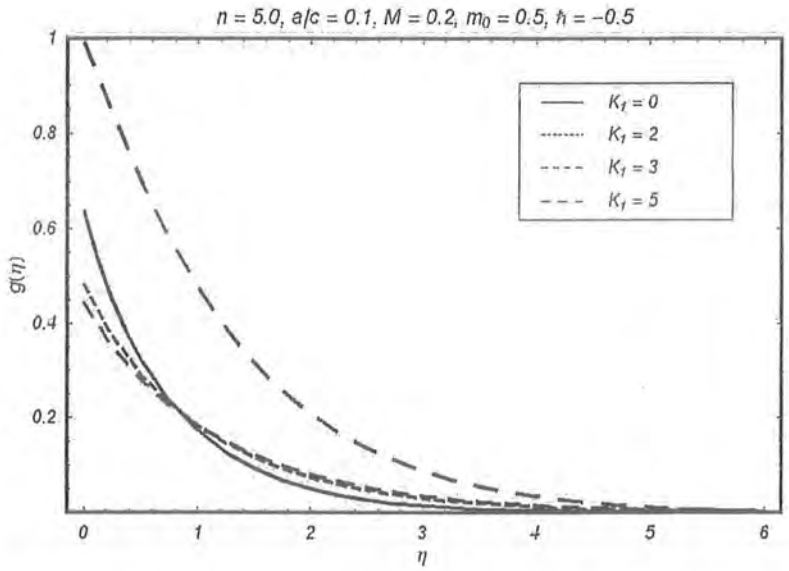

Fig. 8.4(a,b): Influence of material parameter K_1 on the velocity component f' and the micro-rotation velocity g.

(a)

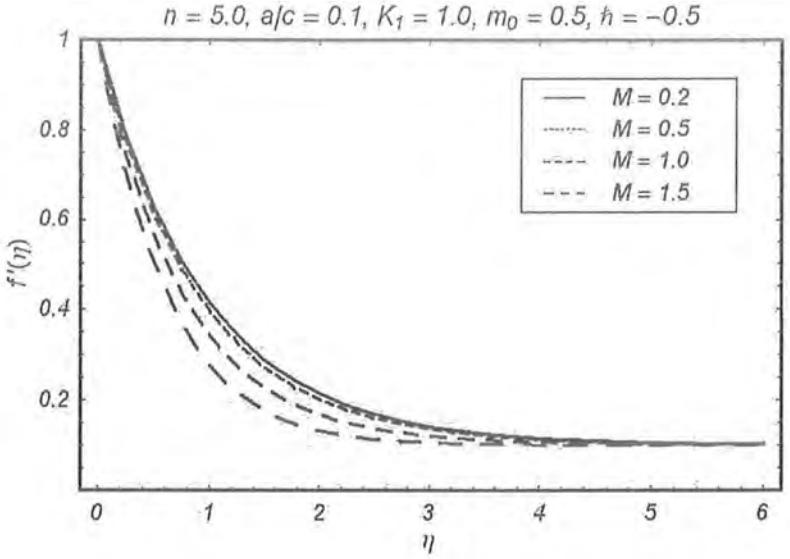

(b)

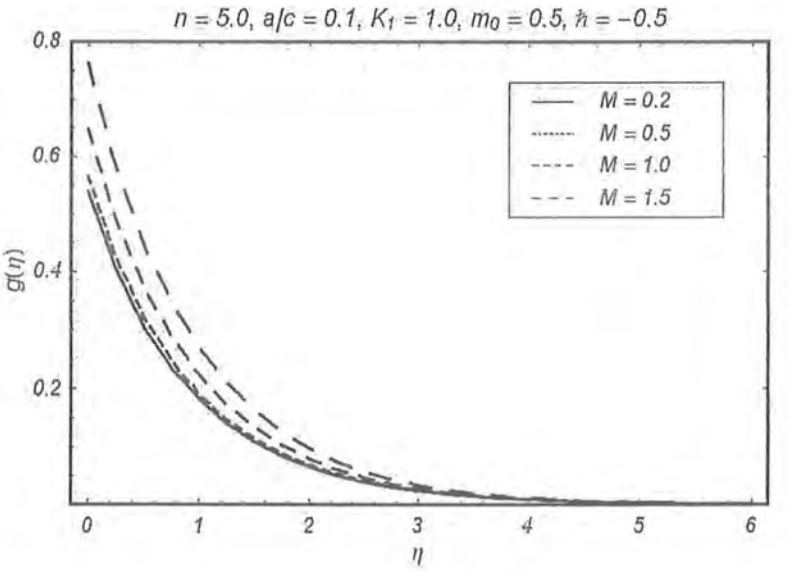

Fig. 8.5(a,b): Influence of magnetic parameter M on the velocity component f' and the micro-rotation velocity g.

(a)

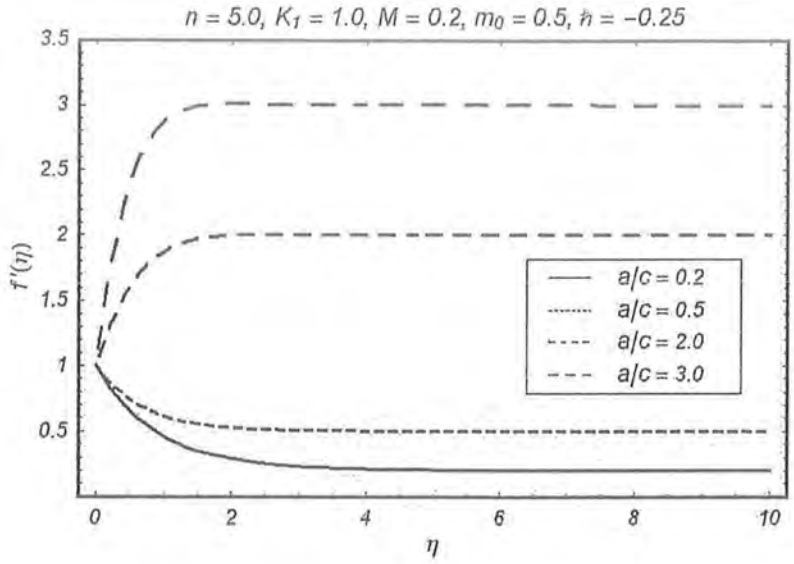

(b)

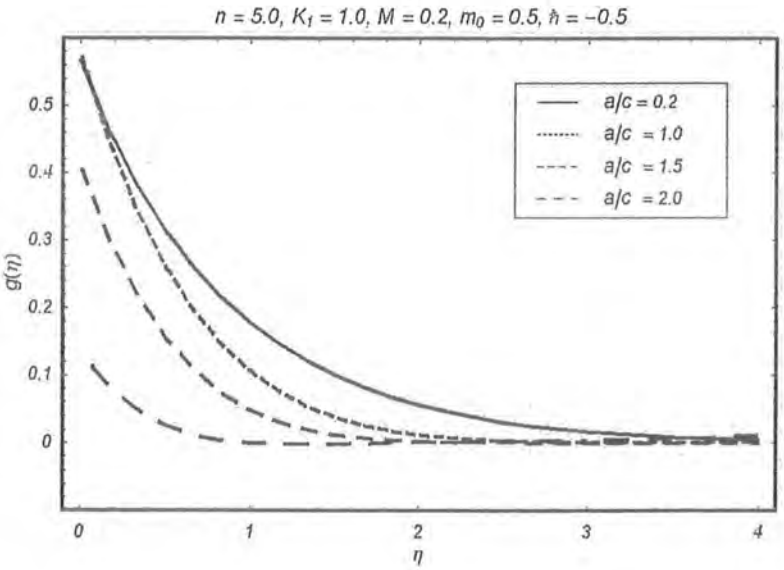

Fig. 8.6(a,b): Influence of stagnation point parameter a/c on the velocity component f' and the micro-rotation velocity g.

a/c	$K_1 = 0$		$K_1 = 1$		$K_1 = 2$	
	Ref. [149]	Present Results	Ref. [149]	Present Results	Ref. [149]	Present Results
0.01	−0.9980	−0.99802	−1.3653	−1.36525	−1.6183	−1.61814
0.02	−0.9958	−0.99578	−1.3622	−1.36222	−1.6147	−1.61454
0.05	−0.9876	−0.98757	−1.3512	−1.35119	−1.6015	−1.60146
0.10	−0.9694	−0.96938	−1.3268	−1.32681	−1.5726	−1.57263
0.20	−0.9181	−0.91810	−1.2579	−1.25792	−1.4914	−1.49136
0.50	−0.6673	−0.66732	−0.9175	−0.91750	−1.0893	−1.08934
1.00	0.0000	0.00000	0.0000	0.00000	0.0000	0.00000
2.00	2.0175	2.01750	2.8062	2.8063	3.3595	3.35941
3.00	4.7296	4.72928	6.6024	6.6023	7.9345	7.9344

Table 8.1. Comparison of homotopy-Pade approximations with the results of Nazar et al. [149] when $n = 1$, $M = 0$, $m_0 = 0$.

a/c	$K_1 = 0$		$K_1 = 1$		$K_1 = 2$	
	Ref. [149]	Present Results	Ref. [149]	Present Results	Ref. [149]	Present Results
0.01	−0.9980	−0.99802	−1.2224	−1.22232	−1.4116	−1.41142
0.02	−0.9958	−0.99578	−1.2196	−1.21958	−1.4084	−1.40825
0.05	−0.9876	−0.98757	−1.2095	−1.20953	−1.3967	−1.39665
0.10	−0.9694	−0.96938	−1.1872	−1.18725	−1.3709	−1.37092
0.20	−0.9181	−0.91810	−1.1244	−1.12445	−1.2984	−1.29840
0.50	−0.6673	−0.66732	−0.8172	−0.81722	−0.9437	−0.94365
1.00	0.0000	0.0000	0.0000	0.0000	0.0000	0.0000
2.00	2.0175	2.01750	2.4710	2.47095	2.8532	2.85321
3.00	4.7296	4.72928	5.7925	5.79216	6.6885	6.6882

Table 8.2. Comparison of homotopy-Pade approximations [20, 20] with the results of Nazar et al. [149] when $n = 1$, $M = 0$, $m_0 = 1/2$.

n	Cortell [148]	HAM solution
0.0	0.627547	0.627547
0.2	0.766758	0.766837
0.5	0.889477	0.889544
0.75	0.953786	0.953956
1.0	1.0	1.0
1.5	1.061587	1.061601
3.0	1.148588	1.148593
7.0	1.216847	1.216851
10.0	1.234875	1.234874
20.0	1.257418	1.257423
100.0	1.276768	1.276773

Table 8.3. Values of the wall shear stress $-f''(0)$ when $K_1 = \gamma_1 = j = 0$ and $M = a/c = 0$.

n	$m_0 = 0$	$m_0 = 1/2$
0.0	−0.768871	−0.714672
0.5	−1.15945	−1.04908
0.75	−1.25676	−1.12981
1.0	−1.32681	−1.18725
1.5	−1.42134	−1.26380
3.0	−1.55692	−1.37142
5.0	−1.62982	−1.42799
7.0	−1.66581	−1.45551
10.0	−1.69508	−1.47768
20.0	−1.73212	−1.50538
50.0	−1.75606	−1.52306
100.0	−1.76436	−1.52914

Table 8.4. Results obtained by the homotopy-Pade approximations [20, 20] for different values of the non-linear stretching parameter n when $K_1 = 1$, $a/c = 0.1$ and $M = 0$.

n	M	$m_0 = 0$	$m_0 = 1/2$	n	M	$m_0 = 0$	$m_0 = 1/2$
1	0.2	−1.35984	−1.21681	10	0.2	−1.72041	−1.49982
	0.5	−1.50982	−1.35038		0.5	−1.84454	−1.60824
	0.7	−1.65704	−1.48075		0.7	−1.97308	−1.72032
	1	−1.93058	−1.72147		1	−2.21773	−1.93321
1.5	0.2	−1.45175	−1.29087	20	0.2	−1.75699	−1.52703
	0.5	−1.59398	−1.41705		0.5	−1.87925	−1.63345
	0.7	−1.73593	−1.54234		0.7	−2.00631	−1.74394
	1	−2.00139	−1.77538		1	−2.24859	−1.95436
3	0.2	−1.58444	−1.39573	50	0.2	−1.78065	−1.54401
	0.5	−1.71685	−1.51242		0.5	−1.90183	−1.64958
	0.7	−1.81574	−1.63088		0.7	−2.02801	−1.75907
	1	−2.10634	−1.85353		1	−2.26887	−1.96794
5	0.2	−1.65610	−1.45109	100	0.2	−1.78886	−1.55038
	0.5	−1.78390	−1.56325		0.5	−1.90968	−1.65514
	0.7	−1.91531	−1.67826		0.7	−2.03558	−1.76428
	1	−2.16448	−1.89565		1	−2.27598	−1.97262

Table 8.5 :. Results obtained by the homotopy-Pade approximations [20, 20] for different values of the non-linear stretching parameter n when $M = 0.2, 0.5, 0.7, 1$, $a/c = 0.1$ and $K_1 = 1$.

Chapter 9

Mixed convection flow of a micropolar fluid bounded by a nonlinear stretching sheet

This chapter aims to investigate the steady two-dimensional mixed convection flow of a micropolar fluid over a non-linear stretching sheet. The governing non-linear partial differential equations are transformed into coupled non-linear ordinary differential equations. The series solution of the non-linear problem is obtained by utilizing the homotopy analysis method (HAM). The convergence of the obtained series solutions is carefully checked. The physical significance of interesting parameters on the flow and the thermal fields are shown through graphs and discussed in detail. The values of wall shear stress, couple wall stress and the local Nusselt number are tabulated. Comparison is also made with the corresponding results of viscous fluid with no mixed convection and an excellent agreement is noted.

9.1 Flow analysis

Consider the steady two-dimensional, incompressible flow of a micropolar fluid over a non-linear stretching surface in the region $y > 0$. The geometry of the problem is shown in Fig. 9.1. Two equal and opposite forces are applied along the x-axis so that the wall is stretched non-linearly by keeping the origin fixed at $y = 0$. The non-linear variation of the x-component

of the velocity is $u_w = cx^n$, c (> 0) is constant of proportionality and n is a power index. The gravitational acceleration, g_c, acts in the downward direction. The temperature of the outside surface of the sheet is maintained at a constant temperature of T_w and far away from the sheet temperature is T_∞, where $T_w > T_\infty$. The temperature difference between the body surface and the surrounding micropolar fluid generates a buoyancy force, which results in an upward convective flow. Neglecting viscous dissipation, the boundary layer equations for micropolar fluid are given in the following form:

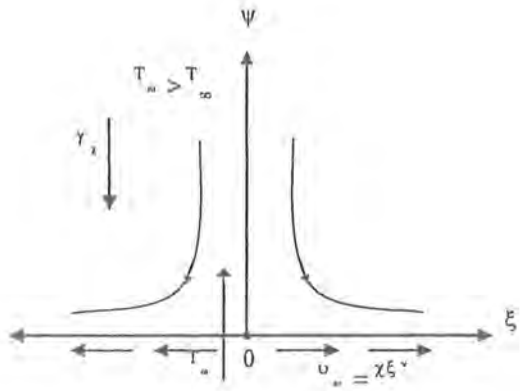

Fig. 9.1. Physical model and coordinate system

$$\frac{\partial u}{\partial x} + \frac{\partial v}{\partial y} = 0, \tag{9.1}$$

$$u\frac{\partial u}{\partial x} + v\frac{\partial u}{\partial y} = \left(\nu + \frac{k}{\rho}\right)\frac{\partial^2 u}{\partial y^2} + \frac{k}{\rho}\frac{\partial N}{\partial y} + g_c\beta_T\left(T - T_\infty\right), \tag{9.2}$$

$$u\frac{\partial N}{\partial x} + v\frac{\partial N}{\partial y} = \frac{\gamma_1}{\rho j}\frac{\partial^2 N}{\partial y^2} - \frac{k}{\rho j}\left(2N + \frac{\partial u}{\partial y}\right), \tag{9.3}$$

$$u\frac{\partial T}{\partial x} + v\frac{\partial T}{\partial y} = \frac{\alpha}{\rho c_p}\frac{\partial^2 T}{\partial y^2}. \tag{9.4}$$

In above equations u and v indicate the velocity components in the x- and y-directions, respectively, N the micro-rotation or angular velocity whose direction of rotation is in the xy-plane, ρ the fluid density, ν the fluid kinematic viscosity, β_T the thermal expansion coefficient, α

the thermal diffusivity, c_p the specific heat, T the temperature and j, γ_1 and k the respective microinertial per unit mass, spin gradient viscosity and vortex viscosity.

The above partial differential equations subject to the following conditions:

$$\begin{aligned} u &= cx^n, \quad v = 0, \quad N = -m_0\frac{\partial u}{\partial y}, \quad T = T_w, \quad \text{at} \quad y = 0, \\ u &\to 0, \quad N \to 0, \quad T \to T_\infty \quad \text{as} \quad y \to \infty. \end{aligned} \tag{9.5}$$

According to the study of reference [149], the definition of γ_1 is

$$\gamma_1 = \left(\mu + \frac{k}{2}\right) j, \tag{9.6}$$

where m_0 $(0 \leq m_0 \leq 1)$ is a constant, μ the fluid dynamic viscosity, and $j = \nu/cx^{1-n/2}$ the reference length. Also $m_0 = 0$ corresponds to $N = 0$ indicating the concentrated particle flows in which the microelements close to the wall surface are unable to rotate. This case is also known as the strong concentration of mircoelements. For $m_0 = 1/2$, one obtains the weak concentration of mircoelements. This value of m_0 indicates the vanishing of anti-symmetric part of the stress tensor. Here both cases of $m_0 = 0$ and $m_0 = 1/2$ are considered. As given by [149], $m_0 = 1$ is used for the modelling of turbulent boundary layer flow. However, it can easily be shown that for $m_0 = 1/2$ the governing equations can be reduced to the classical problem of steady boundary layer flow of a viscous incompressible fluid near the plane wall.

To write the flow equations in simpler form, the following non-dimensional quantities are introduced:

$$\begin{aligned} \eta &= \sqrt{\frac{c(n+1)}{2\nu}}x^{\frac{n-1}{2}}y, \quad N = cx^n\sqrt{\frac{c(n+1)}{2\nu}}x^{\frac{n-1}{2}}g(\eta), \quad \theta(\eta) = \frac{T - T_\infty}{T_w - T_\infty}, \\ u &= cx^n f'(\eta), \quad v = -\sqrt{\frac{c\nu(n+1)}{2}}x^{\frac{n-1}{2}}\left[f(\eta) + \frac{n-1}{n+1}\eta f'(\eta)\right]. \end{aligned} \tag{9.7}$$

Through Eq. (9.7), the continuity equation (9.1) is identically satisfied and Eqs.(9.2) – (9.5) give

$$(1 + K_1)f''' + ff'' - \frac{2n}{n+1}f'^2 + K_1 g' + \frac{2}{n+1}\lambda\theta = 0, \tag{9.8}$$

$$\left(1 + \frac{K_1}{2}\right)g'' + fg' - \frac{3n-1}{n+1}f'g - \frac{2K_1}{n+1}(2g + f'') = 0, \tag{9.9}$$

$$\theta'' + \Pr f\theta' = 0, \tag{9.10}$$

$$\begin{aligned} f &= 0, \quad f' = 1, \quad g = -m_0 f''(0), \quad \theta = 1 \quad \text{at} \quad \eta = 0, \\ f' &\to 0, \qquad g \to 0, \qquad \theta \to 0 \qquad \text{as} \qquad \eta \to \infty. \end{aligned} \tag{9.11}$$

In above equations the prime signifies the differentiation with respect to η, $K_1 = k/\mu (> 0)$ the vortex viscosity or the material parameter, $\Pr = \mu c_p/\alpha$ the Prandtl number and the constant $\lambda (\geq 0)$ is the buoyancy or mixed convection parameter defined by

$$\lambda = \frac{Gr_x}{\mathrm{Re}_x^2}, \tag{9.12}$$

where $Gr_x = g_c \beta_T (T_w - T_\infty) x^3/\nu^2$ is the local Grashof number and $\mathrm{Re}_x = u_w x/\nu$ is the local Reynolds number.

The physical quantities of interest are the skin friction coefficient C_f and the local Nusselt number Nu_x, which are defined as

$$C_f = \frac{\tau_w}{\rho u_w^2}, \qquad Nu_x = \frac{x q_w}{\alpha (T_w - T_\infty)}, \tag{9.13}$$

in which the wall shear stress τ_w and the heat transfer q_w from the plate are

$$\tau_w = \left[(\mu + k) \frac{\partial u}{\partial y} + kN \right]_{y=0}, \qquad q_w = -\alpha \frac{\partial T}{\partial y}_{y=0}. \tag{9.14}$$

In non-dimensional form, the above quantities reduce to

$$C_f \, \mathrm{Re}_x^{1/2} = \left(1 + \frac{K_1}{2} \right) f''(0), \qquad Nu_x \, \mathrm{Re}_x^{-1/2} = -\theta'(0). \tag{9.15}$$

The next section contains the series solutions of Eqs. (9.8) – (9.11) by employing homotopy analysis method (HAM).

9.2 Homotopy analysis solutions

For the series solutions using HAM, it is obvious that the velocity profiles $f(\eta)$, $g(\eta)$ and the temperature field $\theta(\eta)$ can be expressed by the set of base functions

$$\left\{ \eta^k \exp\left(-n\eta\right) \middle| \, k \geq 0, n \geq 0 \right\} \tag{9.16}$$

in the form

$$f\left(\eta\right) = a_{0,0}^0 + \sum_{n=0}^{\infty} \sum_{k=0}^{\infty} a_{m,n}^k \eta^k \exp\left(-n\eta\right), \tag{9.17}$$

$$g\left(\eta\right) = b_{0,0}^0 + \sum_{n=0}^{\infty} \sum_{k=0}^{\infty} b_{m,n}^k \eta^k \exp\left(-n\eta\right), \tag{9.18}$$

$$\theta\left(\eta\right) = \sum_{n=0}^{\infty} \sum_{k=0}^{\infty} c_{m,n}^k \eta^k \exp\left(-n\eta\right), \tag{9.19}$$

where $a_{m,n}^k$, $b_{m,n}^k$ and $c_{m,n}^k$ are the coefficients. Based on the *rule of solution expressions* by Eqs. (9.11) and (9.17) – (9.19), it is straightforward to choose

$$f_0\left(\eta\right) = 1 - \exp(-\eta), \tag{9.20}$$

$$g_0(\eta) = m_0 \exp(-\eta), \tag{9.21}$$

$$\theta_0(\eta) = \exp(-\eta) \tag{9.22}$$

as our initial approximations of $f(\eta)$, $g(\eta)$ and $\theta(\eta)$. Besides that we select the auxiliary linear operators $\mathcal{L}_f\left(f\right)$ and $\mathcal{L}_{g,\theta}\left(f\right)$ as

$$\mathcal{L}_f\left(f\right) = \frac{d^3 f}{d\eta^3} - \frac{df}{d\eta}, \tag{9.23}$$

$$\mathcal{L}_{g,\theta}\left(f\right) = \frac{d^2 f}{d\eta^2} - f, \tag{9.24}$$

satisfying the following properties:

$$\mathcal{L}_f\left[C_1 + C_2 \exp(\eta) + C_3 \exp(-\eta)\right] = 0, \tag{9.25}$$

$$\mathcal{L}_{g,\theta}\left[C_4\exp(\eta)+C_5\exp(-\eta)\right]=0 \tag{9.26}$$

in which C_i, $i=1-5$ are the arbitrary constants. If $p\,(\in[0,1])$ is an embedding parameter and $\hbar_f$, $\hbar_g$ and $\hbar_\theta$ indicate the embedding and non-zero auxiliary parameters, respectively then the zeroth-order deformation problems are of the following form

$$(1-p)\,\mathcal{L}_f\left[\widehat{f}\,(\eta;p)-f_0\,(\eta)\right]=p\hbar_f\mathcal{N}_f\left[\widehat{f}\,(\eta;p)\,,\widehat{g}\,(\eta;p)\,,\widehat{\theta}\,(\eta;p)\right], \tag{9.27}$$

$$(1-p)\,\mathcal{L}_g\left[\widehat{g}\,(\eta;p)-g_0\,(\eta)\right]=p\hbar_g\mathcal{N}_g\left[\widehat{f}\,(\eta;p)\,,\widehat{g}\,(\eta;p)\right], \tag{9.28}$$

$$(1-p)\,\mathcal{L}_\theta\left[\widehat{\theta}\,(\eta;p)-\theta_0\,(\eta)\right]=p\hbar_\theta\mathcal{N}_\theta\left[\widehat{\theta}\,(\eta;p)\,,\widehat{f}\,(\eta;p)\right], \tag{9.29}$$

subject to the boundary conditions

$$\widehat{f}\,(0;p)=0,\quad \widehat{f}'\,(0;p)=1,\quad \widehat{g}\,(0;p)=-m_0\widehat{f}''\,(0;p)\,,\quad \widehat{\theta}\,(0;p)=1, \tag{9.30}$$

$$\widehat{f}'\,(\infty;p)=0,\qquad \widehat{g}\,(\infty;p)=0,\qquad \widehat{\theta}\,(\infty;p)=0, \tag{9.31}$$

in which we define the non-linear operators $\mathcal{N}_f$, $\mathcal{N}_g$ and $\mathcal{N}_\theta$ as

$$\begin{aligned}\mathcal{N}_f\left[\widehat{f}\,(\eta;p)\,,\widehat{g}\,(\eta;p)\right] &= (1+K_1)\frac{\partial^3\widehat{f}\,(\eta;p)}{\partial\eta^3}+K_1\frac{\partial\widehat{g}\,(\eta;p)}{\partial\eta}+\frac{2}{n+1}\lambda\widehat{\theta}\,(\eta;p)\\ &\quad+\widehat{f}\,(\eta;p)\frac{\partial^2\widehat{f}\,(\eta;p)}{\partial\eta^2}-\frac{2n}{n+1}\left(\frac{\partial\widehat{f}\,(\eta;p)}{\partial\eta}\right)^2,\end{aligned} \tag{9.32}$$

$$\begin{aligned}\mathcal{N}_g\left[\widehat{f}\,(\eta;p)\,,\widehat{g}\,(\eta;p)\right] &= \left(1+\frac{K_1}{2}\right)\frac{\partial^2\widehat{g}\,(\eta;p)}{\partial\eta^2}-\frac{2K_1}{n+1}\left(2\widehat{g}\,(\eta;p)-\frac{\partial^2\widehat{f}\,(\eta;p)}{\partial\eta^2}\right)\\ &\quad+\widehat{f}\,(\eta;p)\frac{\partial\widehat{g}\,(\eta;p)}{\partial\eta}-\frac{3n-1}{n+1}\frac{\partial\widehat{f}\,(\eta;p)}{\partial\eta}\widehat{g}\,(\eta;p)\,,\end{aligned} \tag{9.33}$$

$$\mathcal{N}_\theta\left[\widehat{\theta}\,(\eta;p)\,,\widehat{f}\,(\eta;p)\right]=\frac{\partial^2\widehat{\theta}\,(\eta;p)}{\partial\eta^2}+\mathrm{Pr}\,\widehat{f}\,(\eta;p)\frac{\partial\widehat{\theta}\,(\eta;p)}{\partial\eta}. \tag{9.34}$$

For $p=0$ and $p=1$, the above zeroth-order equations (9.27) – (9.29) have the solutions

$$\widehat{f}\,(\eta;0)=f_0\,(\eta)\,,\qquad \widehat{g}\,(\eta;0)=g_0\,(\eta)\,,\qquad \widehat{\theta}\,(\eta;0)=\theta_0\,(\eta)\,, \tag{9.35}$$

and

$$\widehat{f}(\eta;1)=f(\eta),\qquad \widehat{g}(\eta;1)=g(\eta),\qquad \widehat{\theta}(\eta;1)=\theta(\eta). \tag{9.36}$$

When p increases from 0 to 1 then $\widehat{f}(\eta;p)$, $\widehat{g}(\eta;p)$ and $\widehat{\theta}(\eta;p)$ vary from $f_0(\eta)$, $g_0(\eta)$ and $\theta_0(\eta)$ to $f(\eta)$, $g(\eta)$ and $\theta(\eta)$. Expanding $\widehat{f}$, $\widehat{g}$ and $\widehat{\theta}$ in Taylor series with respect to p, we have

$$\widehat{f}(\eta;p)=f_0(\eta)+\sum_{m=1}^{\infty}f_m(\eta)\,p^m, \tag{9.37}$$

$$\widehat{g}(\eta;p)=g_0(\eta)+\sum_{m=1}^{\infty}g_m(\eta)\,p^m, \tag{9.38}$$

$$\widehat{\theta}(\eta;p)=\theta_0(\eta)+\sum_{m=1}^{\infty}\theta_m(\eta)\,p^m, \tag{9.39}$$

in which

$$f_m(\eta)=\frac{1}{m!}\frac{\partial^m\widehat{f}(\eta;p)}{\partial p^m}\bigg|_{p=0},\quad g_m(\eta)=\frac{1}{m!}\frac{\partial^m\widehat{g}(\eta;p)}{\partial p^m}\bigg|_{p=0},\quad \theta_m(\eta)=\frac{1}{m!}\frac{\partial^m\widehat{\theta}(\eta;p)}{\partial p^m}\bigg|_{p=0}, \tag{9.40}$$

where $\hbar_f$, $\hbar_g$ and $\hbar_\theta$ are chosen in such a way that these series are convergent at $p=1$. Therefore we have through Eq. (9.35) that

$$f(\eta)=f_0(\eta)+\sum_{m=1}^{\infty}f_m(\eta), \tag{9.41}$$

$$g(\eta)=g_0(\eta)+\sum_{m=1}^{\infty}g_m(\eta), \tag{9.42}$$

$$\theta(\eta)=\theta_0(\eta)+\sum_{m=1}^{\infty}\theta_m(\eta). \tag{9.43}$$

Differentiating the zeroth-order equations (9.27)$-$(9.29) m times with respect to p, then setting $p=0$, and finally dividing by $m!$ we have the mth-order deformation equations

$$\mathcal{L}_f\left[f_m(\eta)-\chi_m f_{m-1}(\eta)\right]=\hbar_f\mathcal{R}_m^f(\eta), \tag{9.44}$$

$$\mathcal{L}_g\left[g_m(\eta)-\chi_m g_{m-1}(\eta)\right]=\hbar_g\mathcal{R}_m^g(\eta), \tag{9.45}$$

$$\mathcal{L}_\theta \left[\theta_m(\eta) - \chi_m \theta_{m-1}(\eta)\right] = \hbar_\theta \mathcal{R}_m^\theta(\eta), \tag{9.46}$$

with the following boundary conditions

$$f_m(0) = f'_m(0) = g_m(0) - m_0 f''(0) = \theta_m(0) = 0, \tag{9.47}$$

$$f'_m(\infty) = g_m(\infty) = \theta_m(\infty) = 0, \tag{9.48}$$

where

$$\mathcal{R}_m^f(\eta) = (1+K_1) f'''_{m-1} + K_1 g'_{m-1} + \frac{2}{n+1}\lambda\theta_{m-1} + \sum_{k=0}^{m-1}\left[f_{m-1-k} f''_k - \frac{2n}{n+1} f'_{m-1-k} f'_k\right], \tag{9.49}$$

$$\mathcal{R}_m^g(\eta) = \left(1+\frac{K_1}{2}\right) g''_{m-1} - \frac{2K_1}{n+1}(2g_{m-1} - f''_{m-1}) - \sum_{k=0}^{m-1}\left[g'_{m-1-k} f_k - \frac{3n-1}{n+1} g_k f'_{m-1-k}\right], \tag{9.50}$$

$$\mathcal{R}_m^\theta(\eta) = \theta''_{m-1} + \Pr \sum_{k=0}^{m-1} \theta'_{m-1-k} f_k, \tag{9.51}$$

and

$$\chi_m = \begin{cases} 0, & m \le 1, \\ 1, & m > 1. \end{cases} \tag{9.52}$$

The general solutions of equations (9.44) – (9.48) are given by

$$\begin{aligned} f_m(\eta) &= f_m^*(\eta) + C_1 + C_2 \exp(\eta) + C_3 \exp(-\eta), \\ g_m(\eta) &= g_m^*(\eta) + C_4 \exp(\eta) + C_5 \exp(-\eta), \\ \theta_m(\eta) &= \theta_m^*(\eta) + C_6 \exp(\eta) + C_7 \exp(-\eta), \end{aligned} \tag{9.53}$$

in which $f_m^*(\eta)$, $g_m^*(\eta)$ and $\theta_m^*(\eta)$ denote the special solutions of Eqs. (9.44) – (9.46), and the integral constants C_i, $(i = 1, 2...7)$ are determined by the boundary conditions (9.47) and (9.48). In order to satisfy the boundary conditions at infinity, we must put C_2, C_4 and C_6 equal to zero.

In this way, it is easy to solve the linear non-homogeneous Eqs. (9.44) – (9.46) by using Mathematica one after the other in the order $m = 1, 2, 3.....$

9.3 Convergence of the derived solutions

The total explicit analytic series solutions of the functions f, g and θ are given in Eqs. (9.41) – (9.43). The convergence of these series and rate of the approximation for homotopy analysis method (HAM) strongly depends upon the value of the auxiliary parameters $\hbar_f$, $\hbar_g$ and $\hbar_\theta$, as pointed out by Liao [90]. In order to find the range of admissible values of $\hbar_f$, $\hbar_g$ and $\hbar_\theta$, the $\hbar$-curves are plotted in Fig. 9.2(a,b) for the 15th-order of approximation at different values of emerging parameters K_1, m_0, n, λ and Pr. In Fig. 9.2(a) for $f''(0)$, $g'(0)$ and $\theta'(0)$ the $\hbar$-curves are plotted for $K_1 = m_0 = 0.2$, $n = 0.5$, $\lambda = 0.2$ and $\mathrm{Pr} = 0.2$. For simplicity we can put $\hbar_f = \hbar_g = \hbar_\theta = \hbar$, so that the range for values of $\hbar$ for f is $-1.6 \leq \hbar \leq -0.2$, for g is $-1.7 \leq \hbar \leq -0.1$ and similarly for θ is $-1.9 \leq \hbar \leq -0.2$. Fig. 9.2(b) shows the range for values of $\hbar$ when $K_1 = m_0 = 0.5$, $n = 1.5$, $\lambda = 1$ and $\mathrm{Pr} = 0.5$. From this Fig. the ranges for suitable values of $\hbar$ for f are $-1.3 \leq \hbar \leq -0.2$, for g are $-1.3 \leq \hbar \leq -0.1$ and for θ are $-1.65 \leq \hbar \leq -0.2$, respectively. From Fig. 1(a,b) we can say that the range of admissible values of $\hbar$ depends upon the values of involving physical parameters of the flow problem. It is also evident from this Fig. that the series in Eqs. (9.41) – (9.43) converge in the whole region of η when $\hbar = -0.8$. Table 9.1 is prepared to show the convergence of the series solutions given in Eqs. (9.41) – (9.43) for different order of approximations using homotopy-Pade approximation. Homotopy-Pade approximation helps us to obtain the fast convergent of the series solutions.

(a)

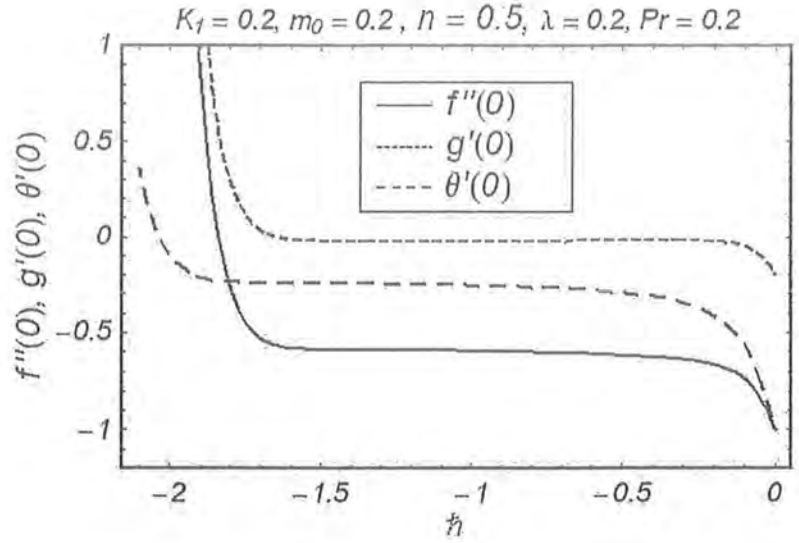

(b)

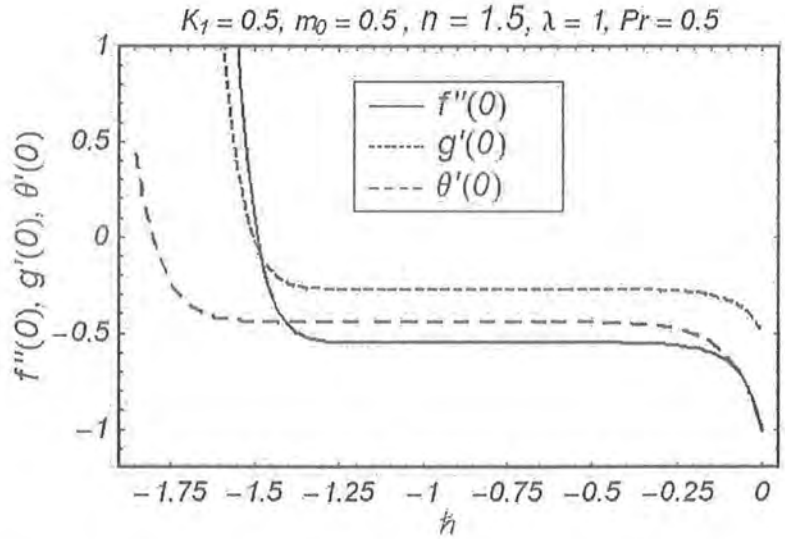

Fig. 9.2. The $\hbar$-curves of $f''(0)$, $g'(0)$ and $\theta'(0)$ at 15th-order of approximations.

Homotopy-Pade approximations $[m, m]$	$-f''(0)$	$-g'(0)$	$-\theta'(0)$
$[1, 1]$	0.92817	0.19007	0.35855
$[5, 5]$	0.93689	0.19164	0.14812
$[10, 10]$	0.93597	0.19153	0.13126
$[15, 15]$	0.93450	0.19148	0.13093
$[18, 18]$	0.93456	0.19147	0.13010
$[20, 20]$	0.93454	0.19147	0.13009
$[24, 24]$	0.93454	0.19147	0.13011
$[30, 30]$	0.93454	0.19147	0.13011
$[40, 40]$	0.93454	0.19147	0.13011

Table 9.1. Convergence of series solutions using homotopy-Pade approximation when $K_1 = 0.1$, $\lambda = \Pr = m_0 = 0.1$ and $n = 1.5$.

9.4 Results and discussion

This section presents the influence of physical parameters on the velocity f', the micro-rotation velocity g and the temperature field θ. For this purpose, Figs. 9.3 – 9.12 have been plotted to analyze the effects of power index of plate velocity n, the material parameter or vortex viscosity K_1, the buoyancy or the mixed convection parameter λ and the Prandtl number Pr on the velocity component f', the micro-rotation velocity g and the temperature profile θ, respectively. Tables 9.2−9.6 are made to show the values of the skin-friction coefficient $C_f \operatorname{Re}_x^{1/2}$ and the Nusselt number $Nu_x \operatorname{Re}_x^{-1/2}$ for viscous ($K_1 = \gamma_1 = j = \lambda = 0$) and micropolar fluids for various parameters of interest, respectively.

To see the variations of power index of plate velocity n, the material parameter or vortex viscosity K_1, the buoyancy or the mixed convection parameter λ on the velocity filed f', Figs. 9.3 – 9.5 have been plotted. Fig. 9.3 indicates that as the nonlinearity of the stretching surface (n) increases the velocity f' decreases. The boundary layer thickness also decreases as n increases. Fig. 9.4 illustrates the effects of vortex viscosity K_1 on the velocity f'. It can be seen from this Fig. that the velocity f' is an increasing function of K_1. The boundary layer

thickness is also increased for large values of K_1. Fig. 9.5 shows the distributions of the velocity f' for various values of the buoyancy parameter λ. It is noted that the velocity f' increases when λ increases. The boundary layer thickness also increases for large values of λ in this case.

Figs. $9.6 - 9.8$ have been made to see the effects of n, K_1 and λ on the micro-rotation velocity g. Fig. 9.6 depicts the influence of power index of plate velocity n on the micro-rotation velocity g. It is found that initially g is an increasing function of n but after $\eta > 1$, it decreases for large values of n. The boundary layer thickness increases as n increases in case of micro-rotation g when compared with the velocity f'. From this Fig. we can see that g has quite opposite results when compared with Fig. 9.3. The variation of vortex viscosity or the material parameter K_1 responsible for micropolar fluid on g is shown in Fig. 9.7. It is observed that initially g decreases by increasing the values of K_1. It can also be seen from this Fig. that the micro-rotation velocity g is greater when compared with the viscous case ($K_1 = 0$) for large values of K_1. The boundary layer thickness also decreases as K_1 increases. Fig. 9.8 depicts the effects of the buoyancy parameter λ on g. The micro-rotation velocity g is a decreasing function of λ. The boundary layer thickness is decreased for large values of λ.

In order to see the variations of n, K_1, λ and Pr on the temperature profile θ, the Figs. $9.9 - 9.12$ are displayed. Fig. 9.9 gives the influence of the factor causes the nonlinear plate velocity n on the temperature field θ. It is noted that the temperature θ increases by increasing n. The thermal boundary layer thickness also increases when n increases. Fig. 9.10 elucidates the effects of the material parameter K_1 on the temperature θ. The temperature profile θ is a decreasing function of K_1. It is evident from this Fig. that such decrease occurs at very large values of K_1. The thermal boundary layer thickness also decreases when K_1 increases. Fig. 9.11 shows the variations of the mixed convection parameter λ on the temperature θ. It is found that θ decreases by increasing the buoyancy effects. But the thermal boundary layer thickness is decreased for large values of λ. The influence of the Prandtl number Pr on the temperature field θ can be seen in Fig. 9.12. As expected, the temperature θ deceases by increasing the values of the Prandtl number Pr. The thermal boundary layer thickness also decreases for large values of Pr.

Tables 9.2 and 9.3 are made for the values of the wall shear stress $-f''(0)$ (or the skin friction coefficient $C_f \operatorname{Re}_x^{1/2}$) and the local Nusselt number $Nu_x \operatorname{Re}_x^{-1/2}$ for viscous fluid ($K_1 = \gamma_1 = j = 0$)

and the comparison is shown with the existing numerical results of viscous fluid ([148]). Table 9.2 shows that the magnitude of the wall shear stress $-f''(0)$ increases when n increases. Table 9.3 gives the values of the local Nusselt number $Nu_x \operatorname{Re}_x^{-1/2}$ for different values of n and Pr. It is noted that the local Nusselt number $Nu_x \operatorname{Re}_x^{-1/2}$ decreases for large values of n but it increases by increasing the Prandtl number Pr. From the comparison of these two tables it is noted that the agreement of the HAM solution for viscous fluid with the existing numerical results in reference [148] is excellent.

Table 9.4 – 9.6 are prepared just to see the values of the skin friction coefficient $C_f \operatorname{Re}_x^{1/2}$ and the local Nusselt number $Nu_x \operatorname{Re}_x^{-1/2}$ for different parameters of interest in both the cases of $m_0 = 0$ and $m_0 = 1/2$, respectively using homotopy -Pade approximation for viscous fluid $K_1 = 0$. Table 9.4 displays the variations of the skin friction coefficient $C_f \operatorname{Re}_x^{1/2}$ and the local Nusselt number $Nu_x \operatorname{Re}_x^{-1/2}$ for Newtonian fluid ($K_1 = 0$) when $\lambda = 1$ and $\mathrm{Pr} = 0.72$ in case of $m_0 = 0$ and $m_0 = 1/2$. It is observed that both the magnitudes of the skin friction coefficient $C_f \operatorname{Re}_x^{1/2}$ increases and the local Nusselt number $Nu_x \operatorname{Re}_x^{-1/2}$ decreases when n increases, respectively and the same observation is noted in both the cases of $m_0 = 0$ and $m_0 = 1/2$. Table 9.5 gives the values of the skin friction coefficient $C_f \operatorname{Re}_x^{1/2}$ and the local Nusselt number $Nu_x \operatorname{Re}_x^{-1/2}$ for micropolar fluid ($K_1 \neq 0$) when $\lambda = 1$ and $\mathrm{Pr} = 0.72$ in the cases of $m_0 = 0$ and $m_0 = 1/2$. It is evident from this table that for micropolar fluid ($K_1 = 1$) the magnitude of the skin friction coefficient $C_f \operatorname{Re}_x^{1/2}$ increases while the local Nusselt number $Nu_x \operatorname{Re}_x^{-1/2}$ decreases for large values of n. But this change in skin friction coefficient is larger in case of $m_0 = 1/2$ when compared with $m_0 = 0$, and this situation is quite opposite for the local Nusselt number. The variations of K_1 and the Prandtl number Pr on the skin friction coefficient $C_f \operatorname{Re}_x^{1/2}$ and the local Nusselt number $Nu_x \operatorname{Re}_x^{-1/2}$ can be seen in Table 9.6 when $n = 1.5$ and $\lambda = 1$ in both the cases of $m_0 = 0$ and $m_0 = 1/2$, respectively. The magnitudes of the skin friction coefficient $C_f \operatorname{Re}_x^{1/2}$ and the local Nusselt number $Nu_x \operatorname{Re}_x^{-1/2}$ increase by increasing K_1 and Pr. The increment in the skin friction coefficient is larger in case of $m_0 = 1/2$ when compared with $m_0 = 0$ for large values of K_1 and Pr and is quite opposite for the local Nusselt number.

9.5 Concluding remarks

The highly non-linear problem of mixed convection flow of a micropolar fluid has been analyzed in this chapter. Analytic solutions of governing momentum and energy equations have been obtained. The HAM solutions for viscous fluid which are yet not available in the literature can be deduced as the limiting cases of the present analysis. The HAM solutions in viscous fluid with no mixed convection are compared with the numerical results [148] and an excellent agreement is found. The influence of the buoyancy parameter, the micropolar material parameter, n and the Prandtl number have been systematically examined. The following main features of the velocity and temperature profiles can be withdrawn from the discussion section:

- The velocity f' is reduced by n and increases when K_1 and λ increase.
- The magnitude of g decreases by increasing n, K_1 and λ.
- The temperature increases with n but decreases as K_1, λ and Pr increases.
- The skin friction coefficient increases with n, K_1 and Pr for viscous and micropolar fluids with and without mixed convection.
- The local Nusselt number decreases with n and increases by increasing K_1 and Pr for viscous and micropolar fluids.
- The HAM solutions with no mixed convection can be deduced by choosing $\lambda = 0$. Such solutions with no mixed convection in a viscous fluid can be obtained by taking $\lambda = K_1 = \gamma_1 = j = 0$.

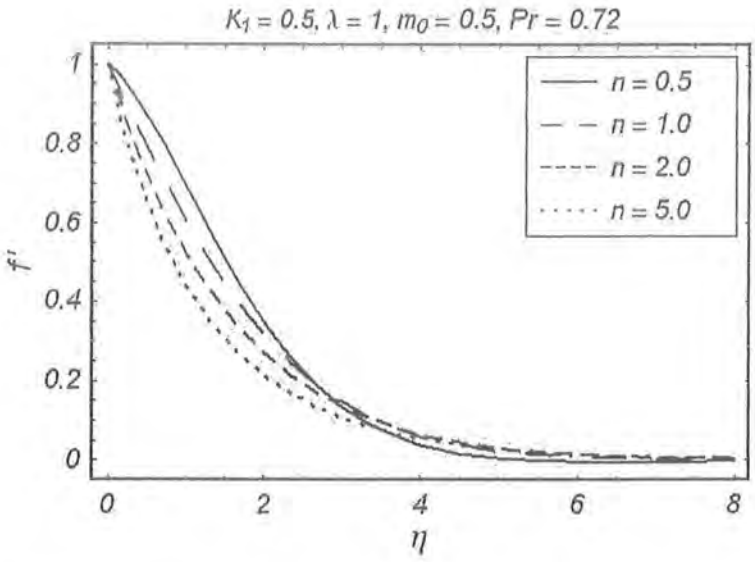

Fig. 9.3. The effects of the power index of surface velocity n on the velocity filed f' verses η.

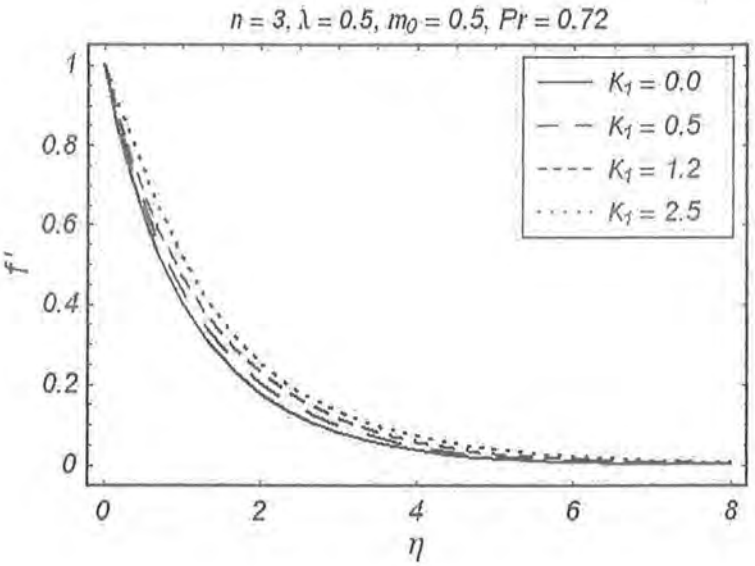

Fig. 9.4. The effects of the vortex-viscoty or the material parameter K_1 on the velocity field f' verses η.

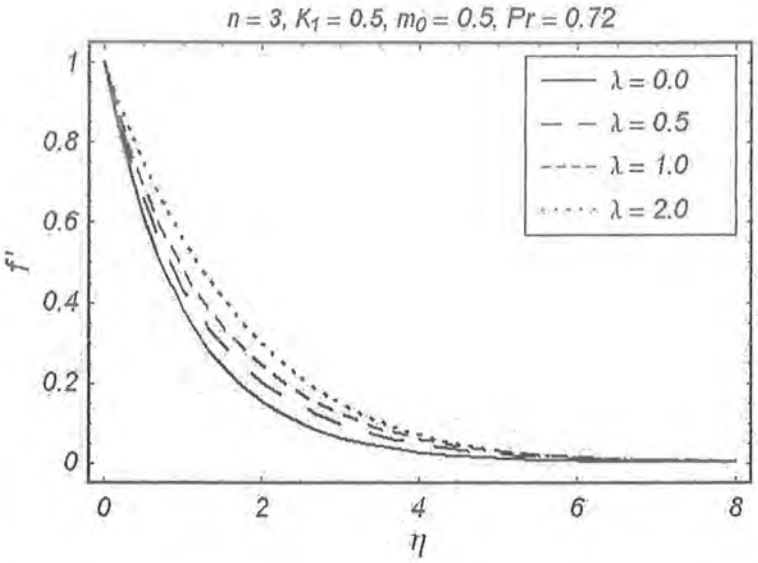

Fig. 9.5. The effects of the buoyancy or mixed convection parameter λ on the velocity field f' verses η.

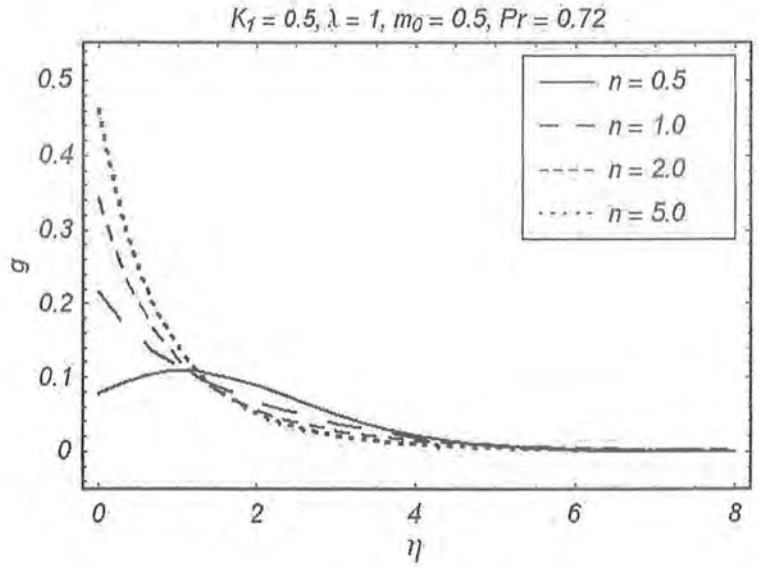

Fig. 9.6. The effects of the power index of surface velocity n on the micro-rotation velocity g verses η.

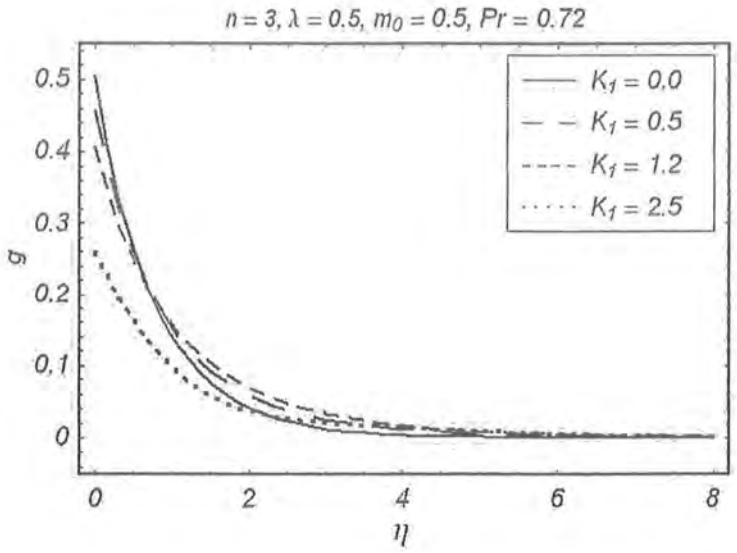

Fig. 9.7. The effects of the vortex-viscosity or the material parameter K_1 on the micro-rotation velocity g verses η.

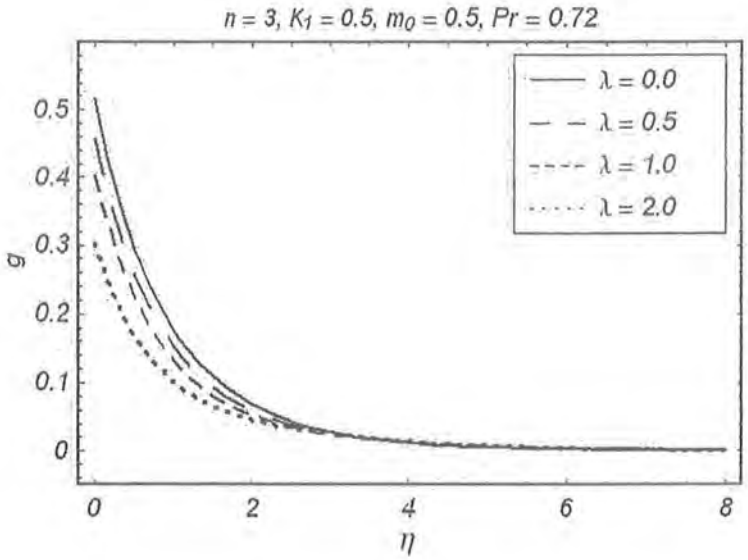

Fig. 9.8. The effects of the buoyancy or mixed convection parameter λ on the micro-rotation velocity g verses η.

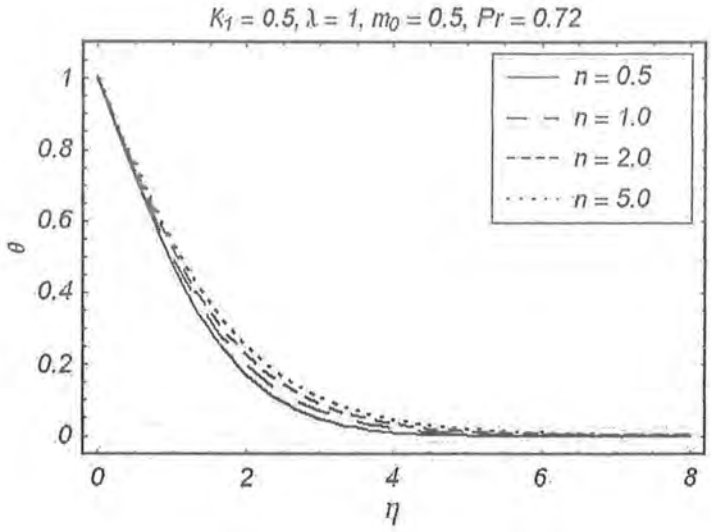

Fig. 9.9. The effects of the power index of surface velocity n on the temperature field θ verses η.

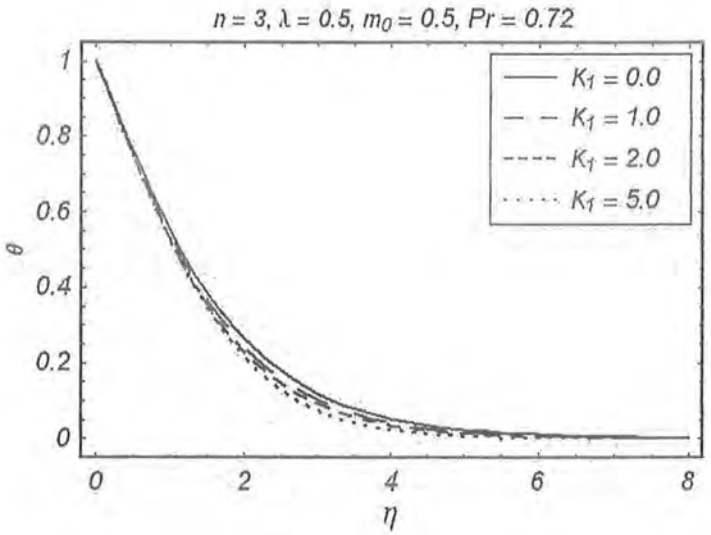

Fig. 9.10. The effects of the vortex-viscoty or the material parameter K_1 on the temperature field θ verses η.

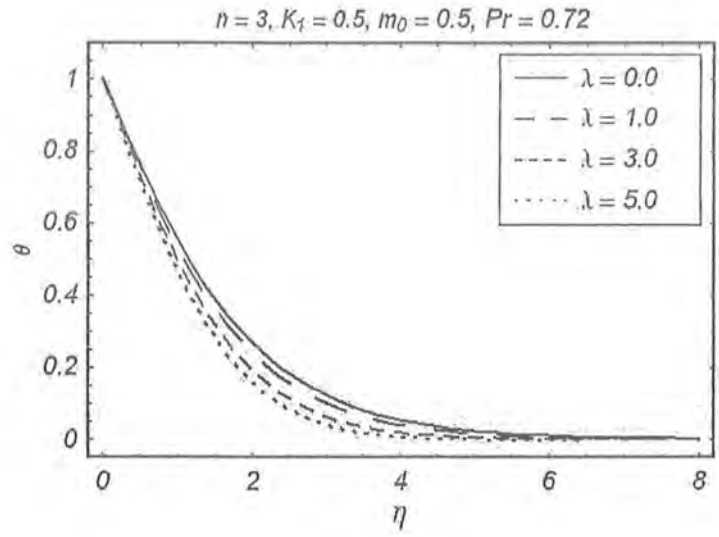

Fig. 9.11. The effects of the buoyancy or mixed convection parameter λ on the temperature field θ verses η.

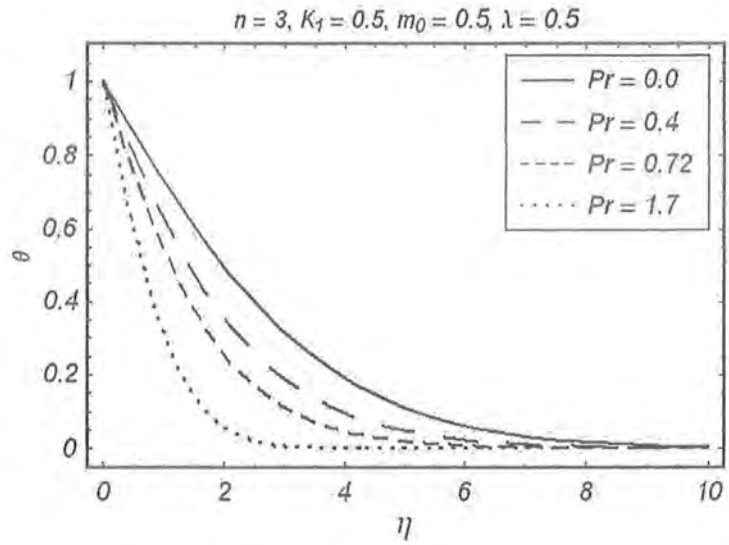

Fig. 9.12. The effects of the Prandtl number Pr on the temperature field θ verses η.

n	Cortell [148]	HAM solution
0.0	0.627547	0.627555
0.2	0.766758	0.766837
0.5	0.889477	0.889544
0.75	0.953786	0.953957
1.0	1.0	1.0
1.5	1.061587	1.061601
3.0	1.148588	1.148593
7.0	1.216847	1.216850
10.0	1.234875	1.234875
20.0	1.257418	1.257424
100.0	1.276768	1.276774

Table 9.2. Values of the wall shear stress $-f''(0)$ for viscous fluid when $K_1 = \gamma_1 = j = \lambda = 0$.

		Cortell [148]	HAM solution	Cortell [148]	HAM solution
Ec	n	$\Pr = 1$	$\Pr = 1$	$\Pr = 5$	$\Pr = 5$
0.0	0.2	0.610262	0.610202	1.607175	1.607925
	0.5	0.595277	0.595201	1.586744	1.586833
	1.5	0.574537	0.574730	1.557463	1.557672
	3.0	0.564472	0.564662	1.542337	1.542145
	10.0	0.554960	0.554878	1.528573	1.528857

Table 9.3. Values of the local Nusselt number $Nu_x \operatorname{Re}_x^{-1/2}$ for viscous fluid when $K_1 = 0$, $\gamma_1 = j = \lambda = 0$.

Homotopy-Pade app.		$K_1 = 0, m_0 = 0$		$K_1 = 0, m_0 = 1/2$	
$[m, m]$	n	$C_f \operatorname{Re}_x^{1/2}$	$Nu_x \operatorname{Re}_x^{-1/2}$	$C_f \operatorname{Re}_x^{1/2}$	$Nu_x \operatorname{Re}_x^{-1/2}$
[25, 25]	0.2	0.22178	0.61715	0.22178	0.61715
[15, 15]	0.75	−0.31176	0.56849	−0.31176	0.56849
[15, 15]	1.0	−0.44320	0.55528	−0.44320	0.55528
[12, 12]	1.5	−0.61992	0.53639	−0.61992	0.53639
[12, 12]	3.0	−0.87283	0.50604	−0.87283	0.50604
[12, 12]	7.0	−1.07672	0.47655	−1.07672	0.47655
[12, 12]	10.0	−1.13200	0.46714	−1.13200	0.46714
[12, 12]	20.0	−1.20256	0.45361	−1.20256	0.45361
[12, 12]	100.0	−1.26507	0.43923	−1.26507	0.43923

Table 9.4. Values of the skin friction $C_f \operatorname{Re}_x^{1/2}$ and the local Nusselt number $Nu_x \operatorname{Re}_x^{-1/2}$ for viscous fluid ($K_1 = 0$) when $\lambda = 1$ and $\Pr = 0.72$.

Homotopy-Pade app.		$K = 1, m_0 = 0$		$K = 1, m_0 = 1/2$	
$[m, m]$	n	$C_f \operatorname{Re}_x^{1/2}$	$Nu_x \operatorname{Re}_x^{-1/2}$	$C_f \operatorname{Re}_x^{1/2}$	$Nu_x \operatorname{Re}_x^{-1/2}$
[20, 20]	0.2	0.07791	0.61944	0.093194	0.62025
[15, 15]	0.75	−0.41927	0.58259	−0.49564	0.57803
[13, 13]	1.0	−0.54447	0.57275	−0.64181	0.56671
[12, 12]	1.5	−0.71435	0.55894	−0.83876	0.55067
[12, 12]	3.0	−0.96020	0.53768	−1.12087	0.52548
[12, 12]	7.0	−1.16000	0.51884	−1.34726	0.50218
[10, 10]	10.0	−1.21421	0.51341	−1.40815	0.49514
[10, 10]	20.0	−1.28316	0.50625	−1.48519	0.48548
[10, 10]	100.0	−1.34359	0.49973	−1.55227	0.47608

Table 9.5. Values of the skin friction $C_f \operatorname{Re}_x^{1/2}$ and the local Nusselt number $Nu_x \operatorname{Re}_x^{-1/2}$ for micropolar fluid ($K_1 \neq 0$) when $\lambda = 1$ and $\Pr = 0.72$.

Homotopy-Pade app.			$n = 1.5, m_0 = 0$		$n = 1.5, m_0 = 1/2$	
$[m, m]$	K	Pr	$C_f \operatorname{Re}_x^{1/2}$	$Nu_x \operatorname{Re}_x^{-1/2}$	$C_f \operatorname{Re}_x^{1/2}$	$Nu_x \operatorname{Re}_x^{-1/2}$
[12, 12]	0.0	0.72	−0.61992	0.53639	−0.61992	0.53639
[12, 12]	0.2		−0.64146	0.54215	−0.66972	0.53975
[12, 12]	0.5		−0.67003	0.54937	−0.73709	0.54422
[12, 12]	0.7		−0.68807	0.55350	−0.77902	0.54693
[12, 12]	1.0		−0.71435	0.55894	−0.83876	0.55067
[15, 15]	2.0		−0.79736	0.57276	−1.01928	0.56107
[25, 25]	1.0	0.0	−0.34602	0.019608	−0.39979	0.019608
[20, 20]		0.2	−0.56008	0.27352	−0.65749	0.27110
[16, 16]		0.5	−0.66850	0.45475	−0.78452	0.44870
[15, 15]		0.72	−0.71435	0.55894	−0.83876	0.55067
[15, 15]		1.0	−0.75479	0.67335	−0.88703	0.66284
[20, 20]		3.0	−0.87215	1.24369	−1.02932	1.22607

Table 9.6. Values of the skin friction $C_f \operatorname{Re}_x^{1/2}$ and the local Nusselt number $Nu_x \operatorname{Re}_x^{-1/2}$ for micropolar fluid ($K_1 \neq 0$) when $\lambda = 1$.

Bibliography

[1] H. Schlichting, Boundary Layer Theory, McGraw-Hill, New York, 1964.

[2] B. C. Sakiadis, Boundary layer behavior on continuous solid surfaces: I Boundary layer equations for two dimensional and axisymmetric flow, AIChE. J. 7 (1961) 26.

[3] B. C. Sakiadis, Boundary layer behavior on continuous solid surfaces: II Boundary layer on a continuous flat surface, AIChE. J. 7 (2) (1961) 221.

[4] L. J. Crane, Flow past a stretching plate, Z. Angew. Math. Phys. 21 (1970) 645.

[5] P. S. Gupta and A. S. Gupta, Heat and mass transfer on a stretching sheet with suction or blowing, Can. J. Chem. Eng. 55 (1977) 744.

[6] M. H. Davies, A note on elastico-viscous boundary layer flows, ZAMP 17 (1996) 189.

[7] K. R. Rajagopal, A. S. Gupta and A. S. Wineman, On a boundary layer theory for non-Newtonian fluids, Appl. Sci. Eng. Lett. 18 (6) (1980) 875.

[8] K. R. Rajagopal, Boundary layers in non-linear fluids, in: M.D.P. Monteivo Marques, J.F. Rodriques, (Eds.), Trends in Applications of Mathematics to Mechanics, Pittman Monographs and Surveys in Pure and Applied Mathematics, vol. 77, Longman, New York, 1995, p. 209.

[9] K. R. Rajagopal and A.S. Gupta, An exact solution for the flow of a non-Newtonian fluid past an infinite porous plate, Meccanica 19 (1980) 158.

[10] M. Pakdimirli, Conventional and multiple deck boundary layer approach to second and third grade fluids, Int. J. Eng. Sci. 32 (1994) 141.

[11] H. Markovitz and B. D. Coleman, Advances in Applied Mechanics, vol. 8, Academic Press, New York (1964).

[12] K. R. Rajagopal, T. Y. Na and A. S. Gupta, Flow of viscoelastic fluid over a stretching sheet, Rheol Acta 23 (1984) 213.

[13] W. C. Troy, E. A. Overman, H. G. B. Ermentrout and J. P. Keener, Uniqueness of flow of a second order fluid past a stretching sheet, Quart. Appl. Math. 44 (1987) 753.

[14] W. D. Chang, The non-uniqueness of the flow of a viscoelastic fluid over a stretching sheet, Quart. Appl. Math. 47 (20) (1989) 365.

[15] B. N. Rao, Technical Note: Flow of a fluid of second grade over a stretching sheet, Int. J. Non-Linear Mech. 31 (4) (1996) 547.

[16] B. Siddappa and M. S. Abel, Non-Newtonian flow past a stretching plate, Z Angew Math. Phys. 36 (1985) 890.

[17] V. M. Soundalgekar, Stokes problem for elastic-viscous fluid, Rheol. Acta 13 (1974) 177.

[18] B. Siddappa and B. S. Khapate, Rivlin-Ericksen fluid flow past a stretching sheet, Rev. Roum. Sci. Tech. Ser. Mech. (Appl.) 2 (1976) 497.

[19] D. W. Beard and K. Walters, Elastic-viscous boundary layer flows. Part I. Two dimensional flow near a stagnation point, Proc. Camb. Philol. Soc. 60 (1964) 667.

[20] H. I. Andersson, MHD flow of a viscoelastic fluid past a stretching surface, Acta Mech. 95 (1992) 227.

[21] A. Acrivos, M. Shah and S. S. Petersen, Momentum and heat transfer in laminar boundary layer flows of non-Newtonian fluids past external surfaces, AIChE J. 6 (1960) 312.

[22] W. R. Schowalter, The application of boundary-layer theory to power-law pseudoplastic fluids: similarity solutions, AIChE J. 6 (1960) 25.

[23] A. C. Srivastava, The flow of a non-Newtonian liquid near a stagnation point, ZAMP 9 (1958) 80.

[24] J. E. Danberg and K. S. Fansler, A non similar moving wall boundary-layer problem, Quart. Appl. Math. 34 (1976) 305.

[25] S. Abel, K.V. Prasad and A. Mahaboob, Buoyancy force and thermal radiation effects in MHD boundary layer visco-elastic fluid flow over continuously moving stretching surface, Int. J. Thermal Sci. 44 (2005) 465.

[26] P. D. Ariel, MHD flow of a viscoelastic fluid past a stretching sheet with suction, Acta Mech. 105 (1994) 49.

[27] P. S. Datti, K. V. Prasad, M. S. Abel and A. Joshi, MHD visco-elastic fluid flow over a non-isothermal stretching sheet, Int. J. Eng. Sci. 42 (2004) 935.

[28] M. A. Seddeek, Heat and mass transfer on a stretching sheet with magnetic field in a visco-elastic fluid flow through a porous medium with heat source or sink, Comput. Mater. Sci. 38 (2007) 781.

[29] R. Cortell, Similarity solutions for flow and heat transfer of a viscoelastic fluid over a stretching sheet, Int. J. Non-Linear Mech. 29 (1994) 155.

[30] M. Massoudi and C. E. Maneschy, Numerical solution to the flow of a second grade fluid over a stretching sheet using the method of quasi-linearization, Appl. Math. Comput. 149 (2004) 165.

[31] R. Cortell, Flow and heat transfer of a fluid through a porous medium over a stretching surface with internal heat generation/absorption and suction/blowing, Fluid Dyn. Res. 37 (2005) 231.

[32] R. Cortell, A note on flow and heat transfer of a viscoelastic fluid over a stretching sheet, Int. J. Non-Linear Mech. 41 (2006) 78.

[33] R. Cortell, Flow and heat transfer of an electrically conducting fluid of second grade over a stretching sheet subject to suction and to a transverse magnetic field, Int. J. Heat Mass Transfer 49 (2006) 1851.

[34] R. Cortell, Effects of viscous dissipation and work done by deformation on the MHD flow and heat transfer of a viscoelastic fluid over a stretching sheet, Phys. Lett. A 357 (2006) 298.

[35] T. Hayat, Z. Abbas and M. Sajid, Series solution for the upper-convected Maxwell fluid over a porous stretching plate, Phys. Lett. A 358 (2006) 396.

[36] R. Cortell, MHD flow and mass transfer of an electrically conducting fluid of second grade in a porous medium over a stretching sheet with chemically reactive species, Chem. Eng. Process 46 (2007) 721.

[37] R. Cortell, Toward an understanding of the motion and mass transfer with chemically reactive species for two classes of viscoelastic fluid over a porous stretching sheet, Chem. Eng. Process 46 (2007) 982.

[38] A. Chakrabarti and A. S. Gupta, Hydromagnetic flow heat and mass transfer over a stretching sheet, Quart. Appl. Math. 33 (1979) 73.

[39] R. S. R. Gorla, Unsteady mass transfer in the boundary layer on a continuous moving sheet electrode, J. Electrochem. Soc. 125 (1978) 865.

[40] H. I. Andersson, O. R. Hansen and B. Olmedal, Diffusion of a chemically reactive species from a stretching sheet, Int. J. Heat Mass Transfer 37 (1994) 659.

[41] H. S. Takhar, A. J. Chamkha and G. Nath, Flowand mass transfer on a stretching sheet with a magnetic field and chemically reactive species, Int. J. Eng. Sci. 38 (2000) 1303.

[42] F. T. Akyildiz, H. Bellout and K. Vajravelu, Diffusion of chemically reactive species in a porous medium over a stretching sheet, J. Math. Anal. Appl. 320 (2006) 322.

[43] I. G. Currie, Fundamental Mechanics of Fluids, McGraw-Hill Inc., New York, 1993.

[44] R. G. Larson, Constitutive Equations for Polymer Melts and Solutions, Butterworths, Boston, 1988.

[45] G. K. Rajeswari and S. L. Rathna, Flow of a particular class of non-Newtonian visco-elastic and visco-inelastic fluids near a stagnation point, Z. Angew. Math. Phys. 13 (1962) 43.

[46] R. T. Davies, Boundary layer theory for viscoelastic liquids, Proceedings of the 10th Midewestern Mechanics Conference, 1967, p. 1145.

[47] M. Van Dyke, Perturbation Methods in Fluid Mechanics, Academic Press, New York, 1964.

[48] K. R. Frater, On the solution of some boundary-value problems arising in elastico-viscous fluid mechanics, Zamp. Angew. Math. Phys. 21 (1970) 134.

[49] I. Teipel, Stagnation point flow of a non-Newtonian second-order fluid, Trans. CSME 12 (1988) 57.

[50] V. K. Garg and K. R. Rajagopal, Stagnation point flow of a non-Newtonian fluid, Mech. Res. Commun. 17 (1990) 415.

[51] M. Pakdemirli, E. S. Suhubi, Similarity solutions of boundary layer equations for second-order fluids, Int. J. Eng. Sci. 30 (1992) 611.

[52] P. D. Ariel, A hybrid method for computing the flow of viscoelastic fluids, Int. J. Numer. Methods Fluids 14 (1992) 757.

[53] R. W. Serth, Solution of a viscoelastic boundary layer equation by orthogonal collocation, J. Eng. Math. 8 (1974) 89.

[54] R. L. Fosdick and K. R. Rajagopal, Anomalous features in the model of second-order fluids, Arch. Ration. Mech. Anal. 70 (1979) 145.

[55] J. E. Dunn and K. R. Rajagopal, Fluids of differential type: critical review and thermodynamic analysis, Int. J. Eng. Sci. 33 (1995) 689.

[56] P. D. Ariel, On extra boundary condition in the stagnation point flow of a second-grade fluid, Int. J. Eng. Sci. 40 (2002) 145.

[57] R. B. Bird, R. C. Armstrong and O. Hassager, Dynamics of Polymeric Liquids, vols. 1 and 2, second ed., Wiley, New York, 1987.

[58] K. Sadeghy, M. Sharifi, Blasius flow of viscoelastic fluid: a numerical approach, Int. J. Appl. Mech. 9 (2) (2004) 399.

[59] K. Sadeghy, A. H. Najafi and M. Saffaripour, Sakiadis flow of an upperconvected Maxwell fluid, Int. J. Non-linear Mech. 40 (2005) 1220.

[60] R. K. Bhatnagar, G. Gupta and K. R. Rajagopal, Flow of an Oldroyd-B fluid due to a stretching sheet in the presence of a free stream velocity, Int. J. Non-linear Mech. 30 (3) (1995) 391.

[61] T. Hagen and M. Renardy, Boundary layer analysis of the Phan-Thien-Tanner and Giesekus model in high Weissenberg number flow, J. Non-Newtonian Fluid Mech. 73 (1997) 181.

[62] M. Renardy, High Weissenberg number boundary layers for the upperconvected Maxwell fluid, J. Non-Newtonian Fluid Mech. 68 (1997) 125.

[63] P. S. Lawrence and B. N. Rao, Heat transfer in the flow of a viscoelastic fluid over a stretching sheet, Acta Mech. 93 (1992) 53–61.

[64] N. M. Bujurke, S. N. Biradar and P. S. Hiremath, Second order fluid flow past a stretching sheet with heat transfer, Z Angew Math. Phys. 38 (1987) 653.

[65] B. S. Dandapat, A. S. Gupta, Flow and heat transfer in a viscoelastic fluid over a stretching sheet, Int. J. Non-linear Mech. 24 (3) (1989) 215.

[66] D. Rollins and K. Vajravelu, Heat transfer in a second order fluid over a continuous stretching surface, Acta Mech. 89 (1991) 167.

[67] M. I. Char, Heat and mass transfer in a hydromagnetic flow of viscoelastic fluid over a stretching sheet, J. Math. Anal. Appl. 186 (1994) 674.

[68] S. Bhattacharya, A. Pal and A. S. Gupta, Heat transfer in the flow of a visco-elastic fluid over a stretching surface, Heat Mass Transfer 34 (1998) 41.

[69] K. Vajravelu and D. Rollins, Heat transfer in electrically conducting fluid over a stretching surface, Int. J. Non-Linear Mech. 27 (2) (1992) 265.

[70] P. D. Ariel, Two dimensional stagnation-point flow of an elastico-viscous fluid with partial slip, ZAMM 88 (2008) 320.

[71] P. D. Ariel, Axisymmetric flow due to a stretching sheet with partial slip, Comput. Math. Appl. 54 (2007) 1169.

[72] P. D. Ariel, T. Hayat and S. Asghar, The flow of a elastico-viscous fluid past a stretching sheet with partial slip,

[73] P. D. Ariel, Generalized three-dimensional flow due to stretching sheet, ZAMM 83 (2003) 844.

[74] P. D. Ariel, A numerical algorithm for computing the stagnation-point flow of a second grade fluid with/without suction, J. Comput. Appl. Math. 59 (1995) 9.

[75] P. D. Ariel, Axisymmetric flow of a second grade fluid past a stretching sheet, Int. J. Eng. Sci. 39 (2001) 529.

[76] H. R. Nataraja, M. S. Sharma and B. N. Rao, Non-similar solutions for flow and heat transfer in a visco-elastic fluid over a stretching sheet, Int. J. Non-Linear Mech. 33 (1998) 357.

[77] R. M. Sonth, S. K. Khan, M. S. Abel and K. V. Prasad, Heat and mass transfer in a visco- elastic fluid flow over an accelerating surface with heat source/sink and viscous dissipation, Heat Mass Transfer 38 (2002) 213.

[78] H.I. Andersson, R. O. Hansen and B. Holmedal, Diffusion of a chemically reactive species from a stretching sheet, Int. J. Heat Transfer 37 (4) (1994) 659.

[79] K. V. Prasad, S. Abel and S. K. Khan, Momentum and heat transfer in viscoelastic fluid flow in a porous medium over a non-isothermal stretching sheet, Inter. J. Numer. Method Heat Fluid Flow 10 (2000) 786.

[80] K. V. Prasad, S. Abel, S. K. Khan and P. S. Datti, Non-Dracy forced convective heat transfer in a viscoelastic fluid flow over a nonisothermal stretching sheet, J. Porous Media 5 (1) (2002) 41.

[81] S. K. Khan, M. S. Abel and R. M. Sonth, Viscoelastic MHD flow heat and mass transfer in a over porous stretching sheet dissipation of energy and stress work, Heat Mass Transfer 40 (2003) 47.

[82] P. Sam Lawrence and B. N. Rao, Reinvestigation of the non-uniqueness of the flow of visco-elastic fluid flow over a stretching sheet, Quat. Appl. Math. 51 (3) (1993) 401.

[83] S. Abel, P. H. Veena, K. Rajagopal and V. K. Paveen, Non-Newtonian magnetohydrodynamic flow over a stretching sheet with heat and mass transfer, Int. J. Non Linear Mech. 39 (2004) 1067.

[84] K. Vajravelu and J. Nayfeh, Convective heat transfer at a stretching sheet, Acta Mech. 96 (1–4) (1993) 47.

[85] A. Postelnicu, T. Grosan and I. Pop, The effect of variable viscosity on forced convection flow past a horizontal flat plate in a porous medium with internal heat generation, Mech. Res. Commun. 28 (2001) 331.

[86] A. Postelnicu, T. Grosan and I. Pop, Free convection boundary layer over a vertical permeable plate in a porous medium with internal heat generation, Int. Commun. Heat Mass Transfer 27 (5) (2000) 729.

[87] A. Postelnicu and I. Pop, Similarity solutions of free convection boundary layers over vertical and horizontal surfaces in porous media with internal heat generation, Int. Commun. Heat Mass Transfer 26 (8) (1999) 1183.

[88] Emad M. Abo-Eldahab and Mohamed A. El Aziz, Blowing/suction effect on hydromagnetic heat transfer by mixed convection from an inclined continuously stretching surface with internal heat generation/absorption, Int. J. Therm. Sci. 43 (2004) 709.

[89] J. Harris, Rheology and Non-Newtonian Flow, Longman, London, 1977.

[90] S. J. Liao, Beyond perturbation: introduction to homotopy analysis method, Boca Raton: Chapman & Hall/CRC Press; 2003.

[91] S. J. Liao, On the proposed homotopy analysis technique for non-linear problems and its applications. Ph. D. dissertation, Shanghai Jiao Tong University 1992.

[92] S. J. Liao, A uniformly valid analytic solution of 2D viscous flow past a semi-infinite flat plate, J. Fluid Mech., 385 (1999) 101.

[93] S. J. Liao, An analytic solution of unsteady boundary-layer flows caused by an impulsively stretching plate, Comm. Non-linear Sci. Numer. Simm. 11 (2006) 326.

[94] S. J. Liao and A. Campo, Analytic solutions of the temperature distribution in Blasius viscous flow problems, J. Fluid Mech., 453 (2002) 411.

[95] S. J. Liao, On the analytic solution of magnetohydrodynamic flows of non-Newtonian fluids over a stretching sheet, J. Fluid Mech., 488 (2003) 189.

[96] S. J. Liao, A new branch of solutions of boundary-layer flows over a permeable stretching plate, Int. J. Non-Linear Mech. 42 (2007) 819.

[97] S. J. Liao, A new branch of solutions of boundary-layer flows over an impermeable stretched plate, Int. J. Heat and Mass Transfer, 48/12 (2005) 2529.

[98] S. J. Liao, An analytic solution of unsteady boundary-layer flows caused by an impulsively stretching plate, Comm. Non-linear Sci. Numer. Simm. 11 (2006) 326.

[99] H. Xu and S. J. Liao, Series solutions of unsteady magnetohydrodynamic flows of non-Newtonian fluids caused by an impulsively stretching plate, J. Non-Newtonian Fluid Mech. 129 (2005) 46.

[100] H. Xu, S. J. Liao and G. X. Wu, A family of new solutions on the wall jet, European J. Mech. B/Fluids 27 (2008) 322.

[101] J. Cheng, S. J. Liao, R. N. Mohapatra and K. Vajravelu, Series solutions of nano boundary layer flows by means of the homotopy analysis method, J. Math. Anal. Appl. 343 (2008) 233.

[102] S. Abbasbandy, The application of homotopy analysis method to nonlinear equations arising in heat transfer, Phys. Lett. A 360 (2006) 109.

[103] Y. Tan and S. Abbasbandy, Homotopy analysis method for quadratic Recati differential equation, Commu. Non-linear Sci. Numer. Simul. 13 (2008) 539.

[104] S. Abbasbandy and F. S. Zakaria, Soliton solutions for the fifth-order KdV equation with the homotopy analysis method, Nonlinear Dyn. 51 (2008) 83.

[105] M. Inc, On numerical solution of Burger's equation by homotopy analysis method, Phys. Lett. A 372 (2008) 356.

[106] S. Abbasbandy and E.J. Parkes: Solitary smooth hump solutions of the Camassa–Holm equation by means of the homotopy analysis method, Chaos, Solitons & Fractals 36 (2008) 581.

[107] S. Abbasbandy: Homotopy analysis method for heat radiation equations, Int. Comm. in Heat and Mass Transfer 34 (2007) 380.

[108] S. Abbasbandy: The application of homotopy analysis method to solve a generalized Hirota–Satsuma coupled KdV equation, Phys. Lett. A 361 (2007) 478.

[109] A. Sami Bataineh, M.S.M. Noorani , I. Hashim. On a new reliable modification of homotopy analysis method. Commun. Nonlinear Sci. Numer. Simul. 14 (2009) 409.

[110] A. Sami Bataineh, M.S.M. Noorani , I. Hashim. The homotopy analysis method for Cauchy reaction–diffusion problems. Physics Letters A 372 (2008) 613.

[111] S. P. Zhu, A closed-form analytical solution for the valuation of convertible bonds with constant dividend yield, Anziam Journal 47 (2006) 477.

[112] T. Hayat, Z. Abbas and M. Sajid: Heat and mass transfer analysis on the flow of a second grade fluid in the presence of chemical reaction, Phys. Lett. A 372 (2008) 2400.

[113] T. Hayat, M. Sajid and M. Ayub: A note on series solution for generalized Couette flow, Comm. Non-linear Sci. Numer.Simu. 12 (2007) 1481.

[114] T. Hayat, M.A. Farooq, T. Javed and M. Sajid: Partial slip effects on the flow and heat transfer characteristics in a third grade fluid, Nonlinear Analysis: Real World Applications (In press).

[115] T. Hayat and T. Javed: On analytic solution for generalized three-dimensional MHD flow over a porous stretching sheet, Phys. Lett. A, 370 (2007) 243.

[116] Y. Wu, C. Wang and S. J. Liao, Solving solitary waves with discontinuity by means of the homotopy analysis method, Chaos Solitons & Fractals 26 (2005) 177.

[117] Z. Abbas, M. Sajid and T. Hayat, MHD boundary layer flow of an upper-convected Maxwell fluid in porous channel, Theor. Comp. Fluid Dyn. 20 (2006) 229.

[118] M. Sajid, T. Hayat and S. Asghar, Non-similar analytic solution for MHD flow and heat transfer in a third-order fluid over a stretching sheet, Int. J. Heat Mass Transfer 50 (2007) 1723.

[119] M. Sajid, T. Hayat and S. Asghar, On the analytic solution of steady flow of a fourth grade fluid, Phys. Lett. A 355 (2006) 18.

[120] T. Hayat, T. Javed and M. Sajid, Analytical solution for rotating flow and heat transfer analysis of a third-grade fluid, Acta Mech. 191 (2007) 219.

[121] F. M. Allan, Derivation of the Adomian decomposition method using the homotopy analysis method, Appl. Math. Comput. 190 (2007) 6.

[122] H. Xu, X. C. You and I. Pop, Analytical approximation for laminar film condensation of saturated stream on an isothermal vertical plate, Appl. Math. Modelling 32 (2008) 738.

[123] A. Alizadeh-Pahlavan and K. Sadeghy, On the use of homotopy analysis method for solving unsteady MHD flow of Maxwellian fluids above impulsively stretching sheet, Commun. Nonlinear Sci. Numer. Simul. 14 (2009) 1355.

[124] B. Yao, Approximate analytical solution to the Falkner-Skan wegde flow with the permeable wall of uniform suction, Commun. Nonlinear Sci. Numer. Simul. 14 (2009) 3320.

[125] P.M. Fitzpatrick: Advancecd Calculus. PWS publishing company, Boston, MA (1996).

[126] S.J. Liao and K.F. Cheung: Homotopy analysis of a nonlinear progressive waves in deep water, J. Eng. Math. 45, (2003) 105 .

[127] V. K. Garg and K. R. Rajagopal, Flow of non-Newtonian fluid past a wedge, Acta Mech. 88 (1991) 113.

[128] A. Bejan, Convection Heat Transfer (2^{nd} edition), Wiley, New York, 1995.

[129] N. Afzal, A. Badaruddin and A. A. Elgarvi, Momentum and heat transport on a continuously flat surface moving in a parallel stream, Int. J. Heat Mass Transfer 36 (1993) 3399

[130] M. V. A. Bianchi and R. Viskanta, Momentum and heat transfer on a continuous flat surface moving in parallel counter flow free stream. Wärme- und Stoffübertr. 29 (1993) 89.

[131] M. Kumari and G. Nath, MHD boundary-layer flow of a non-Newtonian fluid over a continuously moving surface with a parallel free stream. Acta Mechanica 146 (2001) 139.

[132] C. Y. Wang, Liquid film on an unsteady stretching sheet, Quart. J. Appl. Math. 48 (1990) 601.

[133] R. Usha and R. Sridharan, On motion of a liquid film on an unsteady stretching surface, ASME Fluids Eng. 150 (1993) 43.

[134] H. I. Andersson, J. B. Aarseth, N. Braud and B. S. Dandapat, Flow of a power law fluid film on an unsteady stretching surface, J. Non-Newtonian Fluid Mech. 62 (1996) 1.

[135] I. C. Liu and H. I. Andersson, Heat transfer in a liquid film on an unsteady stretching sheet, Int. J. Ther. Sci. (in press).

[136] C. H. Chen, Heat transfer in a power-law fluid film over a unsteady stretching sheet, Heat Mass Transfer 39 (2003) 791.

[137] C. Wang and I. Pop, Analysis of the flow of a power-law fluid film on an unsteady stretching surface by means of homotopy analysis method, J. Non-Newtonian Fluid Mech. 138 (2006) 161.

[138] J. A. Shercliff, A text Book of Magnetohydrodynamics, Pergamon press, Elmsford, New york, 1965.

[139] N. D. Nanousis, Theoretical magnetohydrodynamic analysis of mixed convection boundary layer flow over a wedge with uniform suction or injection, Acta Mech. 138 (1999) 21.

[140] K. Vajravelu and J. Rivera, Hydromagnetic flow at an oscillating plate, Int. J. Non-Linear Mech. 38 (2003) 305.

[141] T. Hayat, M. Zumurad, S. Asghar and A. M. Siddiqui, Magnetohydrodynamic flow due to non-coaxial rotations of a porous oscillating disk and a fluid at infinity, Int. J. Eng. Sci. 41 (2003) 1177.

[142] J. N. Tokis, Hydromagnetic unsteady flow due to an unsteady plate, Astrophys. Space Sci. 58 (1978) 167.

[143] I. Pop, M. Kumari and G. Nath, Conjugate MHD flow past a flat plate, Acta Mech. 106 (1994) 215.

[144] K. Vajravelu and T. Roper, Flow and heat transfer in a second grade fluid over a stretching sheet, Int. J. Non-Linear Mech. 34 (1999) 1031.

[145] T. R. Mahapatra and A. S. Gupta, Heat transfer in stagnation-point flow towards a stretching sheet, Heat and Mass Transfer 38 (2002) 517.

[146] A. Ishak, R. Nazar and I. Pop, Mixed convection boundary layers in the stagnation-point flow toward a stretching vertical sheet, Meccanica 41 (2006) 509.

[147] R. Nazar, N. Amin, D. Filip and I. Pop, Unsteady boundary layer flow in the region of the stagnation point on the stretching sheet, Int. J. Eng. Sci. 42 (2004) 1241.

[148] R. Cortell, Viscous flow and heat transfer over a nonlinearly stretching sheet, Appl. Math. Computation 184 (2007) 864.

[149] R. Nazar, N. Amin, D. Filip and I. Pop, Stagnation point flow of a micropolar fluid towards a stretching sheet, Int. J. Non-Linear Mech. 39 (2004) 1227.

[150] G. Ahmadi, Self-similar solution of incompressible micropolar boundary layer flow over a semi-infinite flat plate, Int. J. Eng. Sci. 14 (1976) 639.

[151] S. K. Jena and M. N. Mathur, Similarity solutions for laminar free convection flow of a thermo-micropolar fluid past a nonisothermal flat plate, Int. J. Eng. Sci. 19 (1981) 1431.

[152] G. S. Guram and A. C. Smith, Stagnation flows of micropolar fluids with strong and weak interactions, Comput. Math. Appl. 6 (1980) 213.

[153] J. Peddieson, An application of the micropolar fluid model to the calculation of turbulent shear flow, Int. J. Eng. Sci. 10 (1972) 23.

[154] K. Vajravelu and J. R. Cannon, Fluid flow over a nonlinear stretching sheet, Appl. Math. Computation. 181 (2006) 609.